Local Stability Analysis of Hydrogen Bonding and Other Non-Covalent Interactions

by

Laura Albrecht

Submitted in partial fulfilment of the requirements
for the degree of Doctor of Philosophy

at

Dalhousie University
Halifax, Nova Scotia
November 2014

For my parents,
who have always believed that I was capable of anything,
and for my big brother and my big sister,
with love.

♥

"What an abyss of uncertainty, whenever the mind feels overtaken by itself; when it, the seeker, is at the same time the dark region through which it must go seeking and where all its equipment will avail it nothing. Seek? More than that: create. It is face to face with something which does not yet exist, which it alone can make actual, which it alone can bring into the light of day."

— Marcel Proust

Table of Contents

List of Tables

List of Figures

Abstract

Bader's quantum theory of atoms in molecules (QTAIM) is used to evaluate local atomic stabilities in clusters of molecules. The total energy of a molecular system is decomposed into atomic contributions determined quantum mechanically through evaluation of the electron density contained within atomic basins. Stability is defined by changes in the atomic energy. These stabilities are used to interpret energetic changes within molecules as they form non-covalent interactions, including hydrogen bonding, beryllium bonding and halogen bonding, as well as combined instances of each. The stabilities are then represented using a unique method of visualization, whereby atom size represents the magnitude of the energy change and atom colour represents sign of energy change (positive or negative). Local stabilities in small methanol $(MeOH)_{n=2-4}$, formaldehyde $(H_2C=O)_{n=2-4}$, and water $(H_2O)_{n=2-6}$ clusters reveal a clear increase in the magnitude of atomic stability when cooperative interactions are present. This energy increase is not observed for non-cooperative or anti-cooperative interactions in formaldehyde and water clusters. For methanol clusters the cooperative stability is clearly localized at the hydroxyl group. Local atomic and molecular energies give new insight into the interaction of water wires with alkali metals, alkaline earth metals and halide ions and, finally, local atomic stabilities show the existence of strong cooperative effects for beryllium-hydrogen bond interactions and beryllium-halogen bond interactions, which are in some cases very intense.

List of Abbreviations and Symbols Used

SYMBOLS

Å	angstrom
a.u.	atomic unit of energy
c_{ik}	orbital coefficients
D	deuterium
e	electron charge
e	Euler's number (2.718281828)
E	energy
E_0	ground state energy
$E_{AVE}HB$	average hydrogen bond energy
E_{int}	interaction energy
E_{tot}	total energy
E_{xc}	exchange-correlation energy
E(A)	atomic energy evaluated with AIMAll
ΔE(A)	atomic stability evaluated with AIMAll
E(Ω)	energy of atomic basin
F	Fock matrix (Chapter 3)
$\hat{F}$	Fock operator
f_i	orbital occupation
F^σ	Fermi correlation
G(Ω)	gradient kinetic energy of atomic basin
ΔG	Gibbs energy
$\hat{h}$	one-electron Hamiltonian operator
$\hat{H}$	Hamiltonian operator
ħ	reduced Planck constant
$\hat{J}$	Coulomb operator
J(ρ)	Coulomb repulsion energy
K	kelvin
$\hat{K}$	exchange operator
K(Ω)	Schrödinger kinetic energy of atomic basin
L(Ω)	atomic Laplacian
m	mass
N(Ω)	population of atomic basin
$\hat{p}$	momentum operator
ps	picosecond
q(A)	atomic charge evaluated with AIMAll
q(Ω)	charge of atomic basin
r	electron coordinates
$\mathbf{r}_s$	point on a surface S (Chapter 3.8)
Ry	Rydberg unit of energy
S	overlap matrix
T	kinetic energy
$\hat{T}$	kinetic energy operator

T_0	non-interacting kinetic energy
$T(\rho)$	interacting kinetic energy
$T(\Omega)$	kinetic energy of atomic basin
V	potential energy
$\hat{V}$	potential energy operator
$V_{ee}(\rho)$	electron-electron interaction energy
z_Ω	nuclear charge of atomic basin
γ	virial ratio
Δ	change in
ε	bond ellipticity
ε_i	energy eigenvalue
λ	curvature of the density
Λ	Hessian matrix
Λ_{ij}	Lagrange multipliers
v	potential field
π	pi orbital
ρ_{BCP}	electron density at bond critical point
$\rho(r)$	electron density, probability density
$\rho(r_c)$	electron density at critical point
σ	electron spin
σ	critical point signature (Chapter 3.8)
$\sigma*$	antibonding orbital (Chapter 4, Chapter 6)
Σ	summation over
$\Upsilon(\mathbf{r})$	potential energy density, virial field
ϕ_k	atomic orbital
ψ_i	molecular orbital
Ψ	n-body wavefunction
ω	critical point rank
Ω	atomic basin
∂	partial derivative
∇	$(x\frac{\partial}{\partial x} + y\frac{\partial}{\partial y} + z\frac{\partial}{\partial z})$

ABBREVIATIONS

1D	one-dimensional
2D	two-dimensional
3D	three-dimensional
ADF	Amsterdam Density Functional
AIM	atoms in molecules
AIMD	*ab initio* molecular dynamics
ATR	attenuated total reflection
AVE	average
B3LYP	Becke, three-parameter, Lee-Yang-Parr
BAR	bond activation reinforcement
BCP	bond critical point
BO	bond order (Chapter 3.8)
BO	Born-Oppenheimer
BSSE	basis set superposition error
CBS	complete basis set
CC	coupled cluster
CCP	cage critical point
cGTO	contracted gaussian-type orbitals
CI	configuration interaction
CP	counterpoise
CPMD	Car-Parrinello molecular dynamics
CPU	central processing unit
CT	charge transfer
DFT	density-functional theory
DNA	deoxyribonucleic acid
D-PCM	dielectric polarizable continuum medium
EDA	energy decomposition analysis
GGA	generalized gradient approximation
GTO	gaussian-type orbitals
H^+	proton
H-bond	hydrogen-bond
HB	hydrogen bond
HB-BCP	hydrogen-bond bond critical point
HF	Hartree–Fock
HK	Hohenberg-Kohn
Hz	Hertz
IEF	integral equation formalism
INS	inelastic neutron scattering
IR	infrared
IUPAC	international union of pure and applied chemistry
KS	Kohn-Sham
KS-DFT	Kohn-Sham density-functional theory
LCAO	linear combination of atomic orbitals
LDA	local density approximation

MBE	many body effects
MBIE	many body interaction energy
MBPT	many body perturbation theory
MC-SCF	multi-configurational self-consistent field
MD	molecular dynamics
Me	methyl group
MES	minimum energy search
MET	many electron theory
MM	molecular mechanics
MP2	second order Møller-Plesset perturbation theory
MO	molecular orbital
M06	Minnesota 06
mol	mole
MPN	n^{th} order Møller-Plesset perturbation theory
MRD	magnetic relaxation dispersion
NBO	natural bond order
NCP	nuclear critical point
NIR	near infrared
NMR	nuclear magnetic resonance
NPA	natural population analysis
OH	alcohol group
ONIOM	Our own N-layered Integrated molecular Orbital and Molecular mechanics
PCM	polarizable continuum medium
PES	potential energy surface
QM	quantum mechanics
QTAIM	quantum theory of atoms in molecules
RCP	ring critical point
SAS	solvent accessible surface
SANS	small angle neutron scattering
SCF	self-consistent field
SCRF	self-consistent reaction field
SCVS	self-consistent virial scaling
SDTQ	singles, doubles, triples, quadruples
SES	solvent excluded surface
SFG	sum frequency generation
SHG	second harmonic generation
SP	single point
STDEV	standard deviation
STO	Slater-type orbitals
UV	ultraviolet
VDW	van der Waals
VMD	visual molecular dynamics
XAS	X-ray absorption spectroscopy
XDM	exchange-hole dipole moment correction
ZPE	zero point energy

Acknowledgements

A sincere thank you to my supervisor, Russ Boyd, for the gentle encouragements and for showing so much confidence in me. I have always felt lucky to be a member of the Boyd Group.

Thank you to my wonderful family, East coast to the West coast, for your love and support.

Thank you to my friends, who are still my friends even though I've ignored you for 5 years.

I would also like to thank Katherine Darvesh for introducing me to computational chemistry; my committee members Axel Becke, Don Weaver, and Jan Rainey, for taking me on as their student and for making committee meetings so enjoyable; Giselle Andrews and Cheryl Stanton for all their administrative help; Ross Dickson for the great ACENet support; Hugo Bohórquez, without whom I might never have appreciated 10 pm office time; Michelle Lu for her insight and her humor; and finally thank you to all the teachers who took the time to show me that learning is a passion.

...I promised, O blessed St. Jude, to be ever mindful of this great favor, to always honor you as my special and powerful patron, and to gratefully encourage devotion to you.
Amen.

Chapter 1   Introduction

In the broad range of topics studied using computational methods, the importance of water and the role of solvation cannot be overstated. It is known that solvation can affect the stability and conformation of systems like proteins and nanostructures, and solvation studies typically focus on the effect of the solvent on the solute. But there is also the question of how these solutes can in turn impact the energy and structure of the surrounding solvent. This becomes very important for protein folding, where the entropy and enthalpy of solvation play a critical role in formation of secondary and tertiary protein structure. Many commonly used computational methods give poor predictions of water behaviour on local levels. A deeper understanding of water's local stability and configuration in the presence of solute molecules is of primary interest. Evaluating these local stabilities is difficult because most analyses report total energies, either obtained experimentally in bulk or theoretically using a variety of approaches. A unique solution to this problem is found in Bader's quantum theory of atoms in molecules (QTAIM) [1], which provides a well-established method to partition total molecular electron densities into non-overlapping local values that can be attributed to the atoms in the molecules. From the local atomic values it is possible to evaluate local stability in the molecule through changing atomic energies. Matta *et al*. [2] demonstrated this in a study of bond dissociation of aliphatic hydrocarbons. Later, Taylor *et al*. [3] evaluated local stabilities for folded telomere structures and then visually represented the results in a way that highlighted important areas of stabilization and destabilization. In this thesis, the QTAIM local stability analysis is extended to consider water-water and water-solute interactions.

The structure of this thesis is as follows. Chapter 2 introduces some properties of water and its hydrogen bonding interactions, with a discussion of experimental approaches for the observation of hydrogen bonds and water molecules. Chapter 3 introduces technical details regarding the computational evaluation of molecules, with a special focus on QTAIM in Section 3.8. In Chapter 4 and Chapter 5, QTAIM is used to evaluate local stabilities within small water clusters from n=2-5 [4] and six minima on the water hexamer potential energy surface [5]. Chapter 6 and Chapter 7 present a study of the water dimer and trimer interacting with two BeX_2 derivatives [6] and a series of water

wires interacting with alkali, alkaline earth metal and halide ions. Chapter 8 and Chapter 9 demonstrate atomic energy analysis of the cooperativity present in a range of non-covalent interactions, including hydrogen bonding [7] and beryllium bonding combined with halogen bonding [8]. The majority of these chapters have been published in peer reviewed journals and are presented in this thesis as-published, with introductory and summarizing sections included for each chapter. This thesis concludes with some proposed future work and finally a summary of important conclusions.

Each molecular system studied here is of key importance in the literature: small water clusters have long been test cases for benchmarking new methods, the water hexamer may provide a model for the behaviour of liquid water, water wires have an integral role in transport across cell membranes, and cooperativity is one of the most important and common characteristics shared by non-covalent interactions. Yet perhaps the most exciting aspect of this thesis is the opportunity to quantitatively evaluate local energy changes in molecular systems on the basis of the electron density – a real, physical observable. In this way, Bader's quantum theory of atoms in molecules serves as a unique bridge between experiment and theory [9].

Chapter 2   Water, Hydrogen Bonds and Cooperativity

What a fascinating thing, water. That such a small molecule can hold so many answers and yet hide so many secrets. Water has a large array of unusual properties in pure form and as a solvent [10]. Some of these properties include: a liquid-phase density maximum, an unusually high boiling point and high heat capacity, a low coefficient of thermal expansion, non-monotonic compressibility with temperature, an unusually high number of crystalline polymorphs, and an unusual preferential arrangement around hydrophobic solutes which results in a negative entropy change for the solvent. Although many properties of water can be measured experimentally, at the molecular level the behaviour of water is still unknown. The unique properties of water are generally attributed to the nature of its hydrogen bond (H-bond) network. The hydrogen bond is a curious phenomenon that has historically been difficult to describe conclusively [11]. In 2011, an IUPAC task force published a report which provided an internationally recommended definition of the hydrogen bond (designated as X—H···Y) [12]: *The hydrogen bond is an attractive interaction between a hydrogen atom from a molecule or a molecular fragment X–H in which X is more electronegative than H, and an atom or a group of atoms in the same or a different molecule, in which there is evidence of bond formation*. They define several criteria necessary for the presence of a hydrogen bond, including: an electrostatic charge-transfer interaction that leads to formation of a partially covalent bond between H and Y; a polarization of the X—H bond resulting in an increase in the H···Y bond strength due to increasing electronegative character of Y; an optimal X—H···Y angle of 180°; an increasing X—H bond length and decreasing H···Y bond length indicating a strengthening of the hydrogen bond (often observed through a red-shift in the IR spectra of the bond vibrations); characteristic NMR signatures that include pronounced deshielding for H in X—H; and, finally, to be experimentally observed, H-bond formation should have a Gibbs energy greater than the thermal energy in the system.[1]

---

[1] The IUPAC recommendation states that: "For hydrogen bonding to have any practical significance, it should be thermally stable. Hence, a hydrogen-bonded complex, between donor and acceptor molecules, produced in a supersonic beam or a cryogenic matrix, may not be found in a room temperature mixture of the two molecules" [12].

Note that these are guideline criteria and there is an element of subjectivity in the interpretation of each case.

When several hydrogen bonds are present in a system a phenomenon called cooperativity can be observed. Cooperativity is a deviation from the pairwise additivity of the bonding interactions, so that the combined stability of a hydrogen-bonded system containing cooperative bonds can be greater than the sum of the isolated individual bonds. This is especially observed in small water clusters; in particular, the trimer through pentamer water clusters are most stable in cyclic arrangements where each water can accept a H-bond from and donate a H-bond to its neighbouring waters [13]. Cooperativity also provides increased stability in biological systems such as DNA and protein secondary structures [14, 15]. Not all hydrogen bonding interactions are cooperative. In some arrangements it is possible for several H-bonds to have a net stability that is equivalent to, or even lower than, the sum of the isolated interactions. These are referred to as non-cooperative and anti-cooperative interactions, respectively [7].

Although much is known about hydrogen bonds and water structures, they are notoriously difficult to model correctly using available theoretical methods. Their dependence on long-range interactions renders many of the commonly applied computational methods unusable, as they do not easily account for diffuse effects [16]. The methods that can account for these interactions are often too expensive to be applied to systems larger than a few molecules [17]. Furthermore, hydrogen bonds are highly sensitive to quantum effects, and the distinct possibility of quantum proton tunnelling must also be considered [18]. Nevertheless, improved equipment, increasing computer power and growing knowledge of the nature of hydrogen bond networks continuously builds our repertoire of information.

2.1 Experimental Observations of Hydrogen Bonds and Water

The experimental study of water has changed considerably since the early 18th century, when it was first noted that combining two parts hydrogen gas and one part common air with a measure of energy would produce a "dew-like substance" [19]. Today, we have tools that allow us to see inside those dew droplets and observe the very

water molecules as they perform their complicated dance. The following sections highlight some current experimental methods used to study water and hydrogen bonds. The rapid dynamics of the small water molecule combined with its ability to establish H-bonds in a large variety of ways makes it a particularly difficult molecule to observe and measure. This overview is separated into two sections: measurement of hydrogen bonds and measurement of water. Although many of the methods used to observe water molecules are analogous to those used to observe H-bonds in larger structures, the purpose of the second section is to highlight the experimental difficulty in pinpointing the presence of the water molecule itself, which lends some explanation as to why inclusion of water has been largely neglected in experimental practices (and also theoretical analyses). The reader is referred to [20] for a more detailed description of each method.

2.1.1 Observing Hydrogen Bonds

Experimental measurements of hydrogen bonds began early in the 20th century. Calorimetric results showed strikingly different latent heats of evaporation for H_2O, HF, and NH_3, compared to liquids of similar substances but whose interaction was predominantly due to van der Waals forces.[2] There are two categories predominant in hydrogen bond (HB) observation: absorption methods and emission or scattering methods. These methods are summarized in Table 2.1.

_____

[2] van der Waals forces are non-covalent interactions between molecules which can be either attractive or repulsive. They include permanent dipole interactions, permanent dipole and induced dipole interactions (polarization), and induced dipole interactions (dispersion).

Table 2.1 Methods for experimental analyses of hydrogen bonds (HBs).

Absorption Methods		
Microwave Spectroscopy	- 3-300 GHz frequency range - Requires gas phase samples at low temperature with a permanent electronic dipole	- Very precise; provides fundamental data on HB geometry and proton transfer - Restricted to simple molecules because of gas-phase criterion
IR spectroscopy	- 400-4000 GHz range - Requires simple compounds with little spectra overlap	- Less expensive equipment than microwave spectroscopy but gives lower resolution
Nuclear Magnetic Resonance (NMR)	- 100-1000 MHz frequency range - Can observe spectra in solution environments	- Very precise; high resolution - Provides structural determination of macromolecules (including proteins) - Can directly observe HBs in proteins [21]
X-ray absorption spectroscopy	- 10^{20} Hz frequency range - Requires stable X-ray beam	- Atom-specific probe, can indirectly provide precise local structural information - Some controversy surrounds the limits of XAS sensitivity for HB analysis in water [22]
Emission (Scattering) Methods		
X-ray and Neutron Diffraction	- Can be applied to very small crystalline samples - Small scattering factor for H means low precision for HBs (improved by deuterium substitution)	- Precise determination of the structure of crystalline molecular complexes - Useful for liquids, *e.g.* to provide O-O distances to determine of average HB values
Raman spectroscopy	- Generally used for intermonomer symmetric vibrations below 400 GHz - Complementary to IR	- Not sensitive to HBs, but useful for situations such as studying liquid water or other aqueous media where hypersensitivity is undesirable
Incoherent Neutron Scattering	- Generally accessible outside of IR region, below 400 GHz - Complicated to implement	- Takes advantage of the exceptionally large incoherent cross-section scattering of H-atom - Reports H-atom vibrations

2.1.2 Observing Water Molecules

Most approaches described in this subsection are applicable to the analysis of water in macromolecular species such as proteins. Some macroscopic global experimental approaches are listed as well as the classical molecular methods and, finally, a more detailed description of the uses of IR is given.

2.1.2.1 Global Methods

Useful for the study of macroscopic quantities, global methods do not provide information at a molecular level.

Thermogravity and calorimetry are generally used together. Thermogravity yields sorption isotherms by measuring the weight of water molecules that naturally embed in a sample in a saturated (humid) environment. Calorimetry is used to measure phase transitions as the temperature is varied. These phase transitions have indicated that embedded water clusters in the sample exhibit properties differing from those of bulk water [23]. Enthalpies of formation of H-bonds formed by the water molecules that have been inserted in the sample are often higher than corresponding enthalpies in liquid water.

Dielectric measurements require frequencies less than a few GHz. They analyze collective motion in a sample, returning the conductivity of the sample at varying levels of hydration. This conductivity is a result of proton transfers and is highly sensitive to isotope substitution. At a critical value of hydration (~0.2) the conductivity of some proteins begins to increase exponentially [24]. This threshold is closely related to the occurrence of enzyme activity and may be a result of the ability of water to form a 2D conductive sheath around the protein [20].

2.1.2.2 Classical Molecular Methods

These methods include X-ray and neutron scattering and NMR spectroscopy and can yield information on a molecular level.

X-ray scattering requires perfect ordering of crystals and is useful for specific cases such as ice and crystalline hydrates. When water is the only species present in the sample, radial distribution functions can provide averaged distance information. This is well documented for liquid water and various forms of ice. Because of their inherent disorder, it is difficult to obtain precise water data for many biological macromolecules. There are specific cases where water molecules have been identified using X-rays, such as the observation of proton wires in bacteriorhodopsin [25, 24], and cases where the water molecules may form a sort of "structural bridge" between two potentially H-bonding groups which are far apart. Note that in these cases the water molecules are the point of structural order rather than disorder, and this generally requires a presence of a minimum of water molecules so that disordered waters do not disrupt the observations.

Neutron scattering is complementary to X-ray scattering, with the advantage that hydrogen atoms can be substituted for deuterium, with improved precision for isolating positions of D-bonds. Small-angle neutron scattering (SANS) can detect small clusters of H_2O molecules. Although the small angle limits the resolution, a process of elimination combining H and D scattering patterns can be used to determine the position of these atoms with better precision (sometimes referred to as isotopic contrast approach). Inelastic neutron scattering (INS) is useful for determining water structure in low frequency regions where IR and Raman encounter difficulties. These methods have been applied to hydration dynamics of proteins [26].

NMR spectroscopy can observe H-bonding directly in small samples through chemical shifts or indirectly by establishing relaxation times for known groups. This is useful for H_2O molecules when embedded in a macromolecule because the H-bond dynamics are more rapid than those of the non-water H-bonds of the macromolecule itself. The method, called relaxometry or nuclear magnetic relaxation dispersion (MRD), is useful for hydration dynamics of proteins and some synthetic polymers [27]. MRD has been useful in understanding the role of water molecules in protein folding.

2.1.2.3 Vibrational Spectroscopy

    The methods discussed in this section are predominantly IR-based. This method has developed into a sensitive and precise approach to observe the presence of hydrogen bonds in water-solute interactions.

Attenuated total reflection (ATR) passes the IR beam through a high refractive index crystal that undergoes total reflection. The diluted IR beam reduces the ratio of transmitted to incident intensity so that the ATR analysis can achieve a much higher signal-to-noise ratio than transmission-based IR. ATR is a useful method for observing bulk water because it avoids the oversaturation limit. This has been applied in determining the similar density of the liquid water H-bond network and the ice H-bond network. Because IR can be performed on solvated species, it is a great advantage in the study of ions in solution as well as the structure of water at various interfaces. Hydrating water molecules can be discerned from bulk water because of their varying H-bond strengths.

IR spectroscopy on thin samples minimizes the amount of sample rather than the light passing through it. This is particularly effective for studying the hydration of macromolecules with a total water thickness of less than 1 μm, avoiding the presence of bulk water contaminating the spectra. It is possible to obtain a quantitative measure of the water molecules present in the sample as well as the nature of the bonding interactions.

Time-resolved nonlinear IR spectroscopy. With this method it is possible to obtain information about the dynamics of the environment surrounding the H-bond vibrations as well as the nature of the vibrations themselves. Furthermore, this method is isotope-sensitive: deuterated species have a significantly different relaxation time for various bending and stretching vibrations. H/D substitution/dilution methods are especially useful for resolving the structure and dynamics of water around solvated ions and simple organic molecules.

Near infrared (NIR) and Raman spectroscopic methods are also useful tools for the observation of water and water-interactions, complementary to IR measurements. They absorb in a region of much lower saturation and can therefore provide information similar to that of ATR but at a lower cost because they are much simpler to implement. Although they are effective in a very limited range, they are useful for analysis of water presence in the food and medicine industries.

Sum frequency generation vibrational spectroscopy (SFG) is a powerful tool for evaluating molecular information at liquid interfaces [28]. It is a nonlinear spectroscopic analysis involving simultaneous evaluation in the visible-UV region and the IR region. This method has proven particularly useful for evaluation of the solvation properties of ions at vapor-liquid and liquid-liquid interfaces, with special attention to hydrogen bond orientation in these environments [29]. A special case of SFG is second harmonic generation (SHG), which has also been used to probe air-water interfaces.

Although there have been incredible advances in the equipment and techniques for experimental observation of water and water interactions, many of these approaches require highly specialized equipment and are difficult if not impossible to perform on a broad spectrum of samples. In light of this, the benefits of the relatively low-cost implementation of theoretical methods become very evident, either to supplement available experimental data, or to make predictions about details inaccessible to experiment.

Chapter 3   Theoretical Methods

An overview of some theoretical methods has been included in this section to outline the inherent strengths and limitations of the methods used within this thesis. In the following section the Schrödinger equation and its development into Hartree–Fock theory is briefly explained. Post-Hartree Fock methods and density-functional theory are then introduced as well as basis sets and solvent models. Methods to evaluate the potential energy surface of clusters and molecules are introduced next. The chapter concludes with an in-depth look at Bader's quantum theory of atoms in molecules. These theoretical methods have been included because they are largely applied in the following research. The reader is also referred to the resources referenced in the chapter for more in-depth discussions of the chapter material.

3.1 The Schrödinger Equation and More

The ability to describe chemical phenomena using computational methods began with Schrödinger's combination of the de Broglie equation with wave behaviour equations, yielding mathematical expressions (called wavefunctions) that could successfully represent the behaviour of electrons [30]. These wavefunctions are single-valued, continuous and finite, and have to be normalized so that they integrate to the exact number of electrons present in the system. To satisfy the Pauli exclusion principle, the wavefunctions are also antisymmetric with respect to the permutation of any two electrons. The Schrödinger model thus turned the one-dimensional Bohr model of atoms into a three-dimensional model capable of exactly describing a system of electrons, protons and neutrons. Written in operator form, the time-independent Schrödinger equation is

$$\hat{H}\Psi = E\Psi \tag{3.1}$$

where $\hat{H}$ is the Hamiltonian, E is the energy of the system, and Ψ is an N-body wavefunction. The Hamiltonian is a quantum mechanical equivalent to the classical total energy, but with the kinetic (T) and potential (V) energy terms replaced by their

respective quantum operator representations, $\hat{T} = \frac{\hat{p}^2}{2m}$ and $\hat{V} = V$, where $\hat{p}$ is the momentum operator, $\hat{p} = -i\hbar\nabla$, and m is mass. This yields the expression

$$\hat{H} = \hat{T} + \hat{V} = \frac{-\hbar^2}{2m}\nabla^2 + V(r) \tag{3.2}$$

The Schrödinger equation is simplified by applying the Born-Oppenheimer (BO) approximation [31] and considering only the time-independent solution; however, because of the quantum behaviour of electron-electron interactions, even with these approximations it is too complicated for practical application. This solution to the Schrödinger equation can therefore be solved only for simple, one-electron systems, *e.g.* the hydrogen atom.

Hartree–Fock (HF) theory presented the first approximation yielding a manageable solution. If the wavefunction is represented as a single Slater determinant of N orbitals, ψ_N, that satisfy the Pauli exclusion principle due to its antisymmetry, *i.e.*:

$$\Psi = \frac{1}{\sqrt{N!}} \begin{vmatrix} \psi_{1(x_1)} & \psi_{1(x_2)} & \cdots & \psi_{1(x_N)} \\ \psi_{2(x_1)} & \psi_{2(x_2)} & \cdots & \psi_{2(x_N)} \\ \vdots & \vdots & & \vdots \\ \psi_{N(x_1)} & \psi_{N(x_2)} & \cdots & \psi_{N(x_N)} \end{vmatrix} \tag{3.3}$$

(space and spin coordinates are included in the x variable), then applying the Hamiltonian to this wavefunction will yield a set of Hartree–Fock equations which are one-electron equations resembling single-particle Schrödinger equations. They include a kinetic energy contribution, an electron-nuclear interaction, an electrostatic potential arising from the distribution of N electrons, and an exchange term which guarantees that like-spin electrons will avoid each other:

$$\varepsilon_i\psi_i(\mathbf{r}) = \left(-\frac{1}{2}\nabla^2 + V_{nuc}(\mathbf{r})\right)\psi_i(\mathbf{r}) + \sum_j \int d\mathbf{r}' \frac{|\psi_j(\mathbf{r}')|^2}{|\mathbf{r}-\mathbf{r}'|}\psi_i(\mathbf{r})$$

$$- \sum_j \delta_{\sigma_i\sigma_j} \int d\mathbf{r}' \frac{\psi_j^*(\mathbf{r}')\psi_i(\mathbf{r}')}{|\mathbf{r}-\mathbf{r}'|}\psi_j(\mathbf{r}) \tag{3.4}$$

Here ε_i is the energy eigenvalue associated with $\psi_i(\mathbf{r})$, $\mathbf{r}$ represents the electron coordinates, V_{nuc} is the electron-nuclear potential and i and j are two electrons. To solve this expression numerically it is first assumed that the one-electron solutions for a multi-electron atom will closely resemble the one-electron solutions for the hydrogen

atom (*i.e.* an atomic orbital), and then the unknown molecular orbitals (ψ_i) are expressed as some linear combination of a finite (basis) set of these atomic-like orbitals, called basis functions,

$$\psi_i = \sum_k^M c_{ik}\phi_k \tag{3.5}$$

where ϕ_k are the atomic orbital representations and c_{ik} are orbital coefficients. This is the linear combination of atomic orbitals (LCAO) approximation. Combining the LCAO approximation with the HF equations yields the Roothaan-Hall equations:

$$\sum_v^\eta \left(F_{\mu v} - \varepsilon_i S_{\mu v} \right) c_{vi} = 0 \tag{3.6}$$

where ε_i are orbital energies, S is an overlap matrix between the basis functions, and F is the Fock matrix:

$$F_{\mu v} = H_{\mu v} + \sum_a \sum_{\lambda\sigma} C_{\lambda a} C_{\sigma a}^* \left[2(\mu v|\sigma\lambda) - (\mu\lambda|\sigma v) \right] \tag{3.7}$$

The first term, $H_{\mu v}$, is a one-electron Hamiltonian matrix and the second term incorporates the electron repulsion missing from the one-electron term. The Fock operator yielding this matrix is a combination of the one-electron Hamiltonian operator ($\hat{h} = \frac{-\nabla^2}{2} + \sum_A \frac{-Z_A}{r_{iA}}$), the Coulomb operator ($\hat{J} = \int d\mathbf{r}' \frac{|\psi_j(\mathbf{r}')|^2}{|\mathbf{r}-\mathbf{r}'|}$), and the exchange operator ($\hat{K}\,\psi_i(\mathbf{r}) = \int d\mathbf{r}' \frac{\psi_j^*(\mathbf{r}')\psi_i(\mathbf{r}')}{|\mathbf{r}-\mathbf{r}'|}\,\psi_j(\mathbf{r})$):

$$\hat{F} = \hat{h} + \sum_n \left[2\hat{J} - \hat{K} \right] \tag{3.8}$$

The methods that derive from the solutions to the Roothaan-Hall equations are Hartree–Fock or *ab initio* methods and the corresponding energy is the Hartree–Fock energy. While relatively easy to obtain, and applicable to fairly large systems (the computing cost for HF scales as N^4, where N is the number of basis functions), in Hartree–Fock theory each electron can only see the others as an average potential. This removes any possibility of correlation between the electrons and results in an overestimation of the electron-electron repulsion, yielding an energy that is too high. The correlation energy is defined as the difference between the HF energy and experiment.

Note that HF theory fails especially in situations of bond breaking or bond formation, as the electrons will not be correctly localized on the nuclei when the bond is stretched.

3.2 Post Hartree−Fock Methods

Post Hartree−Fock methods have been developed which greatly improve the original limitations. These methods are generally of two classes: variational and perturbative. Both methods have unique advantages and are commonly implemented in the literature. In variational methods the ground state energy (E_0) is known to be a minimum of the expectation value of all possible trial functions $\psi(x)$:

$$E_0 \leq \int \psi^*(x)\widehat{H}\psi(x)dx \tag{3.9}$$

By variation of these trial functions one can optimize the expression to find the lowest energy, yielding a good estimate to the Hamiltonian. Variational methods include configuration interaction (CI) and multi-configurational self-consistent field (MC-SCF). They are systematic, accurate, and converge to the correct answer, but can be very CPU intensive and non-size consistent.

An alternative method is a perturbative approach. Perturbation techniques first separate the exact equation into two parts: an exactly solvable expression that will yield an approximate solution, and an expression that corrects the first expression but cannot itself be exactly solved. Consider the equation

$$\widehat{H} = \widehat{H}_0 + \widehat{V} \tag{3.10}$$

$\widehat{H}$ gives the exact but unsolvable expression, $\widehat{H}_0$ gives the solvable but inexact expression, and $\widehat{V}$ is the perturbation that corrects $\widehat{H}_0$. This perturbation is assumed to be small compared to $\widehat{H}_0$. Commonly used perturbative approaches include the MPN methods developed by Møller and Plesset in the 1930's and the coupled cluster (CC) approaches[3], which derive from the many electron theory (MET) originally developed by Sinanoğlu in 1961. These methods are generally efficient and are size-consistent;

---

[3] Although not strictly categorized as perturbative, CC methods are closely related to many-body perturbative approaches and often include perturbative approximations.

however, they can be non-convergent and are not always appropriate for complex species. For example, CC methods rely heavily on the choice of a good starting reference ($\hat{H}_0$), and MP methods oscillate around convergence, meaning there is no guarantee that MP3 (third order MP theory) will provide a more accurate result than MP2 (second order MP theory). Second-order perturbations are considered acceptable for accurate results with relatively reasonable scaling. For benchmarking quality calculations, coupled cluster methods are generally used. The most common CC method is CCSD(T), which is based on an iterative solution of the single and double (SD) excitations with a non-iterative perturbative correction for the triples (T). The CCSD(T) approach is a good compromise between the chemical accuracy of the higher-order CCSDT (full triples) method and the computational efficiency of low order many-body perturbation theory (MBPT). Even with this compromise the CCSD(T) method scales at N^7. The scaling behaviour of some *ab initio* methods are listed in Table 3.1.

Table 3.1: Scaling behaviour of some *ab initio* methods.

Scaling Behaviour[a]	Method
N^4	HF
N^5	MP2
N^6	MP3, CISD, CCSD, QCISD
N^7	MP4, CCSD(T), QCISD(T)
N^8	MP5, CISDT, CCSDT
N^9	MP6
N^{10}	MP7, CISDTQ, CCSDTQ

[a]N is the number of basis functions.

3.3 Møller-Plesset Perturbation Theory

Because the Møller-Plesset perturbative method is frequently used in this thesis it will be discussed in further detail. This approach is based on the many-body Rayleigh-Schrödinger perturbation theory. To begin, consider that the nature of the ground state Hartree–Fock approximation to the Schrödinger solution yields an exactly solvable expression that is slightly incorrect due to the missing electron correlation. The electron correlation energy, however, is generally only a small percent of the total energy

(typically about 1%); such a small correction could thus be considered a perturbation of the exact solution. The Hartree–Fock approximation is thus an ideal starting point for a perturbative investigation of the exact solution to the Schrödinger equation. In 1934, Møller and Plesset [32] demonstrated a simplified approach to obtain the perturbative corrections by combining the treatment of the Hartree-Fock solution as a zeroth order approximation to the energy, together with Brillouin's theorem, which states that the first order correction to the energy and charge density will be equal to zero.

Møller-Plesset perturbation theory (MP) is desirable in part because of its size extensivity, meaning that it can be easily compared over calculations involving varying numbers of electrons, and the predicted energy for every order of perturbation of the system scales with the number of non-interacting particles present in the system. A very important characteristic of the MP method is that it evaluates diffuse systems and can correctly evaluate reaction barriers at relatively low cost. MP methods also include the dispersion interactions of electrons, which are not accounted for in many popular density-functional theory methods. Because of the computational cost of higher order MP (*i.e.* fourth order and greater), most calculations are restricted to small or medium sized systems calculated at the second order (MP2).

3.4 Density-functional Theory

An important property of the wavefunction is its description of the probability density, which is the foundation for density-functional theory (DFT). The probability density gives the probability of finding an electron within a small volume element dr, while all other N-1 electrons have position and spin defined as averages by the wavefunction:

$$\rho(\mathbf{r}) = N \int |\Psi(\mathbf{x}_1, \mathbf{x}_2, \dots, \mathbf{x}_N)|^2 \, ds_1 d\mathbf{x}_2 \dots d\mathbf{x}_N. \tag{3.11}$$

The probability density integrates to the number of electrons in the system and vanishes at infinity. The electron density is a physically observable quantity and can be measured experimentally, *e.g.* using X-ray diffraction. To define the probability of not one but two electrons, having defined spins σ_1 and σ_2, within two small volumes $d\mathbf{r}_1$ and $d\mathbf{r}_2$, with the

remaining N-2 electrons having averaged-out positions and spins, the *pair density* is written as:

$$\rho_2(\mathbf{x_1}, \mathbf{x_2}) = N(N-1) \int \cdots \int |\Psi(\mathbf{x_1}, \mathbf{x_2}, \dots, \mathbf{x_N})|^2 d\mathbf{x_3} \dots d\mathbf{x_N} \qquad (3.12)$$

The pair density integrates to the number of pairs in the system and also vanishes at infinity.

Hohenberg and Kohn proved two ground-breaking theorems in 1964 [33]. The first is that every external potential is associated with a unique electron density and every electron density is associated with a unique external potential. The second states that the total density $\rho(\mathbf{r})$ can be used as a trial variation function in multi-electron theory, indicating that any positive definite N-representable trial density that integrates over all space to give the total number of electrons in the system will have an energy greater than the ground state energy. The first theorem shows that all properties of an N-electron system can be considered as *functionals* of the potential (v) because the potential maps to the wavefunction (v→Ψ) and the wavefunction determines all properties. The ground state energy functional is written as:

$$E_0 = E[\rho(\mathbf{r})] = T[\rho(\mathbf{r})] + V_{ee}[\rho(\mathbf{r})] + \int V_{ext}\rho(\mathbf{r}) \qquad (3.13)$$

where $T[\rho(\mathbf{r})]$ is the electronic kinetic energy, $V_{ee}[\rho(\mathbf{r})]$ is the electron-electron interaction, and $\int V_{ext}\rho(\mathbf{r})$ is the energy of the electron-nucleus interactions resulting from the external potential. The second theorem requires $E_v(\rho') \geq E_v(\rho)$ for all *v-representable* trial densities of ρ'.

A difficulty in DFT arises because the Hohenberg-Kohn (HK) theorems require an *exact* form of a functional that maps the ground state density with the ground state energy, but give no indication of how to construct this functional. Also, the requirement of *potential*-representability (as well as N-representability) is very difficult to satisfy in practice. Kohn and Sham published the solution to this v-representability problem in 1965 [34], introducing a *noninteracting* system of electrons with the same density ($\rho(\mathbf{r})$) as the interacting system. It assumes that the resulting noninteracting v-representabilities from this density can be mapped onto interacting v-representabilities. It is thus possible to set up a noninteracting reference system with a Hamiltonian in which there is an

effective local potential that will yield the exact density of the interacting system. The wavefunction of the non-interacting electrons is just the correlation-free Slater determinant, consisting of N Kohn-Sham orbitals, ψ_i^{KS}. These are similar to the orbitals described in Hartree–Fock theory except that rather than approximating the true N-electron wavefunction they exactly represent the N-electron noninteracting wavefunction. From the Kohn-Sham orbitals one can obtain the density (as in HF theory):

$$\rho_0(\mathbf{r}) = 2 \sum_{i=1}^{N} (\psi_i^{KS})^2 \qquad (3.14)$$

This noninteracting system can also be used to define the exact noninteracting kinetic energy, $T_0(\rho)$, which is related to the interacting kinetic energy, $T(\rho)$, by a small correction term, ΔT_c:

$$T_0(\rho) = -\frac{1}{2} \sum_i 2 \int \psi_i \nabla^2 \psi_i = T(\rho) - \Delta T_c \qquad (3.15)$$

By replacing the electron-electron interaction energy, $V_{ee}(\rho)$, with the exactly known classical Coulomb repulsion energy of the charge distribution, $J(\rho)$, the original HK ground state energy can be rewritten as:

$$E_0 = T(\rho) + V_{ee}(\rho) = T_0(\rho) + J(\rho) + E_{xc}(\rho) \qquad (3.16)$$

Here the E_{xc} is the exchange-correlation energy and represents all non-classical contributions to the energy, including electron-electron interaction and corrections for self-interactions and the noninteracting kinetic energy, ΔT_c. Recall that $T_0(\rho)$ and $J(\rho)$ are *exact* solutions for the non-interacting system, and therefore E_{xc}, a relatively small percentage of the total energy, is the only expression that needs to be approximated.

This remarkable solution to the HK problem is only useful if there is a way to approximate the functional which yields an accurate value for E_{xc}. Quality of the "density functional" is thus hinged on the quality of the chosen exchange-correlation functional. The heart of developing density-functional theory is centered on finding better and better approximations to E_{xc}. This is no simple challenge as there is no systematic way to improve the approximate functionals. Despite this, theoreticians have formulated approaches that can very accurately incorporate the exchange-correlation interaction between electrons in most systems. For a detailed review of the progression of their

18

development, from local density approximations (LDA) through generalized gradient approximations (GGA) to hybrid functionals such as the ever popular B3LYP, the reader is referred to Koch and Holthausen's text: A Chemist's Guide to DFT [35]. For a detailed discussion of the nature of E_{xc}, including the character of the "electron hole" and other insightful discussions the reader is referred to Chapter 6 of this same reference, as well as section 6.4 in Jensen's Introduction to Computational Chemistry [36].

A major concern for DFT methods was their initial inability to include dispersion interactions. Because of their accessibility and efficiency, DFT methods are commonly applied to large biological systems including proteins and enzymes. Although DFT can represent the stationary states of these systems at very low cost, weak interactions such as hydrogen bonding and van der Waals interactions are common in these systems and early DFT failed to correctly represent these important non-covalent interactions. This can be partially circumvented by including an empirical dispersion term, such as has been developed by Grimme [37] and Wu and Yang [38], or the exchange-hole dipole moment (XDM) dispersion correction of Becke and Johnson [39, 40]. Empirical corrections add minimal costs and can yield very good approximations. Reference [41] provides a thorough discussion of some current DFT-based techniques for including dispersion.

3.5 Basis Sets

Due to the impact of choosing the correct basis set on the calculation's accuracy, the fundamentals of basis sets should be introduced. Recall that the wavefunction, Ψ, was originally represented as a Slater determinant, which is an antisymmetrized product of the orbitals that represent the electrons in the system. These orbitals are in turn described by a linear combination of a finite set of functions known as basis functions:

$$\psi_i = \sum_k^M c_{ik}\phi_k \tag{3.17}$$

The shape of these orbitals can be defined in many plausible ways. A "minimal" basis set is defined as the simplest way of describing each electron in the system using atomic orbitals. For a minimal basis, Slater-type orbitals (STOs) were originally applied because they correctly describe the shape of an atomic orbital:

19

$$\phi_k = Ae^{-\alpha r} \tag{3.18}$$

However, STOs have a complicated description, including a discontinuity (cusp) at their apex which makes their application in practice very difficult. The next best approximation is a Gaussian type orbital (GTO), which approximates the shape of the STO but does not have a discontinuous cusp (see Figure 3.1) and is much simpler to describe. In order to better approximate the shape of the STO (because this represents the actual shape of the desired atomic orbital) the primitive GTOs can be factorized into Cartesian parts and a linear combination of several different GTOs having different exponential values can be used to describe one STO. These are referred to as contracted GTOs (cGTOs). The notation STO-nG denotes that n Gaussians have been used to represent each STO in a minimal basis set.
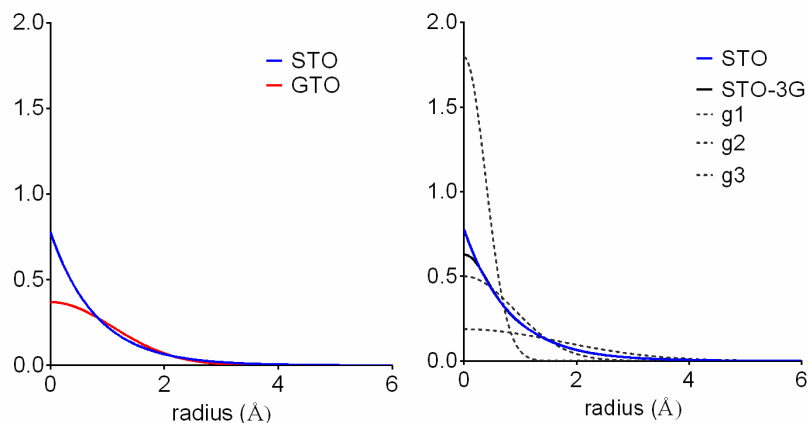
Figure 3.1: On left: STO s-orbital for hydrogen plotted in blue showing cusp at r = 0 (center of nucleus) as well as one GTO orbital plotted in red showing that $\Delta\phi_i$ approaches zero at the nucleus. On right: GTO expansion (STO-3G) in black nearly reproduces STO (blue) except at r = 0 (nuclear cusp). Dashed lines are the three GTO wavefunctions that comprise the STO-3G basis set.

   Minimal basis sets are centered on the nuclei and provide an accurate description for atoms in spherical or near-spherical environments. They are, however, insufficient to accurately describe polarized molecular systems where the electron density may be shifted away from the atom center (into bonding regions, for example). This shortcoming can be rectified by splitting the description of the atomic orbitals in the minimal basis into

two or more contraction/expansion functions which have different radial extents. If only the valence electrons are split they are termed split-valence functions, simplifying the calculation by assuming that the core electrons can be well-represented by the atomic orbital (a fairly accurate assessment). Polarization is included by increasing the angular flexibility of the basis functions through supplementing heavy atoms with a set of d functions and hydrogen atoms with a set of p functions. An increased angular flexibility on the hydrogen atoms is particularly important for describing weakly interacting systems such as van der Waals interactions and hydrogen bonds. Diffuse functions (with low exponential values) can be included to increase the range of the valence orbitals. These are also important for weak interactions such as van der Waals forces and hydrogen bonds.

John Pople developed one of the most commonly applied basis sets, made popular by the Gaussian suite of programs. This set optimizes the orbital coefficients at a Hartree–Fock level, with the s and p contracted GTOs associated with the same quantum number given the same exponential constant (note that the coefficients for these cGTOs are different). Pople's nomenclature for basis functions has standardized the terminology for general application. The Pople basis set can be described by the formula: k-nlmG, where k describes the number of primitives used for the core atomic orbitals; n, l, and m describe the type of splitting and number of primitives that are used for the valence function; and G refers to the gaussian type orbitals. The basis used can be supplemented with terms for inclusion of polarization (*) and diffuse functions (+). For example, the popular 6-31+G(*) basis set has 6 primitives used for each core orbital, 3 primitives and 1 primitive for each split valence, and a diffuse set of functions (+) plus one polarization set of functions (*) added to non-hydrogen atoms only.

Thom Dunning later considered that because the Pople basis set were optimized using Hartree–Fock, they may not perform well for correlated systems. He optimized basis sets using correlated configuration interaction wavefunctions, designed to converge smoothly as they approached the complete basis set limit (*i.e.* an infinite number of basis functions). These are called correlation consistent basis sets and have nomenclature that differs from the Pople basis sets. For example, "cc-pVXZ" describes a "correlation consistent, polarized valence X-zeta basis" where X refers to the level of splitting of the

valence functions: double (D), triple (T), quadruple (Q), 5, 6, 7, and so on. The Dunning basis sets include polarization by definition. It is also possible to augment the basis set with diffuse functions using the aug- prefix. One diffuse function of each function type in use for a given atom is added. For example, the aug-cc-pVTZ basis places s, p, and d diffuse functions on hydrogen atoms, and p and d, or d and f diffuse functions on B through Ne and Al through Ar, respectively.

3.5.1 Basis Set Superposition Error

A further concern with respect to the accuracy of the chosen basis set is the possibility that the overlap of unoccupied orbitals might lower the energy of a complex with respect to its infinitely separated fragments. This is called the basis set superposition error (BSSE). The nature of this error is a result of the ability for basis functions present on one fragment to augment those on the second fragment, improving the accuracy of the energy calculated for the interacting structure. This augmentation is not present for the separated fragments and therefore the conditions for the comparison are no longer equal. In a very small way it is similar to evaluating pieces of a reaction using different basis sets and then directly comparing their energies.

One of the most common solutions to this error is the counterpoise (CP) correction as proposed by Boys and Bernardi [42]. In the CP correction scheme a single point energy for the separated fragments is calculated within the presence of the basis set for the complex. The extra empty orbitals are usually called ghost orbitals. This modification can only partially correct for BSSE because the presence of the empty orbitals may influence the geometry of the fragment complex, which is unaccounted for. Some modified schemes incorporate a geometry optimization with the ghost orbitals present in an attempt to improve the accuracy of the CP corrections [43, 44].

There are some cases where BSSE corrections are intentionally not included; for example, if it is generally known that a theory or method overestimates interaction energies the BSSE can provide a "fortuitous cancellation of errors". Benchmark studies also reveal that as the size of the basis set increases the BSSE is minimized [45]; for systems with very large basis sets it may not be necessary to include a BSSE correction.

3.6 Solvent Models

The importance of solvent interactions, combined with increases in computing capacity, has prompted researchers to develop a variety of methods for including a solvent-like environment. These methods range from the dramatically simplified effect of treating the solvent as a uniform polarizable medium, to explicitly including the solvent molecules at varying levels of theory. Although ideal, the computational cost of including explicit solvent molecules at the quantum chemical level is often prohibitive. Reducing the solvent representation to an empirical or semi-empirical model is possible using, for example, QM/MM and ONIOM methods[4], and is often implemented in situations where the physical presence of the solvent molecule may be important (*e.g.* for waters inside an enzyme pocket). In order to provide a more complete description of the current approaches that classically include explicit solvent, an entry in the appendices has been included to briefly describe properties of some common water models. See Appendix A.1 for further information.

Even the simplified approach of a continuum model can have profound effects on the final structure of optimized systems. Bond lengths are altered and charge separations are stabilized, *e.g.*, zwitterionic glycine is more stable when modeled with an implicit solvent than in gas phase, correlating with experiment. Energies are also affected dramatically, especially when ions are present: the effect of implicit solvation on an ion can change the total stability by hundreds of kJ mol^{-1}. This method is applied in Chapter 7 and the following section will therefore introduce continuum solvation models, in particular the polarizable continuum model used for self-consistent reaction fields (PCM-SCRF) as

---

[4] QM/MM is a combined quantum mechanics and molecular mechanics method which allows the area of interest (the solute) to be represented quantum mechanically and the solvent area to be represented using a molecular mechanics description. ONIOM is a method available in the Gaussian code, originally developed by Morokuma and coworkers [154]. The acronym stands for "Our own N-layered Integrated molecular Orbital and molecular Mechanics".

applied in the Gaussian 09 program.[5] Further information on this and other models is also available in several reviews and reports [46-50].

3.6.1 Continuum Models

Continuum models treat the solvent as a uniform polarizable medium surrounding a cavity which contains the solute molecule. The free energy of solvation is a sum of the energy required to form the cavity and the dispersion/repulsion and electrostatic interactions between solute and solvent:

$$\Delta G_{solvation} = \Delta G_{cavity} + \Delta G_{dispersion-repulsion} + \Delta G_{electrostatic} \qquad (3.19)$$

Several factors affect how $\Delta G_{solvation}$ is evaluated. These include cavity definition and how its contribution is calculated, calculation of the solute's charge distribution, and the description of the electric medium. For SCRF calculations, the step-wise quantum optimization of the solute molecule presents the need for communication between the changing solute and responding solvent: the calculated electronic structure of the solute will induce a solvent response which in turn influences the solute's electronic structure, and thus must be evaluated at each optimization step. The ease of this evaluation depends partially on the cavity description, which should have a physical meaning, exclude the solvent and contain as much as possible of the solute charge distribution. A simple spherical cavity can be solved analytically, as in the Onsager model; however, the crudeness of this approach yields very poor accuracy. The default method in Gaussian 09 is the integral equation formalism (IEF) PCM [51], and uses van der Waals (vdW) radii to define the cavitation term and then defines the dispersion-repulsion term by tracing out the solvent accessible surface (SAS) along a parameter-scaled vdW surface with a probe sphere that has its radii adjusted to reflect the solvent (see Figure 3.2). This describes the non-solvent accessible cavities which may be present in the solute. The solvent excluded surface (SES) is used to evaluate the electrostatic term. Evaluation of the surface charges

---

[5] Not only is there a wide variety of available solvent models, the implementation in quantum chemistry modelling software is also diverse. For example, the Q-Chem implementation of an IEF-PCM model is in some respects wholly different from the Gaussian 09 algorithm.

(defining the reaction field) is achieved by tessellating the SES and calculating one point charge per surface element. The IEF method is a combination of Gaussian's original dielectric PCM (D-PCM) with inclusion of a careful outlying charge correction that renders it less sensitive to diffuse solute charge distributions.
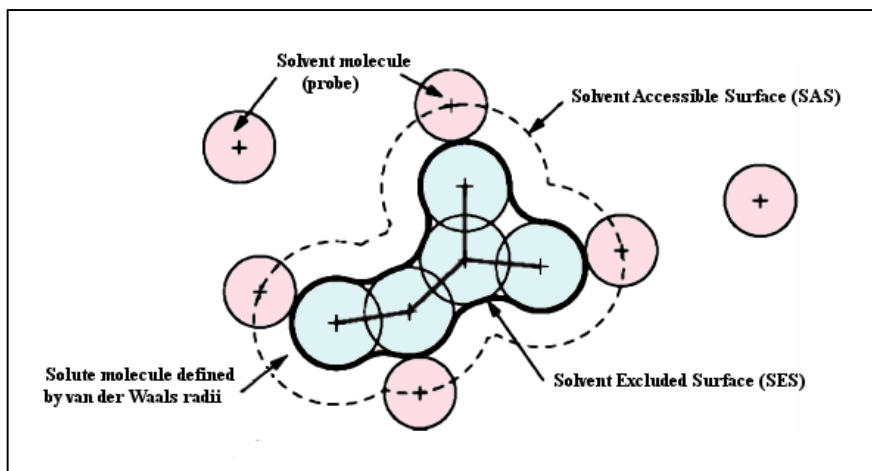
Figure 3.2: Solvent accessible and solvent excluded surfaces defined by a probe molecule and the atomic van der Waals surface of the solute molecule.

3.7 Potential Energy Surfaces and Minimization Techniques

The methods used for minimum energy searches (MESs) [52] and to describe potential energy surfaces (PESs) become increasingly important when exploring highly complicated PESs, such as in water cluster minimizations. Minimum energy searches attempt to locate the global or local energy minimum of a molecule. The potential energy surface represents the relationship between the geometry of a molecule and its energy. In quantum mechanics this energy is defined using the wavefunction associated with the arrangement of nuclei. The PES is used to define stationary points corresponding to stable minima and transition structures, and to map the lowest energy pathways between them. This information can be represented graphically as in Figure 3.3. Valleys show lowest energy paths between stationary points, saddle points are transition states, and the paths connecting them are reaction coordinate paths. The lowest points in a valley or depression are the local minima and the lowest point on the PES is the global minimum.
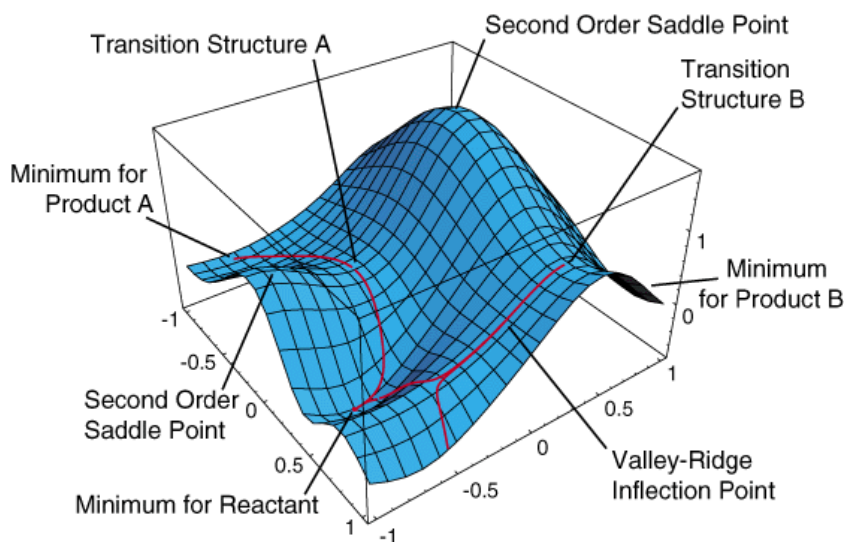
Figure 3.3: Example potential energy surface for the reaction of two species A and B. The red line traces out the reaction coordinate path (graphic reproduced from [53]).

The type of stationary point can be determined through the Hessian index, which is the number of negative eigenvalues present in the force constant matrix. This also corresponds to what are called "imaginary vibrational frequencies". A stable minimum should have a Hessian index of zero and transition states have Hessian indexes of 1. It is possible to follow the negative eigenvalues represented in the Hessian index to travel to stable minima.

Computational packages employ various algorithms to search for the local and global minima on this PES. Probably the most well-known algorithm used for minimum energy searching is the Berny optimizer [54] available in the Gaussian program, although other approaches are available. For large systems such as proteins or explicitly solvated molecules the PES is often too complicated to evaluate using quantum mechanics (QM) and molecular mechanics (MM) approaches can be used to obtain a reasonable starting point for subsequent QM analysis. These approaches minimize a potential energy function, which describes the energy of the system as a function of the nuclei based on classical parameters. Because there is no electronic description, quantum phenomena such as covalent bond-breaking cannot occur. Several classes of minimization methods

26

commonly applied in MM minimization techniques include search, gradient, and Newton. See Table 3.2 for a brief description of these approaches.

Table 3.2: Minimization techniques commonly used in molecular mechanics to isolate local and global minima on a PES.

Method	Advantages	Disadvantages
Search methods use only values of the function itself. Often used as a starting point when the system is far from the minimum	- Very simple code to implement - Will always find a minimum	- Slow and inefficient for large numbers of optimized variables (*i.e.* anything greater than 10)
Gradient methods use values of the function as well as its gradient. A "conjugated gradient approach" is the most commonly used.	- Have a greater convergence rate than search methods - Do not require a large amount of memory	- May fail to converge
Newton methods use values of the function as well as first and second derivatives.	- Rapid convergence	- Extensive memory requirements for 2nd derivatives

There is also the possibility that the minimum found will be a local minimum rather than a global minimum. One method to search for the global minimum is simulated annealing, which involves increasing the temperature to provide enough energy to allow the structure to move out of a local minimum valley, and then very slowly cooling the system in an attempt to allow the structure to reach the global minimum conformation. Monte Carlo simulations can also be useful for global minima searches where non-physical transitions are required; in this method a large number of conformations are sampled and the lowest energy structures are reported [55].

3.8 Quantum Theory of Atoms in Molecules

The electron density of an atom in a molecule or crystal determines its additive contribution to all properties of the total system, its transferability being determined by a paralleling degree of transferability in the atom's virial field, the virial of the Ehrenfest force exerted on its electron density.

 – R. F. W. Bader [56]

The quantum theory of atoms in molecules (QTAIM) was developed by Richard Bader and his collaborators over the course of several decades, beginning in 1963. The insight into the electronic makeup of molecules resulting from this theory has proven it to be a very useful tool for interpreting many chemical phenomena. In this chapter several concepts contained within QTAIM theory are explored. These include: the physics of molecules and atoms defined as open systems; the concept of an atom's virial field and the importance of the Ehrenfest forces acting on its electron density; the ability to define the properties of an atom-within-a-molecule using the Heisenberg equation of motion; and the principle of stationary action. While this chapter cannot possibly cover all the details of QTAIM, it should introduce sufficient theory for an understanding of some of its strengths, limitations, and applications. Armed with these concepts the reader will be able to critically assess the research presented in later chapters based on QTAIM analysis. For a more thoroughly complete description of QTAIM and its varied applications the reader is referred to references such as [1] and [57].

3.8.1 Topology and Quantum Chemistry

All observable properties of a molecule can be determined by its electron density. The electron density of a molecule is a function of the density of its electrons described in real space, $\rho(r)$. It is a physical, three-dimensional "object" that can be measured using experimental methods. The foundation of QTAIM stems from the ability to describe this density using a topological approach, yielding details about the nature of the attractive and repulsive interactions that guide the electronic and nuclear components of any molecular (or atomic) system. The electron density topology is dominated by the

presence of nuclear attractors. The surface decays rapidly away from these points, resulting in a distinct pattern of peaks and valleys; see for example the electron density of the water trimer, Figure 3.4, which includes a contour map as well as a three-dimensional representation of the density in the plane of the central hydrogens.

Gradient vectors of the electron density, $\nabla \rho(\boldsymbol{r})$, define trajectories containing information of physical importance. Sets of these trajectories terminate at the maxima found at each nucleus, which is why the nuclei are termed *attractors*. These trajectories (also called gradient paths) trace out defined basins within the molecular system; a basin encompasses a set of gradient paths terminating at an attractor. Each attractor (nucleus) is thus associated with its surrounding basin and an "atom" is defined as the combination of a basin with its nuclear attractor (see Figure 3.5). The surface bounding the basin is defined by a zero-flux condition ($\nabla \rho(\boldsymbol{r}) \cdot \boldsymbol{n} = 0$, see eq. 3.26) and is not crossed by any gradient vector.
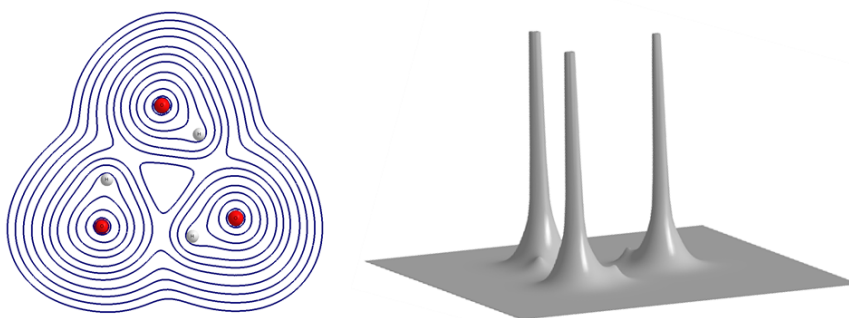
Figure 3.4 Electron density of water trimer in the plane of the three central hydrogens as a contour map (left) and projected in three dimensions (right).
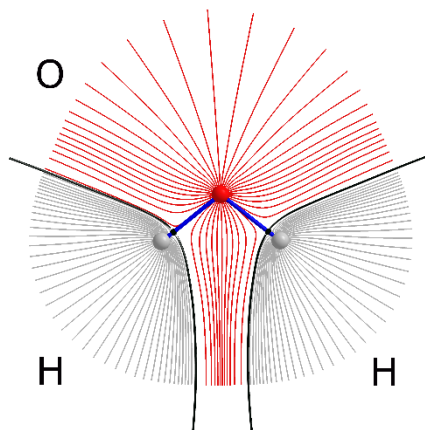
Figure 3.5: Water monomer showing bond paths (in blue), atomic basins described by gradient paths terminating at nuclear attractors (red=oxygen, grey=hydrogen), and the interatomic surfaces (black lines) defining the boundaries of the atomic basins.

As in any topology terminology, points where the gradient is zero ($\nabla\rho(r) = 0$) are considered *critical points* and indicate either the maxima at the nuclei or local maxima, minima, and saddle points in the valleys between nuclei. Nuclear maxima are called nuclear critical points (NCP). The remaining critical points are defined by their Hessian matrix, consisting of the second derivatives of $\rho(r)$ which are elements of the tensors $\nabla\nabla\rho(r)$ and can be diagonalized and written as:

$$\Lambda = \begin{pmatrix} \dfrac{\partial^2\rho}{\partial x'^2} & 0 & 0 \\ 0 & \dfrac{\partial^2\rho}{\partial y'^2} & 0 \\ 0 & 0 & \dfrac{\partial^2\rho}{\partial z'^2} \end{pmatrix} = \begin{pmatrix} \lambda_1 & 0 & 0 \\ 0 & \lambda_2 & 0 \\ 0 & 0 & \lambda_3 \end{pmatrix} \qquad (3.20)$$

$\lambda_1, \lambda_2, \lambda_3$ are the curvatures of the density at critical points and describe the changing terrain of the surrounding electron density. Critical points are assigned a rank (ω) and a signature (σ) based on the value and sign of their curvature values, written as (ω, σ). The rank is the number of non-zero values for the curvatures[6] and the signature is the net sign of the sums of the curvatures' signs. The rank and signature of the critical points defines

---

[6] Cases where zero curvatures are present at a critical point indicate a mathematical instability and generally are not found in equilibrium charge distributions. Careful attention should be paid to any critical point with $\omega<3$.

their type: nuclear, bond, ring, or cage. The four types of stable critical points are summarized in Table 3.3.

Table 3.3: Rank and signature values for stable critical points, their corresponding density description, and the critical point type they describe.

(ω, σ)	Type of ρ	Type of critical point
(3,-3)	ρ is a local maximum	Nuclear critical point (NCP)
(3,-1)	ρ is a maximum in one plane and a minimum along a third axis perpendicular to this plane	Bond critical point (BCP)
(3,+1)	ρ is a minimum in one plane and a maximum along a third axis perpendicular to this plane	Ring critical point (RCP)
(3,+3)	ρ is a local minimum	Cage critical point (CCP)

The total number of all critical points is restricted by the Poincaré-Hopf relationship for isolated molecules and the Morse equation for infinite crystals[7]:

$$n_{NCP} - n_{BCP} + n_{RCP} - n_{CCP} = \begin{cases} 1 & \text{isolated molecule} \\ 0 & \text{infinite crystal} \end{cases} \tag{3.21}$$

Sets of lines that either connect critical points or originate at infinity and terminate at critical points are instructive in defining the bonding interactions between atoms and the interatomic surfaces that separate the atoms. The path of maximum electron density connecting two nuclei is called a bond path and generally describes a chemical bond. Information regarding the nature of this bond can be determined by the properties of the critical point corresponding to a maximum along this bond path (the bond critical point). An example of critical points and bond paths is shown in Figure 3.6. If only the nuclear attractor critical points and the lines of maximum density (bond paths) connecting them are represented it is called the molecular graph; this recovers the network of bonds that would generally be applied under chemical considerations.

---

[7] Note that satisfaction of this relationship is not a guarantee that all possible critical points have been isolated. It is possible (although unlikely) that two missing critical points could cancel, *e.g.* if a RCP and a CCP were missing.
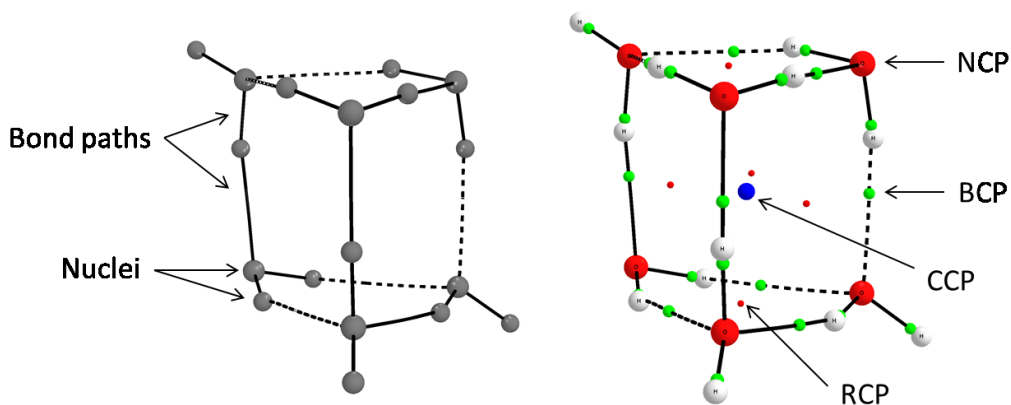
Figure 3.6: Molecular graph (on left) and molecular graph plus critical points (on right) for water hexamer prism. Critical points are labelled as in Table 3.3.

The bond critical point is a special case in the topology of a molecule because the traditional character of a bond, such as in covalent, ionic, and weak interactions, can be recovered by evaluating its properties and the properties of the electron density at the critical point. Returning to the Hessian matrix, (3.20), the trace of this Hessian is the Laplacian of the density:

$$\nabla^2\rho(\boldsymbol{r}) = \nabla \cdot \nabla\rho(\boldsymbol{r}) = \frac{\partial^2\rho}{\partial x^2} + \frac{\partial^2\rho}{\partial y^2} + \frac{\partial^2\rho}{\partial z^2} = \lambda_1 + \lambda_2 + \lambda_3 \tag{3.22}$$

In cases where $\nabla^2\rho(\boldsymbol{r}) < 0$ at the BCP there is an open shell interaction, such as in covalent bonds. Polar bonding, *i.e.* C—X (X = O, N, F), can have an accumulation of density at the BCP but the Laplacian at this BCP may be of either sign. When electron density is depleted between the nuclei, as in the case where $\nabla^2\rho(\boldsymbol{r}) > 0$, then it is a closed shell interaction, such as ionic or hydrogen bonding. The plane in which the density accumulates can also yield information as to the character of the bond. This is determined by the ellipticity of the bond, ε:

$$\varepsilon = \frac{\lambda_1}{\lambda_2} - 1 \tag{3.23}$$

Cylindrically symmetrical bonds occur when $\lambda_1 = \lambda_2$ and are typical of single or triple bond interactions. Double bonds show a deviation from $\lambda_1 = \lambda_2$, indicating an increase in π-character of the bond.

32

The value of the electron density at the bond critical point (ρ_{BCP}) is related to the strength of the chemical bond between the two nuclei: the bond order (BO).[8] The relationship between ρ_{BCP} and BO is dependent on the nature of the interacting nuclei, and can generally be defined as:

$$BO = e^{A(\rho_{BCP}-B)} \tag{3.24}$$

where A and B are constants specific to the nature of the bonding atoms. Another measure of the bond order is the electron delocalization between the bonded atoms. This "delocalization index" is an evaluation of the amount of exchange that occurs between the electrons in the basin of atom A and the electrons in the basin of atom B. It is defined for closed shell systems as:

$$\delta(A,B) = 2|F^{\alpha}(A,B)| + 2|F^{\beta}(A,B)| \tag{3.25}$$

where F^{σ} is the Fermi correlation. This is described in detail in section 1.7.6 in reference [57].

The ρ_{BCP} values for hydrogen bonds (HB-BCPs) can range over two orders of magnitude, *i.e.* ~0.002 a.u. to ~0.2 a.u. [11], and linear relationships between the bond strength and ρ_{BCP} have been reported for hydrogen bonded systems [58]. The lower end of the HB-BCP range corresponds to weak closed-shell interactions with positive $\nabla^2\rho$ values and the upper end corresponds to very strong interactions with negative $\nabla^2\rho$ values, indicating covalent bonding properties [11]. The water dimer has hydrogen bond BCP that is in the middle of this spectrum, 0.0247 a.u. at the MP2/aug-cc-pVTZ level of theory [4].

3.8.2 Partitioning the Electron Density Into Atomic Contributions

QTAIM can describe a system of critical points and bond paths that represent the interacting subunits of a molecule using only the observable physical density in real space and without any qualitative or quantitative derivations in the form of molecular or atomic

---

[8] The bond order is a method of quantifying the amount of bonding interaction between two atoms. It is defined as ½ the difference between the number of bonding electrons and the number of anti-bonding electrons present in the bond.

orbitals. Although it seems evident that the $\rho(\mathbf{r})$ topology can describe the chemical nature of the atoms in their molecules, it is imperative to prove the ability to construct this topology from purely quantum mechanical methods. If the atom is to truly exist as the fundamental building block of a molecule, the topological atom and the quantum atom must coincide within that molecule [1]. The following discussion justifies this within the zero-flux principle, followed by a description of atomic properties that are available because of this partitioning ability.

In QTAIM, an atom is defined quantum mechanically as a region of real space (Ω) containing a nucleus that is bounded by surfaces through which there is a zero flux in the gradient vector field of the electron density. The zero-flux boundary condition is:

$$\nabla\rho(\mathbf{r}_s) \cdot n(\mathbf{r}_s) = 0, \qquad \text{for every point } \mathbf{r}_s \text{ on the surface } S(\mathbf{r}_s) \qquad (3.26)$$

The surfaces may be bounded by other atoms (interatomic surfaces) or may be bounded by infinity. These atoms are considered open systems: they are subject to fluctuations in charge and momentum felt through their boundaries. This status as an open system is the key to exactly partitioning the molecule into substituent atoms.

The Schwinger principle (a generalization of the principle of stationary action) yields a variational derivation of Heisenberg's equation of motion for any observable [59]. The relevance of the Schwinger principle for QTAIM is that it allows one to derive a quantum description of an open system, but only on the condition that the system satisfies the boundary conditions in equation 3.26. The derivation results in an identical expression for the change in action and content for both open and isolated systems, indicating that the total-molecular isolated system and its constituent atomic closed systems are described by the same physics (with the necessary constraint of the zero-flux condition). With this understanding, the molecular species that is partitioned into atomic basins will have measurable values for electronic properties such as atomic charges, volumes, energies, and the degree of electron delocalization between two basins. In mathematical terms, if these properties are said to be the expectation value of some operator $\hat{O}$, the Schwinger

principle allows us to say that its expectation value, $\langle \hat{O} \rangle$, averaged over all space, is the sum of the expectation values for $\hat{O}$ averaged over all the atoms in the molecule[9],

$$\langle \hat{O} \rangle_{molecule} = \sum_{i}^{\substack{all\ atoms\ in \\ the\ molecule}} \left(N \int_{\Omega_i} \int \left\{ \frac{1}{2} [\Psi^* \hat{O} \Psi + (\hat{O} \Psi)^* \Psi] d\tau' \right\} d\mathbf{r} \right)$$

$$= \sum_{i}^{\substack{all\ atoms\ in \\ the\ molecule}} \left(N \int_{\Omega_i} \rho_O\ d\mathbf{r} \right) = \sum_{i}^{\substack{all\ atoms\ in \\ the\ molecule}} O(\Omega_i)$$

(3.27)

meaning that the molecular expectation value is also the summation of the atomic expectation values for that molecule. The ability to partition the molecular species into exact and chemically meaningful atomic basins opens up a wealth of applications for this method, including atomic population and charge, atomic volume, atomic kinetic energy, the Laplacian, and total atomic energy. These atomic properties will be described briefly in the following section. The reader is also referred to references [1] and [57] for a more detailed analysis of the further applications, in particular section 1.8 in [57]. The following definitions will closely follow the text from that section.

3.8.3 Atomic Properties

If $\hat{O}$ is a one-electron operator (or a sum of one-electron operators), then the average of a property O over an atomic basin Ω, O(Ω), is:

$$O(\Omega) = \langle \hat{O} \rangle_\Omega = \frac{N}{2} \int_\Omega d\mathbf{r} \int d\tau' \left[\Psi^* \hat{O} \Psi + (\hat{O} \Psi)^* \Psi \right]$$

(3.28)

The *atomic population* can be easily obtained by setting the operator $\hat{O}$ to $\hat{1}$, giving

$$N(\Omega) = \int_\Omega \rho(\mathbf{r})\ d\mathbf{r}$$

(3.29)

Note that this can also be written explicitly in terms of the electron spin populations. The *atomic charges*, q(Ω), are simply obtained by subtracting the electron atomic population from the atomic nuclear charge, Z_Ω:

$$q(\Omega) = Z_\Omega - N(\Omega)$$

(3.30)

---

[9] $\int d\tau'$ symbolizes integration over the coordinates of all electrons but one and summation over all spins.

The *atomic volume* is defined by the interatomic surfaces and an appropriately chosen isodensity surface where the basin would otherwise extend to infinity. The *atomic kinetic energy*, $T(\Omega)$, can be described using either the Schrödinger kinetic energy operator:

$$K(\Omega) = -\frac{\hbar^2}{4m}N\int_\Omega d\mathbf{r}\int d\tau' \,[\Psi\nabla^2\Psi^* + \Psi^*\nabla^2\Psi] \tag{3.31}$$

or the gradient kinetic energy operator:

$$G(\Omega) = -\frac{\hbar^2}{2m}N\int_\Omega d\mathbf{r}\int d\tau' \,\nabla_i\Psi^*\cdot\nabla_i\Psi \tag{3.32}$$

Though both descriptions of the kinetic energy differ locally, they will integrate to the same value over all space. The local difference between them is a term proportional to the Laplacian, $L(\Omega)$:

$$\begin{aligned}
L(\Omega) &= K(\Omega) - G(\Omega)\\
&= -\frac{\hbar^2}{4m}N\int_\Omega d\mathbf{r}\,[\nabla^2\,\rho(\mathbf{r})]\\
&= -\frac{\hbar^2}{4m}N\int dS(\Omega,\mathbf{r})\,\nabla\rho(\mathbf{r})\cdot n(\mathbf{r})\\
&= 0 \;\forall\; \nabla\rho(\mathbf{r})\cdot n(\mathbf{r}) = 0
\end{aligned} \tag{3.33}$$

Integration over proper open quantum systems that exactly conserve the zero-flux condition (*i.e.* atomic basins) reduces the Laplacian to zero and the kinetic energy expectation values are equal:

$$K(\Omega) = G(\Omega) = T(\Omega) \tag{3.34}$$

Satisfaction of this equality is a good measure for the accuracy of the integration results.

3.8.4 Atomic Energies

Because of its importance in later chapters, the *atomic energy*, $E(\Omega)$, deserves further discussion. The atomic energy for an atom in a molecule at its equilibrium geometry relies on satisfaction of an atomic virial theorem which applies to the potential energy density, $Y(\mathbf{r})$. Also called the virial field, $Y(\mathbf{r})$ is the effective potential field experienced by an electron at a point $\mathbf{r}$ in a many-particle system:

$$Y(\mathbf{r}) = N\int d\tau'\{\psi^*(-\mathbf{r}\cdot\nabla\hat{V})\psi\} = -\mathbf{r}\cdot\nabla\overleftrightarrow{\sigma} \tag{3.35}$$

$-\nabla\overleftrightarrow{\sigma}$ is related to the force density (see section 6.1 in reference [1]). This virial field differs from the traditional description of the potential energy, $V(\mathbf{r})$, which expresses the

total electron-nuclear attractive and electron-electron and nuclear-nuclear repulsive energies, in that it also contains the virials of the external (Feynman) forces acting on the nuclei [60]. These virial forces vanish at equilibrium geometry. $Y(\mathbf{r})$ is always negative and its integral over all space gives the total potential energy of the molecule. There is a relation between the local statement of the virial field, the kinetic energy and the Laplacian:

$$\frac{\hbar^2}{4m}\nabla^2\rho(\mathbf{r}) = 2G(\mathbf{r}) + Y(\mathbf{r}) \tag{3.36}$$

where $G(\mathbf{r})$ is the kinetic energy for the system from (3.32).

The partitioning of a total molecular energy into atomic subunits is no trivial matter and relies on the ability to express the whole system as proper open sub-units. Recall that the molecular kinetic energy density can be expressed in two ways: apply the Schrödinger operator to give $K(\mathbf{r})$,

$$K(\mathbf{r}) = -\frac{\hbar^2}{4m}N\int d\tau' \, [\Psi\nabla^2\Psi^* + \Psi^*\nabla^2\Psi] \tag{3.37}$$

or apply the gradient kinetic energy operator to give $G(\mathbf{r})$,

$$G(\mathbf{r}) = -\frac{\hbar^2}{2m}N\int d\tau'\nabla\Psi^* \cdot \nabla\Psi \tag{3.38}$$

These equations yield

$$K(\mathbf{r}) = G(\mathbf{r}) - \frac{\hbar^2}{4m}\nabla^2\rho(\mathbf{r}) \tag{3.39}$$

Partitioning the molecule into some arbitrary volume, ω, and integrating over this volume gives

$$K(\omega) = G(\omega) - \frac{\hbar^2}{4m}N\int_\omega dr\,\nabla\cdot\nabla\rho \tag{3.40}$$

The volume integral can be transformed into a surface integral using Gauss's theorem

$$K(\omega) = G(\omega) - \frac{\hbar^2}{4m}N\int dS(\omega,\mathbf{r})\nabla\rho\cdot n(\mathbf{r}) \tag{3.41}$$

From (3.41) the kinetic energy values are only equivalent when the surface vanishes for $\nabla\rho\cdot n(\mathbf{r}) = 0$, which relies on ω being a proper open system, Ω.

Returning to the local virial theorem (3.36), integration over Ω results in a statement of the atomic virial:

$$-2T(\Omega) = Y(\Omega) \tag{3.42}$$

37

Recall that in the absolute equilibrium minima, where there are no Feynman forces acting on the nuclei, the virial equals the average potential energy of the molecule, $V = \Upsilon$, and (3.42) becomes

$$V(\Omega) = -2T(\Omega) \tag{3.43}$$

The total atomic energy $E(\Omega)$ is the sum of the kinetic and potential atomic energies. From (3.34), the atomic kinetic energy is $K(\Omega) = G(\Omega) = T(\Omega)$ and from above, (3.43), the potential energy is $V(\Omega) = -2T(\Omega)$. Therefore

$$E(\Omega) = T(\Omega) - V(\Omega) = T(\Omega) - 2T(\Omega) = -T(\Omega) = \frac{1}{2}V(\Omega) \tag{3.44}$$

Summation of all atomic energies over the molecule will yield the total molecular energy.

The outcome of $E(\Omega) = -T(\Omega) = \frac{1}{2}V(\Omega)$ relies on the evaluation of an electron density arising from a perfectly equilibrated system (because of the virial theorem restriction). In practice, there will remain some forces on the nuclei which will cause the ratio of $-V/_T$ to deviate from 2. If this deviation is small, it can be corrected by scaling the energies with the virial ratio ($\gamma = -V/_T$) by introducing a scale factor, $(1 - \gamma)$, to the energy at the end of a wavefunction calculation. This scaling, however, can lead to forces on the nuclei and make the energy nonstationary with respect to the variational parameters in the wavefunction [61, 62]. For very accurate evaluations of the atomic energies it is possible to introduce a self-consistent virial scaling (SCVS) [63]. This variationally scales the electronic and nuclear coordinates during the self-consistent optimization so that at each step the wavefunction will satisfy the molecular virial theorem, resulting in an *ab initio* wavefunction or first order density matrix that yields a satisfied virial theorem (see Appendix A.2 for details on implementing SCVS in Gaussian 09).

In the following chapters, changes in atomic energies ($\Delta E(\Omega)$) are used to define local stabilities in molecules. Building on the chemical convention that a decrease in the energy of a system indicates an increase in stability for that system [64], a negative energy change for an atom (*i.e.* $\Delta E(\Omega) < 0$) is defined here as stabilizing, and a positive atomic energy change is destabilizing [3]. Note that while a large increase in energy may indicate a large "destabilization", this destabilization could be paired with an even larger nearby stabilization, indicating an overall favourable interaction. For example, in the case

of the water dimer [4] the hydrogen atom involved in the H-bond has an increase in energy (*i.e.* is destabilized), yet the H-bond is overall stabilizing because of the even greater lowering in energy for the oxygen atoms involved.

3.8.5 Some Practical Considerations for the Application of AIMAll

There are several software packages that implement Bader's QTAIM analysis of molecular systems. Some of these include: Bader Charge Analysis from the Henkelman Group at University of Texas at Austin [65], ABINIT from the ABINIT Group [66], and Amsterdam Density Functional (ADF) from Vrije Universiteit in Amsterdam and the University of Calgary in Canada [67]. ADF also has a third party program, Xaim from Universitat Rovira I Virgili in Spain [68], which can be used for QTAIM analysis. Many research groups also employ unpublished codes written "in-house". This thesis applies the AIMAll software package from McMaster University in Canada [69]. This began as code written by Richard Bader's research group, and then was heavily modified and extended by Todd A. Keith. The program is easy to implement, reliable, robust, and relatively fast and efficient. There is also excellent support available from Dr. Keith. As with any software there are particular tips that help ensure proper use and therefore correct results. Because QTAIM may not be as globally recognized as other popular software used in this report, it is prudent to include some advice so that an individual may repeat or continue the research here, or apply these techniques to their own interests. More details (and much of the following discussion) can be found on the AIMAll website: aim.tkgristmill.com, as well as some details in Appendix A.3.

AIMQB (the integration code in the AIMAll package) requires an accurate electron density, readily obtained via computational analysis. The Gaussian 09 program [70] was used for all calculations in this thesis. The necessary density information is stored in a checkpoint file created during the calculation, and this can be formatted to produce a .fchk file that AIMQB can read and subsequently use to produce the appropriate wavefunction file (.wfx, .wfn) for the AIM analysis. The .wfx files are currently limited

39

to the first order electron density matrix, expressed in a molecular orbital (MO) basis.[10] For HF or KS-DFT the MOs are the canonical SCF spatial or spin orbitals. In the case of post-SCF cases such as MP2, they are the natural (spin) orbitals, *i.e.* the eigenvectors of the first order (alpha and beta) density matrix. Note that for single-determinate methods like HF and KS-DFT the first order density matrix can determine all properties of the system, however for post-SCF multi-determinate methods the first-order density matrix provides only one-electron properties and two-electron density properties must be estimated from the one-electron density matrix.[11]

With respect to accuracy of the calculations, the success of the integrations is confirmed in two ways: the atomic integrations correctly reproduce the total number of electrons, and the integrated values of the atomic Lagrangian, L(A), approach zero. Due to numerical integration errors this will generally never be exact. AIMAll will report a "significant integration error" if any value of L(A) is greater than 0.01 a.u., if the sum of all L(A)s is greater than 0.01 a.u., or if the difference in molecular charge and the sum of atomic charges, q(A), is greater than 0.01 a.u. A "potentially significant integration error" is reported if any of these values are between 0.002 and 0.01 a.u. These accuracy criteria should be evaluated to suit the needs of the results. For the data presented in this report, all L(A) values must be less than 0.001 a.u. to be considered acceptable. If this target is not met, the "problem atoms" are re-integrated using a more accurate integration method available in AIMAll (such as 1st or 3rd order Promega or, as a last resort, Sculpt), a finer interatomic surface mesh, or a higher basin quadrature.

3.8.6 Energy Scaling for DFT Wavefunctions

As described above, the virial theorem for a molecule at a stationary state on the potential energy surface reduces to $-V/T = 2$, where V and T are the potential and kinetic energies, respectively, giving an expression for atomic energy, $E(\Omega)$,

---

[10] Molecular orbitals are expressed in terms of their normalized linear expansion in raw primitive Cartesian Gaussian basis functions.

[11] In AIMAll, the two-electron density properties are estimated using the Müller approximation of the two-electron density matrix in terms of natural orbitals of the one-electron density matrix [350].

$$E(\Omega) = -T(\Omega) = -\frac{1}{2}V(\Omega) \qquad (3.43)$$

By definition, the sum of E(Ω) for all atoms in a molecule returns the molecular energy, E. Because the wavefunctions used in practice are approximate, there will be some deviation from this virial relationship and summation of E(Ω) does not exactly yield E. Ideally, one would minimize this deviation by applying self-consistent virial scaling, SCVS [63, 71], however, in practice this can be very computationally costly and furthermore is not currently available for DFT methods in the Gaussian 09 software. An alternative and much cheaper approach is to simply scale the final atomic energy components by the amount of deviation from the virial relationship,

$$E_{scaled}(\Omega) = T(\Omega)(1 + \gamma) \qquad (3.44)$$

where $\gamma = -V/T$. This provides satisfactory results for comparison of energies in different systems because $(1 + \gamma)$ is usually small and γ generally scales linearly with $T(\Omega)$. In the case of Kohn-Sham (KS) DFT, the kinetic energy is obtained from KS molecular orbitals (KS-MOs) and $T(\Omega)$ is actually $T_0(\Omega)$, the non-interacting kinetic energy. This deviates from the total kinetic energy by

$$T(\Omega) = T_0(\Omega) + \Delta T_C(\Omega) \qquad (3.45)$$

Where $\Delta T_C(\Omega)$ is the correlation kinetic energy contained in the exchange-correlation functional [72-73].

The implication for QTAIM analysis is that the relationship used to define the scaling factor is no longer $V/T = \gamma$, but is actually $V/T_0 = \gamma$ and is thus missing $\Delta T_C(\Omega)$, which can vary in size depending on the atom and may be positive or negative [13]. The use of $(1 + \gamma)$ to scale the energies now becomes only a first approximation to the correct energy and will either over- or underestimate the actual value [13]. Because of this, it may be prudent in some cases to make use of unscaled energies, with the understanding that these atomic energies may not sum to yield the total molecular energy (see, for example, Chapter 9).

Chapter 4 Visualizing Internal Stabilization in Weakly Bound Systems Using Atomic Energies: Hydrogen Bonding in Small Water Clusters
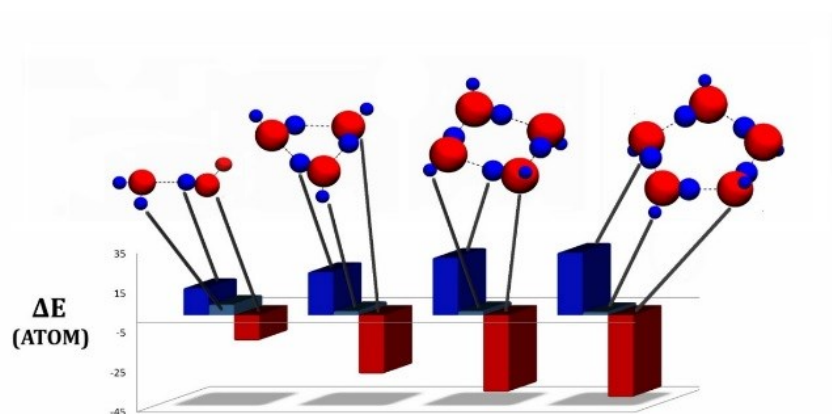
This chapter presents the first study applying atomic energies to evaluate local properties of a set of hydrogen-bonded water clusters. It demonstrates that the changes in local (atomic) energies can reflect the cooperativity that is observed in water-water hydrogen bonding. Global minimum clusters $(H_2O)_n$, n=2−5, provide a well-studied test-set for evaluating the QTAIM energy analysis, and the level of theory used (MP2/aug-cc-pVTZ) has been previously established as a reliable and accurate method for evaluation of water clusters. Total energies as well as geometries are used to support the atomic energies results. The method of visualization, whereby atom size represents the magnitude of energy change and atom colour represents sign of energy change (positive or negative), is also presented as a useful tool for visual inspection of local stabilities of the systems.

4.1 Abstract

Atomic energies are used to visualize the local stabilizing and destabilizing energy changes in water clusters. Small clusters, $(H_2O)_n$, from n=2 to 5, at MP2/aug-cc-pVTZ geometries are evaluated using energies defined by the quantum theory of atoms in molecules (QTAIM). The atomic energies reproduce MP2 total energies to within 0.005 kcal mol^{-1}. Oxygen atoms are stabilized for all systems and hydrogen atoms are destabilized. The increased stability of the water clusters due to hydrogen bond cooperativity is demonstrated at an atomic level. Variations in atomic energies within the clusters are correlated to the geometry of the waters and reveal variations in the hydrogen bond strengths. The method of visualization of the energy changes applied here is especially suited for application to large biomolecules.

4.2 Introduction

Biochemical processes such as protein folding and enzyme docking rely on a delicate balance of weakly stabilizing interactions [14]. Although the total energy change during these processes is typically very small, it may involve large local energy fluxuations [74-75]. These localized energy changes can be a result of weak interactions such as hydrogen bonding, π-stacking, van der Waals forces, steric interferences and hydrophobic interactions, and may either stabilize or destabilize the system. Current experimental techniques such as X-ray crystallography [76] and NMR [77] provide atomic-level resolution of protein structures, allowing researchers to identify specific protein interactions. Combined with computational simulation, an understanding of these interactions leads to the development of highly specific target molecules designed to manipulate biological systems, especially in the area of drug design [78]. The ability to understand, and therefore manipulate, protein interactions would be enhanced with an understanding of the localized energy changes occurring in the system as the proteins interact [79-81]. This local energy is not readily available with traditional methods since they report total energy changes for the system, either obtained experimentally in bulk or theoretically using *ab initio*, density functional, semi-empirical or empirical approaches.

Small model systems are often used to observe the interaction energies of isolated species within proteins; however, they do not represent the important long-range interactions necessary for protein stability [82]. Evaluating protein systems through use of atomic energies would accurately represent the local areas of stabilization and destabilization crucial for understanding intermolecular interactions.

A well-established method for atomic energy evaluation is Bader's quantum theory of atoms in molecules (QTAIM) [1]. QTAIM has been applied in a number of situations to assess the implications of atomic energy changes, such as in the breaking of carbon-carbon bonds [2] and a study of the conformation and tautomerization of amino acids [83]. These reports focus on either strong bonding interactions or intramolecular interactions in small molecules. Previously in our group, we have applied the QTAIM method to evaluate the guanine quadruplex formation in the study of telomeres [3]. Areas of stabilization and destabilization within this large system were highlighted through a study of the changing atomic energies after folding. Furthermore, Taylor *et al.* [3] introduced a novel graphical way of representing these atomic energy changes and the resulting analysis has proven beneficial to the study of telomeric species [84]. The use of atomic energies to assess local areas of biochemical stability in weakly interacting species remains a fairly novel concept and shows great promise for future studies.

To explore the effectiveness and versatility of the atomic energy changes approach it is instructive to examine in detail small water clusters for which a large amount of experimental and theoretical data is available [45, 85-97]. The hydrogen bonding ability of water makes it a uniquely complicated substance that is difficult to measure exactly and to study theoretically. Water clusters exhibit cooperative enhancement, whereby the average hydrogen bond strength increases with an increase in the number of hydrogen bonds present in the system [13, 97-98]. This cooperativity is partially responsible for an increased stability observed in many large hydrogen bonded systems, including protein substructures [15]. Analysis of hydrogen bonded systems should reflect the potential cooperative nature of the bonding interactions. We report here the atomic energy changes in water molecules as they interact to form minimum energy clusters, $(H_2O)_n$, n=2-5. Our intent is to represent changes in atomic stability and thus localized system stability by estimating changes in atomic energies using the quantum theory of atoms in molecules

approach, and furthermore to visualize these changes using the approach of Taylor *et al.*
[3].

4.3 QTAIM Atomic Energies

Bader and his colleagues have shown that it is possible to partition the electron density of a molecular system into constituent open systems bounded by zero-flux surfaces [1, 57, 99-103]. These open systems, called atomic basins, describe the physical properties of atoms in molecules. Integration over the atomic basins yields atomic information such as population and energy. The QTAIM method has been applied in a wide variety of systems, both theoretical and experimental [60, 104-108]. Of particular importance to this study, it is an effective tool for evaluating weak bonding interactions.

4.4 Computational Details

Single point energy calculations were performed on a set of global minima water systems, $(H_2O)_n$, n=1-5, at the MP2/aug-cc-pVTZ level of theory using Gaussian 09 [70]. The geometries were obtained from a benchmark analysis reported by Santra *et al.* at the same level of theory [109]. As a source of reference data, Møller-Plesset Perturbation theory [32] has widely been applied to examine hydrogen bonded systems. It is a suitable method to obtain accurate structural and electronic values for hydrogen bonded water clusters to within 0.001 Å and 0.01 kcal mol^{-1} [45, 89, 96, 109]. The choice of the augmented correlation-consistent polarized triple zeta basis set, as defined by Dunning and coworkers [110], produces very accurate results for water systems [96, 109]. The MP2 energies reported herein reproduce results from previous studies [45, 109], and were corrected for basis set superposition error (BSSE) via the counterpoise (CP) correction method of Boys and Bernardi [42]. The uncorrected and *a priori* CP-corrected MP2 values for the dissociation energy of the water dimer are known to overshoot or undershoot, respectively, the complete basis set value [109, 111-112]. While the magnitude of this error decreases with an increase in basis set size, it will also increase

with cluster size [45]. We therefore provide both corrected and uncorrected values in this study.

MP2 generated wavefunctions were analyzed using the AIMAll suite of programs to calculate atomic energies [69]. Atomic energies are also reported with a CP-type BSSE correction. The accuracy of QTAIM analysis is greatly dependent on the satisfaction of the atomic and molecular virial theorems. As described by Cortés-Guzmán and Bader [71], the atomic virial theorem states that the energy of an atom in a molecule, E(A), is equal to its negative kinetic energy, T(A), and must satisfy the ratio $\gamma = -V/T = 2$, where V is the total potential energy for an equilibrium geometry. Since this is rarely exactly satisfied with post Hartree–Fock calculations, atomic energy values are scaled by a factor of $(1-\gamma)$. As a measure of the accuracy of the integrations, the Laplacian of the electron density should integrate to zero. This ensures that the sum of atomic kinetic energies exactly yields the molecular kinetic energy [113]. The accuracy threshold for integration of atomic basins was maintained at a Laplacian value of 1×10^{-4} a.u. for all atoms. Graphics were created using the VMD software [114].

4.5 Results and Discussion

The optimized water structures are shown in Figure 4.1. Hydrogen bonds are denoted by dashed lines. The interaction energies, ΔE_n, for the formation of water clusters are defined as the difference between the electronic energy of the cluster, E_n, and the energy of an appropriate number of monomers, $nE(H_2O)$, where $E(H_2O)$ is the energy of a water molecule and n is the number of water molecules present in the cluster:

$$\Delta E = E_n - nE(H_2O) \tag{4.1}$$

Stabilization energies for the atoms, $\Delta E(A)$, are defined as the difference between the energy of an atom in a water cluster, $E(A)_{cluster}$, and the energy of the same atom in a water molecule, $E(A)_{H_2O}$:

$$\Delta E(A) = E(A)_{cluster} - E(A)_{H_2O} \tag{4.2}$$

The total energies and interaction energies are reported in Table 4.1. Atomic energies and stabilization energies are reported in Table 4.2. Stabilized and destabilized atoms are indicated by negative and positive energy changes, respectively. The effect of the BSSE

46

correction is to lower the magnitude of the computed energy change. The BSSE corrected values are included in italics in the tables. The E_n values obtained from the QTAIM calculations recover the uncorrected MP2 energies to within 0.005 kcal mol^{-1} for all systems and BSSE corrected energies to within 0.02 kcal mol^{-1} for all systems except the dimer, which differs by 0.23 kcal mol^{-1}. The corrected virial ratio values for all water clusters are within 0.0016 of the exact value of 2. The sum of BSSE corrected atomic energies recovers the total cluster BSSE corrected QTAIM energies exactly, for all systems.
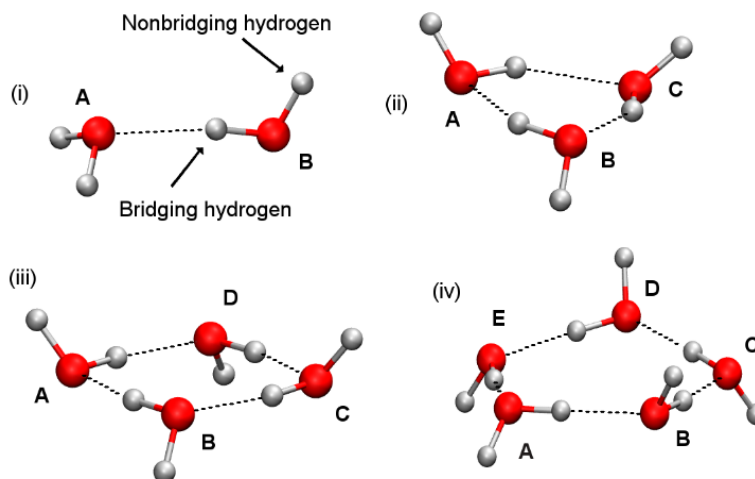
Figure 4.1 MP2 optimized water clusters: (i) dimer, (ii) trimer, (iii) tetramer, (iv) pentamer. Labels A-E correspond to the waters within the clusters. Bridging and non-bridging hydrogens are labeled for the dimer.

Table 4.1 Total MP2 and QTAIM energies E_n and interaction energies ΔE_n for water monomer and water clusters $(H_2O)_n$, n=1-5.[a,b]

	E_n				ΔE_n			
	MP2		QTAIM		MP2		QTAIM	
H_2O	-76.328992		-76.328992					
$(H_2O)_2$	-152.666241	*-152.665858*	-152.666252	*-152.665499*	-5.18	*-4.94*	-5.19	*-4.72*
$(H_2O)_3$	-229.012934	*-229.010823*	-229.012939	*-229.010837*	-16.29	*-14.96*	-16.29	*-14.97*
$(H_2O)_4$	-305.361536	*-305.357823*	-305.361542	*-305.357821*	-28.59	*-26.26*	-28.60	*-26.26*
$(H_2O)_5$	-381.704873	*-381.707835*	-381.704864	*-381.707801*	-37.60	*-39.45*	-37.59	*-39.43*

[a] E_n values are in hartrees, ΔE_n values are in kcal mol^{-1}. [b] Values in italics are BSSE corrected.

Table 2.1 Methods for experimental analyses of hydrogen bonds (HBs).

Cluster H₂O	E(A)						ΔE(A)					
	Non-bridging hydrogen		Bridging hydrogen		Oxygen		Non-bridging hydrogen		Bridging hydrogen		Oxygen	
H₂O	-0.348833				-75.631383							
(H₂O)₂												
A	-0.340323	*-0.340604*			-75.656839	*-75.655837*	5.34	*5.17*			-15.97	*-15.35*
A	-0.340322	*-0.340603*					5.34	*5.16*				
B	-0.354490	*-0.354474*	-0.326909	*-0.327168*	-75.647369	*-75.646812*	-3.55	*-3.54*	13.76	*13.60*	-10.03	*-9.68*
(H₂O)₃												
A	-0.345342	*-0.345957*	-0.313550	*-0.313990*	-75.678977	*-75.677228*	2.19	*1.81*	22.14	*21.87*	-29.87	*-28.77*
B	-0.345282	*-0.345876*	-0.313380	*-0.313872*	-75.679132	*-75.677328*	2.23	*1.86*	22.25	*21.94*	-29.96	*-28.83*
C	-0.345793	*-0.346383*	-0.313384	*-0.313833*	-75.678100	*-75.676368*	1.90	*1.54*	22.25	*21.96*	-29.32	*-28.23*
(H₂O)₄												
A-Dᶜ	-0.345446	*-0.345981*	-0.301514	*-0.302456*	-75.693425	*-75.691018*	2.13	*1.79*	29.69	*29.10*	-38.93	*-37.42*
(H₂O)₅												
A	-0.346747	*-0.347197*	-0.297251	*-0.298363*	-75.696276	*-75.693764*	1.31	*1.03*	32.37	*31.67*	-40.72	*-39.14*
B	-0.346189	*-0.346631*	-0.297301	*-0.298456*	-75.697534	*-75.694957*	1.66	*1.38*	32.34	*31.61*	-41.51	*-39.89*
C	-0.345680	*-0.346142*	-0.297062	*-0.298197*	-75.698606	*-75.696032*	1.98	*1.69*	32.49	*31.78*	-42.18	*-40.57*
D	-0.345437	*-0.345893*	-0.297360	*-0.298503*	-75.698524	*-75.695958*	2.13	*1.85*	32.30	*31.58*	-42.13	*-40.52*
E	-0.346861	*-0.347332*	-0.297219	*-0.298288*	-75.696818	*-75.694314*	1.24	*0.94*	32.39	*31.72*	-41.06	*-39.49*

[a] E(A) values are in hartrees, ΔE(A) values are in kcal mol⁻¹, values in italics are BSSE corrected. [b] Labels A-E correspond to labeling in Figure 4.1.
[c] Waters in the tetramer are equivalent due to symmetry.

Table 4.2 QTAIM atomic energies E(A) and atomic stabilization energies ΔE(A) for water clusters (H₂O)ₙ, n=1-5.[a,b]

Figure 4.2 shows the atomic energy changes of the water clusters schematically; stabilized and destabilized atoms are red and blue, respectively, and the sphere diameter is proportional to the magnitude of $\Delta E(A)$. This style of representation, introduced by Taylor *et al.* [3], provides a useful method of visual analysis for observing localized areas of energy change within complicated systems. It is evident from visual inspection that cluster formation stabilizes the oxygen atoms and destabilizes the hydrogen atoms, with the exception of the non-bridging hydrogen attached to the donor oxygen in the dimer system. In this case the non-bridging hydrogen attached to the donor oxygen shows a stabilization of -3.55 kcal mol^{-1}. The uniqueness of the dimer system can be attributed to its non-cyclic nature. In the remaining cyclic water clusters the destabilization of the non-bridging hydrogens is significant: 1.91 to 2.23 kcal mol^{-1} for the trimer and tetramer, and 1.31 to 2.13 kcal mol^{-1} for the pentamer.
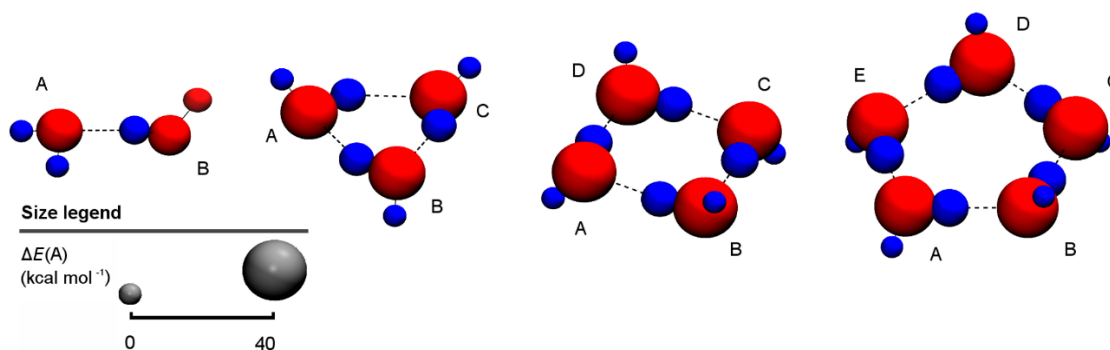
Figure 4.2 Localized energy changes for cluster formation: (i) dimer, (ii) trimer, (iii) tetramer, and (iv) pentamer. Stabilized atoms are red and destabilized atoms are blue. The sphere diameter is proportional to $\Delta E(A)$.

There is strong evidence for the presence of charge transfer (CT) in the formation of hydrogen bonds [13, 98, 115-116]. In the CT description due to Weinhold [116], the lone pair on the accepting oxygen interacts with an empty hydride antibond of the donating O-H atoms, $n_O \rightarrow \sigma^*_{OH}$. Occupancy of the antibonding orbital raises the energy of the O-H species while stabilizing the oxygen. The stabilization increases as the cluster size increases, as a result of hydrogen bond cooperativity. This can be described through changing cluster geometry: decreasing O$\cdots$O distances coupled with increasing O-H covalent bond lengths indicate a weakening of the covalent OH bond and strengthening

of the H⋯O hydrogen bond interaction. Furthermore, there is an increasingly linear O-H⋯O angle as the size of the ring increases. These properties are well supported by the atomic energy changes observed here. The destabilization of the bridging hydrogens increases from 13.76 kcal mol^{-1} in the dimer to an average of 22.21, 29.70, and 32.38 kcal mol^{-1} in the trimer, tetramer and pentamer, respectively. The oxygen atoms are significantly stabilized by -15.97 and -10.03 kcal mol^{-1} in the dimer and an average of -29.71, -38.95, and -41.52 kcal mol^{-1} in the trimer through pentamer, respectively. Figure 4.3 illustrates these changes in atomic energies as cluster size increases. It is evident that as the number of hydrogen bonded waters in the system increases, the magnitude of $\Delta E(A)$ increases for all atoms and tends towards a maximum amount. This is consistent with the exponential form of the cooperativity effect [117]. Furthermore, the energy difference between the bonding atoms increases in the same manner as the average hydrogen bond strength within the clusters. For example, the difference in $\Delta E(A)$ between the oxygen and bridging hydrogens of the trimer is approximately 51.9 kcal mol^{-1}, versus that of the tetramer at 68.6 kcal mol^{-1} and pentamer at 73.9 kcal mol^{-1}. This supports the hypothesis of previous studies applying atomic energy changes, whereby it was stated that a greater local change in atomic energy corresponded to a greater amount of local stabilization or destabilization [3, 13].
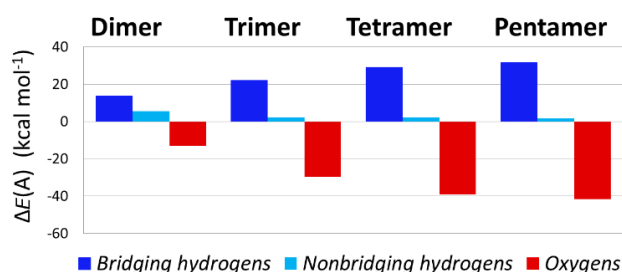
Figure 4.3 Change in atomic energy $\Delta E(A)$, for all atoms in clusters $(H_2O)_n$, n=2-5. $\Delta E(A)$ is averaged over the waters in each cluster. In the dimer average, the non-bridging hydrogen attached to the donating water is not included.

We have also considered QTAIM and natural population analysis (NPA) atomic charges, q(A). The change in atomic charge, $\Delta q(A)$, is evaluated in the same manner as the change in atomic energy: $\Delta q(A) = q(A)_{cluster} - q(A)_{H2O}$. These values are represented

in Figure 4.4. It is obvious that the atomic charges for bridging hydrogens and oxygens reflect the trends observed in the atomic energies: the magnitude of $\Delta q(A)$ increases as the system stability increases. As expected, NPA charges are ~25% smaller than QTAIM charges and their $\Delta q(A)$s are diminished (atomic charges are available in the supporting information). For the dimer through pentamer systems, the QTAIM (NPA) change in atomic charge increases for bridging hydrogens from 0.038 to 0.079 e (0.014 to 0.041 e) and decreases for oxygens from -0.028 to -0.083 e (-0.017 to -0.050 e). The QTAIM (NPA) $\Delta q(A)$s for non-bridging hydrogens are 0.014 e (0.012 e) for the dimer and 0.004 to 0.005 e (0.009 to 0.010 e) for the trimer through pentamer. Interestingly, the NPA $\Delta q(A)$s for non-bridging hydrogens in the trimer through pentamer systems are nearly twice the QTAIM $\Delta q(A)$s, and remain consistent for both NPA and QTAIM for the trimer through pentamer ($\pm$ 0.001 e). The non-bridging hydrogens thus do not reflect the same trend in $\Delta q(A)$ as is observed in $\Delta E(A)$.
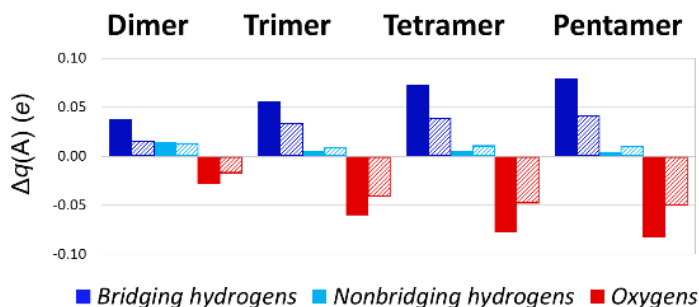
Figure 4.4 Change in atomic charge $\Delta q(A)$, for all atoms in clusters $(H_2O)_n$, n=2-5. $\Delta q(A)$ is averaged over the waters in each cluster. In the dimer average, the non-bridging hydrogen attached to the donating water is not included. QTAIM charges are solid bars, NPA charges are patterned bars.

The QTAIM energy of a water molecule within a cluster, E_W, is defined as the summation of the energies of the constituent atoms in that water molecule:

$$E_W = \Sigma E(A)_W \qquad (4.3)$$

The stabilization of a water molecule due to cluster formation, ΔE_W, is defined as the difference between the energy of the water molecule within the cluster and a free water molecule, $E(H_2O)$:

$$\Delta E_W = E_W - E(H_2O) \qquad (4.4)$$

The molecular energies and stabilization energies for the waters in all clusters are reported in Table 4.3. The average hydrogen bond energy, $E_{AVE}HB$, is the energy of formation for the cluster, ΔE_n, divided by the number of hydrogen bonds present in the system, n_{HB}:

$$E_{AVE}HB = \frac{\Delta E_n}{n_{HB}} \qquad (4.5)$$

ΔE_W and $E_{AVE}HB$ are plotted in Figure 4.5. The cooperative effect is generally quantified by the increase in the average hydrogen bond strength, *i.e.* $E_{ave}HB$. Figure 4.5 demonstrates that by directly calculating the molecular energy change of the hydrogen bonded waters (ΔE_W) we reproduce the same hydrogen bond energy changes as was obtained from averaged energies. Thus the change in molecular energy, as defined through atomic energies, represents the stabilization observed from cooperativity.
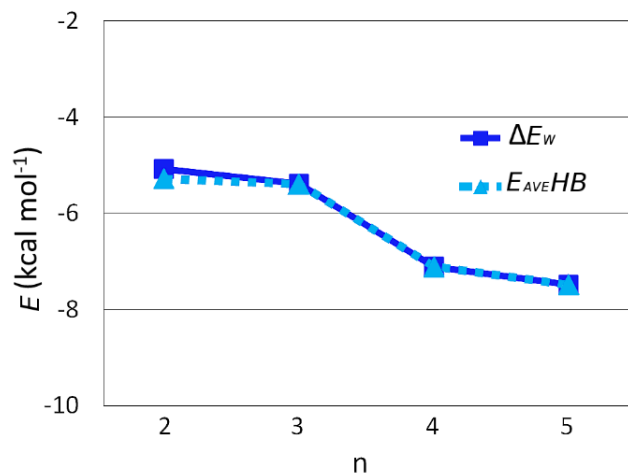
Figure 4.5 Total QTAIM energy changes of water molecules (ΔE_W), and average hydrogen bond energy ($E_{AVE}HB$), for water clusters $(H_2O)_n$, n=2-5. ΔE_W values are averaged over the waters in each cluster.

Table 4.3 QTAIM energies, E_W, stabilization energies, ΔE_W, and average hydrogen bond energies, $\Delta E_{AVE}HB$, for water monomer and clusters $(H_2O)_n$, n=1-5.[a,b]

	E_W		ΔE_W		$\Delta E_{AVE}HB$	
H_2O	-76.328992					
$(H_2O)_2$						
A	-76.337484	*-76.337044*	-5.29	*-5.02*		
B	-76.328768	*-76.328455*	0.18	*0.37*	-5.19	*-4.72*
$(H_2O)_3$						
A	-76.337874	*-76.337181*	-5.53	*-5.10*	-5.43	*-4.99*
B	-76.337784	*-76.337067*	-5.49	*-5.04*		
C	-76.337263	*-76.336571*	-5.16	*-4.73*		
$(H_2O)_4$						
A-D[c]	-76.340378	*-76.339448*	-7.11	*-6.53*	-7.15	*-6.57*
$(H_2O)_5$						
A	-76.340274	*-76.339324*	-7.08	*-6.48*	-7.52	*-7.89*
B	-76.341024	*-76.340044*	-7.55	*-6.94*		
C	-76.341348	*-76.340372*	-7.75	*-7.14*		
D	-76.341320	*-76.340354*	-7.74	*-7.13*		
E	-76.340898	*-76.339934*	-7.47	*-6.87*		

[a] E_W values are in hartrees, ΔE_W and $\Delta E_{AVE}HB$ values are in kcal mol^{-1}. [b] Values in italics are BSSE corrected. [c] Waters in the tetramer are equivalent due to symmetry.

It is interesting to note that the values of $\Delta E(A)$ are not consistent for all waters within each cluster. In the trimer system the $\Delta E(A)$ values for the oxygens vary by about 0.7 kcal mol^{-1}, non-bridging hydrogens by 0.3 kcal mol^{-1}, and bridging hydrogens are consistently destabilized within 0.1 kcal mol^{-1}. The changes in energies for atoms in the pentamer vary by up to 1.5 kcal mol^{-1}, 0.9 kcal mol^{-1}, and 0.2 kcal mol^{-1} for the oxygens, non-bridging hydrogens and bridging hydrogens, respectively. These atomic energy variations are reflected in the water molecules: ΔE_W values for the trimer system differ by up to 0.4 kcal mol^{-1} and the pentamer by 0.7 kcal mol^{-1}. The tetramer does not show any variation in ΔE_W or $\Delta E(A)$. Although these energy differences are close to a limit of accuracy previously stated by Bader in 1987 (~1 kcal mol^{-1}) [103], it has been recently reported that there exists a variation in hydrogen bond strengths within the different water clusters [118]. Considering this, and the precision of the QTAIM energies with respect to MP2 energies, we conclude that these atomic energy differences are not simply numerical artifacts.

These molecular and atomic energy differences are furthermore correlated with the slight geometrical differences observed in the clusters. Referring to Figure 4.1, we see that the puckered trimer adopts C_1 symmetry with two hydrogens pointing above the oxygen plane, and one below. Waters A and B are slightly more stabilized than water C, by ~0.4 kcal mol^{-1}. As a hydrogen bond acceptor, water C has the least favourable geometry: the hydrogen bond between waters A and C slightly lengthened (0.02 Å) and more bent (2.5°) compared to the other two hydrogen bonds in the system (geometries for the optimized clusters are available in the supporting information). The pentamer system also has a puckered ring and adopts C_1 symmetry. Waters B and E, which have a ΔE_W of -7.55 and -7.47 kcal mol^{-1}, respectively, and C and D, which have a ΔE_W of -7.75 and -7.74 kcal mol^{-1}, respectively, adopt mirrored configurations. The water molecule at the peak of the pentamer structure (A) has the lowest amount of stabilization, -7.08 kcal mol^{-1}. As a hydrogen bond acceptor, water A has the least favourable geometry: the hydrogen bond between A and E is slightly elongated (0.01Å), with a bond angle slightly more bent (2.5-3.3°) than the other hydrogen bonds present. The tetramer shows no relevant variation in the atomic or molecular QTAIM energies, which is expected due to its S_4 symmetry. Considering that the symmetrical tetramer is the only structure for water clusters n=2-6 that does not undergo an experimentally observed bifurcation of hydrogen bonds [119], it is possible that this observation of atomic energy distribution may indicate sites of preferential protonation or structural transformation, and could be explored in more depth. What is most relevant for this work is that the reported atomic energies are able to quantify the geometrical differences observed in the water cluster systems.

4.6 Conclusions

We demonstrate the use of atomic energies to describe the internal energy changes in weakly bound systems, applied to water clusters, $(H_2O)_n$, from n=2 to 5. The reported energies obtained from the quantum theory of atoms in molecules method reproduce highly accurate MP2/aug-cc-pVTZ values to within 0.005 kcal mol^{-1}. The change in atomic energies is correlated to a change in atomic stability within the clusters and reflects the overall increased stability due to hydrogen bond cooperativity. The variations

in atomic energies observed within the clusters are attributed to slight differences in the geometry of the waters, and may prove useful as a predictive method for the preferential site of protonation or transformation in water clusters. The atomic energy changes can be represented graphically in order to easily view important energetic changes occurring in the system. This method of evaluating energy change is shown to be a direct way of evaluating the areas of stabilization and destabilization in weakly bound systems, and will be of benefit for studies of larger and more complicated biomolecular structures.

4.7 Acknowledgements

Supporting Information Available: Geometric parameters for MP2 optimized water molecules, QTAIM atomic properties, and NPA charges. This material is available free of charge via the Internet at http://pubs.acs.org.

4.8 Chapter Summary and Relevance

In this chapter atomic energies were successfully used to visualize the local energy changes in small water clusters. MP2/aug-cc-pVTZ total energies are accurately reproduced at the atomic level, to within 0.005 kcal mol^{-1}. It is found that the energy change for oxygen atoms is always negative, indicating oxygen stabilization in hydrogen bonding, and the energy change for hydrogen atoms is always positive, indicating hydrogen destabilization in hydrogen bonding. The hydrogen bond cooperativity – demonstrated by a non-linear increase in stability of the water clusters as the number of hydrogen bonds increases – is reflected by a similar non-linear change in stability for the oxygen and hydrogen atoms. Small variations in atomic energies within the water clusters are correlated to the geometry of the interacting water molecules and reveal variations in hydrogen bond strengths, in particular for the pentamer cluster. Finally, the visual depiction incorporating a colour-coded and size-dependent representation of the relative energy changes provides a striking picture of the distribution of stability within the water clusters. This first study of small clusters with QTAIM energies has proven to be a reliable and insightful approach to the study of hydrogen bond cooperativity.

Chapter 5   Atomic Energy Evaluation of Eight Low-Lying Water Hexamer Structures
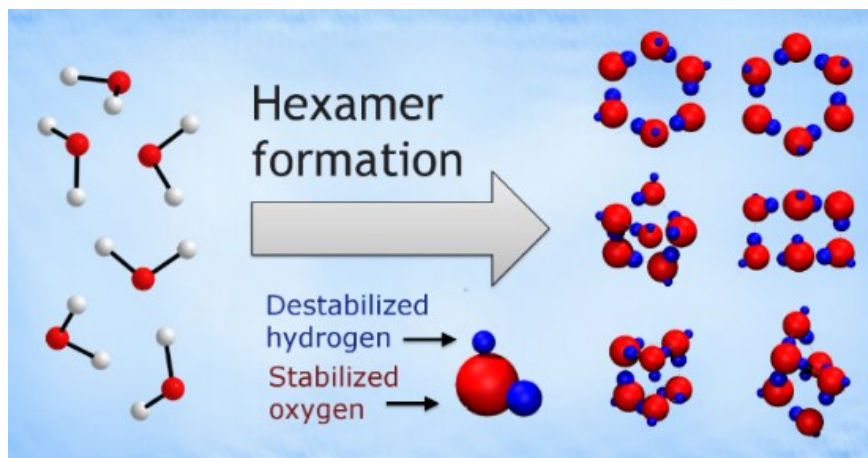
Having established the capacity for QTAIM atomic energies to represent cooperativity in simple, linear hydrogen bonding, as well as the suitability of the MP2/aug-cc-pVTZ method for this analysis of water molecules, we further explore the utility of QTAIM energies in more complicated hexamer systems. The $(H_2O)_6$ potential energy surface (PES) is extremely complex, with over 15 structural motifs representing local minima that are within 3 kcal mol^{-1} of the global minimum. The hexamer PES has undergone intense experimental as well as computational analysis, and contains a further dimension of hydrogen bonding where a water molecule may have up to three bonding partners and the opportunity to interact cooperatively or anti-cooperatively. The eight lowest energy water hexamers (prism, cage, boat 1, boat 2, bag, chair, book 1 and book 2), will be evaluated in a similar manner as in Chapter 4. This chapter was a collaborative effort; the contribution of this author was supervision of the ab inito calculations, performing the QTAIM calculations and drafting and editing the manuscript.

5.1 Abstract

Atomic energies are used to describe local stability in eight low-lying water hexamers: prism, cage, boat 1, boat 2, bag, chair, book 1, and book 2. The energies are evaluated using the quantum theory of atoms in molecules (QTAIM) at MP2/aug-cc-pVTZ geometries. It is found that the simple, stabilizing cooperativity observed in linear hydrogen-bonded water systems is diminished as clusters move from nearly planar to three-dimensional structures. The prism, cage and bag clusters can have local water stabilities differing up to 5 kcal mol^{-1} as a result of mixed cooperative and anti-cooperative interactions. At the atomic level, in many cases a water may have a largely stabilized oxygen atom but the net water stability will be diminished due to strong destabilization of the water's hydrogen atoms. Analysis of bond critical point (BCP) electron densities shows that the reduced cooperativity results in a decrease in hydrogen bond strength and an increase in covalent bond strength, most evident in the prism. The chair, with the greatest cooperativity, has the largest average electron density at the BCP per hydrogen bond, while the cage has the largest total value for BCP density at all hydrogen bonds. The cage also has the second largest value (after the prism) for covalent bond critical point densities and an oxygen-oxygen BCP which may factor into the experimentally observed stability of the structure.

5.2 Introduction

The current understanding of the exceptional properties of water is founded in part on studies of small-to-large water clusters. The combined theoretical and experimental analyses of the past decades [17, 120-124] provide insight into the complex interactions that define essential hydrogen bonding (HB) in water, particularly the cooperative behaviour that is a result of non-additive contributions to the HB total energy [10, 13, 91, 116, 125-134]. Characterization of hydrogen bonding within small water clusters reveals a unique distribution of the stability for each cluster size and configuration. These studies are important for a variety of applications, for example understanding water behaviour at biomembrane surfaces, inside enzyme active sites, and the formation of clathrate hydrates

in the atmosphere. Characterization of water clusters is also necessary for the continuing development of force field methods. It is now possible to directly study small water clusters in the gas phase using a variety of experimental methods, and low energy structures for the hexamer, heptamer and nonamer water clusters have recently been isolated [135-136]. The water hexamer in particular has garnered significant interest (see references cited in reference [137], as well as references [138-151]) because it is the first water cluster to have a three-dimensional (3D) configuration as its global minimum structure; this is possibly a result of the additive components in HBs being more important than non-additive components for a 3D configuration [13]. This shift in the character of water's hydrogen bonding approaches its expected behaviour in bulk water [152-153]. The potential energy surface (PES) of the water hexamer is very complicated, containing many minima in a narrow energy range. For example, there are over 15 structural motifs representing local minima that are within 3 kcal mol^{-1} of the global minimum [150]. Characterization of the true global minimum energy structure for the hexamer water cluster has been the source of intense debate over the past two decades, with theoretical reports ranging between the cage and prism structures. A recent experimental study concludes that the cage is the minimum energy structure [135] while theoretical reports maintain that the prism has the lowest energy (before zero-point energy correction) [148, 151].

A further aspect of water cluster research is that, along with finding minima on PESs, it is necessary to understand the distribution of stability within each cluster configuration that allows one particular arrangement of water molecules to be more stable than another slightly different arrangement. To that end, there are several theoretical approaches which consider the distribution of energetics within water clusters. One such approach is to use theoretical energy decomposition analyses (EDAs) to determine individual contributions to bond strength. These are usually based on the seminal work of Kitaura and Morokuma [154] and have been developed in many ways to decompose the interaction energies [155-162]. In general, the complicated approaches of EDA models often require simplifying assumptions so that application to even moderately sized structures is feasible. For example, the contributions to the total energy from four-body or higher interactions in water clusters are generally presumed negligible [132] and so these higher

order terms are often truncated in the EDAs. Four-body effects, however, can impact the interaction energy of the water hexamer by up to 4.4% [13], a significant amount for the PES of the hexamer. An unambiguous picture of the stability within water clusters requires a direct analysis of their substituent energy properties, without truncation or fitted model assumptions.

We report atomic and molecular stabilities in a quantitative fashion using Bader's quantum theory of atoms in molecules (QTAIM) analysis [1]. This approach has been demonstrated in previous reports to accurately describe energy changes at an atomic level [3, 4, 6]. We evaluate the eight lowest energy isomers of the water hexamer: prism, cage, boat 1, boat 2, bag, chair, book 1, and book 2. These clusters represent 2D through 3D geometries, including a range of hydrogen bond configurations, yet remain within 3 kcal mol^{-1} on the hexamer potential energy surface. See Table 5.1 for the relative energy ordering of the hexamers as well as the number of hydrogen bonds per cluster. Using QTAIM topology we provide a distinct picture of the atomic stabilization within each water hexamer configuration to show that the small energy range for such a large variation in cluster geometries is a result of competing cooperative and anti-cooperative interactions present in the 3D clusters. We apply a simple method of visualization to represent the distribution of stabilization within the complicated water clusters [3].

Table 5.1 Relative stabilities of eight water hexamers and the number of hydrogen bonds formed in each cluster.

Hexamer	Boat 2	Boat 1	Chair	Bag	Book 2	Book 1	Cage	Prism
Relative stability[a]	2.62	2.53	1.59	1.29	0.78	0.46	0.06	0.00
Number of HBs	6	6	6	7	7	7	8	9

[a] Stability is relative to the interaction energy for the prism structure, in kcal mol^{-1}.

5.3 Computational details

The hexamers were optimized at the MP2/aug-cc-pVTZ level of theory [32] using Gaussian 09 Rev.C.01 [70]. Cartesian coordinates for the structures were obtained from a study by Chen and Li [149]. No symmetry constraints were applied in the optimization and all final geometries have C_1 symmetry. It has been reported previously that enforcing C_2 symmetry for the boat structures will increase the energy by ~0.015 kcal mol^{-1} [148];

we do not constrain our optimizations as it is important for the QTAIM analysis that there are no residual forces on the atoms resulting from a non-equilibrium structure. The influence of zero-point energy (ZPE) vibrations in water hexamers can be large enough to impact their stability order [148]; however, Dahlke *et al*. [163] report that ZPE corrections at the MP2 level do not reproduce the CCSD(T) relative energy ordering, despite having the lowest error of any methods tested in the study. The QTAIM analysis does not include ZPE corrections, nor are thermal or entropic contributions present in the atomic breakdown of the molecules.

Self-consistent virial scaling (SCVS) was implemented for all optimizations to ensure that the wavefunctions fully satisfy the virial theorem, as outlined in reference [71]. The MP2 wavefunctions generated were analyzed using the AIMAll suite of programs [69] to calculate atomic energies according to Bader's quantum theory of atoms in molecules [1]. The accuracy threshold for atomic basin integrations was maintained at a Laplacian value of 1×10^{-4} a.u. for all atoms, giving a maximum per atom error of 0.06 kcal mol^{-1}. To gauge the impact of SCVS, we also compared our results to non-SCVS calculations. The non-SCVS values for the atomic energies deviate from SCVS values by up to 1.7 kcal mol^{-1} for the oxygen atoms and 0.24 kcal mol^{-1} for the hydrogen atoms, about 0.1% of the individual atomic energy. The atomic kinetic energies used in this discussion have been scaled post-calculation using a virial factor to account for any remaining deviation from virial satisfaction (this value is essentially zero for the SCVS calculations but was implemented so as to remain consistent with other discussions). Relevant atomic properties and virials for all systems (scaled and unscaled) are available in the supporting information, as well as bond critical point data and geometries for the hexamer structures. The graphical descriptions of the atomic energy changes in Figures 5.2-5.6 were generated using the VMD software to represent the atomic energy changes quantitatively [114].

Previous reports conclude that the basis set superposition error (BSSE) will decrease the MP2 energy by ~1 kcal mol^{-1} consistently for each hexamer configuration [149]. The complete basis set value is presumed to lie between the corrected and uncorrected energy [45, 109, 111-112]. For the hexamers, the energy ordering of the configurations does not change with inclusion of BSSE corrections, either for total energies or for substituent

energetic contributions [149]. Furthermore, Ramirez *et al*. [90] have suggested that counterpoise corrections fail for some hydrogen bonding clusters. We therefore chose not to include a BSSE correction.

5.4 Results and Discussion

The atomic energy changes were obtained in the same manner as in previous reports, [4, 6] whereby the change in energy per atom is the difference between the energy of the atom (A) in the isolated water monomer and the energy of the same atom in a water cluster: $\Delta E(A) = E(A)_{cluster} - E(A)_{monomer}$. The atomic energy changes for all atoms and for the atoms summed into their respective waters are reported in Table 5.2 and Table 5.3. In the following discussion we divide the hexamer clusters into systems according to their geometries: two-dimensional (2D) are the chair, boat 1 and boat 2 systems and three-dimensional (3D) are bag, book 1, book 2, cage, and prism structures. Note that although the boat structures have been classified as "2D", they are not truly planar, having a bend across the plane of the waters of ~113°. Hydrogens participating in a hydrogen bond are HB-hydrogens and those that are not participating in a hydrogen bond are non-HB hydrogens. 2D systems have only two HBs per water, however in the 3D systems one water may participate in up to three hydrogen bonds by either donating or accepting an extra HB. These multiple-bonding water types are represented in Figure 5.1 as single donor, single acceptor (**sd,sa**); single donor, double acceptor (**sd,da**); and double donor, single acceptor (**dd,sa**). In the following discussion the atomic energy stabilities will be first discussed for the 2D systems (chair and boat), then the 3D systems (book, bag, cage and prism), and then a general discussion of the bond critical points (BCPs) in the QTAIM topology follows.

Table 5.2. Atomic energy changes (kcal mol^{-1}) for atoms in the hexamer clusters.

water label[a]	A		B		C		D		E		F	
atom[b]	O	H1	O	H1	O	H1	O	H1	O	H1	O	H1
		H2		H2		H2		H2		H2		H2
Prism	-47.7	12.4	-33.9	12.5	-38.2	28.8	-37.5	11.4	-37.7	25.0	-48.4	36.6
		23.3		15.0		3.3		16.2		5.1		5.7
Cage	-37.6	26.6	-47.8	15.0	-42.8	30.2	-35.0	14.9	-48.5	35.6	-38.3	27.3
		2.0		23.6		5.1		13.1		5.8		3.0
Book 1	-35.8	26.6	-48.1	35.6	-44.6	33.9	-44.2	33.9	-47.2	25.2	-34.7	25.7
		2.2		5.4		2.6		2.0		12.9		1.0
Book 2	-35.9	26.2	-47.5	34.9	-43.7	33.8	-43.8	33.4	-45.7	23.7	-35.6	26.6
		2.7		5.2		2.5		2.1		12.7		1.3
Bag	-47.1	37.7	-31.1	22.4	-47.6	19.0	-29.7	21.1	-46.2	35.6	-46.0	34.5
		4.2		1.3		19.0		1.5		2.5		2.2
Chair	-43.0	33.5	-43.0	33.4	-43.0	33.5	-43.0	33.5	-43.0	33.4	-43.0	33.5
		1.8		1.8		1.8		1.8		1.8		1.8
Boat 1	-42.5	32.8	-41.5	32.8	-41.5	33.1	-41.5	33.1	-42.7	33.4	-42.5	32.8
		1.9		1.9		1.1		1.1		1.6		1.9
Boat 2	-41.9	32.9	-41.7	32.5	-43.0	33.5	-41.9	32.9	-41.7	32.5	-43.0	33.5
		1.3		1.8		2.0		1.3		1.8		2.0

[a] Labels A-F correspond to the waters indicated in Figures 5.2-5.6. [b] Hydrogen atom can be HB-hydrogens (H1) or non-HB hydrogens (H2). Occurrences where both hydrogen atoms participate in HBs are labeled in their respective figures.

Table 5.3. Total energy change (kcal mol^{-1}) for each water molecule in hexamer clusters, defined as the sum of the water's constituent atoms. Total energy (ΔE_{total}) is the sum of all constituent atomic energy changes in each cluster.

cluster	A	B	C	D	E	F	ΔE_{total}
Prism	-12.0	-6.5	-6.1	-9.9	-7.6	-6.0	-48.0
Cage	-9.0	-9.2	-7.4	-7.1	-7.2	-8.0	-48.0
Book 1	-7.0	-8.1	-7.1	-8.4	-9.1	-7.9	-47.6
Book 2	-7.0	-7.5	-7.4	-8.3	-9.3	-7.7	-47.2
Bag	-5.2	-7.5	-9.6	-7.1	-8.2	-9.3	-46.7
Chair	-7.7	-7.7	-7.7	-7.7	-7.7	-7.7	-46.4
Boat 1	-7.8	-7.3	-7.6	-7.8	-7.3	-7.6	-45.5
Boat 2	-7.8	-7.4	-7.5	-7.8	-7.4	-7.5	-45.4

Figure 5.1 Bonding arrangements for multiply bonded water molecules in 3D structures. Each water can have up to three neighbour waters, and may either i) donate one hydrogen bond and accept one hydrogen bond (single donor, single acceptor, sd,sa), ii) donate one hydrogen bond and accept two hydrogen bonds (single donor, double acceptor, sd,da), or iii) donate two hydrogen bonds and accept one (double donor, single acceptor, dd,sa).

5.4.1 2D Structures: chair, boat 1, and boat 2

Figure 5.2 Localized energy changes for 2D hexamer cluster formation: i) chair, ii) boat 1, iii) boat 2. Stabilized atoms are red and destabilized atoms are blue. The sphere diameter is proportional to the atomic energy stabilization, $\Delta E(A)$, so that an atom with a larger energy change will have a larger sphere radius. The bottom row shows the deviation from planarity in the boat *vs.* chair clusters.

A visual representation of the atomic energy changes within the 2D clusters (chair, boat 1 and boat 2) is shown in Figure 5.2. As with previous reports, the oxygen atoms (in red) are stabilized at the expense of the hydrogen atoms (in blue) and the HB-hydrogens have a much greater destabilization than the non-HB hydrogens. Each water in a cluster

64

has been labelled from **A-F**. For these systems the stabilization of each atom type is relatively uniform: oxygens are stabilized by ~-42 kcal mol^{-1}, HB-hydrogens are destabilized by ~33 kcal mol^{-1}, and non-HB hydrogens are destabilized by ~2 kcal mol^{-1}. The net stabilization for each water in the clusters is ~-8 kcal mol^{-1}. This distribution of stabilization per water molecule is analogous to what was observed in the trimer through pentamer cyclic structures [4], however with a small increase in stability per water (~0.5 kcal mol^{-1}) as a result of the increased cooperativity in the larger systems.

The consistent atomic stabilization is a result of a uniform HB environment where each water molecule donates one hydrogen and accepts one oxygen to form single donor, single acceptor (**sd,sa**) arrangements having similar HB geometries. The uninterrupted **sd,sa** chain allows for strong cooperative interactions and is the source of the increased stability in the 2D cyclic conformations, despite having fewer hydrogen bonds than the 3D configurations. In fact, the more symmetrically balanced the **sd,sa** arrangement is, the greater the cooperativity that is observed; *e.g.* the chair configuration is more stable than the boat configurations. The enhanced cooperativity in the chair system is reflected in the total energy changes for its atoms: the chair has the largest values for the stabilization of its oxygens (-43 kcal mol^{-1}) and the largest values for destabilization of donor hydrogens (~34 kcal mol^{-1}) of the three 2D systems. In the slightly bent boat 1 and boat 2 systems, there is a small non-uniform distribution of energy, reflected in small differences in atomic stabilizations. Waters **B** and **E** donate into hydrogen bonds which are slightly lengthened (by ~0.01 A) with narrowed OH$^{...}$O bond angles (by ~ 2.5º), have smaller amounts for ΔE(oxygen) and ΔE(hydrogen), and are slightly less stable overall. A lengthening of the hydrogen bond can indicate weakening bond strength, reflected also in the decrease in cooperative stability as indicated by smaller atomic energy changes. Interestingly, in the boat systems the most stabilized waters (**A**, **D**), which also have the largest change in their constituent atomic energies, donate HBs to the least stabilized waters (**B**, **E**), so that the weakening of one water results in a strengthening of its neighbour water. This effect becomes far more complicated in the three-dimensional systems.

5.4.2 3D Structures: book 1, book 2, bag, cage, prism

It is quickly recognized in the book 1, book 2, bag, cage and prism structures that the atomic stabilization in the three-dimensional systems is not as uniform as in the two-dimensional systems. Energy changes for oxygen atoms in all 3D systems range from -49 to -30 kcal mol^{-1}, HB-hydrogens from 11 to 38 kcal mol^{-1} and non-HB hydrogens have destabilization values from 1 to 6 kcal mol^{-1}. The net stabilization for individual waters is between -12 and -6 kcal mol^{-1} in the prism, -10 and -5 kcal mol^{-1} in the bag, and -9 and -7 kcal mol^{-1} in the cage, book 1 and book 2.

To interpret the large variations in atomic stabilities within the 3D water clusters we consider the environment of each water-water interaction and its resulting impact on the potential for cooperative enhancement of hydrogen bond strength. Although analysis of cooperativity is straightforward in the planar cyclic systems (each water has only one donor and one acceptor), the 3D hexamer geometries exhibit a combination of possible bonding arrangements where a water molecule may interact with up to three other water molecules by either donating or accepting hydrogen bonds. Each HB interaction can be classified as either largely cooperative or largely anti-cooperative: a cooperative interaction is stabilizing and an anti-cooperative interaction is destabilizing [127-128]. The stabilizing value of each interaction depends on the bonding character of the waters forming the hydrogen bond as well as the bonding interactions of their neighbouring waters [130-137]. Waters which donate two hydrogen bonds have an increased capacity for cooperativity and waters accepting two hydrogen bonds have a decreased capacity for cooperative stabilization.

5.4.2.1 Book 1 and Book 2

Figure 5.3 represents the atomic energy changes for book 1 and book 2. The book configurations could be considered transition structures between 2D and 3D, having an extra hydrogen bond splitting the simple cyclic cooperative environment into two rings. One water donates two and accepts one hydrogen bond (**E**) and its neighbour water must thus accept two hydrogen bonds and donate one (**B**). The double donating water has a strongly stabilized oxygen (-47 kcal mol^{-1} in book 1 and -46 kcal mol^{-1} in book 2) and

66

only moderately destabilized HB-hydrogens (25 and 13 kcal mol^{-1} for book 1 and 24 and 13 kcal mol^{-1} for book 2) resulting in a net stabilization of -9 kcal mol^{-1} for each **dd,sa** water. The double accepting water (**B**) also has a strongly stabilized oxygen (-48 kcal mol^{-1}), however, it has a significantly large destabilization for the non-HB hydrogen (5 kcal mol^{-1}) and this detracts from the overall stability of the water, resulting in a net stabilization of -7 kcal mol^{-1}.
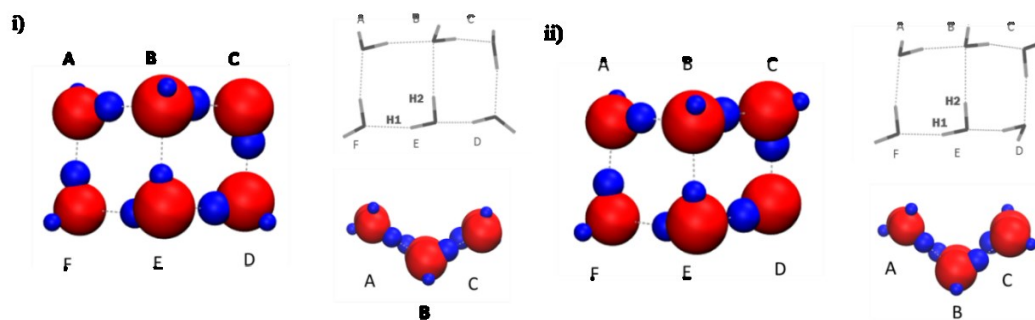
Figure 5.3 Localized energy changes for 3D hexamer cluster formation: i) book 1, ii) book 2. Stabilized atoms are red and destabilized atoms are blue. The sphere diameter is proportional to the atomic energy stabilization, $\Delta E(A)$. The wireframe structures indicate hydrogen labelling for waters where both hydrogens participate in HBs; in all other cases H1 is the HB hydrogen and H2 is the non-HB hydrogen. The lower right image shows the deviation from planarity of the book clusters.

This picture of water stability matches what is observed in various arrangements of water trimers and tetramers, where a double donor water arrangement is overall more stable than a double acceptor water [127]. It has been reported that double donating interactions are cooperatively stabilizing and double accepting interactions may be considered anti-cooperative and destabilizing [128]. It is interesting to note that it is the non-interacting hydrogen on water **B** that "pays the price" for the additional HB, while the oxygen remains largely stabilized. If we next consider the water which donates a hydrogen bond *to* the double donor (**D**) and the water receiving a hydrogen bond *from* the double donor (within the outer ring structure, **F**) they also have increased overall stability (8 kcal mol^{-1}). Their stabilization at the atomic level, however, is quite different: the receiving water and its nearest neighbour (**F** and **A**) have a significantly lowered relative stability of their oxygen (only -35 to -36 kcal mol^{-1} *vs.* -46 and -47 kcal mol^{-1} in **E**) however a decreased destabilization of their HB-hydrogen (~26 kcal mol^{-1}) results in the

net stabilization of -8 and -7 kcal mol^{-1}. It may be that the second neighbour (**A**) has lowered ΔEs because it donates to a double accepting water. Considering HB lengths, the waters with shorter HBs show an increased stability, with the exception of water **F**. In this case its HBs are ~0.1 Å longer than neighbouring waters; however it has a net stability greater than expected (by about 1 kcal mol^{-1}). This may be attributed to the surprisingly small change in atomic energy of its non-HB hydrogen: ΔE(hydrogen) is only 1 kcal mol^{-1}. These energetic observations indicate that the extra bond formed in the system has a cooperative effect on the waters which form the ring that donates to the double donor water, and an anti-cooperative effect on the waters which form the ring that receives from the double donor water.

5.4.2.2 Bag

Figure 5.4 Localized energy changes for formation of 3D bag hexamer. Stabilized atoms are red and destabilized atoms are blue. The sphere diameter is proportional to the atomic energy stabilization, ΔE(A). The wireframe structure indicates hydrogen labelling for waters where both hydrogens participate in hydrogen bonds; in all other cases H1 is the HB hydrogen and H2 is the non-HB hydrogen.

Although the bag system has the same number of hydrogen bonds as the book systems, it has a lower net stabilization. Figure 5.4 represents the atomic energy changes in the bag configuration. As with the book systems, there are four waters which adopt simple single donor, single acceptor HB arrangements (**B**, **D**, **E**, **F**), one water which has a double donor, single acceptor arrangement (**C**), and one has a single donor, double acceptor arrangement (**A**). As in the book structures, the double donating water is the

most stabilized (-10 kcal mol^{-1}) and the double accepting water is the least stabilized (-5 kcal mol^{-1}). The oxygen stabilization is similar (-48 kcal mol^{-1} for **C** and -47 kcal mol^{-1} for **A)**, and thus it is the hydrogen destabilization that determines the net stabilization: double donating **C** has both HB-hydrogens destabilized by 19 kcal mol^{-1} and double accepting **A** has a HB hydrogen destabilized by 38 kcal mol^{-1} and a non-HB destabilized by 4 kcal mol^{-1}. Waters **B** and **D** are both **sa,sd** with similar neighbour environments: each receives from a **dd,sa** water and donates to a **sd,da** water and has a net stabilization of ~-7 kcal mol^{-1}. The distribution of atomic values for these waters is similar as well: the oxygen in **D** is stabilized by -30 kcal mol^{-1} and in **B** by -31 kcal mol^{-1}; the HB hydrogen in **D** is destabilized by 21 kcal mol^{-1} and in **B** by 22 kcal mol^{-1}; and the non-HB hydrogen in **D** is destabilized by 2 kcal mol^{-1} and in **B** by 1 kcal mol^{-1}. The slightly reduced stabilization of **D** *vs.* **B** can be understood in terms of slightly lengthened hydrogen bonds associated with **D** (0.03 and 0.02 Å longer). Waters **E** and **F** are both also **sd,sa** waters, however their neighbour environments differ from **B** and **D** in that **E** accepts from a double accepting water and **F** donates to a double donating water. This is similar to the arrangements of **C** and **D** in the book systems where the recipient of a hydrogen bond from a double acceptor has a slightly lower stability than the water donating to a double donor: **E** has a net stabilization of -8 kcal mol^{-1} and **F** has a net stabilization of -9 kcal mol^{-1}. The increased stability for these waters versus the analogous waters in the book structures is reflected by a greater stabilization of the bag **E** and **F** oxygen atoms (-46 kcal mol^{-1}), the HB-hydrogens' destabilization of 36 and 35 kcal mol^{-1}, and non-HB hydrogens' destabilization of 3 and 2 kcal mol^{-1}. It is apparent in the bag structure that for **sd,sa** environments the net stabilization depends largely on neighbouring waters, *i.e.* whether it receives a HB from a double donating or a double accepting water. As in the book structures, the double donating water is more stable than the double accepting water.

5.4.2.3 Cage

Figure 5.5 represents the atomic energy changes in the cage cluster. There are 8 hydrogen bonds and an even distribution of bonding type environments for the waters:

two are single donors, single acceptors (**F**, **A**), two are double donors and single acceptors (**B**, **D**), and two are single donors but are double acceptors (**C**, **E**).
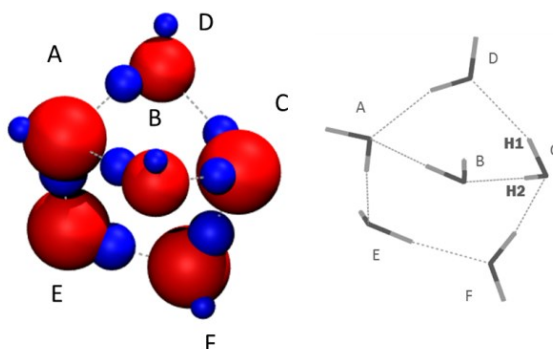

Figure 5.5. Localized energy changes for formation of 3D cage hexamer. Stabilized atoms are red and destabilized atoms are blue. The sphere diameter is proportional to the atomic energy stabilization, $\Delta E(A)$. The wireframe structure indicates labelling for waters where both hydrogens participate in HBs; in all other cases H1 is the HB hydrogen and H2 is the non-HB hydrogen.

In the cage system the impact of a neighbouring water on net stability is evident. Consider the two double donor waters **B** and **D**, having a stabilization of -9 kcal mol^{-1} and -7 kcal mol^{-1}, respectively. The lower stability in **D** is a result of its neighbouring water molecules: it donates hydrogen bonds to two waters which are both double accepting oxygens, creating an anti-cooperative interaction. **B** donates to a **sd,sa** water (**A**) and to a **dd,sa** water (**C**), which allows for an enhanced cooperative interaction with **A**. Much larger values for the atomic stabilizations of **B** *vs.* **D** reinforce this cooperative picture: the oxygen is stabilized by -48 kcal mol^{-1} in **B** but only -35 kcal mol^{-1} in **D** and the HB-hydrogens are destabilized by 24 and 15 kcal mol^{-1} in **B**, compared to 15 and 13 kcal mol^{-1} in **D**. In the double accepting waters, **E** and **C**, the total stabilization is the same for both (7 kcal mol^{-1}) however at the atomic level **E**'s larger oxygen stabilization (-49 kcal mol^{-1} in **E** *vs.* -42 kcal mol^{-1} in **C**) is offset by an equally larger HB hydrogen destabilization (36 kcal mol^{-1} for **E** *vs.* 30 kcal mol^{-1} for **C**). The non-HB hydrogen in **E** is slightly more destabilized than in **C**, 6 kcal mol^{-1} *vs.* 5 kcal mol^{-1}. Since water **E** donates to a double donating water (**B**), it has a greater cooperative stability than **C**, which donates to a single donating, single accepting water (**F**). Comparing the two single donating, single accepting waters (**F**, **A**), water **F** donates to a double accepting water, receives from a double accepting neighbour, and is stabilized by -8 kcal mol^{-1}. Water **A** donates to a

70

double donating water and receives from a double donating water and is stabilized by -9 kcal mol^{-1}. The atomic energy values for **F** and **A** are similar: oxygens are both stabilized by -38 kcal mol^{-1} and HB-hydrogens are both destabilized by 27 kcal mol^{-1}; however, the non-HB hydrogen is destabilized by 3.0 kcal mol^{-1} in **F** and only 2.0 kcal mol^{-1} in **A**. The double donating system is slightly more cooperatively stabilized than the double accepting system. What is interesting is that the non-bonding hydrogen again pays the price for the less favourable double accepting interactions. The cage structure also has an interesting topology point which may affect the overall cluster stability: it has an oxygen-oxygen bond critical point between waters **D** and **B**. The critical point topology of the clusters is discussed in a later section.
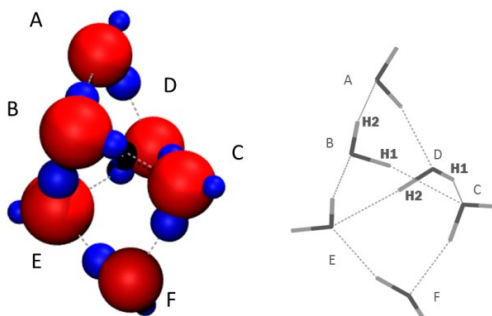
5.4.2.4 Prism
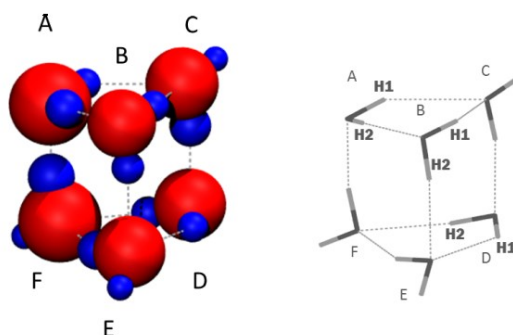
Figure 5.6 . Localized energy changes for formation of 3D prism hexamer. Stabilized atoms are red and destabilized atoms are blue. The sphere diameter is proportional to the atomic energy stabilization, ΔE(A). The wireframe structure indicates labelling for waters where both hydrogens participate in HBs; in all other cases H1 is the HB hydrogen and H2 is the non-HB hydrogen.

Figure 5.6 represents the atomic energy changes in the prism configuration. In the prism system, there are no singly-accepting and singly-donating waters; instead, all waters interact with three other water molecules, either as double donor, single acceptors (**A**, **B**, **D**) or as single donor, double acceptors (**C**, **E**, **F**). The **dd,sa** waters **A** and **D** are highly stabilized, by -12 and -10 kcal mol^{-1}, respectively, with atomic values of -48 and -38 kcal mol^{-1} for oxygens in **A** and **D** respectively, 23 and 12 kcal mol^{-1} for the HB-hydrogens in **A** and 16 and 11 kcal mol^{-1} for the HB-hydrogens in **D**. The strongly stabilized **A** receives from a single donor, double acceptor (**F**) and donates to one **sd,da**

and one **dd,sa**. Water **D**, which is slightly less stabilized than **A** and has smaller atomic energy changes, donates to two **sd,sa** waters, and has a reduced cooperative stability versus **A**. The final double donor, single acceptor water, **B**, has a total stabilization of only -6 kcal mol. The oxygen in **B** is stabilized by -34 kcal mol^{-1}, and its HB-hydrogens are destabilized by 15 and 12 kcal mol^{-1}. Although it is a double donor, which means an opportunity for increased cooperative stability, it receives a HB from a double donor and donates to two waters which are both double acceptors – these are anti-cooperative interactions and result in a lower net stabilization. Waters **C**, **E** and **F** also provide an interesting opportunity for analysis: **E** has a net stabilization of -8 kcal mol^{-1} and atomic stabilities of -38 kcal mol^{-1} for the oxygen, 25 kcal mol^{-1} for the HB hydrogen, and 5 kcal mol^{-1} for the non-HB hydrogen; **C** has a net stability of -6 kcal mol^{-1} and atomic stabilities of -38 kcal mol^{-1} for the oxygen, 29 kcal mol^{-1} for the HB hydrogen, and 3 kcal mol^{-1} for the non-HB hydrogen; and **F** has a net stabilization of -6 and atomic stabilities of -49 kcal mol^{-1} for the oxygen, 37 kcal mol^{-1} for the HB hydrogen, and 6 kcal mol^{-1} for the non-HB hydrogen. The atomic energy changes in **C** and **E** are similar for oxygens and HB-hydrogens whereas in **F** the oxygen and HB hydrogen have a much stronger stabilization and destabilization, a difference of about 10 kcal mol^{-1} each. Water **F** accepts one HB from a double donor water and one HB from a single donor water whereas waters **C** and **E** receive both of their hydrogen bonds from waters which are double donors. The large atomic energy changes in **F** (which only receives from one double donor) indicate that there is greater cooperativity present than in **E** and **C**. It is the large destabilization of **F**'s non-HB hydrogen that serves to give it a net lower stability, resulting from the anti-cooperative **sd,da** environment. It is particularly evident in the prism structure that the local stability of a water molecule is highly dependent on the type of bonding interactions with its neighbouring water molecules. In the prism case it is also evident that the stability of the *non*-HB hydrogen can have a significant impact on the overall stability of the water cluster. A further consideration regarding the electronic behaviour in these water interactions is the impact of higher order electron correlation (*i.e.* not available in MP2 analysis). These correlation effects influence the relative interaction energies of the six hexamer isomers discussed above [17-148] removing the near degeneracy of the prism and cage structures. The 3D structures are more stabilized

than the planar structures [88], with the largest influence of correlation observed for the planar structures [148]. Returning to our analysis of the cooperativity within each system, it is evident that these higher order correlation effects become most important when cooperativity is highest (planar, chair) and least important when it is diminished (3D, prism). The removal of near-degeneracy between the prism and cage isomers with inclusion of higher order correlation serves to emphasize the different interactions present in these systems that contribute towards their net stabilization.

To summarize the bonding interactions in the 3D clusters, the distribution of atomic energies discussed for all systems show that 1) relative to the other waters within the cluster, a double donating water in general is more stabilized and a double accepting water in general is less stabilized, 2) the stability of any water depends largely on the bonding environment of its neighbouring waters so that donating or accepting a HB to or from a double donating water is more stabilizing than donating or accepting a HB to or from a double accepting water, and 3) an increased 3D character of the water clusters yields an increased destabilization of the non-HB hydrogens. The amount of cooperative enhancement in the stability of a water molecule within these clusters may be inferred through the magnitude of the differences in their substituent atomic stabilities [4].

5.4.3 Bond critical point analysis

Previous reports have shown that the total electron density at bond critical points (BCPs) in water clusters is directly related to the overall stability of the structure [90]. We plot this relationship for the water hexamers in Figure 5.7. To further categorize the relative stabilities of the structures, total BCP densities were separated into contributions from either hydrogen bond (HOH$\cdots$O) or covalent bond (O-H) critical points. With respect to the total bond critical point density, increasingly stable clusters have increased density at BCPs. Interestingly, the cage, which is slightly less stable than the prism, has a total BCP density that is slightly (0.004 a.u.) higher. The cause for this may in part be due to an O-O bond critical point in the cage structure which increases the total BCP density by 0.0049 a.u.; the O-O BCP is discussed in more detail in the next section. In the relationship between hydrogen bond critical points (HBCPs) and total stability the prism

is a clear deviant, with a much lower total HBCP density despite having the greatest number of hydrogen bonds. The cage has the highest total hydrogen bond critical point density. For total density at covalent bond critical points there is no clear linear relation between the total covalent BCP density and the overall stability for the clusters, however, it is evident that systems having larger total HBCP densities also have smaller total covalent BCP density, again with the exception of the cage and prism structures.
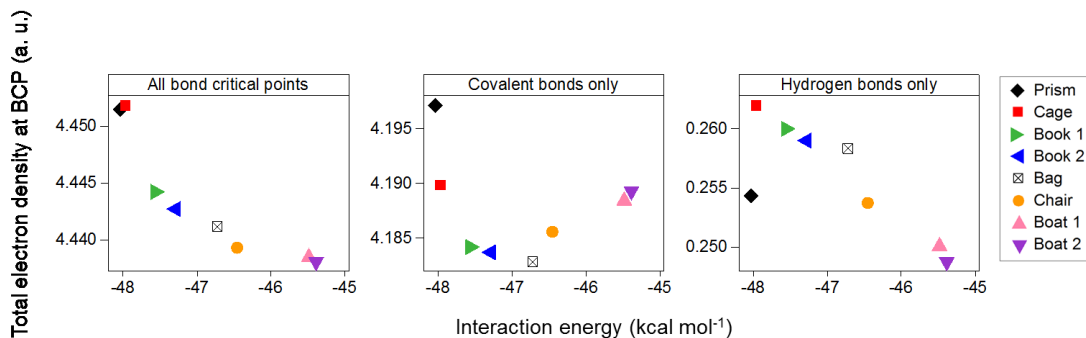
Figure 5.7 Total electron densities for bond critical points plotted relative to the interaction energy of each hexamer cluster. Left panel: all BCPs in the cluster (including cage O-O BCP). Center panel: only covalent (O-H) BCP densities. Right panel: only hydrogen bond (OH···O) BCP densities.

The stability distribution observed in the critical point densities reflects the cooperative influence on the hydrogen bonding in the clusters. Consider the prism, cage and chair systems, with nine, eight and six hydrogen bonds, respectively. The chair cluster has a simple donor acceptor arrangement forming hydrogen bonds that are enhanced by a strong cooperativity. The total density of the six HBCPs in the chair structure is 0.2537 a.u., which is 0.1055 a.u. greater than six "non-cooperative" HBs (defining a non-cooperative HB as that of an isolated water dimer, with HBCP density of 0.0247 a.u.). Although the cage has complicated bonding interactions, an equal distribution of **dd,sa**, **sd,sa** and **sd,da** waters results in a minimal amount of anti-cooperative interactions present and thus the possible cooperative interactions are maximized. The cage has a total HBCP density of 0.2620 a.u. which is 0.0644 a.u. greater than eight non-cooperative hydrogen bonds. For the prism, the equal number of double donor and double acceptor interactions, with no single donor, single acceptors, results in two strongly stabilized waters but also two waters which have a greatly reduced

stabilization from forced anti-cooperative interactions. The prism has a total HBCP density of 0.2543 a.u., which is only 0.0320 a.u. greater than would be expected for nine non-cooperative bonds. Considering the individual HBCP densities in the prism, we also note that there are five hydrogen bonds that have HBCP densities *lower* than that of the dimer. There are four such HBCPs in the cage, two in the bag, one in each book 1 and book 2, and none in the 2D chair and boat structures. The bond critical point values for all structures can be found in Figure 5.8.
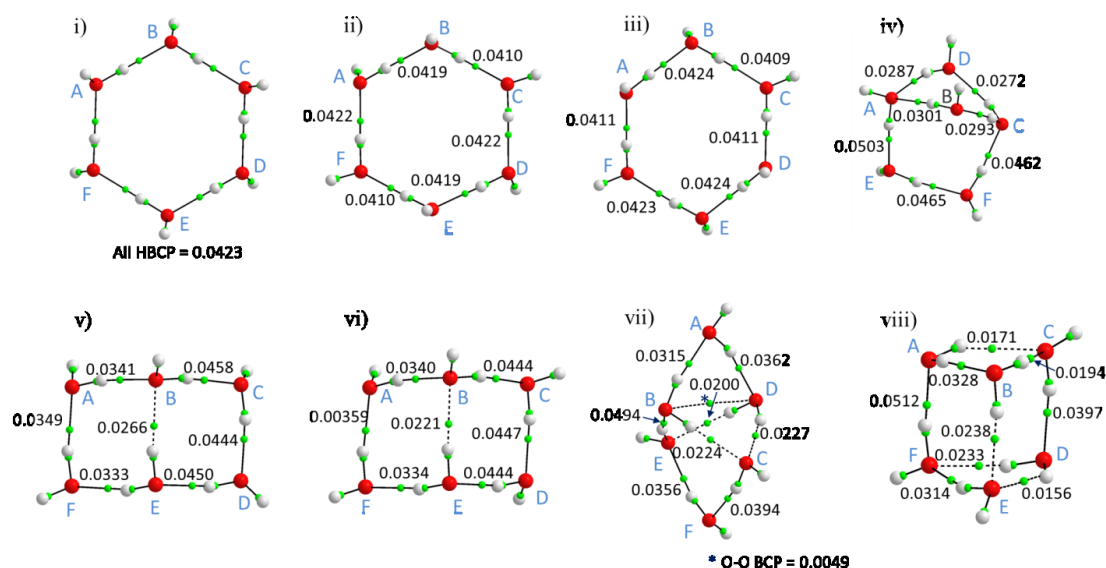
Figure 5.8 Molecular graph plots of hexamer structures showing bond critical point electron density values (a.u.) for all hydrogen bonds plus O-O interaction in cage structure. The HBCP value for the dimer is 0.0247 a.u. Complete critical point data (including covalent bonds) is available in the supporting information. Plots were created using AIMAll.

5.4.4 Oxygen-oxygen bond critical point

As well as the expected covalent and hydrogen bond critical points in the cage water clusters, there is also an oxygen-oxygen (O-O) bond critical point found between waters **D** and **B**. Pakiari and Eskandari [164] studied a set of enol forms of *cis*-β-diketones and have provided detailed analysis on what constitutes a stabilizing O-O interaction for those systems, including bond lengths, density at BCPs and ellipticity. We note that in the cage cluster the O-O distance is 0.51 Å longer than the longest reported O-O distance in the Eskandari study (2.90 Å) and has a BCP density of 0.0049 a.u., just over half of their

reported lowest value (0.0088 a.u.). Jenkins *et al*. [165] have closely studied the critical point topology for clusters of 4, 5, and 6 waters. They report that structures containing O-O critical points with highly strained bond paths (designated by the deviation of bond path length, BPL, from the bond length) can be more energetically stable if they obey Bernal-Fowler ice rules, but are otherwise unfavourable. In the cage cluster reported here the BPL deviation is very small, only 0.005 Å. Although Jenkins *et al*. do not discuss an O-O bond critical point for the cage structure, they report an O-O BCP in the boat structures which is not present in our evaluation at the SCVS MP2/aug-cc-pVTZ level. There is an O-O BCP in the boat structures when evaluated at the SCVS MP2/6-311++G(d,p) level. This impact of *type* of basis set (*e.g.* Pople *vs.* Dunning) on the electron density topology is interesting given the level of theory. We note that the boat O-O BCP, with a very small value of electron density (0.00024 a.u.) and very large ellipticity (2.33), is not a stable point in the density topology. The O-O BCP in the cage is present when evaluated with either Dunning or Pople basis sets. Despite the cage O-O BCP density being significantly larger than in the boat (0.00487 a.u. for the Dunning basis set using SCVS), one might still argue that this is not a stabilizing interaction for the cage structure due to its large ellipticity value (1.85). We would, however, like to point out that there is a low vibrational frequency (O-H-O bending) present in the cage structure that brings the oxygens closer by ~0.2 Å (unscaled). It is possible that this could become a stabilizing interaction when this vibrational mode is accessible to the cluster (*i.e.* at temperatures above 0 K). It could be argued that any geometry change will cause the marginally stable critical point to simply disappear (see reference [1], p. 84), however given the non-vanishing value of electron density at the BCP this is not likely. We conclude that this O-O BCP is a stable point on the cage topology and contributes to the overall stability of the cage structure.

5.5 Summary and Conclusions

In this report we used changes in atomic energies to describe the local stabilization of water molecules and their constituent atoms in eight low-lying water hexamer clusters: prism, cage, bag, book 1, book 2, chair, boat 1, and boat 2. The atomic energies provide

critical insight into the unequal distribution of stability within each cluster and a reduced potential for cooperative stability as the dimensionality of the clusters increases from 2D to 3D, where the hydrogen bonds may be either cooperatively stabilized or anti-cooperatively destabilized. In the chair system, all hydrogen bonds are cooperatively stabilized to an equal extent, resulting in similar energy changes within each atom type (oxygens, hydrogen bonding (HB) hydrogens and non-HB hydrogens). In the boat systems, small deviations from symmetry result in similarly small deviations in distribution of atomic stability; narrowed OH⋯O angles and increased bond lengths reflect the lowered atomic stabilizations in the waters. For the 3D systems (boat 1, boat 2, bag, cage and prism), the atomic stabilization varies widely depending on the water in question and the bonding interactions of its neighbours. The number of HBs for each water, as well as the arrangement and number of hydrogen bonds formed by neighbouring waters, can enhance or diminish the net stabilization. In general, waters which donate both hydrogens to form double donating interactions have an increased stabilization and waters which accept two hydrogen bonds experience a decrease in stabilization, as a result of cooperative and anti-cooperative effects. Similarly, waters that interact with a double donor water are more stabilized than waters that interact with a double acceptor water. In many cases a water molecule may have a largely stabilized oxygen atom but an overall stabilization that is diminished due to the destabilization of the water's hydrogen atoms. In the prism structure the formation of a maximum number of hydrogen bonds (with all waters either doubly donating or doubly accepting) comes at the price of a lowered overall decrease in the strength of most of these hydrogen bonds along with a large destabilization of the non-HB hydrogen atoms.

Bond critical point (BCP) electron densities indicate that the chair system has the greatest cooperative stability of the clusters, with the highest values of electron density at hydrogen bond BCPs and reduced covalent BCP densities. The cage is at a balance point having both large covalent BCP densities and large hydrogen bond BCP densities. The overall stability in the prism is largely due to strong covalent bonds rather than strong hydrogen bonds; it has the lowest average BCP density per HB. The cage structure also has an oxygen-oxygen bond critical point which may factor into the experimentally observed stability of the structure.

77

5.6 Acknowledgements

Supporting Information

Geometric parameters for SCVS-MP2 optimized water hexamers and QTAIM atomic properties including bond critical point data. This material is available free of charge via the Internet at http://pubs.acs.org.

5.7 Chapter Summary and Relevance

In this chapter, as in Chapter 4, it is found that the oxygen atoms are stabilized and the hydrogen atoms are destabilized in the water hexamers. The planar-like hexamer systems (chair and boat 1 and 2) continue the trend of a non-linear increase in atomic energy change as number of hydrogen bonds increases (cooperative stability) as was observed for the trimer to pentamer clusters. This cooperative trend is diminished when clusters change from nearly planar to three-dimensional. The prism, cage, and bag clusters can have local water stabilities differing up to 5 kcal mol^{-1} as a result of mixed cooperative and anti-cooperative interactions. Atomic energies reveal that in many cases a water molecule may have a largely stabilized oxygen atom but the net water stability will be diminished due to the destabilization of the water's hydrogen atoms. Analysis of bond critical point (BCP) electron densities shows that the reduced cooperativity results in a decrease in hydrogen bond strength and an increase in covalent bond strength, as is most evident in the prism. This chapter demonstrates that QTAIM energy analysis is a useful tool to evaluate a variety of complicated water-water hydrogen bond interactions.

Chapter 6   Cooperativity Between Hydrogen Bonds and Beryllium
Bonds in $(H_2O)_nBeX_2$ (n = 1–3, X = H, F) Complexes. A
New Perspective.
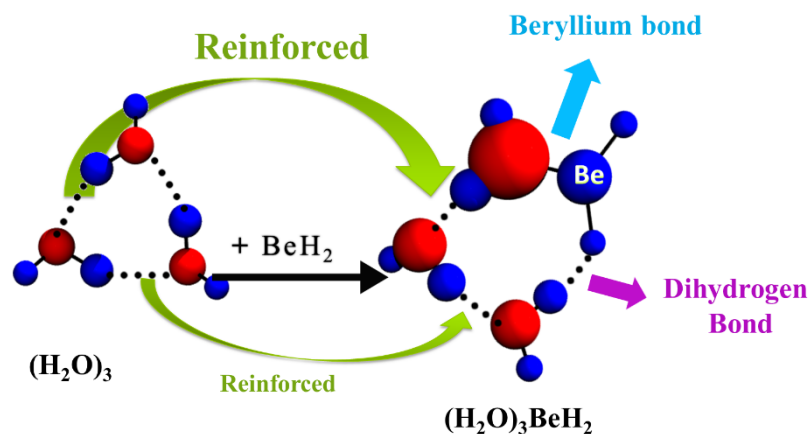
The following chapter was a collaborative effort. The contribution from this author was to provide the QTAIM energies analysis and some discussion related to the atomic energies. The chapter is included in this thesis because it provides a useful example of the application of atomic energy analysis to small cluster systems which incorporate elements other than those in pure water clusters (beryllium and fluorine). It also demonstrates the use of a theoretical method other than MP2 for the analysis of atomic energies.

6.1 Abstract

The interaction of BeX_2 (X = H, F) with water molecules has been analyzed at the B3LYP/6-311+G(3df,2p)//B3LYP/6-31+G(d,p) level of theory. The formation of strong beryllium bonds between water molecules and the BeX_2 derivative triggers significant electron density redistribution within the whole system, resulting in significant changes in the proton donor and proton acceptor capacity of the water molecules involved. Hence, significant cooperative and anti-cooperative effects are present, explaining why there is no case in which the global minimum corresponds to a tetracoordinated beryllium atom. In fact, the most stable clusters can be viewed as the result of the attachment of BeX_2 to the water trimer and the water dimer, respectively, and not as the result of the solvation of the BeX_2 molecule. We have also shown that the decomposition of the interaction energy into atomic components is a reliable quantitative tool to describe all the closed-shell interactions present in the clusters investigated herein, namely hydrogen bonds, beryllium bonds and dihydrogen bonds. Indeed, we have shown that the changes in the atomic energy components are correlated with the changes in the strength of these interactions, and they provide a direct quantitative measure of cooperative effects directly in terms of energies.

6.2 Introduction

Beryllium and its derivatives are extensively used in the chemical industry [166-167] [168]. Just to mention a few of their applications, elemental Be is employed as an alloying agent, in a low percentage, to produce age-hardening alloys such as BeCu [169] [170] with many applications in the electronics industry [171-173]. Its high melting point, low density and high thermal conductivity make it a useful material for heat dissipation [174-175]. Since the 1980's it has been used to fabricate lightweight mirrors with good dimensional stability [176-178]. Due to its low thermal neutron absorption, Be is also employed as moderator in nuclear reactors. Its oxide is a very good heat conductor, but at the same time is an excellent electrical insulator used in telecommunications and in ceramics [179-182]. Its chloride derivative catalyzes the Friedel-Crafts reaction and

forms many interesting complexes [166]. Be and its compounds are however very toxic, mainly if inhaled as dust leading to the so-called *chronic beryllium disease* [183-185]. This has motivated much interest in unraveling the mechanisms behind the high toxicity of this element. In some of these studies it has been suggested that Be acts as a "tetrahedral proton" displacing H^+ from strong hydrogen bonds [186-190]. This implies that strong hydrogen bonds are an ideal binding site for Be. Besides, this new binding mechanism seems to explain how Be migrates through a biological system passing from one protein to another via exchangeable hydrogen bonds [190].

These ideas are essentially based on the formal similarity between H^+ and Be^{2+} ions. Furthermore, neutral beryllium derivatives have been shown to lead to very strong closed-shell interactions with typical Lewis bases, forming what have been named *beryllium bonds* [191] because of their similarity with conventional *hydrogen bonds*, with which they share some common characteristics [191]. One of the most important signatures of many closed-shell interactions is cooperativity, reflected in changes in their strength when more than one of these interactions occurs in the same system. Cooperativity has been extensively studied in hydrogen bonded systems, [127, 192-208] but it is also present in other weak interactions [209]. In this respect, it has been shown very recently that cooperativity is rather strong between beryllium and inter- or intra-molecular hydrogen bonds, in such a way that the strengths of both closed-shell interactions become mutually altered [210]. For instance, the intramolecular hydrogen bond (HB) holding together the imidazole dimer becomes significantly reinforced when the imidazole monomer acting as the proton donor forms a beryllium bond with BeH_2 or BeF_2 [210]. Also of importance, when the BeX_2 molecule is attached to the imidazole acting as the HB acceptor, the HB cleaves and is replaced by a beryllium bond and a dihydrogen bond (structure **a** in Scheme 1). One of the most important findings is that the complex in which Be is tetracoordinated to the two X ligands and the two imidazole molecules (structure **b** in Scheme 1) is not the global minimum on the potential energy surface, as might be expected [210].
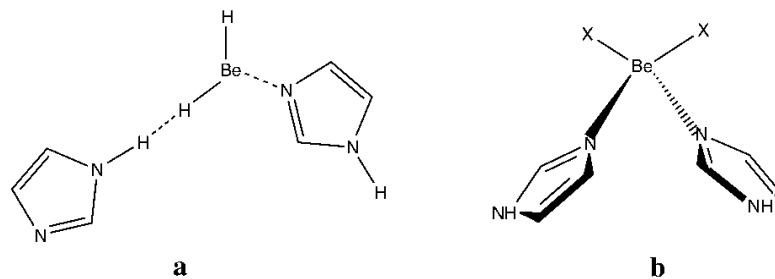
Scheme 1

Hence, although Be has a clear propensity to be tetracoordinated [186, 188, 189, 211-212], the formation of beryllium bonds may favor arrangements in which the level of coordination is clearly smaller, because of the significant electron density redistribution associated with the formation of beryllium bonds.

Since water is ubiquitous in the physiological medium, significant attention was paid to the way in which Be^{2+} interacts with water. It seems well established that Be^{2+} forms tetracoordinated clusters when interacting with water [188, 212-213], followed by the deprotonation of one of the water molecules. It is not evident however whether this arrangement would be preferred when Be is already attached to two ligands but is still able to form stable beryllium bonds. Hence we have considered it of interest to investigate here the effects that beryllium bonds may produce on the hydrogen bonds which stabilize water clusters. For this purpose we have taken as suitable model systems the water dimer and the water trimer interacting with both BeH_2 and BeF_2.

6.3 Computational details

In our theoretical survey of the complexes between the water dimer and trimer with BeX_2 (X = H, F) we have used the B3LYP hybrid density functional method [214-215], because it has been shown to be well suited for the description of water clusters [196, 216-217], provided that a sufficiently flexible basis set is used. As well, this hybrid functional provides a reliable description of beryllium bonds [191]. More importantly, B3LYP has been shown, using G4 calculations as a reference, to be a reasonable choice when trying to describe simultaneously beryllium bonds and hydrogen bonds [210]. In fact other functionals that performed better than B3LYP as far as the description of HBs

83

is concerned, such as X3LYP, M05-2X, M06-2X or B97-D methods, turn out to not be a good alternative when both beryllium bonds and hydrogen bonds coincide in the same system [210]. This is because they underestimate the strength of the former, but overestimate the strength of the latter, whereas the B3LYP approach slightly underestimates the strength of both closed-shell interactions [210]. Nevertheless, using the clusters of BeH_2 with two water molecules as a suitable benchmark case we have verified that the relative stability order found at the B3LYP level is in agreement with the one obtained through CCSD(T)/cc-aug-pVQZ single point calculations carried out on CCSD/6-31+G(d,p) optimized geometries (see Table B.1 of the supporting information Appendix B.3).

For the geometry optimizations and the evaluation of the harmonic vibrational frequencies a 6-31+G(d,p) basis set expansion was used. Final energies were evaluated in single point calculations carried out with a larger 6-311+G(3df,2p) basis set. The harmonic vibrational frequencies were used to assert that the stationary points found were local minima (having no imaginary vibrational frequencies) on the corresponding potential energy surface (PES). The interaction energies (E_{int}) have been calculated by subtracting from the total energy of each complex the energies of the isolated monomers in their equilibrium conformation.

Beryllium bonds are characterized by a significant charge transfer from the lone-pairs of the Lewis base (in this case the oxygen-lone pairs of a water molecule) towards the empty p orbital of Be and to the $\sigma_{BeX}*$ antibonding orbital of the BeX_2 moiety [191]. An efficient way to quantify these charge transfer interactions is through the NBO second order interactions between the occupied orbitals of the Lewis base (the water cluster) and the empty orbitals of the BeX_2 Lewis acid [218]. Also in the framework of this approach it is possible to calculate the Wiberg bond orders which also provide a good quantitative measure of the strength of the bond [219].

An alternative and complementary view can be obtained through the quantum theory of atoms in molecules (QTAIM) [1, 57], based on a topological analysis of the electron density. Using this approach it is possible to define the so-called molecular graphs of the system as a three-dimensional plot, which shows the positions of the maxima of the density, associated with the positions of the nuclei, as well as the first-order saddle points

(usually called bond critical points, BCPs). The molecular graph is completed by adding the bond paths, which are the lines connecting two neighbor maxima, passing through the BCP between them. The electron density, the Laplacian of the density, and the energy density calculated at the BCPs provide useful information about the strength and nature of the interaction between two atoms in the molecular system.

A further perspective is available within the framework of QTAIM is based on the evaluation of atomic energy components [3-4]. QTAIM defines atoms as open systems bounded by zero flux surfaces, called atomic basins. Integration over these basins yields very accurate atomic information. The QTAIM method is well documented and further technical details for atomic energy evaluation are described in reference [4]. It has been demonstrated [3-4] that atomic energies are a useful tool for describing internal energy changes in weakly bound systems. The changes in atomic energies correlate to changing atomic stabilities within the system, thus giving insight into the distribution of the stabilization and destabilization present in the BeX_2:H_2O moieties. The atomic energy changes for the clusters are calculated with respect to the energy of each atom as it exists in the BeX_2 or H_2O monomer. Gaussian 09 [70] was used to generate the B3LYP/6-31+G(d,p) wave functions which were then analyzed using the AIMAll suite of programs to evaluate the QTAIM properties [69].

6.4 Results and discussion

The molecular graphs of the clusters formed by two and three water molecules with BeH_2 are shown in Figure 6.1. The analogous graphs for the BeF_2 complexes are shown in Figure B.1 of the supporting information (Appendix B.3). Figure 6.1 also includes the molecular graphs of BeH_2, H_2O:BeH_2, water dimer and water trimer, in order to facilitate the discussion of cooperative effects. The nomenclature adopted hereafter is as follows: the water dimer:BeX_2 clusters will be named in general as **WD(BeX$_2$)**. The different stable minima will be identified by adding **a**, **b** to this acronym, following a decreasing stability order. The same convention will be used to name the clusters involving three water molecules, the general acronym being in this case **WT(BeX$_2$)**.
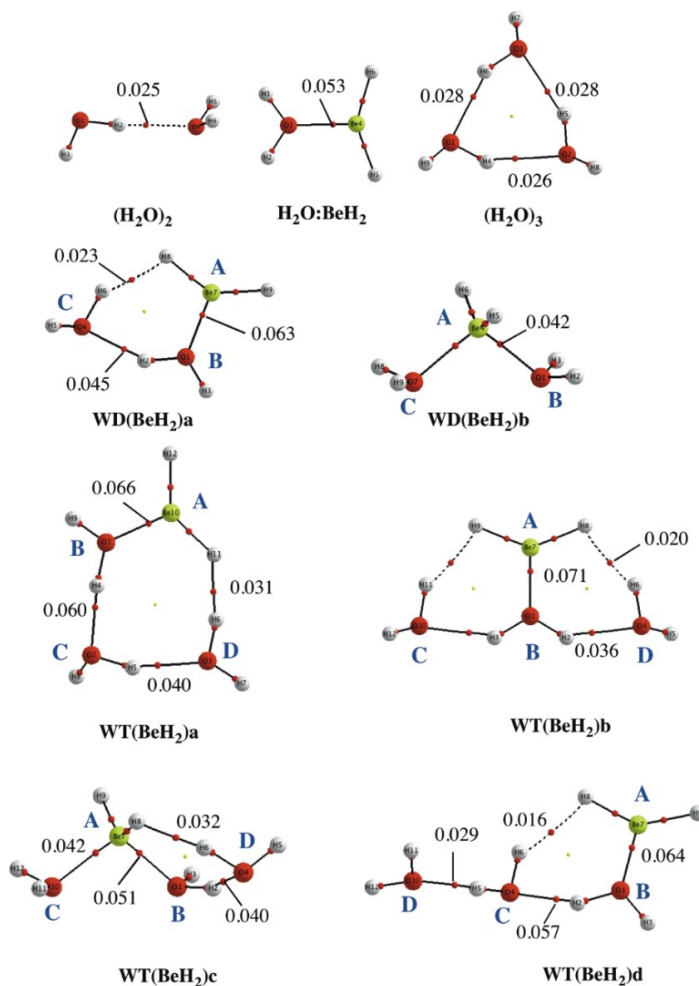
Figure 6.1 Molecular graphs of H$_2$O:BeH$_2$, water dimer, and water trimer and the optimized clusters formed by two and three water molecules with BeH$_2$. Red dots denote BCPs. Electron densities are in a.u. **A** and **B** denote respectively the BeH$_2$ molecule and the water molecule attached to through a beryllium bond.

The corresponding optimized geometries are summarized in Table B.2 of the supporting information. Table B.3 collects the B3LYP/6-31+G(d,p) and B3LYP/6-311+G(3df,2p) total energies. The interaction energies as well as the relative energies of the different complexes, referring to their corresponding global minima, are given in Table 6.1. The interaction energies of the water dimer and water trimer, as well as those of H$_2$O:BeH$_2$ and H$_2$O:BeF$_2$ are also reported to facilitate the analysis of the results. For the sake of simplicity, in what follows we will discuss in detail only the characteristics of

the BeH_2 clusters, which can be easily extended to the clusters that involve BeF_2 as the Lewis acid.

Table 6.1 Interaction energies (E_{int}, kJ mol^{-1})[a] and relative stabilities ($\Delta G°_{298}$, kJ mol^{-1})[b] of the complexes formed between water dimer and water trimer with BeX_2 (X = H, F).

S	WD(BeH₂)s		WD(BeF₂)s		WT(BeH₂)s		WT(BeF₂)s	
	E_{int}	$\Delta G°_{298}$	E_{int}	$\Delta G°_{298}$	E_{int}	$\Delta G°_{298}$	E_{int}	$\Delta G°_{298}$
A	-138.2	0.0	-159.9	0.0	-195.3	0.0	-220.8	0.0
B	-122.9	14.2	-148.1	12.5	-190.4	2.5	-219.1	0.05
C					-182.5	15.8	-214.0	11.7
D					-169.4	17.7	-192.4	19.2

[a] The interaction energies for the water dimer and the water trimer at the same level of accuracy are: -25.1 and -72.4 kJ mol^{-1}, respectively. The interaction energies for complexes $H_2O:BeH_2$ and $H_2O:BeF_2$ are -77.6 and -90.4 kJ mol^{-1}, respectively. [b] Relative stabilities have been calculated at the B3LYP/6-311+G(3df,2p)//B3LYP/6-31+G(d,p) level of theory.

For **WD(BeH₂)** complexes only two stable local minima have been located. Interestingly, the less stable one corresponds to the structure in which Be appears tetracoordinated forming two beryllium bonds with the water molecules. As could be easily anticipated, the interaction energy for the **WD(BeH₂)b** clusters is less than twice that of the $H_2O:BeH_2$ complex since, as shown by the electron densities at the BCP, the two beryllium bonds in **WD(BeH₂)b** are weaker than the one in $H_2O:BeX_2$. This is because in the former Be behaves as a double electron acceptor. The structure of the global minimum (**WD(BeH₂)a**) results from the attachment of the BeX_2 Lewis acid to the HB donor of the water dimer. For BeH_2 this structure is stabilized through the formation of an (O···Be) beryllium bond and a dihydrogen bond between one of the protons of water molecule **C** and an H in the BeH_2 moiety (note that for BeF_2 this latter interaction is replaced by a H···F hydrogen bond). Accordingly, the interaction energy for the **WD(BeH₂)a** complex is larger than the sum of the interaction energies calculated for water dimer and for the H_2O-BeH_2 complex. Note however, that the difference: E_{int}(**WD(BeH₂)a**) - E_{int}(water dimer) - E_{int}($H_2O:BeX_2$) (-35.5 kJ mol^{-1}) does not measure the strength of this additional H···H bond because in the **WD(BeH₂)a** complex non-negligible cooperative effects appear. A perusal of its molecular graph clearly shows that both the OH···O hydrogen bond and the Be···O beryllium bond become reinforced with respect to the isolated water dimer and the $H_2O:BeH_2$ complex. Hence, the enhanced

stability of the **WD(BeH₂)a** complex with respect to **WD(BeH₂)b** is not only due to the fact that the former is stabilized by three closed-shell interactions (one beryllium bond, one HB and one dihydrogen bond) instead of two (beryllium bonds), but also because two of these interactions are reinforced due to cooperativity effects. Indeed the beryllium bond becomes stronger in **WD(BeH₂)a** than in H_2O:BeH₂ because the water molecule **B** interacting with the BeH₂ molecule, is at the same time a proton donor to the water molecule **C**, enhancing its electron donor capacity. This reinforcement of the O···Be interaction is also reflected in the NBO characteristics of this bond. Whereas in the H_2O:BeH₂ complex the O-Be bond has a participation of 6% from the Be orbitals, its participation increases to 8% in the **WD(BeH₂)a** cluster. Also the Wiberg bond order goes from 0.290 to 0.336. The OH···O HB becomes reinforced as well, because the water molecule **B** acting as the HB donor is simultaneously acting as an electron donor to Be, which strongly enhances its proton donor capacity. On the top of that, the donor acceptor capacity of water molecule **C** is enhanced because **C** is not only a proton acceptor with respect to **B**, but also a proton donor in the OH···HBe dihydrogen bond with respect to **A.** Again, this is reflected not only in the increase of electron density at the BCP from 0.025 a.u. to 0.045 a.u., but also in the NBO second order orbital interaction energies, which show that while in the water dimer the interaction between the O lone pair of the HB acceptor and the σ_{OH}* antibonding orbital of the HB donor is 29 kJ mol^{-1}, the same interaction in the **WD(BeH₂)a** cluster amounts to 81 kJ mol^{-1}.

Four different local minima have been located for BeH₂ clusters involving three water molecules. The three less stable complexes arise from the solvation of **WD(BeH₂)a** and **WD(BeH₂)b** with a third water molecule. Starting from **WD(BeH₂)a**, when the third water molecule solvates the water molecule **B** directly interacting with BeH₂, one obtains the C₂ symmetry structure **WT(BeH₂)b**. If the third water molecule solvates water molecule **C** (the one not interacting with the BeH₂ molecule) then the much less stable cluster **WT(BeH₂)d** is obtained. Local minimum **WT(BeH₂)c** arises from the solvation of the Be tretracoordinated **WD(BeH₂)b** complex. Due to the symmetry of this complex, regardless of which water molecule is solvated (**B** or **C**) the resulting cluster is the same. The global minimum **WT(BeH₂)a** was obtained by attaching BeH₂ to one of the oxygen atoms of the water trimer. Although the three oxygens in the water trimer are not strictly

equivalent, no matter which oxygen is chosen for the BeH_2 attachment the optimization always yields **WT(BeH₂)a**. It is important to notice that in this cluster, one of the HBs in the water trimer has been replaced by a beryllium bond and a dihydrogen bond. Similar to what was already found for **WD(BeH₂)a**, in this case the cooperative effects are significant and responsible for the enhanced stability of this structure with respect to the tetracoordinated Be (**WT(BeH₂)b**). Indeed when the molecular graph of the complex **WT(BeH₂)a** is compared with that of **WD(BeH₂)a**, one may observe that besides the new, rather strong, HB formed between **C** and **D** (electron density of 0.040 a.u.), the electron density at the BCP of all the other closed-shell interactions increases: for the beryllium bond between **A** and **B** from 0.063 a.u. to 0.066 a.u., for the HB between **B** and **C** from 0.045 a.u. to 0.060 a.u. and for the dihydrogen bond between **D** and **A**, from 0.023 a.u. to 0.031 a.u. These changes in the electron density distribution reflect the changes in the charge transfer between the monomers integrated in the cluster. In fact, going from **WD(BeH₂)a** to **WT(BeH₂)a**, the O-Be bond further increases the participation of Be orbitals from 8% to 9%, whereas the Wiberg bond order goes from 0.336 to 0.442. Similarly the NBO interaction energy between the O lone pair of water molecule **C** and the $\sigma_{OH}*$ antibonding orbital of the water molecule **B** increases from 81 kJ mol^{-1}in the **WD(BeH₂)a** cluster to 140 kJ mol^{-1} in the **WT(BeH₂)a** cluster.

Cooperative effects also appear in cluster **WT(BeH₂)c**. A comparison of its molecular graph with that of **WD(BeH₂)b** shows that the beryllium bond between **A** and **B** is clearly reinforced whereas the other beryllium bond (between **A** and **C**) remains unperturbed. Also, the HB between both water molecules **B** and **D** is stronger than in the water dimer. Conversely, the formation of **WT(BeH₂)b** leads to both cooperative and anti-cooperative effects. The electron density at the beryllium bond critical point (between **A** and **B**) increases from 0.063 a.u. to 0.071 a.u., when going from **WD(BeH₂)a** to **WT(BeH₂)b** but the electron density at the HB critical points between the water molecules (**C-B** and **B-D**) and at the dihydrogen bond critical points (**A-C** and **A-D**) decreases from 0.045 a.u. to 0.036 a.u. and from 0.023 a.u. to 0.020 a.u., respectively. The enhancement in the stability of the beryllium bond reflects the increase in the electron donor capacity of the water molecule interacting with BeH_2 because it is acting as a double proton donor. For this same reason the HBs between this water molecule and the other two become weaker.

6.5 An alternative perspective in terms of atomic energy components

In this section we will show that the decomposition of the total interaction energy into atomic energy components offers a new perspective for analysis of the bonding characteristics of different closed-shell interactions, also accounting for the observed cooperative effects.

In Figure 6.2 we have plotted the same systems as in Figure 6.1, however the atoms are represented in a way to visually indicate the changes in atomic energy. Atoms experiencing a negative (stabilizing) energy change are red and atoms experiencing a positive (destabilizing) atomic energy change are blue. The size of the spheres representing the atoms is directly correlated to the magnitude of the atomic energy change. Thus a large red atom is greatly stabilized while a small blue atom is slightly destabilized. The values of the atomic energy changes have been labeled. The atomic energy changes are calculated with the respect to their value in the corresponding free monomer, evaluated in its equilibrium conformation. Atomic data for BeH_2 and BeF_2 systems as well as graphs for the $BeF_2:H_2O$ complexes are available in the supporting information (Appendix B.3).

The first conspicuous fact is that in water clusters the oxygen atoms become stabilized, whereas all hydrogen atoms become destabilized. This result quantitatively confirms the idea that the hydrogen atoms strongly contribute to mitigate the electron density redistributions produced by charge donations, ionizations or changes in the electronegativity of the heavy atoms of a molecular system. This explains for instance why the ring strain energy of the three-membered alkyl ring decreases dramatically on going from the perfluorinated cyclopropane molecule to unsubstituted cyclopropane, [220-221] or why the relative stability of carbocations and carboanions [222] decreases with their degree of substitution, and more recently why the interaction energies of $C_2H_2F_2$ with CuF are weaker than those calculated for the unsubstituted parent compound, whereas for C_2F_2, which does not contain hydrogen atoms, gives the opposite result [223].

Figure 6.2 Change in atomic energy for the formation of water dimer, trimer, and BeH$_2$:(H$_2$O)$_n$, n=1-3, systems. Values for the relative energy change of each atom are labeled (kJ mol^{-1}). Stabilized atoms are red, destabilized atoms are blue. Atom size corresponds to the magnitude of energy change. A, B, C, and D denote labels as in Figure 6.1. For hydrogens which are hidden the energy is included in parentheses. The atomic energies for the atoms in BeH$_2$ and H$_2$O monomers are: Be (-3.78x10^5), H (-2.02x10^3), and O (1.98x10^5), H (1.03x10^3), respectively, in kJ mol^{-1}. Structures were prepared using VMD software [114].

When a beryllium bond is formed, for instance in the $H_2O:BeH_2$ complex, the Be atom becomes systematically destabilized along with the hydrogen atoms attached to it, because the measure of stabilization is closely related to the accumulation of electron density on the atom in question. When a dihydrogen bond is formed, for instance in **WD(BeH₂)a**, the hydrogen of water molecule **B** participating in the bond destabilizes more than the H present as a spectator. Conversely, the negatively charged hydrogen atom of **A** participating in the bond is stabilized with respect to the one not directly taking part in it. Similarly, the hydrogen atom which participates in a HB is the one which destabilizes the most. Let us consider, for instance, the water trimer. The three hydrogens participating in the hydrogen bonds have destabilization energies around 100 kJ mol⁻¹, whereas for the H atoms which do not participate in the HBs these values are around 12 kJ mol⁻¹.

Furthermore, the larger the destabilization of the H atom participating in a HB the stronger the HB. This is clearly seen when comparing the values for the water dimer and water trimer. In the former, the relative atomic energy of the H atom participating in the HB is 61 kJ mol⁻¹, whereas in the latter these energies are around 100 kJ mol⁻¹, as it corresponds to stronger HBs in the trimer than in the dimer. Similarly, the greater the destabilization of the Be atom the stronger the beryllium bond in which it participates. Compare, for instance the values of $H_2O:BeH_2$ with those of **WD(BeH₂)a**).

These results clearly show that the changes in the atomic energy components mirror the corresponding changes in the strength of hydrogen bonds, beryllium bonds and dihydrogen bonds and therefore they should be able to account for the cooperative effects. In the previous section we have shown that in cluster **WT(BeH₂)a** cooperative effects reinforce the beryllium bond, the HB between **B** and **C**, and the dihydrogen bond between **D** and **A**. In perfectly harmony with these findings it is observed that on going from **WD(BeH₂)a** to **WT(BeH₂)a** the destabilization energy of the Be bond increases from 312 kJ mol⁻¹ to 324 kJ mol⁻¹ and at the same time the destabilization energy of the H of water molecule **B** participating in the HB, and the H atom of water molecule **D** participating in the dihydrogen bond also increases by 8.2 and 4.3 kJ mol⁻¹, respectively. It is worth noting that in the dihydrogen bond, not only the H of the water molecule becomes more destabilized (by 4.3 kJ mol⁻¹), but the H of the BeH_2 moiety becomes less

destabilized (by 10.8 kJ mol^{-1}). Finally, the atomic energy components also show that the new HB formed between water molecules **C** and **D** is weaker than the one present between **B** and **C**, since the destabilization energy of the H participating in the bond is 48.2 kJ mol^{-1} smaller. This is not surprising if one takes into account that molecule **B** transfers charge to Be and this dramatically enhances its intrinsic acidity and therefore its proton donor capacity. The same trends are observed for the complexes involving BeF$_2$ as shown in Figure B.2 of the supporting information. This figure shows that going from **WD(BeF$_2$)a** to **WT(BeF$_2$)a** the destabilization energies of the Be atom and of the H atoms participating in the **B-C** and **D-A** HBs increase by 5.8, 18.4, and 10.9 kJ mol^{-1}, respectively. Note that coherently, the stabilization energy of the fluorine atoms participating in the F$\cdots$H HB increases, in absolute value, by 19.7 kJ mol^{-1}.

The atomic energy components also account for anti-cooperative effects. This is apparent form the calculated values of cluster **WT(BeH$_2$)b** with respect to those of **WD(BeH$_2$)a**, from which it derives. The Be destabilization energy in the former is 15.9 kJ mol^{-1} larger than in the latter, indicating a clear cooperative effect. Conversely, the destabilization energy of the H atoms of molecules **C** and **D** participating in the HBs decreases by 5.9 kJ mol^{-1}, indicating in this case some anti-cooperativity. The same applies to the H atoms of both water molecules participating in the dihydrogen bonds, whose destabilization energies decrease by 10.0 kJ mol^{-1}. Coherently, the destabilization energy of the H atoms of the BeH$_2$ moiety involved in these dihydrogen bonds increases by 6.1 kJ mol^{-1}.

It should be emphasized that the advantage of using atomic energy components to analyze cooperative effects, with respect to other methods that are based on the analysis of the electron density, is that they provide a quantitative measure of these effects directly in terms of energies. In fact, when the weak interactions involved in the cluster are of the same kind, as for instance in the water trimer, the calculation of the energy of each of the three HBs involved in this cluster using the atomic energy components is straightforward. Additional work, however, is required to see whether it would be possible to calculate the energy of the closed-interactions stabilizing the clusters when they have a different nature, as in **WD(BeX$_2$)** or **WT(BeX$_2$)** complexes.

6.6 Conclusions

The interaction of BeX_2 (X = H, F) with water molecules leads to the formation of strong beryllium bonds. The significant electron density redistribution these closed-shell interactions produce in the whole system results in significant changes in the proton donor and proton acceptor capacity of the water molecules involved. This is evident from significant cooperative and anti-cooperative effects. The existence of cooperativity actually explains why the tetracoordinated beryllium atom is not present in the global minimum of complexes with two or three water molecules. In fact, the most stable clusters can be viewed as the result of the attachment of BeX_2 to the water dimer and the water trimer, rather than as the result of the solvation of the BeX_2 molecule. Thus, in the **WD(BeX$_2$)a** cluster the BeX_2 molecule interacts with the water acting as a HB donor, strongly reinforcing the water-water interaction and closing a ring through the formation of a dihydrogen bond with the HB acceptor. Similarly **WT(BeX$_2$)a** can be viewed as the result of replacing one of the HB in the water trimer with a beryllium bond plus a dihydrogen bond, also resulting in very large reinforcements of the water-water interactions.

We have also shown that the decomposition of the interaction energies in atomic components is a very reliable tool to describe all these closed-shell interactions and that it could very likely be extended to other interactions, such as halogen bonds or agostic interactions. The changes in the atomic energy components are correlated with the changes in the strength of the interactions, and can therefore account for cooperative or anti-cooperative effects.

6.7 Acknowledgments

6.8 Chapter Summary and Relevance

This chapter demonstrates that significant cooperative and anti-cooperative effects are present in the interaction of beryllium halides and its derivatives with small water clusters, which explains the lack of a tetrahedral global minimum for the beryllium interactions. Changes in the atomic energy components are correlated with changes in the strength of a variety of closed-shell interactions, including hydrogen bonds, beryllium bonds and di-hydrogen bonds, and provide a quantitative measure of cooperative effects directly in terms of energies.

Chapter 7   Water Wires Interacting With One or Two Ions
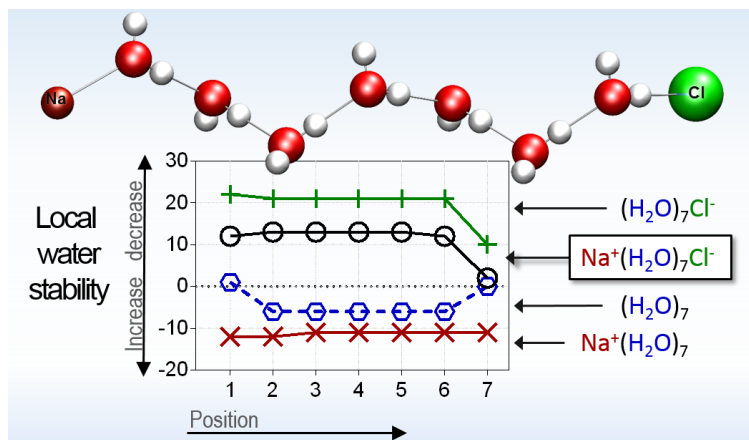
In the following chapter atomic energies are used to evaluate the local changes in water wires as they interact with ions. This local analysis, established in earlier chapters, allows the total stability of the water wire to be decomposed into contributions from the ion *vs.* contributions from the water molecules. An interesting trend is revealed: the stabilizing or destabilizing effect of the ions on the water molecules is correlated to the traditional classification of ions as structure makers or structure breakers. Visualization of atomic energy changes for the protonated water wires emphasizes the usefulness of this method for a simple visual assessment of local changes in stability. In the final section a counter ion is introduced to evaluate the effect of two opposing ions on the water wire. Bond critical point values as well as oxygen-oxygen bond distances are used to support atomic energy analysis.

7.1 Abstract

Water wires provide a necessary function in cells involving the movement of water molecules and ions across membranes. We report a series of high level *ab initio* (MP2) calculations on $(H_2O)_n$ water wires up to n=7, interacting with a set of halide ions and alkali and alkaline earth metal ions ($X = Cl^-, Br^-, F^-, H^+, Li^+, Na^+, K^+, Ca^{2+}$). We use Bader's atoms in molecules analysis (QTAIM) to report the change in local (atomic) stability within the water wire after the ion is introduced. Interaction with F^-, H^+, Li^+, and Na^+ results in the net stabilization of water relative to a neutral water wire. Interaction with K^+, Ca^{2+}, Cl^-, and Br^- yields a net destabilization relative to the neutral water wires. These trends reproduce properties of kosmotropic *vs.* chaotropic ions. Protonation of the water wire results in a clear shift in the local stability, with an asymmetric distribution of energy as the wire increases in length. Hydrogen-bonding H atoms are always destabilized, but the atomic energy for the non-hydrogen bonded H atoms increases for cations and decreases for anions. We also evaluate systems containing two ions, NaCl and KCl, separated by an n=7 water wire. The local water stability in the presence of a counter ion is essentially the sum of the individual influences of each isolated ion.

7.2 Introduction

Water wires are chains of water molecules connected through hydrogen bonds. They can be isolated in metal-organic frameworks [224-226], are present in aqueous acid-base neutralization [227-228] and play a key role in the mechanisms of some enzymes [229] [230]. Of particular importance is the nature of water wires in various forms of confinement, including carbon or boron nanotubes [231-236], hydrophobic crystal channels [237], and peptide-based nanotubes [238-240]. This keen interest is due in part to the fundamental role of water wires in cell life. They have an active role in many biological systems including aquaporins [241], potassium channels [242] and proton channels [243-248]. These membrane pores provide the mechanism for the movement of water molecules, ions and H+ protons in and out of cells [249]. Hydrophilic functional groups lining channel pores may be incorporated into the hydrogen-bonded chains

crossing cell membranes and local environment likely has a large role in the stability and function of water wires. Computational studies on water wires will thus often include a representation of the membrane pore, employing molecular dynamics (MD) analysis to maintain computational efficiency. In the MD approach, chemical interactions are modelled using sophisticated empirical approximations (forcefields) and have the ability to simulate dynamic behaviour of water and ions in the channels. A key shortcoming of forcefield representation is an over-simplified description of water behaviour. Common models such as TIP3P and SPC/E describe water molecules as non-polarizable point charges constrained to a rigid geometry, quantum behaviour such as bond breaking and proton transfer is not possible, and the models are generally parameterized to reproduce bulk water properties (see Appendix A.1). This design significantly influences the final water structure [233]. For example, lack of polarizability can have a substantial effect on the dipoles of water wires inside Gramicidin A channels [250]. Care must be taken when interpreting reports of novel hydrogen bond environments for water-filled channels described using these methods. We note that some approaches, *e.g.* the MS-EVB approach [251], do allow bond-breaking/formation and have been successfully applied to describe proton channels, despite not including water properties such as electronic polarizability and nuclear quantization [252].

An alternative to the MD approach is to use *ab initio* methods to evaluate isolated water wires. Early calculations applied Hartree–Fock (HF) analysis [253-254] to map the potential energy surface of proton transfer in water by evaluating the stability of $H^+(H_2O)_n$ wires in gas phase environment using frozen geometries. More recently, Patharasarthi *et al*. [255] fully optimized neutral water wires up to 20 molecules long using density-functional theory (DFT), HF and Møller-Plesset perturbation (MP2) approaches in gas phase to show that cooperativity increases at a much greater rate for water clusters than water wires. In fact, the systems of 3-7 waters did not form stable linear minima when optimized using the MP2 method but rather tended to optimize as clusters. Karakus *et al*. [256] used DFT to evaluate water wire formation in highly charged environments, in order to study water phenomena observed in mass spectrometry experiments. Sastry *et al*. employed DFT to study the subsequent binding energy of neutral clusters of water molecules [257] and chains of water interacting with a set of

mono- and divalent ions, considering the influence of ions on the cooperativity of the water interaction [258]. They found that cooperativity as well as the ions influence was reduced dramatically after addition of 2-3 water molecules.

Membrane pore channels can be highly ion-selective, and many factors governing their ion selectivity are still unknown. In part, this is because the nature of ion-water interactions remains a unique area of chemical discovery [259-264]. A recent experimental study has shown that water interacts cooperatively with negative ions and anti-cooperatively with positive ions [265], further reinforcing our interest in the nature of ion influence on water. Evaluating the local response of waters to ions in a water wire environment would provide novel insight into the nature of these interactions, perhaps elucidating details of the mechanism behind the impressive ion selectivity of some membrane pores. Such a study also provides an interesting one-dimensional look at the general behaviour of ion-water solvation.

In this report we evaluate the local properties of neutral water wires using MP2 analysis and Bader's quantum theory of atoms in molecules (QTAIM) [1]. We introduce a set of alkali, alkaline earth and halide ions to study how the waters within the water wires are influenced by positive or negative ions. Finally we evaluate two systems with paired-ion interactions to evaluate the influence of a counter ion. The QTAIM analysis provides the ability to isolate the properties of individual waters in each water wire and to directly compare the influence of the ions on the water wire. We also consider local bonding information obtained from bond critical point analysis as well as the geometries of the water wires.

7.3 Computational Methods

We study water wires up to 7 waters in length (~13 Å long) with a helix-type geometry. Although the length of a channel spanning a typical biomembrane may accommodate chains up to 20 waters long [266], the actual length of a water wire is likely to be less: either existing in a narrow region within a pore or interrupted by functional groups lining the channel of the pore. Additionally, the majority of studies on the

structure of hydration of ionic salts use a molar ratio of water to salts between 4-40, with a few studies up to 63 [261]. This corresponds to an approximate mean distance between ions of ~12 Å, on the order of a 7-water chain. The water wires were fully optimized using the MP2 method [32] with a Pople 6-311++G(d,p) basis set using Gaussian 09 [70]. An IEF-PCM water dielectric was included to help stabilize the water wires. The calculations also apply self-consistent virial scaling (SCVS) [61, 71] which improves the quality of the optimized wavefunction by simultaneously minimizing the energy with respect to a scaling factor for all coordinates, molecular orbital coefficients, and the molecular geometry [63]. After the wires were optimized, an ion was introduced at the appropriate end: H^+, Li^+, Na^+, K^+, Ca^{2+} at the hydrogen bond donor end, or F^-, Cl^-, Br^- at the acceptor end, and these structures were then fully optimized using the same level of theory. Frequency calculations were used to ascertain that all structures evaluated were true minima on the very complicated water potential energy surface. We emphasize that these water structures are not global minima, which would likely adopt a clustered geometry, but do represent local minima. The wavefunctions were evaluated using AIMAll [69] to calculate critical points in the electron density topology and to decompose the topology into local atomic contributions. There are many resources which describe critical point analysis in detail, including the correlation between the properties of the electron density at a bond critical point (BCP) and the nature of that bond [57, 267-272]. The local evaluation of atomic energies in water clusters has also been previously described in the literature [4-5, 7].

Local stability ($\Delta E(A)$) of atoms in the neutral water wire (W_n) were evaluated relative to the energy of the isolated water monomer,

$$\Delta E(\text{atom in } W_n) = E(\text{atom in } W_n) - E(\text{atom in monomer}) \qquad (7.1)$$

where n is the number of waters in the water wire and E is its atomic energy. Local atomic stabilities for the water wires plus ions (W_n^X) are evaluated according to the change in atomic energy relative to the neutral water wire,

$$\Delta E(\text{atom in } W_n^X) = E(\text{atom in } W_n^X) - E(\text{atom in } W_n) \qquad (7.2)$$

where X is the interacting ion. $\Delta E(X)$ is evaluated relative to an isolated ion. A decrease in atomic energy ($\Delta E(A)<0$) is stabilizing and an increase in energy ($\Delta E(A)>0$) is

destabilizing. The results are visualized by plotting the molecular system using colour-coded atoms, where an atom with $\Delta E(A){<}0$ is red and atom with $\Delta E(A){>}0$ is blue [3]. The size of the atom is also scaled so that it is proportional to the magnitude of energy change and relative atomic stabilities can be judged by visual inspection. A largely stabilized atom is represented by a large red sphere and a moderately destabilized atom is represented by a moderately sized blue sphere. If the energy change is very small (less than ± 1 kcal mol^{-1}) the atom is non-coloured (white) and will have a relative default sphere size of "1". These figures were generated using the VMD program [114]. All reported atomic energies are scaled by $(1 - \gamma)$ [1], according to the virial relation $\gamma = -V/T = 2$ where V and T are the potential and kinetic energies, respectively.

We define total interaction energy (E_{int}) as,

$$E_{int} = [E(W_n{}^X)] - [nE(H_2O) + E(X)], \qquad (7.3)$$

The relative interaction energy ($E_{int}{}^X$) is for a neutral water wire interacting with an ion. This is defined as the difference between the neutral water wire and the water wire plus the ion:

$$E_{int}{}^X = [E(W_n{}^X)] - [E(W_n) + E(X)], \qquad (7.4)$$

The relative interaction energy is equivalent to the sum of the atomic energy stabilities in the system, so that $E_{int}{}^X \equiv \Sigma \Delta E(A)$, where $E(A)$ is the energy of an atom in $W_n{}^X$. With respect to the effect of basis set superposition error (BSSE) on interaction energy, we use a large basis set which will minimize the BSSE [45]. Furthermore, it has been shown previously that while the effect of BSSE on water wires may lower the interaction energies slightly, all trends remained consistent for the sequential growth of the water wire [258].

7.4 Results and Discussion

7.4.1 Neutral Water Wire
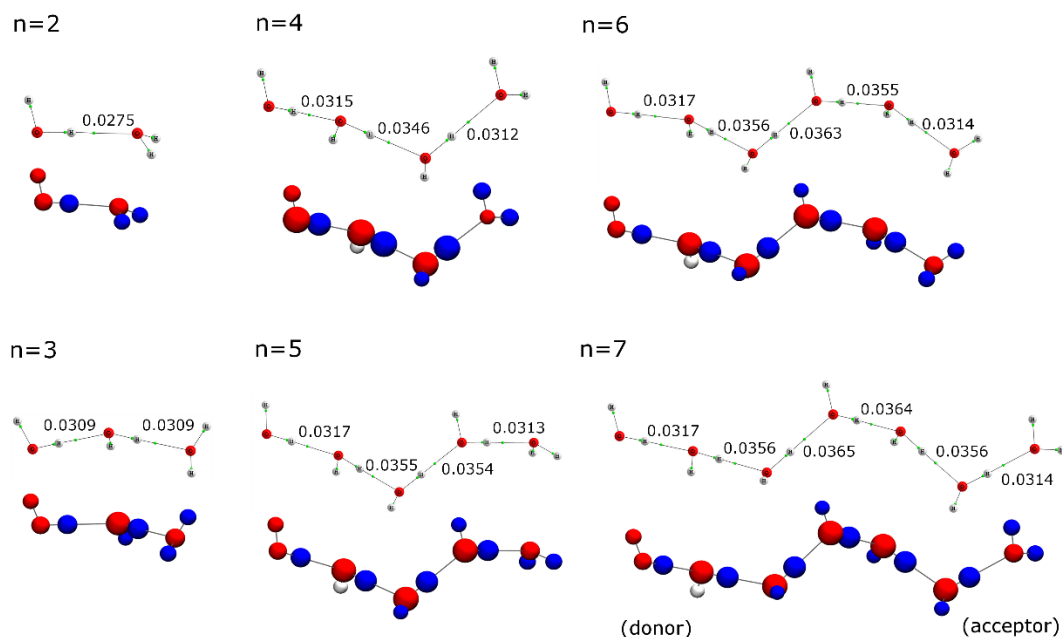
Figure 7.1 Optimized structures of the neutral water wires. Molecular graphs (top) and local energy changes (bottom). Green dots in the molecular graphs are bond critical points. Densities at hydrogen bond critical points are labelled in a.u. For atomic stabilities, stabilized atoms are red and destabilized atoms are blue. The sphere diameter is proportional to the atomic energy stabilization, $\Delta E(A)$, so that an atom with a larger energy change is shown as a larger sphere. For energy changes less than ±1 kcal mol^{-1} the sphere is coloured white. The hydrogen bond donor and hydrogen bond acceptor waters are indicated for the n=7 figure. The donor water will always be the first water from the left.

The optimized structures of the neutral water wires are represented as molecular graphs and as atomic energy stabilities in Figure 7.1. Neutral water chains have been discussed in previous reports and we focus our discussion on the changing local (atomic or water) stabilities of each water wire as length increases, relative to the energy of the water monomer. Local water stability is the sum of the stabilities of the atoms compromising that water. From Table 7.1 it is clear that the stability of the initial

donating water (far left, Figure 7.1) decreases as the chain increases in length, from -2 kcal mol^{-1} (stabilized) to +0.7 kcal mol^{-1} (destabilized), for n increasing from 2 to 7. The final accepting water (far right, Figure 7.1) decreases in stability from -3 to -0.5 kcal mol^{-1}. The central waters are the most stabilized, and also there is a slight asymmetry in the stability of the water wire, with the accepting side being more stable than the donating side. The non-hydrogen bonding hydrogen (H^{nHB}) on the first donating water does not experience significant change in local energy for wires with n=3 or greater. In terms of bond critical point analysis, the strength of the hydrogen bond interaction increases as the chain length increases. This is indicated by increased electron density at the hydrogen-bond bond critical points (HB-BCPs), predominantly at the center of the water wire. While the central waters have the strongest HB interaction, HB-BCPs also reflect the asymmetric distribution of the atomic stabilities: the HBs on the donating side are slightly stronger than the HBs on the accepting side. Previous reports have also indicated that HBs originating from the left or the right may have differing energies (depending on the local environment) [266].

Table 7.1. Energy per water in water wires n=2-7.

W	E(W)^a					
	n=2	n=3	n=4	n=5	n=6	n=7
1	-1.8	-0.6	0.1	0.5	0.8	0.7
2	-2.6	-7.3	-6.7	-6.4	-6.1	-5.9
3		-1.6	-7.0	-6.8	-6.5	-6.3
4			-1.1	-6.7	-6.6	-6.4
5				-0.6	-6.5	-6.3
6					-0.3	-6.2
7						-0.5
T^b	-4	-9	-15	-20	-25	-31

^{a} Energy in kcal mol^{-1}. E(W) = ΣE(H,O). ^{b} T is the total energy, T= ΣE(W) for W$_n$.

7.4.2 Ion Interaction

When the neutral water wires interact with an ion, each water will undergo a change in stability that depends on the nature of the ion. Cations interact with the oxygen at the donor end and anions interact with a hydrogen at the acceptor end. The energy changes

are defined relative to a neutral water wire, demonstrating the extent of the ion's influence if it were to interact with a water wire already formed, *e.g.* in a membrane channel (notwithstanding the environmental effects of the channel itself). The change relative to an isolated water monomer can be obtained by simple addition of the atomic stability of the neutral water wire (W_n) to the atomic stability of the water wire plus the ion (W_n^X).

The total interaction energy (E_{int}) for each ion-plus-water wire is plotted against wire length, n, in Figure 7.2a. It is clear that the ions have an overall stabilizing influence on the water wires and that this stabilization is constant as the length of the water wire increases, with the exception of H^+ where the influence of the extra proton on total stabilization becomes diminished as the chain length increases. The order of ion influence on net stability is $F^- > Cl^- > Br^-$ for anions and $H^+ > Ca^{2+} > Li^+ > Na^+ > K^+$ for cations. In terms of cooperativity ($E_{coop}=E_{int}/n_{HB}$, see Figure 7.2b), the neutral water wire shows the expected slight cooperativity [255] indicated by a gradual increase in interaction energy per hydrogen bond. For the water wires with the ion present, E_{coop} is decreasing, most dramatically in the H^+ case. This apparent loss of cooperativity is likely because the electrostatic ion interaction strongly overshadows the cooperativity of the hydrogen bonds in the water chain.
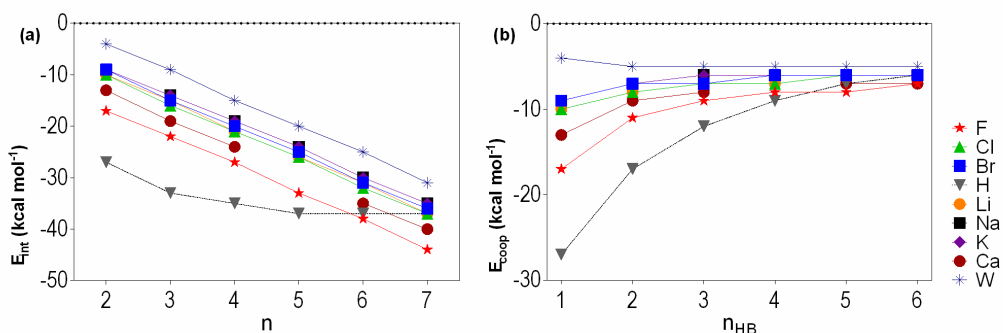
Figure 7.2 Total interaction energy, E_{int}, for ions interacting with water wires n=2-7 (a), and average energy per HB, $E_{coop}=E_{int}/n_{HB}$, where n_{HB}=number of hydrogen bonds (b). The x-axis is the number of water molecules in the chain.

Changes in local atomic stability *vs.* the neutral water wire (W_n) can be obtained by decomposing the relative interaction energy into contributions from each oxygen and hydrogen atom. In Figure 7.3, the stability of each oxygen atom (O), hydrogen bonded

hydrogen atom (H^{HB}), non-hydrogen bonded hydrogen atom (H^{nHB}), and hydrogen atom interacting with an ion (H^X) is plotted along the length of the water wire, for n increasing from 2 to 7 waters. The general shape of the curves, indicating the atomic stability moving from left to right along the water chain, is consistent for all n and the largest change in energy is clearly experienced by the atoms closest to the ion. After ~3 waters, the stabilities attain a constant value. The oxygen atoms are the largest contributor to the net stability of the water wire. Interestingly, the sign of the ion's formal charge does not determine if the oxygen will be stabilized or destabilized: Br^-, Cl^- and K^+ are destabilizing, while F^-, Ca^{2+}, Li^+ and Na^+ are stabilizing. The stability of the oxygens is also dependent on the length of the water wire; with the exception of Ca^{2+}, as the water wire increases in length the energy change for oxygen decreases in magnitude, indicating more or less stability depending on the nature of the ion. This influence on oxygen stability is greatest for Cl^- and K^+, followed by Li^+, Br^- and Na^+. For F^- and Ca^{2+} the oxygen stability is influenced largely by proximity to the ion, and only minimally by the lengthening of the water wire.

For the hydrogen atoms, it is clear that the local energy is not affected by the length of the water wire but depends only on proximity to the ion and the ion charge. This influence on stability approaches zero after ~3 waters from the ion. H^{HB}s are destabilized regardless of ion type, however the H^{nHB}s are destabilized for cation interaction but stabilized for anion interaction. In the cation systems, both hydrogens of the final accepting water molecule are destabilized between +10 to +4 kcal mol^{-1}, with Li^+ having the largest influence. In the anion systems H^X is destabilized between +7 to +3 kcal mol^{-1} while the non-interacting H on the same water is stabilized by -13 to -4 kcal mol^{-1}. Fluoride has the largest influence on the stability of H^X.
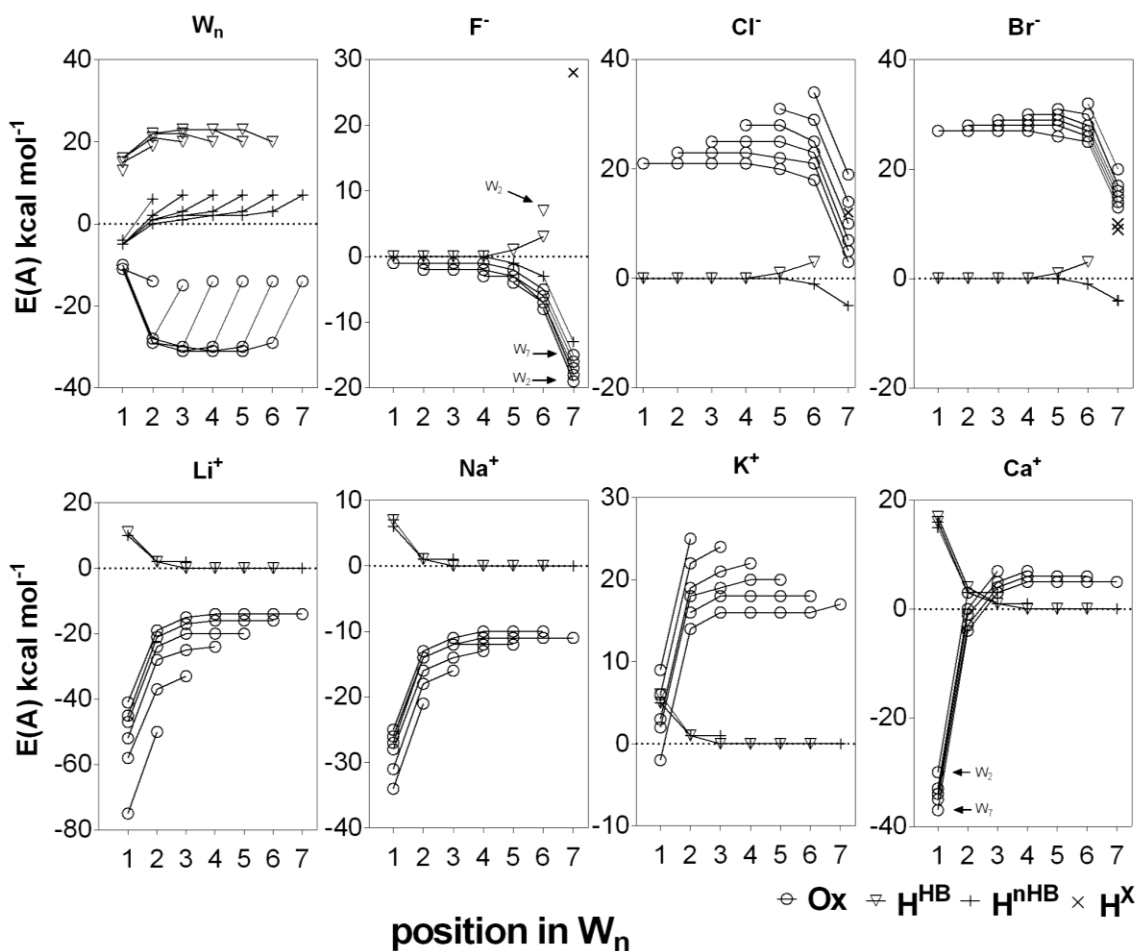
Figure 7.3 Local atomic stabilities for atoms in water wire interacting with ions. Each point on a line represents the stability of an oxygen, H^{HB}, or H^{nHB} atom in a water molecule along the water wire, plotted against the position of that water in the wire, for the set of W_n^X water wires, n=2-7. Oxygens are open circles, hydrogen bonded hydrogens (H^{HB}) are open triangles and non-hydrogen bonded hydrogens (H^{nHB}) are plus signs. For anions, the hydrogen interacting directly with the ion (H^X) is marked as a cross.

While atomic stabilities are useful to discuss the local source of stability in the water wires, it is also instructive to combine these stabilities in order to discuss the contribution to net stability from the water wire *vs.* from the ion. These values are represented in Figure 7.4. E_{int}^X for the ions-plus-water wire reveal a net stability invariant with respect to chain length. When the stability is divided into water *vs.* ion contributions, net stability for the water molecules shows a dependency on the nature of the ion as well as the length of the water wire. For Li^+, Na^+ and F^-, the water chain has an increase in stability as the chain grows in length. For Br^-, Cl^-, K^+, and Ca^{2+} the water chain is increasingly

107

destabilized. Despite having the greatest net stability, fluoride has only a minimal effect on the local energy changes of the waters and ion.
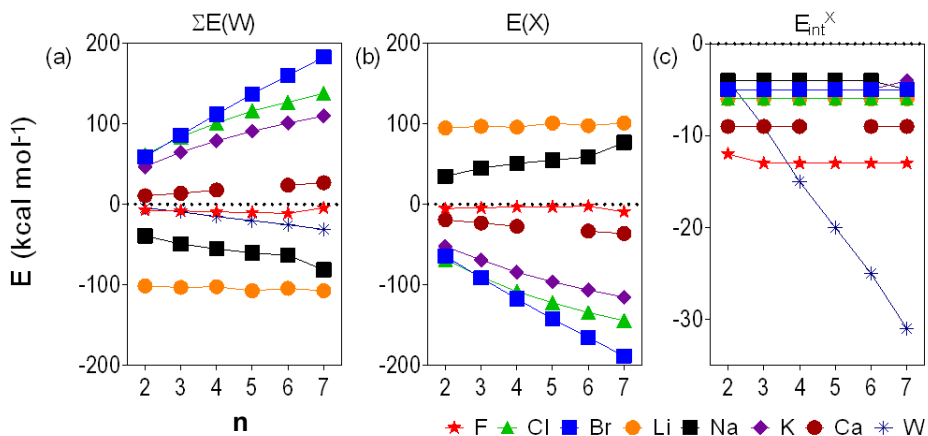
Figure 7.4 a) Total stability for all waters in the wire, b) stability of the ion, c) net stability of the water wire *vs.* the neutral wire (E_{int}^X). The x-axis is length of water wire (n).

7.4.3 BCP and Geometry

Bond critical point analysis is a powerful tool for quantifying the strengths of hydrogen bonding interactions. It has been shown that the magnitude of electron density at the hydrogen-bond bond critical point (HB-BCP) is directly related to hydrogen bond strength [268, 271-272]. To supplement our atomic energy analysis we report the HB-BCP values for each water wire (Figure 7.5). The shape of the plots for neutral water wires indicates greater HB strength in the center of the wire, with weaker HBs at the ends. Addition of the ions has the effect of increasing the electron density at the HB-BCPs predominantly near the point of interaction (right acceptor side for anions and left donor side for cations). For F^-, Cl^-, Li^+ and Ca^{2+} the shape of the curve changes *vs.* the neutral water: density at the HB-BCP nearest the ion is stronger than in the center of the wire, by a significant amount in the case of F^-, Li^+, and Ca^{2+}. Ions Br^-, Na^+ and K^+ maintain a slight maximum for the central HBs. The electron density of the HB furthest from the ion wire does not change *vs.* the neutral water value for all lengths n=3-7. It is

clear that the ion influence on HB strength in the water wires is limited to the waters closest to the ion.
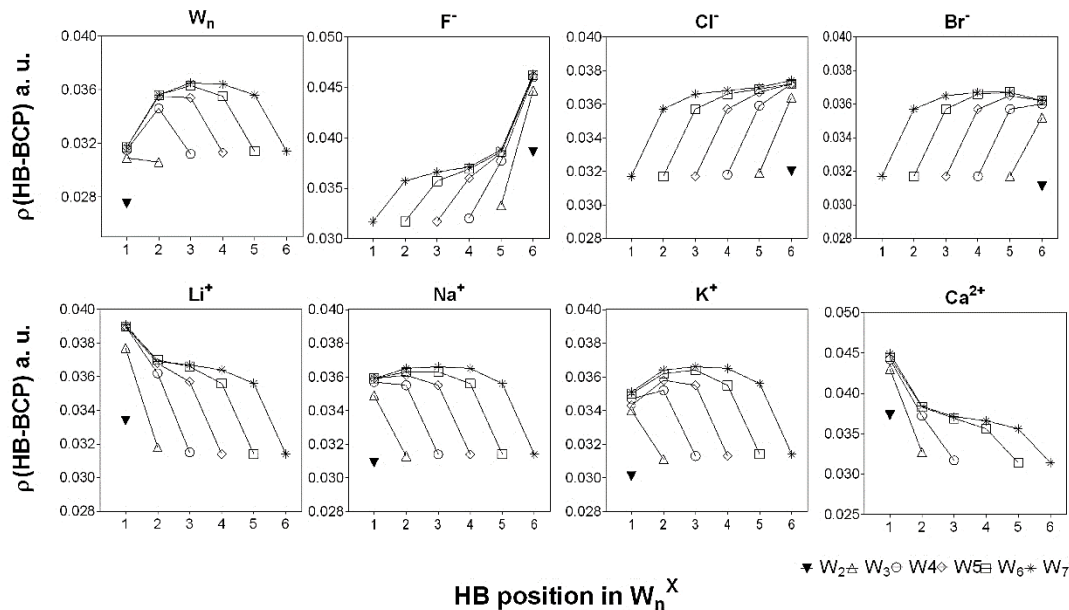
Figure 7.5 Electron density at hydrogen bond critical points for each HB in W_n^X water wires. The x-axis indicates position of the HB in the water wire. The donating water (interacting with cations) is on the left and accepting water (interacting with anions) is on the right.

We also include O-O distances for each water in W_7 and W_7^X in Figure 7.6. The influence of the ion on hydrogen bond length is clearly largest for the waters closest to the ion, which have a significantly shortened O-O bond. Comparing with Figure 7.5, it is clear that the density at HB-BCPs is increased for shortened O-O bonds. The ion which has the greatest influence on BCP density is fluoride, with a HB-BCP increase of 0.015 a.u. The O-O distance for the HB nearest to the ion in W_7^{F-} is shortened by the greatest amount among this series of ions (0.13 Å). Even with such a large influence on the initial water in the chain, the final water HB shows no significant influence from the fluoride's presence. This agrees with the observed minimal change in the atomic stabilities for that final water.

109

Figure 7.6 O-O distances for HBs in W_7 and W_7^X water wires interacting with a) cations and b) anions. Labelled values are O-O distances in Å. The x-axis is the position of the HB in the water wires, beginning from the donor end. In the legend, W indicates the neutral water wire.

7.4.4 Structure Makers and Breakers

Although the impact of the ion decreases sharply after two or three water molecules, the overall energy of each water molecule is still influenced by the presence of the ion, with the oxygen atoms experiencin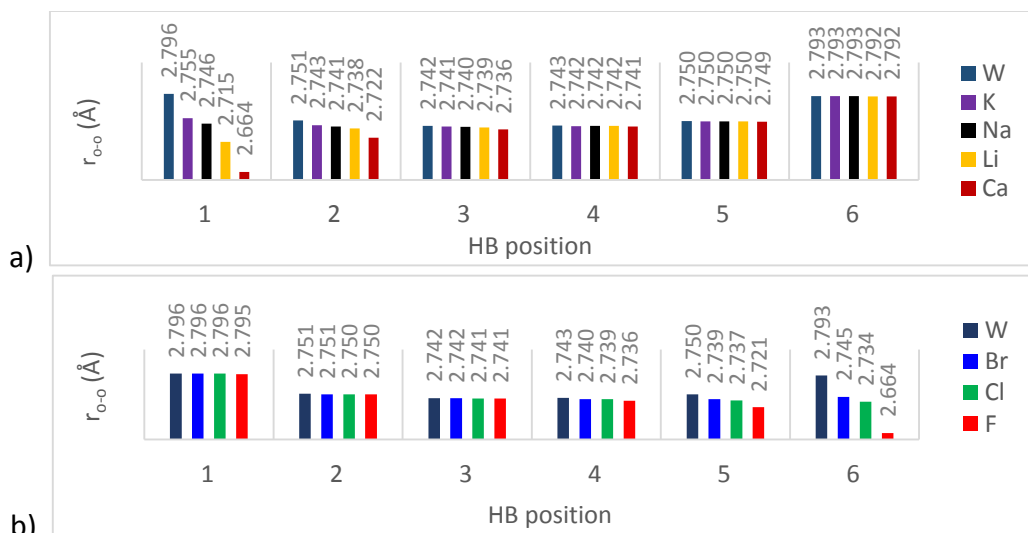g the most significant change in energy. This is the source of the overall stability of the W_n^X wires. What is interesting is that, as mentioned, the sign of the local oxygen stability does not correlate with the sign of the formal charge on the ion. Although the concept of kosmotropes and chaotropes has undergone significant reappraisal over recent years [261], we find it interesting to point out that there is an agreement between the historic division of ions into "structure makers" *vs.* "structure breakers" and the nature of the local stability in the water wires. Ions which are classified as kosmotropes (having a positive ordering effect on the surrounding waters), correspond to those ions which also have a stabilizing influence on the water in the water wires: Li^+, Na^+, F^-. The ions which are chaotropes, which tend towards disordered surrounding water, are those ions which have a destabilizing influence on the water in the water wires: K^-, Cl^-, Br^-. We stress that the net interaction between the water wires and ions is always stabilizing; however, it is interesting that the local nature of this interaction appears to reproduce a trend that has long pervaded the discussion of water-ion solvation.

110

7.4.5 H+ Interaction

The nature of a proton interacting with a water wire is uniquely different from the interaction of the other ions. This is because the addition of H^+ results in a proton transfer to a central water, resulting in the formation of a Zundel ion or a hydronium cation. Because of its importance in biological systems, proton transfer in water wires has been extensively studied [247, 251, 273-274]. While a comprehensive discussion of this phenomenon is beyond the scope of this report, atomic energy analysis offers a unique perspective of the proton transfer in the water wire and we will discuss these results. From plots of the local stabilities in Figure 7.7 it is clear that the oxygens are all stabilized and the hydrogen atoms are all destabilized. There is a clear shift in the local stability as the chain increases in length. The minimum at the second oxygen of the n=2-4 water chain shifts to a minimum at the third oxygen for n=5-7, indicating that the H^+ has migrated from the second to third water as chain length increases. The H^{HB} stabilities show a clear peak for the Hs that bracket this protonated water. Note that when the length increases past n>4, the destabilization of the initial H^{HB} has diminished considerably. H^{nHB} stabilities also show a shift for the third water in the chains with n>3, with a maximum for the hydrogen attached to the newly protonated water molecule, and the H^{nHB}s bracketing this water being similar. The visual representation of the local stabilities in Figure 7.8 clearly shows the movement of the proton as n increases. Notice that the largely stabilized oxygen is no further than 3 waters along the wire, even as n increases to 7.

We have also plotted the hydrogen bond critical point densities for W_n^{H+} (Figure 7.9). It is clear that the protonated water wire has a significant increase in HB strength, skewed towards the beginning of the water wire. The greatest increase in HB-BCP (coinciding with the strongest HB) occurs either between the 2nd and 3rd water for n=3,4 or the 3rd and 4th water for n=5-7. For the wires with an odd number of waters there are two HBs of nearly equal strength, for even numbered water chains there is clearly only one HB which is the most stable.
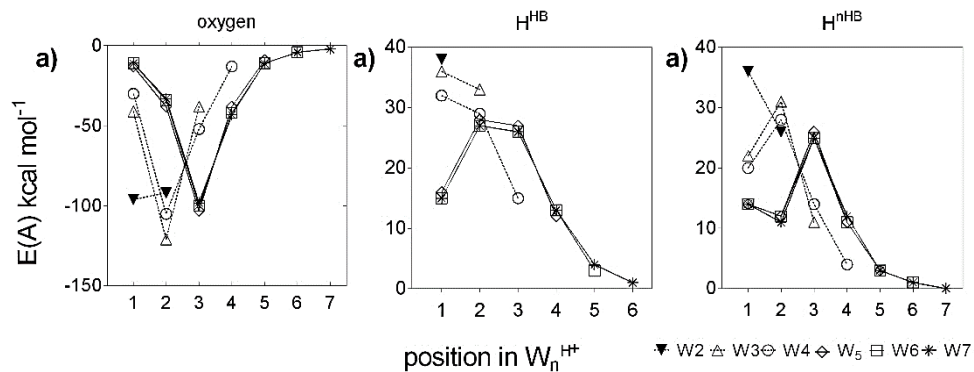
Figure 7.7 Local contributions towards the net stability from a) oxygen atoms, b) hydrogen-bonded hydrogen atoms, c) non-hydrogen bonded hydrogens atoms in W_n^{H+}. For better clarity, the connecting lines for n=2-4 are dashed and for n=5-7 these lines are solid.
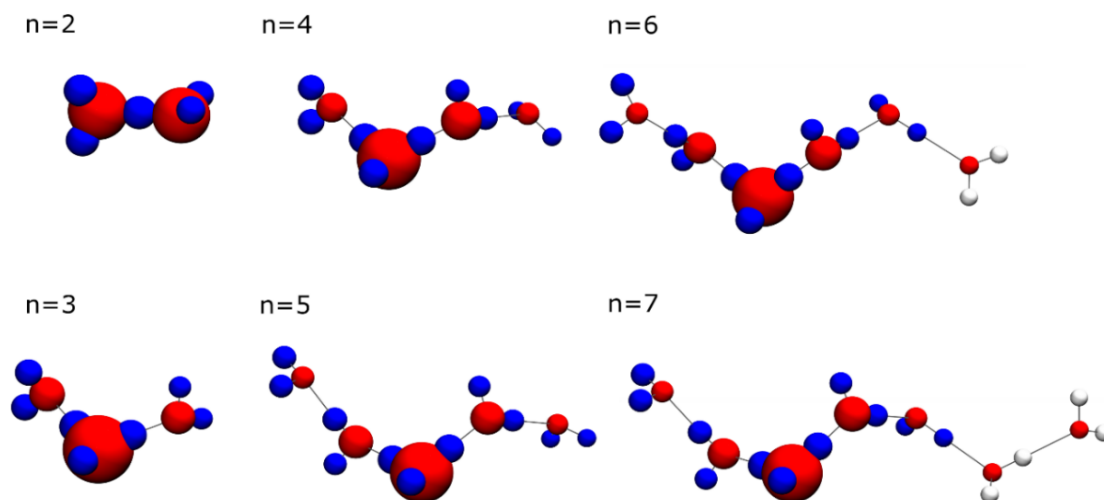

Figure 7.8 Atomic energies for the set of water wires W_n^{H+}, n=2-7. See caption of Figure 7.2 for further information.
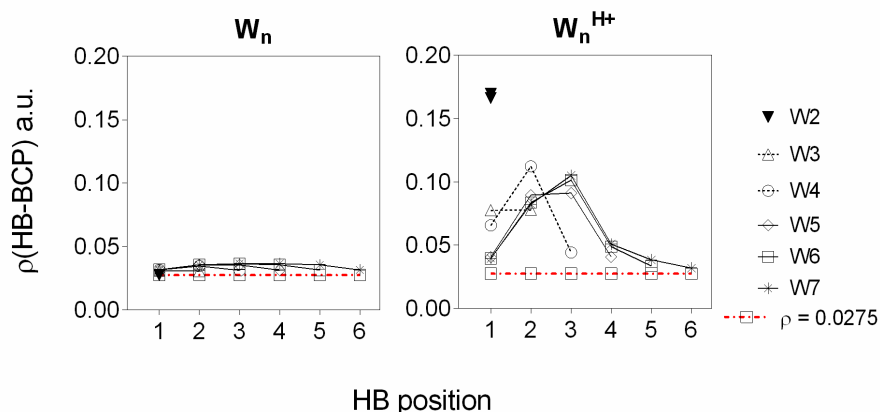
Figure 7.9 Bond critical point values for hydrogen bonds in W_n and W_n^{H+} for n=2-7. Values are in a.u. The HB-BCP density of the water dimer (ρ=0.0275 a.u.) is also included for reference.

7.4.6 Paired-Ion Interactions

An extremely interesting question regarding the nature of ions interacting with water wires is the influence that a counter ion will have on the local stability of the waters. We demonstrate this effect for the n=7 water wires interacting with Na^+ and K^+, including Cl^- as the counter ion. The relative interaction energies of these systems are reported in Table 7.2. E_{int}^X in this case is essentially the sum of the influences of the isolated cation and anion interacting with the water wire. Decomposing the interaction energy into local water stability, the graphs in Figure 7.10 show the net stabilities for the waters in the water wires, as well as stabilities of each oxygen and hydrogen atom. The local energy changes for the atoms in the paired-ion water wires are clearly the combination of the individual ions' influence on the waters in the water wires. For example, the plot of atomic stabilities for H^{nHB} in W_7^{KCl} is a sum of the separate plots of H^{nHB} for W_7^{K+} and W_7^{Cl-}. The oxygen atoms are again influenced the most by the ions, with oxygen stabilization in W_7^{KCl} and W_7^{NaCl} clearly a sum of the single-ion interactions. If each isolated ion destabilizes the oxygen atoms, as in K^+ and Cl^-, the oxygen atoms of the paired-ion water wire (W_7^{KCl}) will have an even greater destabilization. Alternatively, for W_7^{NaCl} the Na^+ stabilizes while Cl^- destabilizes the oxygen atoms, and the combined result has an oxygen stabilization that lies between the isolated ion values. While the shape of the curves for the paired ion interactions are similar, the position of the curve for

113

NaCl is shifted to reveal greater local stabilization per water than KCl. Previous *ab initio* MD studies on NaCl and KCl solvation [264] report that while the structure of the solvation waters for these ion pairs is similar, average residence times in the first solvation shells was nearly double for NaCl vs KCl. The relative HB strengths, as determined by electron density at HB-BCPs, are summarized in Figure 7.11. The shape of the paired-ion curve clearly reveals the combined effects of each ion on the water wires. It would be very interesting to consider the influence of paired-ions for water wires shorter than n=7.

Table 7.2 Interaction energies for isolated ion and paired-ion interaction with a neutral n=7 water wire.

E_{int}^X	W_7^{K+}	W_7^{NA+}	W_7^{CL+}	W_7^{KCL}	W_7^{NACL}	W_7
net stability	-35.3	-35.3	-37.0	-42.0	-41.5	-30.8
relative to W_7	-4.5	-4.5	-6.2	-11.1	-10.7	

[a] Energies in kcal mol^{-1}
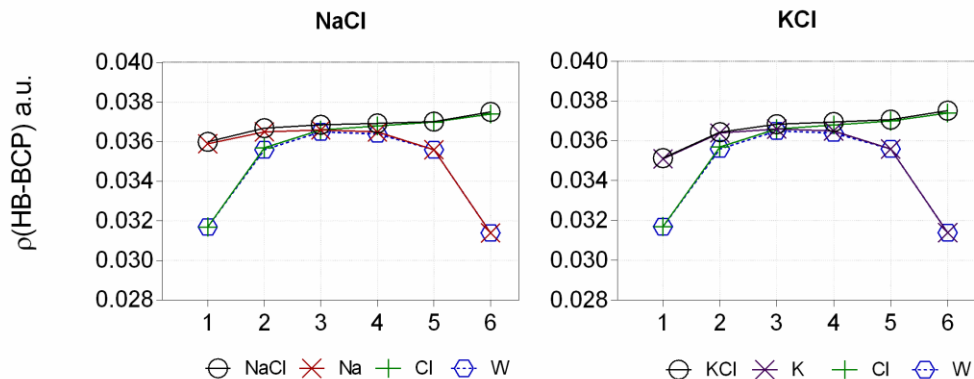
Figure 7.11 Bond critical point electron densities for hydrogen bonds in NaCl (top) and KCl (bottom) water wires. The x-axis indicates hydrogen bond position, where 1 corresponds to the first H-bond.
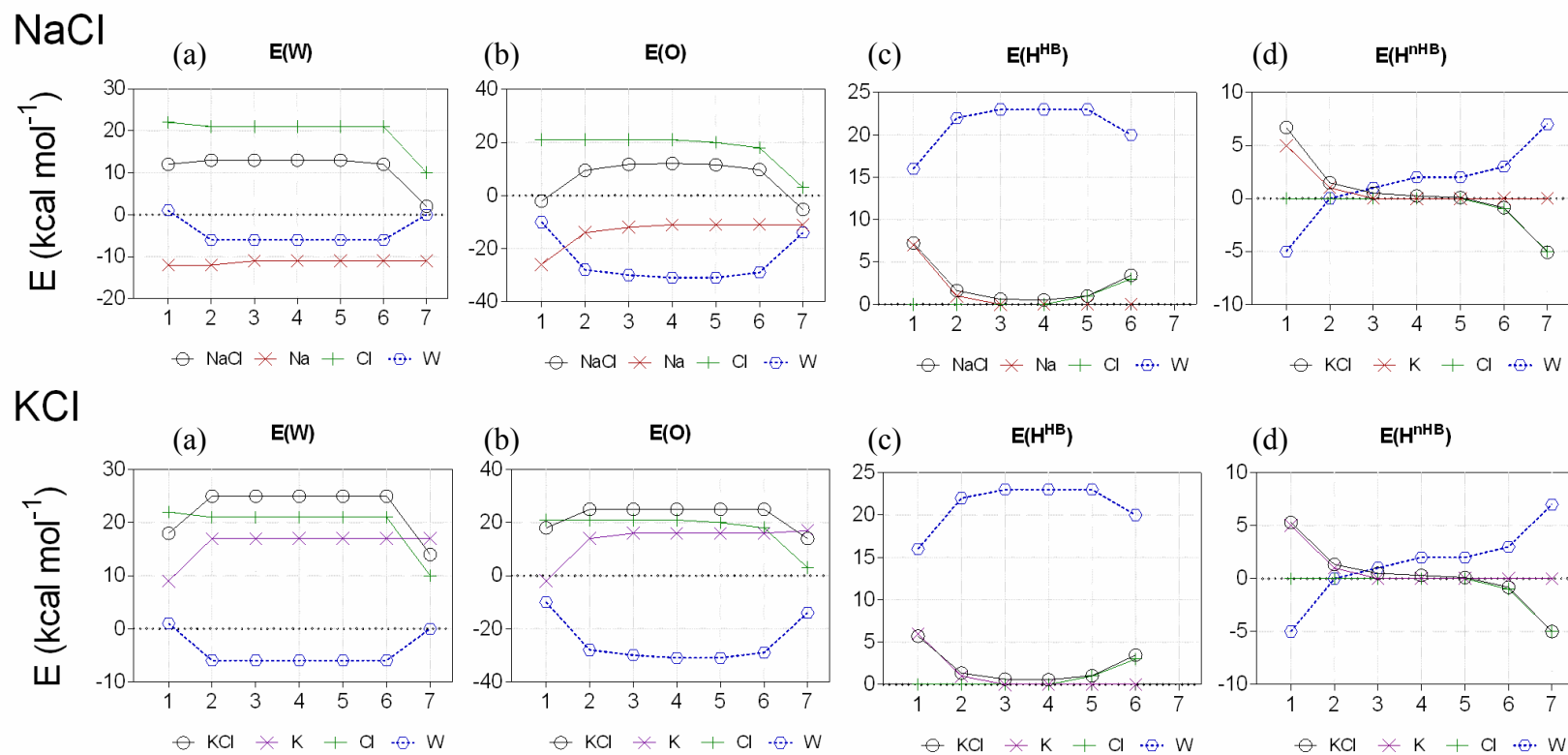
Figure 7.10. Local atomic stabilities for NaCl (top) and KCl (bottom) water wires: (a) Stability per water, (b) stability per oxygen, (c) stability per hydrogen bonded hydrogen, (d) stability per non-hydrogen bonded hydrogen. The x-axis indicates position in water wire.

7.5 Conclusions

In our report we have studied the local stability of one-dimensional helix-type water wires as they interact with a series of ions: $X = Cl^-$, Br^-, F^-, H^+, Li^+, Na^+, K^+, Ca^{2+} as well as the paired NaCl and KCl ions. Stabilities are evaluated at the atomic level using Bader's quantum theory of atoms in molecules. Results show that the stability for the neutral wire is centered in the middle of the wire, having greater atomic energy changes for central waters. The accepting end of the water wire has slightly more stability than the donating end. When an ion is introduced at either the donor (cation) or acceptor (anion) end of the water wire, the local stability reveals the largest influence to be for the first 2-3 waters in the water wire, trending towards a constant local stability for waters further from the ion. Oxygen atoms bear the majority of the energy change, and are stabilized/destabilized depending on the nature of the ion present. The energy change for oxygen atoms does not correlate to formal charge of the ion but rather follows the traditional trends of stabilizing kosmotropes (F^-, H^+, Li^+, and Na^+) *vs.* destabilizing chaotropes (K^+, Cl^-, and Br^-). The local atomic stabilities reflect a large increase in hydrogen bond strength, also confirmed through increased hydrogen-bond bond critical densities and shortened bond distances. When a proton is introduced to a neutral water wire, an asymmetric shift is observed so that the H^+ remains closest to the donor end of the water wire, and the energy changes are greater on the donor side. This is clearly represented using the atomic energies visualization. For the systems where the n=7 water wire interacts with a pair of ions (NaCl and KCl), the net stability for the waters can be clearly decomposed into the isolated contributions from individual ions. Although both ion-water wires have a net stabilization that is nearly equal, the curve for NaCl is reveals greater stabilization per water than KCl.

7.6 Acknowledgements

7.7 Chapter Summary and Relevance

Previous studies have reported the short-range influence of ions on water wires by evaluating sequential hydrogen bond energies as the chain grows in length. The current analysis combines Bader's QTAIM topology critical point analysis with local atomic energy changes to support this picture of a net short-range influence, however there is also an atomic energy change which increases as the wire increases in length. QTAIM energies also provide a unique picture of the classification of the local effects of the ions on the water molecules which correlates with structure maker *vs.* structure breaker ideas of ion solvation. Visualization of the QTAIM energies is a powerful tool to quickly demonstrates this, as well as to highlight the position of the greatest change in local stability when the water wire is protonated. The decomposition of the total energy into local parts is also useful in discussing the combined influence of two ions on a water wire.

Chapter 8   Atomic Energy Analysis of Cooperativity, Anti-cooperativity, and Non-cooperativity in Small Clusters of Water, Methanol, and Formaldehyde.
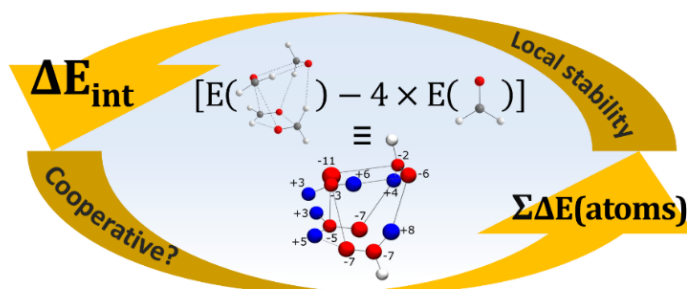
Chapters 4 and 5 revealed that, in the evaluation of cooperative water clusters, local stability increases with increasing cooperativity; however, there is also the question of the influence of changing cluster size on local stability. Is there a dependency for the local atomic energies on the size of the clusters? In order to further evaluate the capacity for atomic energy analysis to distinguish between cooperative and non-cooperative interactions, small clusters (n=2-4) of methanol, water and formaldehyde are evaluated next. These systems demonstrate, respectively, cooperative, anti-cooperative and non-cooperative bonding interactions and therefore provide a useful test case for the influence of system size on atomic energy analysis of weak interactions. The following chapter was published as an invited article in a special issue of Computational and Theoretical Chemistry on "Understanding structure and reactivity from topology and beyond."

8.1 Abstract

The local and regional stabilities in clusters of water, methanol, and formaldehyde up to the tetramers have been analyzed from an atomic energy perspective. We optimize structures at the MP2/6-311++G(d,p) level with some CCSD(T)/6-311++G(d,p) single point energies, and then decompose the electronic densities into atomic parts using the atoms in molecules (AIM) approach. We consider the changes in atomic energy in the clusters *vs.* the isolated monomer. This method of analysis allows us to reveal the variety of stabilities within these hydrogen-bonded clusters, including indications of cooperative, anti-cooperative, and non-cooperative interactions. Cooperatively interacting clusters have increasing stability at the atomic level as the cluster size grows. This is not observed in the anti- and non-cooperative arrangements of water and formaldehyde clusters. The cooperativity in methanol clusters is dominated by the OH regions, with negligible energy change in the methyl regions. Formaldehyde clusters, including the lowest minimum "bucket" cluster, do not show significant cooperativity. Atomic energy analysis is supported with bond critical point data as well as charge and geometric values. We represent the local stability in the clusters using a simple visual approach that allows areas of increased or decreased stability to be easily interpreted.

8.2 Introduction

Characterizing the interactions in molecular systems normally involves interpreting changing geometries and evaluating total energies. Shortened bonds may reveal important areas of stability and decomposing the total energy in terms of electrostatics, charge transfer, or polarization can help us understand the sources of this stability. To add to these standard methods of analysis there is another powerful approach: Bader's topological analysis of the electron density, as described in the atoms in molecules (AIM) theory [1, 57, 275]. The AIM approach provides access to a wealth of information about a molecular system directly from evaluation of its electron density. Many reports apply AIM, using electron density topology to describe properties such as group transferability, relationships between bond critical point values and bond strength, characteristics of

bonding interactions, and other applications that are well described in the literature [57, 267-268, 271, 275-278]. In the AIM method, the electron density of a molecule is partitioned into atomic constituents from which local properties can be determined. This provides a way to directly evaluate the local (atomic) or regional (*e.g.* functional group) changes occurring as molecular systems interact. In this report we use a unique application of AIM density partitioning, one that takes advantage of the ability to evaluate the local energy of each atom in a molecule by integrating over its partitioned density [100]. By evaluating changes in atomic energies when molecules interact, we show that local and regional stabilities can be directly represented both inter- and intramolecularly. Furthermore, we represent this stability using a simple visual method that gives a direct picture of the changing energy within a system.

To demonstrate the effectiveness of the atomic energy analysis we turn our attention to small clusters that can demonstrate either cooperative or non-cooperative interactions. Cooperativity is often described as a non-pairwise increase in stability observed when two or more weak interactions operate in concert. It plays an important role in the stability of many molecular clusters and is a central part of the behaviour of some molecules in condensed medium, *e.g.* in a solvent environment, as well as in processes such as protein folding and enzyme activity. Hydrogen-bonded interactions [12, 279-281] were perhaps the first cooperative systems to be observed, and their cooperativity has been well-studied using experimental, theoretical and combined approaches [13, 116, 127-128, 130, 192, 196, 201-202, 282-293]. Cooperativity also exists between other kinds of weak interactions, such as halogen bonding [111, 209, 294-296] and ion-π [297-298] interactions. Furthermore, the interplay of cooperativity between differing types of weak interactions is also an area of important study [298-299], *e.g.* hydrogen bonds plus halogen bonds [300-302], beryllium bonds plus hydrogen [6] or halogen bonds [8], and hydrogen bonds combined with ion-π interactions [299, 303]. The cooperative behaviour between two bonding interactions is not always a stabilizing association. It can instead result in what is often referred to as anti- or non-cooperative behaviour, where the combination of non-covalent interactions yields a system that is less stabilized than the isolated bonding interactions [299, 304]. This is observed in the linear HCN/HNC$^+$ molecules [305], in some ion-π [303] interactions, and has been observed in various

arrangements of water clusters [5, 127-128]. Anti-cooperativity could have an important role in biological systems, inhibiting molecule docking or minimizing interaction strength despite the presence of multiple bonds that might otherwise be stabilizing. The balance of cooperative and anti-cooperative behaviour within small water clusters may be an important influence in the dynamic behaviour of bulk water [5].

Application of atomic energies to the study of cooperativity is particularly useful because it allows one to diagnose increased or decreased stability without needing to separate the system to explore it, as is the case in fragmentation methods [154, 162, 286, 304]. This is particularly important because cooperative stability is a total molecular result that relies on many-body interactions of the third and higher orders [306] which are often approximated or truncated in energy decomposition approaches. These higher order interactions can have a considerable influence on the total energy, *e.g.* the third and fourth-order many-body interactions in water clusters can contribute more than 20% and 4% to the total interaction energy, respectively [13].

We have previously used this atomic energy analysis to explore cooperative interactions in a variety of systems, including hydrogen bonding in water clusters [5-4] and beryllium bonding combined with hydrogen bonding [6] and halogen bonding [8]. To further explore the ability for atomic energies to represent cooperative behaviour in weakly interacting systems we present here calculations on three sets of small molecular clusters that encompass a range of strong to weak hydrogen bonding. Water, methanol and formaldehyde clusters from n=2-4 are optimized with MP2 theory and then evaluated at the atomic level. Water clusters in cooperative and anti-cooperative arrangement provide an interesting look at anti-cooperativity as well as a standard of comparison to previous studies. Methanol and formaldehyde deliver increased complexity in hydrogen bonding and furthermore formaldehyde clusters can adopt geometries that do not possess cooperative stability; we demonstrate this at the atomic level. We use atomic energies as well as other topological tools available in AIM to analyse the interactions in these clusters and then present their local stabilities visually in a simple and accessible way.

8.3 Computational Methods

8.3.1 Wavefunction evaluation

Previous analysis has demonstrated the suitability of Møller-Plesset second order perturbation theory [32] for the evaluation of cooperativity in water and methanol clusters [282, 290, 307]. Single point coupled cluster calculations were also performed on select systems (methanol and formaldehyde) to verify their energies (see supporting information, Table B.4 in Appendix B.4). We use a large triple zeta basis set including diffuse functions and polarizability on hydrogen and heavy atoms, 6-311++G(d,p), which is important for weak interactions. The large basis set was also chosen to minimize possible BSSE error [308]. We compare this Pople basis set to a similar Dunning basis set (aug-cc-pVTZ) which was previously shown to not require BSSE correction for weak interactions [304], and see that the Pople basis set provides a reasonable compromise for the range of structures evaluated (see supporting information, Table B.5). All molecules have been fully optimized and their vibrational frequencies evaluated to ascertain that they are stationary minima on their potential energy surfaces. Optimizations and frequency calculations were performed using Gaussian 09 [70].

Total stabilization of the clusters is defined by the interaction energy (E_{int}),

$$E_{int} = E(n\text{-mer}) - nE(\text{monomer}), \qquad (8.1)$$

where "n-mer" refers to the dimer, trimer or tetramer (n=2-4). The total cooperativity (E_{coop}) is sometimes defined as the difference between the average hydrogen bond (HB) energy and the energy of a single HB in the dimer structure:

$$E_{coop} = E_{HB} - E_{int}(\text{dimer}), \qquad (8.2)$$

where $E_{HB} = E_{int}/m$, m = number of hydrogen bonds in the cluster. Although this is a useful method of comparison, it is not strictly accurate, as we will discover in the discussion of methanol clusters.

8.3.2 Atoms in molecules evaluation

The atoms in molecules analysis requires an accurate evaluation of the wave function including proper minimization of nuclear forces to reduce deviation from the virial theorem. Ideally we would optimize the systems using self-consistent virial scaling (SCVS) [61, 71], which will simultaneously minimize the energy with respect to a scaling factor for all coordinates, molecular orbital coefficients, and the molecular geometry [63]. We have evaluated the largest of our systems with this approach to ensure that there is no significant deviation in accuracy of the wavefunction as the system size increases (see supporting information, Tables B.6 and B.7). All reported atomic energies are scaled by $(1 - \gamma)$, according to the virial relation $\gamma = -V/T = 2$. Local energy changes are evaluated by calculating the increase or decrease in atomic energy per atom in a cluster relative to the isolated monomer,

$$\Delta E(atom) = E(atom\ in\ complex) - E(atom\ in\ monomer). \qquad (8.3)$$

A decrease in energy ($\Delta E<0$) is stabilizing and an increase in energy ($\Delta E>0$) is destabilizing. The results are visualized by plotting molecular systems using colour-coded atoms [3], where an atom with $\Delta E<0$ is red and atom with $\Delta E>0$ is blue. The size of the atom is also scaled so that it is proportional to the magnitude of energy change. Thus, a largely stabilized atom is represented by a large red sphere and a moderately destabilized atom is represented by a moderately sized blue sphere. If the energy change is very small (less than ± 1 kcal mol^{-1}) the atom is colourless (white) and will have a default sphere size of "1".

AIM analysis also yields other important information from density topology, in particular the characterization of critical points. There are many resources which describe this analysis in detail, including the correlation between the properties of the electron density at a bond critical point (BCP) and the nature of that bond [267-271]. We will use this correlation to support our discussion of the relationship between local stability and atomic energy changes. All AIM analyses were performed within the AIMAll suite [69]. Atomic energy figures were generated using the VMD program [114].

8.4 Results and Discussion

8.4.1 Water clusters

We have previously reported an atomic energy analysis of water clusters from the dimer through to the hexamer [5-4], and the cooperativity in water clusters has also been extensively studied using other theoretical and experimental approaches. From the atomic energy perspective, cooperativity was represented by an increase in stabilization or destabilization of the atoms in the water molecules as the cluster size increased. To extend this analysis we evaluate here a linear trimer system that has a water molecule acting as a double donor: donating two hydrogen bonds and receiving none. This arrangement has previously been shown as anti-cooperative [127, 196]. We were unable to isolate the analogous trimer system with a central water accepting two HBs; in all attempts we found either a saddle point (with two imaginary vibrational frequencies) or the structure collapsed to the global minimum cyclic trimer. We next evaluate an anti-cooperative tetramer system [128] where two waters are double donors and the remaining waters are double acceptors. Here, the double donating water should be more stabilized than the double acceptor [5, 130]. We also include atomic evaluation of the global minimum dimer, trimer and tetramer so that a direct comparison can be made at the current level of theory. A summary of the energy changes is compiled in Table 8.1.

Table 8.1 Summary of energy changes for water clusters.[a]

Cluster		ΔE(A)			$E_{net}(H_2O)$	E_{int}	E_{HB}	E_{coop}
		O	H^{HB}	H^{nHB}				
Dimer								
	A	-14.3	14.6	-3.6	-3.3			
	B	-17.2	7.2	7.2	-2.7	-6.1	-6.1	--
Trimer								
Cyclic cooperative	A	-33.4	23.6	3.8	-6.0			
	B	-33.1	23.6	3.7	-5.8			
	C	-32.8	23.5	3.2	-6.0	-17.8	-5.9	0.2
Linear anti-cooperative	A	-25.3	10.9	10.9	-3.5			
	B	-15.0	5.7	5.7	-3.6			
	C	-15.0	5.7	5.7	-3.6	-10.7	-5.4	0.7
Tetramer								
Cyclic cooperative		-42.4	30.3	4.3	-7.8	-31.3	-7.8	-1.7
Cyclic anti-cooperative	A	-22.2	8.1	8.1	-6.0			
	B	-22.2	8.1	8.1	-6.0			
	C	-25.2	10.9	10.9	-3.4			
	D	-25.2	10.9	10.9	-3.4	-18.8	-4.7	1.4

[a] Energies are in kcal mol^{-1}. Labels A-D refer to monomers in the cluster, see Figure 8.1. ΔE(A) is the stabilization for atom A. H^{HB} is the hydrogen-bonded hydrogen atom and H^{nHB} is the non-hydrogen bonded hydrogen atom. $E_{net}(H_2O)$ is the sum of all atomic energy changes in a given water monomer. E_{int} = [E(n-mer) – nE(monomer)] ≡ ΣΔE(A). E_{HB} and E_{coop} are defined in the text.

Net energy stabilities for the monomers in the clusters show that waters which are HB acceptors in the linear trimer system are more stabilized than those in the dimer system (by ~ 1 kcal mol^{-1}). Local atomic values show smaller energy changes for the accepting waters in the anti-cooperative trimer than in the dimer, by about 2 kcal mol^{-1}. The donating water has essentially the same stabilization as that of the donor molecule in the dimer, although the local energy changes are greater in magnitude (by about 10 kcal mol^{-1} for the oxygen and 4 kcal mol^{-1} for the hydrogen atoms). The electron densities at the hydrogen bond critical points (HB-BCPs, see Figure 8.1) are larger in the dimer, indicating anti-cooperative character. Comparing the two trimer clusters, the cyclic global minimum is more stable than the linear system by 7 kcal mol^{-1}. The atomic energies in this cyclic cluster have larger stabilization for oxygen atoms (by up to ~8 kcal mol^{-1}) and larger destabilization of the hydrogen atoms participating in the hydrogen bonds (by ~13 kcal mol^{-1}). The HB-BCPs are larger in the cyclic system, indicating stronger hydrogen bond formation.
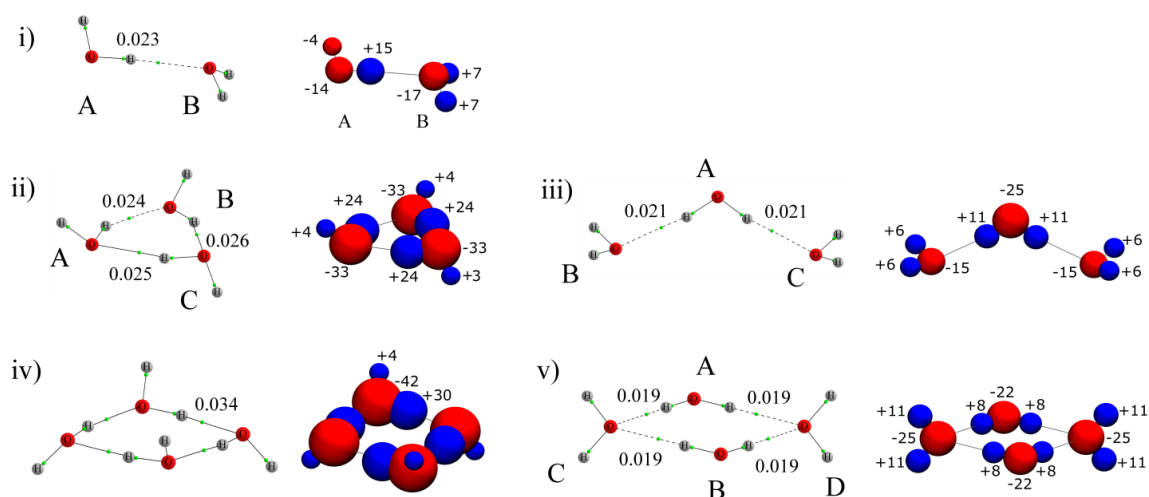
Figure 8.1 Molecular graphs (left) and atomic stabilities (right) of water clusters: i) dimer, ii) cooperative cyclic trimer, iii) anti-cooperative linear trimer, iv) cooperative cyclic tetramer, v) anti-cooperative cyclic tetramer. Green dots in the molecular graphs are bond critical points. Electron densities at hydrogen bond critical points are labeled in a.u. Atomic energies are labeled in kcal mol^{-1}. For clusters with symmetry, monomer energies are only labelled once. Labels and orientation for molecular graphs match those of the atomic energies. For atomic stabilities, stabilized atoms are red and destabilized atoms are blue. The sphere diameter is proportional to the atomic energy stabilization, $\Delta E(A)$, so that an atom with a larger energy change will have a larger sphere radius. For energy changes less than ± 1 kcal mol^{-1} the sphere is coloured white.

Comparing the anti-cooperative trimer cluster with its tetramer analogue, we notice right away that the HB-BCP densities in the tetramer system continue to decrease. This indicates that the four HBs in the tetramer are each weaker than the two formed in the trimer, indicating anti-cooperativity. This is opposite to the cyclic systems where density at HB-BCPs is significantly increased going from trimer to tetramer. The anti-cooperative tetramer cluster is more stable than the linear trimer system by 8 kcal mol^{-1}. Atomic energies show that the net stabilization of the double donor waters in the tetramer are larger than those in the trimer and the double accepting waters are stabilized by about the same amount as the single accepting waters in the trimer. These double accepting waters have non-hydrogen bonded hydrogens (H^{nHB}) that are more destabilized than those of the trimer (by 5 kcal mol^{-1}) and an oxygen atom that is significantly more stabilized (by 10 kcal mol^{-1}). Compare this with the double donating waters, which have a reduced oxygen stabilization combined with a reduced hydrogen destabilization *vs*. the trimer. A greater

stability for double donating waters has been previously observed in water hexamer clusters [5]. Compared to the cooperative tetramer, the energy changes for the H^{HB} and oxygen are significantly diminished, and the energy change for H^{nHB} is increased. This indicates an overall anti-cooperative interaction. Local atomic energies thus reveal a varied distribution of stabilization for individual water molecules within the clusters.

8.4.2 Methanol Clusters

Methanol clusters have been the subject of many experimental studies but only a few theoretical explorations. Some of the discussion has focussed on the cooperativity observed in the formation of methanol clusters. Previous reports [282, 284, 290, 309] indicate that the hydrogen-bond interaction of the methanol clusters strengthens cooperatively as the cluster size increases. The role of the methyl group in the overall stability provides an interesting discussion for the atomic energy analysis. The bonding interactions of methanol are much more restricted than water, with only one HB donor per monomer. Although it is possible that a methanol could act as a double acceptor, we report atomic energy analyses for only the (cooperative) global minima of methanol clusters up to the tetramer. The energy changes are summarized in Table 8.2.

Table 8.2 Summary of energy changes for methanol clusters.[a]

	ΔE(A)						ΔE_{net} (Me)	ΔE_{net} (OH)	E_{net}	E_{int}	E_{HB}	E_{coop}
	O	C	H^{OH}	H^{trans}	H^{inner}	H^{outer}						
Dimer												
A	-21.2	7.5	16.4	-3.4	-1.6	-1.8	0.7	-4.8	-4.1			
B	-11.2	-9.3	6.6	3.3	4.0	4.1	2.0	-4.6	-2.7	-6.8	-6.8	
Trimer												
A	-34.7	0.4	24.5	-1.5	3.0	2.1	3.9	-10.2	-6.3			
B	-35.3	1.9	24.6	-1.2	1.4	2.4	4.4	-10.6	-6.2			
C	-34.9	1.9	24.5	-1.8	1.6	2.2	4.0	-10.4	-6.4	-18.9	-6.3	0.5
Tetramer												
	-44.5	1.0	31.6	-2.1	2.9	2.7	4.4	-12.9	-8.5	-34.0	-8.5	-1.7

[a] Energies in kcal mol^{-1}. Labels A-D refer to monomers in the cluster, see Figure 8.2. ΔE(A) is the stabilization for atom A. $\Delta E_{net}(OH)=\Delta E(O)+\Delta E(H)$, similarly for $\Delta E_{net}(Me)$. $\Delta E_{net}=\Delta E_{net}(OH)+\Delta E_{net}(Me)$. H^{trans} is the hydrogen that is trans to the OH$\cdots$O bond, H^{inner} is the hydrogen atom that points over the ring (towards another hydrogen on the opposite monomer), H^{outer} is the hydrogen that points away from the ring. $E_{int}=[E(n\text{-mer})-nE(monomer)]\equiv\Sigma\Delta E(A)$. E_{HB} and E_{coop} are defined in the text.

The energy changes of the dimer system differ slightly from the ring-like clusters and we will discuss those values first. In the dimer, one molecule can be considered a donor monomer and the other an acceptor monomer (A and B, respectively, in Figure 8.2). Atomic energy changes for carbon and oxygen show that the donor methanol has a destabilized carbon and stabilized oxygen (consistent with the ring clusters) whereas the acceptor methanol has both of these atoms stabilized. The methyl hydrogens on the donor monomer are stabilized by about -2 to -3 kcal mol^{-1}, with the hydrogen trans to the OH group (H^{trans}) having the largest stabilization. The methyl hydrogens of the acceptor monomer are destabilized by about +4 kcal mol^{-1}, and H^{trans} on the acceptor monomer is slightly less destabilized than its neighbour hydrogens. Bond critical point values for the donor monomer show an increase in density at the C–O BCP and decrease in densities for the C-H and O-H BCPs (*vs.* the isolated monomer). The acceptor monomer is opposite this, with the C–O BCP decreasing and the C-H BCPs increasing. The net energy change of the monomers is -2 kcal mol^{-1} for the donor and +4 kcal mol^{-1} for the acceptor. The local atomic energies show a variation in stabilization for the donor *vs.* acceptor methanols, concurrent with previous hydrogen-bonding analyses. Local differences in the methanol dimer have also been discussed previously using bond lengths and vibrations [290], and our results are in perfect agreement with this analysis.
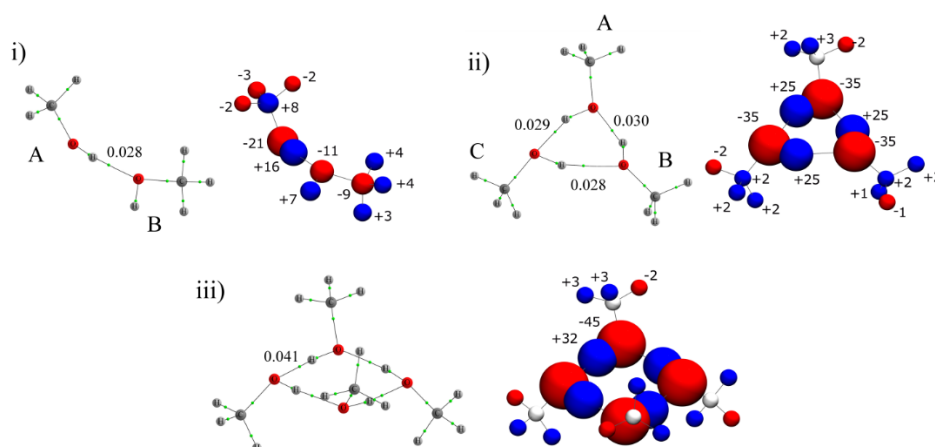

Figure 8.2 Molecular graphs (left) and atomic stabilities (right) of methanol clusters. i) dimer, ii) trimer, iii) tetramer. BCP densities in a.u. and energies in kcal mol^{-1}. For clusters with symmetry, monomer energies are only labelled once. Labels and orientation for molecular graphs match those of the atomic stabilities. See the caption of Figure 8.1 for further details.

For the cyclic clusters of the trimer and tetramer, the local atomic energy changes clearly represent cooperativity. Each oxygen atom is stabilized, with an increase in stabilization for the oxygens in the trimer *vs.* the tetramer (-35 *vs.* -45 kcal mol^{-1}, respectively). The alcohol hydrogen that forms the hydrogen bond (H^{OH}) is concurrently destabilized, with the destabilization increasing from +16 kcal mol^{-1} in the dimer to +25 kcal mol^{-1} in the trimer and +32 kcal mol^{-1} in the tetramer. As in the dimer, H^{trans} has the greatest stabilization (-2 kcal mol^{-1}), whereas the remaining hydrogens are destabilized (+2 kcal mol^{-1}). Bond critical point densities support the greater stabilization of H^{trans}, evident in the slight increase in density at the C-H BCP: +0.004 a.u. in the dimer, +0.003 to 0.005 a.u. in the trimer, and +0.003 a.u. in the tetramer. There is also a small shift in the C-H stretching vibrations, of about 45-50 Hz (unscaled frequencies), for this hydrogen. Thus the atomic energy analysis is again in perfect agreement with previous reports.

The net stabilization per each monomer in the clusters, defined as the sum of all atomic energy changes in a given water monomer, yields the average HB strength: -6.3 kcal mol^{-1} in the trimer and -8.5 kcal mol^{-1} in the tetramer. It was surprising to note that trimer does not actually reveal a net cooperativity per HB if one considers only total energies: the average HB energy in the trimer is 0.5 kcal mol^{-1} less than the dimer hydrogen-bond energy. We tested the accuracy of the MP2 calculations using CCSD(T) single point calculations on the methanol clusters and found that the CCSD(T) results are nearly identical to the MP2 analysis (see Table 8.3). By considering regional energy changes we can further explore the sources of net stability. The energy changes of the alcohol group clearly indicate a cooperative stabilization: the stabilization of the OH group in the trimer is twice that of the OH in the dimer, and in the tetramer it is nearly three times that of the dimer. However, the net stabilization of the cluster depends on the energy change of all the atoms. Despite increased stabilization of the OH groups in the tetramer, the methyl groups in the tetramer and trimer are destabilized by about the same amount (about twice that of the accepting methanol group in the dimer). Thus, the cooperativity present in the trimer is masked because of local destabilization per methyl group. This methyl destabilization is likely a result of the smaller ring formation, where the methyl groups on the trimer are much closer together than in the alternating

arrangement of the tetramer. Notice that carbon atoms have a larger atomic destabilization in the trimer *vs.* the tetramer. The local energy analysis allows us to isolate these local and regional stabilities when discussing cooperativity in hydrogen-bonded systems. Simply decomposing the net interaction into only HB contributions could lead to incorrect assumptions about the cooperative character of the HBs alone.

Table 8.3 MP2 and CCSD(T)//MP2 energies for methanol clusters[a]

Cluster	Energy (Ha)		E_{int}		E_{HB}		E_{coop}	
Monomer	-115.445220	*(-115.477241)*	--	--	--	--	--	--
Dimer	-230.901300	*(-230.965263)*	-6.8	*(-6.8)*	-6.8	*(-6.8)*	--	--
Trimer	-346.365781	*(-346.461647)*	-18.9	*(-18.8)*	-6.3	*(-6.3)*	0.5	*(0.5)*
Tetramer	-461.835152	*(-461.962494)*	-34.1	*(-33.6)*	-8.5	*(-8.4)*	-1.7	*(-1.6)*

[a] Energies in kcal mol^{-1} except where noted otherwise. All structures optimized at MP2/6-311++G(d,p). No ZPE correction. Values in italics are CCSD(T)/6-311++G(d,p)//MP2/6-311++G(d,p) single point evaluations. Definitions for energy terms as in Table 8.1.

8.4.3 Formaldehyde clusters

Formaldehyde is an interesting and important molecule that has only recently undergone much theoretical exploration [285, 293, 310-314]. Formaldehyde dimers have been measured experimentally [315] and *ab initio* and DFT calculations [314-317] reproduce a C_s geometry as the minimum energy dimer structure, matching the experimental results. There is also a planar C_{2h} minimum with a side-by-side interaction (which we refer to as "stacked") that lies within 1 kcal mol^{-1} of the C_s minimum. Larger clusters can demonstrate cooperative stabilization or non-cooperative stabilization, depending on the arrangement of the interacting monomers. The cooperativity in the formaldehyde clusters is diminished compared to that observed in similar systems of formamide clusters [318]. The case of formaldehyde provides an interesting test for the atomic energies analysis: will the energetic changes fully distinguish non-cooperative interactions from cooperative interactions at the atomic level? To investigate this we evaluate both dimer minima (C_s and C_{2h}) as well as three types of trimer and tetramer geometries: circular clusters with only CH···O interactions, stacked clusters which adopt a side-by-side CH···O interaction, and a three-dimensional "bucket" cluster which

131

incorporates additional C−O contacts as well as CH···O bonds (see Figure 8.3). The circular geometry has previously been shown to demonstrate cooperative stabilization, whereas the stacked geometry is reported to be a non-cooperative interaction. The atomic energies for the clusters can be found in Table 8.4.
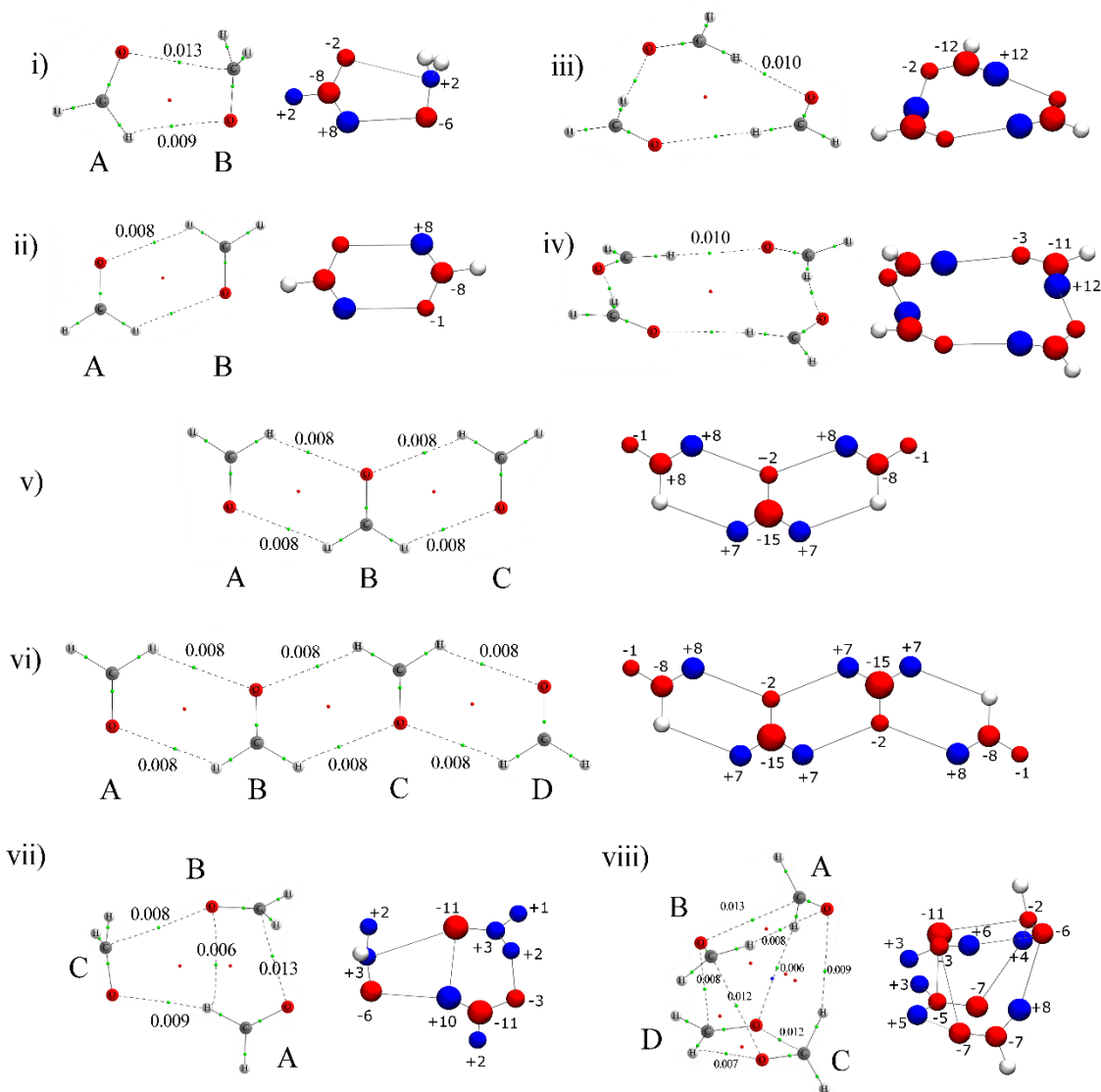
Figure 8.3 Molecular graphs (left) and atomic stabilities (right) of formaldehyde clusters. i) dimer C_s, ii) dimer C_{2h}, iii) cyclic trimer, iv) cyclic tetramer, v) stacked trimer, vi) stacked tetramer, vii) bucket trimer, viii) bucket tetramer. Energies in kcal mol^{-1}. For clusters with symmetry, monomer energies are only labelled once. Labels and orientation for molecular graphs match those of the atomic stabilities. See the caption of Figure 8.1 for further details.

Table 8.4 Summary of energy changes in formaldehyde clusters.[a]

Cluster		ΔE(A)				E_{net} (CH_2O)	E_{int}	E_{HB}	E_{coop}
		O	C	H^{HB}	H^{nHB}				
Dimer									
C_s		-1.2	-7.5	8.0	-0.9	-1.6	-3.2	-1.6	--
C_{2h}	A	-2.3	-7.8	8.1	1.6	-0.5			
	B	-6.5	2.5	0.3	0.3	-3.4	-3.9	-2.0	--
Trimer									
Cyclic		-1.6	-11.9	11.8	-0.6	-2.2	-6.7	-2.2	-0.7
Stacked	A	-0.6	-7.5	7.7	-1.0	-1.4			
	B	-2.1	-15.1	7.0	7.0	-3.3			
	C	-0.6	-7.5	7.7	-1.0	-1.4	-6.16	-1.5	0.0
Bucket	A	-3.0	-10.8	10.0	1.8	-2.0			
	B	-10.9	3.3	1.3	1.7	-4.6			
	C	-6.3	2.5	0.8	1.6	-1.4	-8.03	--	--
Tetramer									
Cyclic		-2.8	-11.2	12.0	-0.5	-2.4	-9.5	-2.4	-
Stacked	A	-0.6	-7.6	7.9	-1.0	-1.3			
	B	-1.8	-15.0	6.9	6.6	-3.3			
	C	-1.8	-15.0	6.9	6.6	-3.3			
	D	-0.6	-7.6	7.9	-1.0	-1.3	-9.17	-1.5	0.1
Bucket	A	-6.5	-1.7	4.1	0.2	-3.8			
	B	-10.8	-3.2	6.4	3.0	-4.6			
	C	-6.7	-6.6	8.3	0.7	-4.2			
	D	-7.1	-2.5	5.1	2.6	-1.9	-14.48	--	--

[a] Energies in kcal mol^{-1}. Labels A-D refer to monomers in the cluster, see Figure 8.3. ΔE(A) is the stabilization for atom A. H^{HB} is the hydrogen-bonded hydrogen atom and H^{nHB} is the non-hydrogen bonded hydrogen atom. E_{net}(CH_2O) is the sum of all atomic energy changes in that monomer. E_{int} = [E(n-mer) – nE(monomer)] ≡ ΣΔE(A). E_{HB} and E_{coop} are defined in the text.

For the dimers, the lowest energy C_s geometry has a C−O contact as well as a CH···O bond whereas the C_{2h} geometry has two CH···O bonds. Monomer A in the C_s dimer (which donates the hydrogen) has a stabilization very similar to that of the monomers in the C_{2h} dimer, with the exception of an increased stabilization on the oxygen and a destabilization of H^{nHB} by just under 2 kcal mol^{-1}; this results in a very small monomer stability of only -0.5 kcal mol^{-1}. The HB acceptor (monomer B) has a stabilization of -3.4 kcal mol^{-1}, which is more than twice the monomer stabilization in the C_{2h} cluster. The local atomic energies in the C_{2h} cluster are smaller than in monomer A, and have a stabilized carbon (+2 kcal mol^{-1}) and a destabilized oxygen (-7 kcal mol^{-1}). The hydrogens on monomer B have negligible energy change, despite a small increase in BCP density for the CH bond (+0.002 a.u.). The BCP value for the C=O bond is decreased as

133

well (by ~0.003 a.u.). A key difference between the two dimers is the CH⋯O and C−O bond critical point densities. The C_s cluster has a CH⋯O BCP of 0.0127 a.u., which is 0.005 a.u. larger than the CH⋯O bond in the C_{2h} dimer. Although the C_s cluster is clearly the more stable of the two geometries, the C_{2h} stacked geometry has similar bonding interactions as the cyclic and stacked clusters. We include it in the discussion to provide a comparison with the changing energies as these clusters increase in size.

In the cyclic geometries, a small amount of cooperative stability is demonstrated as the cluster increases in size. The net stabilization per formaldehyde monomer about 0.7 kcal mol^{-1} greater in the trimer than in the C_{2h} dimer, matching the small increase in stability per hydrogen bond. Considering the local atomic energies, some cooperativity is evident from the increasing magnitude of stabilization or destabilization per atom: carbon atoms are about 4 kcal mol^{-1} more stabilized and the H^{HB} are about 4 kcal mol^{-1} more destabilized in the trimer $vs.$ C_{2h} dimer. An increase in density at the CH⋯O bond critical points of the trimer (by 0.002 a.u.) is supportive of minimal cooperativity. We also notice that the C=O BCPs have a reduced density: 0.392 a.u. in the trimer vs 0.394 a.u. in the C_{2h} dimer. Comparing the cyclic trimer with the cyclic tetramer, minimal cooperativity becomes even more evident. The average energy change per hydrogen bond is only about 0.3 kcal mol^{-1} greater than the trimer system. Concurrently, the local energy changes are also minimal: oxygen atoms have only 1 kcal mol^{-1} increased stabilization and the remaining energy changes are nearly negligible. The net energy change per molecule is -2.4 kcal mol^{-1} (only 0.2 kcal mol^{-1} more stable than in the trimer). Geometric parameters and BCP values also do not indicate serious increase in cooperativity at the tetramer level (see Table 8.5), with values nearly consistent for both systems. In fact, the only geometrical parameter with a non-negligible change is the CH⋯O hydrogen-bond distance, which is directly reflected by the oxygen energy change.

Table 8.5 Some geometric and topological properties of cyclic formaldehyde clusters.

Property[a]	Dimer (C_{2h})	Trimer	Tetramer
BCP(C=O)	0.394	0.392	0.392
BCP(C-H^{HB})	0.281	0.282	0.283
BCP(C-H)	0.277	0.277	0.277
BCP(CH···O)	0.008	0.010	0.010
R(C=O)	1.216	1.218	1.218
R(C-H^{HB})	1.101	1.100	1.100
R(C-H)	1.105	1.105	1.105
R(CH···O)	2.580	2.419	2.408

[a] BCP electron densities are in a.u., distances in Å, angles in degrees, H^{HB} is the hydrogen involved in the HB in the ring.

For the stacked geometries, the average stabilization per HB in the trimer and tetramer clusters is 1.5 kcal mol^{-1}, which is not significantly different from that of the dimer (1.6 kcal mol^{-1}). Local atomic energy changes show a greater stabilization for the central formaldehyde molecules, *i.e.* those that do not have free hydrogens (B in the trimer and B and C in the tetramer). The atomic energies do not reveal cooperativity in the stacked clusters: increasing the number of hydrogen bonds does not reveal significantly different stabilization between the trimer and tetramer clusters. Net stability of central molecules for both trimer and tetramer are -3 kcal mol^{-1} and outer molecules are -1 kcal mol^{-1}. The local atomic stabilizations are also essentially the same in both trimer and tetramer. Bond critical point values agree with the atomic energy stabilization, with BCP densities consistent for both clusters.

The clustered geometries are the most stable of the three arrangements, by about 1 kcal mol^{-1} for the trimer and 5 kcal mol^{-1} for the tetramer. In these systems there are C−O contacts as well as CH···O hydrogen bonds, as was observed in the C_s dimer (for the trimer there is only one extra C−O contact on molecule B, but in the tetramer system all molecules have a C−O contact in addition to a hydrogen-bond interaction). In the trimer system, molecule A has a bifurcated hydrogen bond between the oxygens of the neighbouring molecules. The relatively large destabilization of this bifurcated hydrogen (+10 kcal mol^{-1}) is matched by a large stabilization of its carbon center (-11 kcal mol^{-1}) and only a minimal stabilization of the oxygen atom (-3 kcal mol^{-1}). This is opposite to the other molecules in the cluster, which have largely stabilized oxygens (-6 to -10 kcal

mol^{-1}) and minimally destabilized carbons (~ 3 kcal mol^{-1}). It is also unlike the C and O stabilities in the planar and stacked systems that all have stabilized carbon atoms. The BCP density of the C-H bond that forms the bifurcated hydrogen is increased (0.282 a.u. vs. 0.278-0.280 a.u. for non-bifurcated CH bonds) and the C=O BCP density is decreased (0.392 a.u. vs. 0.393-0.395 a.u. in the other monomers), indicating a weakening of the C=O bond and strengthening of the CH bond. Monomer B and C in this trimer cluster have a bonding environment that is similar to the acceptor monomer in the C$_s$ dimer, with the exception of the oxygen on B forming an extra interaction with the carbon on C. The atomic energies for B and C are also similar: a stabilized oxygen and destabilized carbon and hydrogens. There is an increased stabilization for the doubly interacting oxygen on monomer B, resulting in the largest net stability by about 2 kcal mol^{-1}. With the exception of the hydrogen atoms, there is negligible difference for the atomic stabilities in monomer A of the trimer cluster and the analogous monomer B of the Cs dimer. This could be an indication that there is no cooperative stabilization present here. Indeed, the bond critical point densities are also essentially the same for both monomers.

In the tetramer bucket arrangement there are three different bonding environments. The oxygen atom can form two interactions with two carbon atoms (B), one carbon and one hydrogen atom (C and D) or two hydrogen atoms (A). The net stabilities for the molecules in the cluster are about -4 kcal mol^{-1}, with the exception of D which is only -2 kcal mol^{-1}. Molecule D also has the largest C=O BCP density, and the smallest CH BCP density (with concurrently larger and smaller bond distances). The oxygen of monomer B forms two C−O contacts and has the largest stabilization in the cluster, as was also the case in the trimer cluster.

Comparing the general energy changes for the molecules in the cluster arrangement vs. the planar or stacked system it is clear that there are different sources of stability for each. In the planar and stacked geometries it is the carbon atoms that undergo the greatest stability and the H^{HB}s that undergo the majority of the destabilization; there is a minimal change in oxygen energy for these systems. In the cluster geometries, the ability to form C−O contacts redistributes the energy changes so that the carbon atom now experiences relatively significant stabilization. The destabilization of the hydrogen atoms is also significantly less. The ability to form C−O contacts dominates the lowest energy

structures for these small formaldehyde clusters, as was demonstrated for clusters from the dimer up to the tetramer. There is a very minimal amount of cooperative stability in the clusters, as is demonstrated by consistent atomic energy changes for each bond type despite the number of interactions formed per cluster.

8.5 Conclusions

We have evaluated the local and regional stabilities within clusters of water, methanol and formaldehyde from an atomic energy perspective, comparing our results with bond critical point (BCP) analysis and some geometrical parameters. Water clusters demonstrate both cooperative and anti-cooperative interactions. The cyclic, global minima for the water clusters are cooperative (as has been previously observed) and show increases in local stabilization and destabilization as cooperativity increases. The anti-cooperative, double donating trimer has a stabilization that is only half what is found in the cyclic trimer, and local and regional energy changes are similarly reduced. The anti-cooperative tetramer structure, with both double donating and double accepting water molecules, also has diminished energy changes and reduced electron density at bond critical points. From the atomic energy changes it is clear that the double donating water is more stabilized than the double accepting water; this is not observed from BCP densities because symmetry dictates that the hydrogen-bond BCPs are equivalent.

In the methanol clusters the HB cooperativity defined by total interaction energy is surprisingly negative at the trimer level. We confirm our calculations using CCSD(T) single point energies. The local energy changes, however, strongly support cooperative stability for the OH groups, with increasing atomic stabilization (oxygens) and destabilization (hydrogens) as the cluster size increases. The methyl groups show negligible stability changes, however the hydrogen atoms trans to the OH···O bond have a consistently greater stabilization that the other hydrogens in the methyl group.

For the formaldehyde clusters we consider two minima for the dimer. Our results agree with previous observations that the C_s orientation is more stable than the C_{2h}. A small amount of cooperativity is present in the circular clusters, with slight increases in regional stabilities as well as increasing stabilization and destabilization at the atomic

137

level. The stacked geometries do not show any cooperativity, as is confirmed by both consistent atomic energies and BCP values. The bucket geometries, which can also incorporate C−O contacts, are the most stable of the clusters. We compare energy changes for the C−O contacts in the bucket geometries with the energy changes in the C_s dimer (which also has a C−O contact), and do not find any significant difference in local stability, perhaps indicating that there is no cooperativity in these more stable systems.

8.6 Acknowledgements

Supporting Information

Benchmark data for Dunning basis set, SCVS calculations, and CCSD(T)//MP2 *vs.* CCSD(T)//B3LYP energies. Relevant AIM parameters including charges, scaled and unscaled energies, L(A) values, and BCP energy densities.

8.7 Chapter Summary and Relevance

In this chapter it is demonstrated that local changes in energy are a useful tool to distinguish between cooperative *vs.* non-cooperative and anti-cooperative interactions. Some key findings are as follows: when there is no cooperativity present in the bonding interaction, the local atomic energies remain consistent even as the clusters grow in size; atomic energy analysis of a symmetric cluster (such as the anti-cooperative water tetramer) provides insight into the distribution of stability that is not available using bond critical point values or bond lengths alone; and cooperativity can be localized at the functional group which constitutes the cooperative bonding species, such as the alcohol group in methanol clusters.

Chapter 9   Changing Weak Halogen Bonds into Strong Ones through Cooperativity with Beryllium Bonds
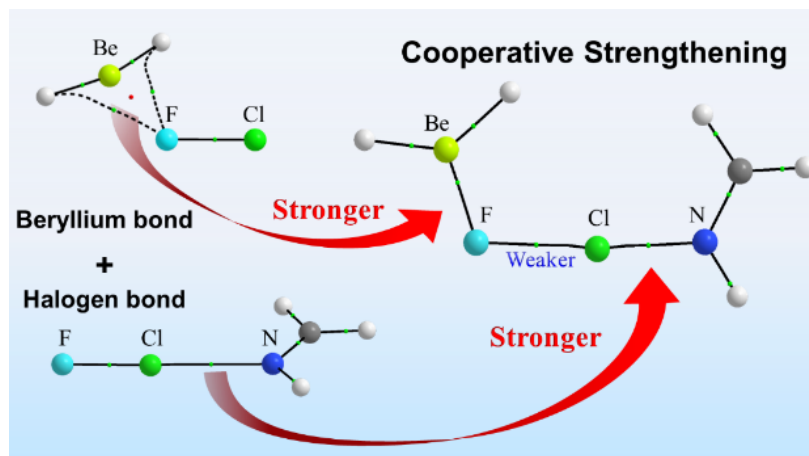
This final chapter was a collaborative effort. The contribution from this author was to provide the QTAIM analysis and some discussion related to the atomic energies. The benchmarking associated with the QTAIM analysis is also contributed from this author. The relevance of this chapter is to provide an example of the application of QTAIM atomic energy analysis to evaluation of multiple non-equivalent closed-shell bonding interactions, and to demonstrate the usefulness of visualization of atomic energy changes for assessment of local stabilities.

9.1 Abstract

The mutual interaction between beryllium bonds and halogen bonds within $H_2Be\cdots FCl\cdots Base$ complexes, where Base includes a wide set of N and O containing Lewis bases, has been studied at the M06-2X/6-31+G(d,p) level of theory. The reliability of this theoretical model was assessed by comparison with *ab initio* CCSD/aug-cc-pVTZ reference calculations. Cooperative effects were investigated within the framework of the atoms in molecules theory (AIM), by analyzing the topology of the electron density and the changes in the atomic energy components. The decomposition of the total stabilization energy into atomic components is found to be a very reliable tool to describe halogen bond interactions. Both the topological analysis of the electron density and the changes in the atomic energy components of the binding energy show the existence of strong cooperative effects between beryllium and halogen bonds, which are in some cases very intense. In general, there is a correlation between the intrinsic basicity of the Lewis base participating in the halogen bond and the resulting cooperativity, in the sense that the stronger the base the larger the cooperative effects.

9.2 Introduction

Cooperativity is one of the most important and common characteristics shared by non-covalent interactions [6, 130, 127, 157, 192-194, 196, 200-202, 204-205, 207, 209, 279, 284-285, 305, 313, 319-333]. It has long been recognized that the stability of water clusters and many other hydrogen bonded polymers has its origin in the fact that the interaction between a hydrogen bond (HB) acceptor and a HB donor is strengthened when one or both of them interact with an additional HB donor or HB acceptor, respectively. In addition to cooperativity, non-covalent interactions such as HBs, dihydrogen bonds [334], halogen bonds [294-295, 335], pnicogen bonds [198, 253, 336-337], etc. share other common characteristics. In most cases these interactions involve closed-shell systems, with electrostatic and polarization or charge-transfer effects commonly contributing to their stability, although the magnitude of various contributions may vary within rather large limits. Recently, it has been shown that one of these closed-

shell interactions – the so-called beryllium bond, which is formed when a typical Lewis base interacts with a BeXY derivative acting as a Be Lewis acid – can lead to rather high interaction energies [191]. The strength of beryllium bonds is not only electrostatic in origin but is also closely related to the large charge-transfer which usually takes place from the Lewis base towards the empty 2p orbital of Be and towards the σ_{BeX}* (or σ_{BeY}*) antibonding orbital. The obvious consequence of this charge transfer is a significant electron density redistribution in the Lewis base which leads to a dramatic enhancement of its intrinsic acidity [338]. Electron density redistributions are also responsible for the cooperativity found between beryllium bonds and hydrogen bonds when these non-covalent interactions stabilize molecular clusters, as has been shown for the interaction of azole dimers [210] and water clusters with BeX_2 derivatives [6]. Strong cooperative effects are also detected when the interaction takes place between ditopic monomers, such as (iminomethyl)beryllium hydride or (iminomethyl)beryllium fluoride [HC(BeX)=NH, X = H, F], in which the molecule has a terminal Lewis basic site (the imino group) and a terminal Lewis acidic site (the BeX group), favouring the self-assembling of the system to form rather stable linear or circular polymers [339].

At the opposite end of the scale as far as the strength of non-covalent interactions is concerned are the so-called halogen bonds [294-295, 335], where the center acting as a Lewis acid is a halogen atom. Many complexes stabilized through halogen bonds have been described in the literature. The aim of this paper is to analyze possible cooperative effects between rather weak interactions, such as halogen bonds, and rather strong interactions, such as beryllium bonds. This analysis will be carried out under the conventional perspective of the atoms in molecules (AIM) theory [1, 57] in terms of the topology of the electron density and its Laplacian. To further this discussion, we will also use an alternative perspective based on the evaluation of atomic energy components [3]. This is also available within the framework of the AIM theory and has been shown to be a rather reliable index to quantitatively describe internal energy changes in weak non-covalent interactions, and has been successfully applied in the analysis of cooperativity between hydrogen bonds in water clusters [4-5] and hydrogen bonds and beryllium bonds in $(H_2O)_nBeX_2$ (n = 1–3, X = H, F) complexes [6].

The idea is to explore the changes undergone by the halogen bond in FCl⋯Base complexes when the FCl in turn forms a beryllium bond with BeH_2 to yield $H_2Be⋯FCl⋯Base$ clusters. To define the set of Lewis bases to be investigated we consider it of interest to include compounds that present basic sites which are commonly found in biological systems. Hence, we have included a set of bases where the basic site is a carbonyl group in a variety of functional environments, namely formaldehyde, acetaldehyde, acetone, formamide, and formic acid. We also consider bases in which the basic site is an amino-type nitrogen. In this case we have included ammonia and its methyl derivatives to check the sensitivity of cooperativity between beryllium and halogen bonds to substituent effects. Finally, to investigate the effect of the hybridization of the basic site, we have included other nitrogen bases such as methanimine, hydrogen cyanide, imidazole and pyridine, in which the nature of the N basic site changes. To these sets we have added tetrahydrofuran as an example of a cyclic ether.

9.3 Computational Details

Since the aim of this study is to evaluate the changes in the strength of halogen bonds that interact cooperatively with beryllium bonds, the first step is to assess the appropriate theoretical method to describe these weak interactions. For this purpose we have chosen, as a benchmark set, N-bases in which the hybridization of the basic site changes, namely ammonia, methanimine and HCN, and also formaldehyde as a good prototype of a carbonyl base. The geometries of the complexes between FCl and the aforementioned benchmark compounds were optimized using the following *ab initio* theoretical models: MP2/aug-cc-pVTZ, CCSD/cc-pVTZ, CCSD/aug-cc-pVTZ, as well as the following density-functional theory (DFT) methods: B3LYP [214-215], M06 [340] and M06-2X [340] in combination with a 6-31+G(d,p) basis set expansion. For all the benchmark complexes the CCSD/aug-cc-pVTZ calculations were used as the common reference. Optimizations and benchmark calculations were performed without symmetry constraints using the Gaussian 09 program [70].

As shown in Figure B.3 of the supporting information (Appendix B.5), MP2 strongly overbinds the complexes, yielding halogen bonds that are up to 0.22 Å too short.

Conversely, CCSD/cc-pVTZ yields distances that are too long (up to 0.11 Å) showing the importance of the diffuse functions. The behavior of B3LYP is similar to that exhibited by MP2, although the optimized distances are slightly longer. No significant differences are observed when the B3LYP functional is replaced by the M06-2X one. However, the agreement between the CCSD/aug-cc-pVTZ halogen bond lengths and those obtained with the M06-2X functional is rather good, and deviations are almost constantly equal to 0.03 Å, indicating that this functional is well suited for the description of weak non-covalent interactions.

The second step of our assessment focused on the basis set expansion. All molecule pairs were re-optimized at the M06-2X/6-311++G(d,p) level, followed with frequency evaluations and AIM analysis [69]. Some benchmark complexes were optimized at the M06-2X/6-311++G(2df,2pd) level, including complexes with acetone, formaldehyde, HCN, methanimine, and methylamine as base. Since we are interested in the use of atomic energy components, that is, the energy obtained for each atom through integration over the corresponding atomic basin as defined in the AIM theory framework [1], we have used as a suitable reference for this assessment the molecular virial ratio (see supporting information, Figure B.3 in Appendix B.5). It can be observed that using the larger 6-311++G(d,p) basis set will improve the virials significantly for the complexes, and that increasing the number of polarization functions to 2df,2pd yields minimal further improvement. Considering atomic stabilities (*i.e.* the effective change in each atom's energy as BeH_2 interacts with FCl-Base to form the $H_2Be\cdots FCl\cdots Base$ complex), the smallest basis set yields energy values very close to the large basis set with increased polarization functions (see Figure B.4 of the supporting information in Appendix B.5, as well as Figure B.5 and Section B.5.2 for further information on unscaled atomic energies and the AIM method). We conclude that the use of the smaller 6-31+G(d,p) basis set is a good compromise between economy and accuracy for this kind of analysis. The same basis set expansion has been used to obtain the corresponding molecular graphs, which are the ensemble of the critical points of the electron density, maxima (nuclei) and first order saddle points (bond critical points), and the zero gradient lines ($\nabla\rho = 0$) or bond paths connecting them. The charge transfer taking place between the interacting subunits has been calculated by means of the natural bond orbital (NBO) method [218].

From the energetic viewpoint, cooperativity can also be also analyzed by means of the many-body interaction energy (MBIE) formalism [117, 126] in which the interaction energy of a ternary ABC complex can be obtained as the sum of two-body energy interactions:

$$\Delta^2 E(AB) = E(AB) = [E(A) + E(B)] \qquad (9.1)$$

(with similar expressions for BC and AC), and three-body energy interactions:

$$\Delta^3 E(ABC) = E(ABC) - [E(A) + E(B) + E(C)]$$
$$- [\Delta^2 E(AB) + \Delta^2 E(AC) + \Delta^2 E(BC)] \qquad (9.2)$$

In equations (1) and (2) *E(A), E(B), E(AB)* are computed with the geometries they have in the ternary complex. Note that the first two terms on the right side of eq. (9.2) define the interaction energy of the ternary complex:

$$E_{int} = E(ABC) - [E(A) + E(B) + E(C)] \qquad (9.3)$$

whereas the binding energy, E_{bind}, is given by a similar expression in which the energy of the monomers is computed at their equilibrium conformations. The MBIE analysis will be carried out at the M062X/6-31+G(d,p) level of theory. We have checked the reliability of this model for some suitable examples by using as a reference the values obtained at the CCSD(T)/aug-cc-pVTZ level of theory (See Table B.11 of the supporting information in Appendix B.5).

9.4 Results and discussion

The molecular graphs of the complexes are shown in Figures 9.1a-9.4a whereas the changes of the atomic energy components upon complex formation are shown in Figures 9.1b-9.4b. The sum of atomic energy changes yields the total energy change for the complex formation. In part (a) of each figure, the first column shows the molecular graph of the complex between FCl and the Lewis base, stabilized by only a halogen bond. The second column shows the original complex now interacting with BeH_2, allowing cooperative effects to arise between the new beryllium bond and the pre-existing halogen bond. In part (b) of each figure, the first column shows the changes in the atomic energies

when the FCl···Lewis base is formed, and the second column shows these changes when the H_2Be··FCl···Lewis base complex is formed.

9.4.1 Amines

In Figure 9.1a the results for ammonia and its successive methyl derivatives are shown. Regarding the first column, we see the expected increase in strength of the Cl···N halogen bond with the number of methyl substituents, reflected in an increase of the electron density at the bond critical point (BCP). Consistently, the Cl···N internuclear distance decreases in the same order. The important result is found in the second column where we see that each halogen bond becomes stronger when the FCl molecule forms a beryllium bond with BeH_2, and this reinforcement also increases with methyl substitution. In fact, whereas the electron density at the Cl···N BCP increases by 0.066 a.u. in the ammonia cluster with BeH_2 interaction, this increase becomes 0.075, 0.080 and 0.081 a.u. for methyl-, dimethyl- and trimethylamine, respectively. Also importantly, the corresponding Be···F beryllium bonds are reinforced as well, and this reinforcement also increases with methyl substitution. Indeed, the electron density at the Be···F BCP for the isolated H_2Be···FCl complex (not shown in the figure) is 0.023 a.u. and when this moiety interacts with a Lewis base to form the corresponding Cl···N halogen bond, the value of the electron density at the Be···F BCP increases to 0.062, 0.070, 0.074 and 0.077 a.u. for ammonia, methyl-, dimethyl- and trimethylamine, respectively.

These cooperative effects are also well described by the atomic energy components, as shown in Figure 9.1b. In this alternative representation of the complexes, each atom is represented by a sphere whose diameter is proportional to the magnitude of the atom's energy change. The sphere is red when the atom experiences a negative (stabilizing) energy change and blue if it experiences a positive (destabilizing) energy change. For atoms with an energy change of less than ± 4 kJ mol^{-1} the sphere is left uncoloured.
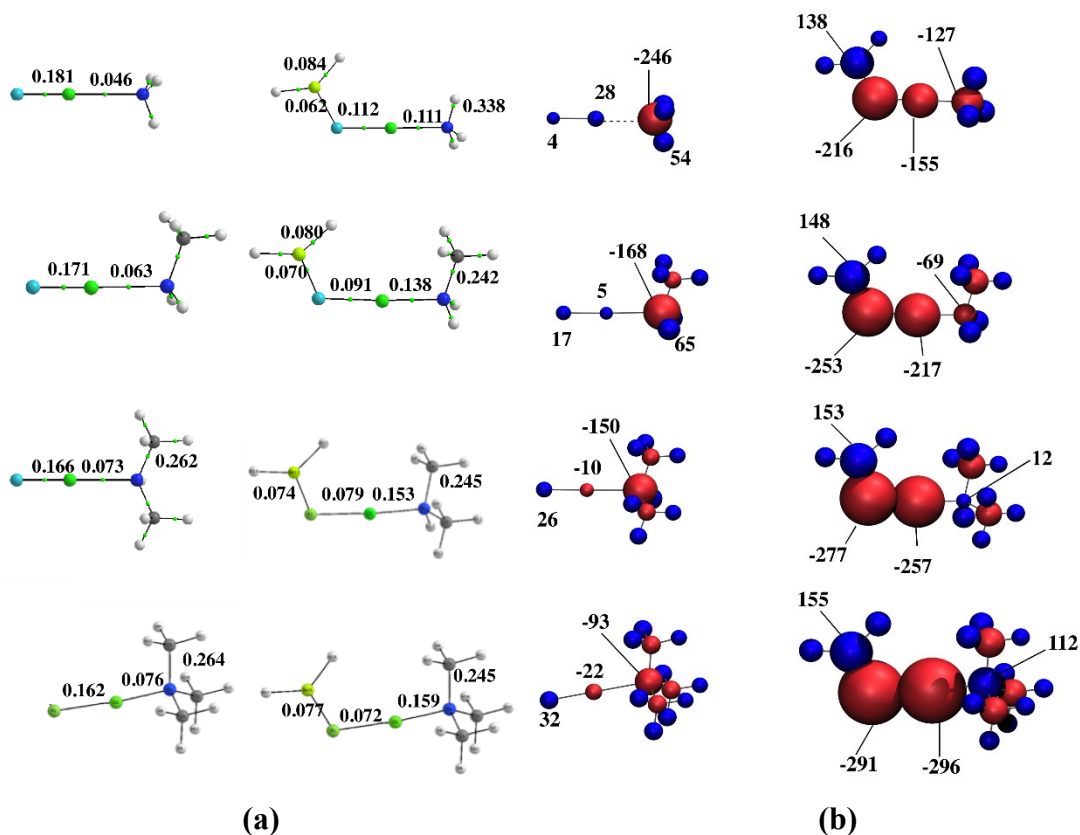
Figure 9.1 Complexes involving ammonia, methyl-, dimethyl- and trimethylamine. **a)** Molecular graphs. Electron densities at the BCPs in a.u. **b)** Change in atomic energy upon formation of the complexes. Values for the relative energy change of each atom are labeled (kJ mol^{-1}). Stabilized atoms are red, destabilized atoms are blue. Atom size corresponds to the magnitude of energy change. Structures were prepared using VMD software [114].

It is clear that in the H$_2$Be··FCl···Lewis base complexes the BeH$_2$ molecule as a whole is destabilized by the interaction, whereas both halogen atoms F and Cl become stabilized and this stabilization increases with methyl substitution. Using this perspective, the relative strengths of the beryllium and halogen bonds are reflected in the stabilization undergone by the F and Cl atoms of the FCl moiety and in the changes observed for the atomic energy components of the BeH$_2$ group and the N atom of the Lewis base. Indeed, the strengthening of the halogen bond on going from ammonia to trimethylamine is reflected by increasing stabilization of the Cl atom and concomitant destabilization of the N atom of the base. Similarly, the strength of the beryllium bond is mirrored in the increasing stabilization of the F atom and the increasing destabilization of the BeH$_2$

147

group. A comparison of the first and second column of Figure 9.1b shows that the aforementioned changes for F and Cl atoms are larger in the $H_2Be\cdots FCl\cdots Base$ complexes than in the $FCl\cdots Base$ ones, due to cooperativity between beryllium and halogen bonds. Indeed, the strength of the halogen bond depends on the electron acceptor capacity of Cl which obviously increases when the FCl molecule forms a beryllium bond in which the F atom behaves as a Lewis base transferring charge to Be, and therefore enhancing the Lewis acidity of Cl. Reciprocally, the beryllium bond becomes also reinforced when a FCl molecule forms a halogen bond with a Lewis base, because the charge transferred from the Lewis base to FCl enhances the basicity of the fluorine center and therefore its electron donor capacity. In the $FCl\cdots Base$ complexes we see this manifest as an increase in the atomic destabilization of F, going from methyl- to trimethylamine.

These changes in the electron donor and electron acceptor ability of the active centers within these complexes are easily detected by an NBO analysis. For example, for the $FCl\cdots NH_3$ complex the NBO analysis shows that this complex is stabilized through the interaction between the N lone-pair of the ammonia molecule and the $\sigma_{FCl}*$ antibonding orbital, the second-order interaction energy between these two orbitals being 137 kJ mol^{-1} and the charge transfer amounting to 0.13 e. Consistently the F-Cl bond length increases from 1.639 Å in the isolated FCl molecule to 1.691 Å in the $FCl\cdots NH_3$ complex. Similarly, for the $H_2Be\cdots FCl$ complex the NBO analysis reveals a charge transfer from one of the lone-pairs of the F atom towards the empty *p* orbital of Be and the $\sigma_{BeH}*$ antibonding orbital. Consistently, the BeH_2 moiety in the $H_2Be\cdots FCl$ complex departs slightly from linearity (the HBeH angle being 162.4º) and the BeH bonds become slightly longer. When both non-covalent interactions are allowed to interact by forming the $H_2Be\cdots FCl\cdots NH_3$ complex, the NBO analysis detects the formation of two new bonds, one between Cl and N with 75% participation of the N orbitals and 25% of the Cl orbitals, and another very polar bond between F and Be, with 94% contribution of F orbitals. Hence, the Cl-N and the Be-F internuclear distances shrink by 0.386 and 0.399 Å, respectively, and the BeH_2 group now becomes significantly bent (HBeH angle 138.1º). Logically, the charge transfers involved in the formation of these two new bonds necessarily decrease the electron density at the F-Cl bond which becomes 0.249 Å longer

in the new complex.

A final point of discussion is to consider the two-body components of the interaction energies. The same discussion of cooperativity that we interpret from the characteristics of the electron density is also observed through the decomposition of the total energy into its many-body contributions. These values are summarized in Table 9.1.

Table 9.1 Binding energies, E_{bind}, interaction energies, E_{int} and the two- and three-body interaction energy components (Δ^2E and Δ^3E) for ABC (A = BeH_2, B = FCl, C = Lewis base) complexes. The values within parentheses correspond to the two-body interactions in the binary AB and BC complexes. All values are in kJ mol^{-1}.

Lewis Base	E_{bind}	E_{int}	$\Delta^2E(AB)$	$\Delta^2E(BC)$	$\Delta^2E(AC)$	$\Sigma\Delta^2E$	Δ^3E
NH$_3$	-105	-231	-73 (-13)	-80 (-56)	-4	-157	-74
Methylamine	-139	-307	-94 (-13)	-117 (-71)	-5	-217	-90
Dimethylamine	-163	-369	-115 (-13)	-151 (-85)	-5	-272	-97
Trimethylamine	-173	-388	-129 (-13)	-182 (-95)	-5	-315	-73

We notice right away that the interaction energies are much larger than the binding energies; this is because of a large distortion in the geometries of the three monomers when they form the complex. The value of Δ^3E clearly shows that in all cases the interaction energy is much larger than the sum of the two-body components of the ternary complex. These two-body interactions are always dominated by the contributions of their nearest neighbors, AB and BC. The third component, AC, is relatively insignificant. Cooperativity is also reflected in the larger (absolute) values of the Δ^2E terms when compared with the interaction energies in the free binary complexes, $H_2Be\cdots FCl$ and $FCl\cdots$Lewis base (values within parentheses). These data are in perfect agreement with our previous discussion: both the $H_2Be\cdots FCl$ beryllium bond and the $FCl\cdots$Lewis base halogen bond are reinforced through cooperativity, and this reinforcement steadily increases with the intrinsic basicity of the Lewis base attached to FCl.

9.4.2 Different N Lewis bases

Cooperativity between beryllium and halogen bonds clearly changes with the nature of the basic site of the Lewis base participating in the halogen bond. This is apparent when

the complexes formed by ammonia, methanimine and HCN are compared. As shown in Figures 9.2a,b the halogen bond formed is strongest with methanimine and weakest with HCN, but what is more important from the perspective of our study is that the reinforcement of both halogen and beryllium bonds, as a result of their cooperativity, follows the same trend: much larger in methanimine than in ammonia, and also larger than in HCN, as shown by the relative increase of the electron densities at the corresponding BCPs (See Figure 9.2a).
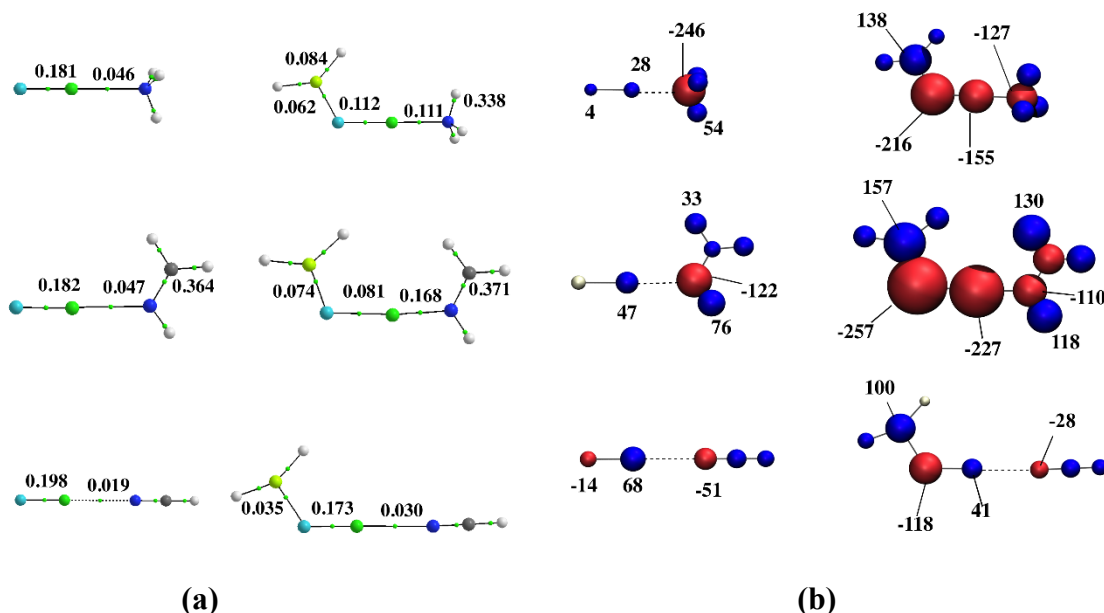

(a)   **(b)**

Figure 9.2 Complexes involving ammonia, methanimine and HCN. **a)** Molecular graphs; **b)** Change in atomic energy upon formation of the complexes. Same conventions as in Figure 9.1.

The same conclusion is reached by analyzing the atomic energy components (see Figure 9.2b). The stabilization of F and Cl is the largest for the methanimine complex and the smallest for the HCN complex. In fact, the Cl atom in the HCN complex is actually destabilized by the BeH_2 interaction. The net stabilization of the atoms in the BeH_2 and FCl atom groups within the HCN complex has a destabilization of +37 kJ mol^{-1}. The same atoms in ammonia and methanimine are overall stabilized by -41 and -56 kJ mol^{-1}, respectively. This feature points to some kind of anti-cooperative effect which cannot be detected just by looking at the electron densities at the BCPs. Indeed, from these electron densities the only thing we can conclude is that they increase much less for the HCN

Lewis base than for ammonia or methanimine. In terms of stability imparted by the formation of the beryllium bond, the binding energy for the interaction of BeH_2 with $FCl\cdots HCN$ is much smaller (-26 kJ mol^{-1}) than in the complexes involving ammonia (-75 kJ mol^{-1}) or methanimine (-96 kJ mol^{-1}). We also note that the F-Cl interaction changes with the BeH_2 interaction, actually becoming weaker the stronger the cooperative influence. What the analysis in terms of the atomic components is showing is that for HCN the lowered atomic stabilization comes not just from the formation of the beryllium and the halogen bonds, but also from the diminished influence of the F-Cl bond. For the complexes involving ammonia and methanimine, the overall cooperative reinforcements of the beryllium and halogen bonds are much larger than the weakening of the FCl bond.

The discussion in terms of two-body interaction energies is again consistent with the picture obtained through the analysis of the electron density. The values summarized in Table 9.2 show a significant difference between binding and interaction energies. These values reach a maximum for methanimine, the most basic compound, and are significantly smaller for HCN, which is the weakest base of the three considered. Also in this case, as observed in the amines, the interaction energy is larger than the sum of the two-body components, which are again dominated by the nearest neighbor contributions.

Table 9.2 Binding energies, E_{bind}, interaction energies, E_{int}, and the two- and three-body interaction energy components (Δ^2E and Δ^3E) for ABC (A = BeH_2, B = FCl, C = Lewis base) complexes. The values within parentheses correspond to the two-body interactions in the binary AB and BC complexes. All values are in kJ mol^{-1}.

Lewis Base	E_{bind}	E_{int}	$\Delta^2E(AB)$	$\Delta^2E(BC)$	$\Delta^2E(AC)$	$\Sigma\Delta^2E$	Δ^3E
NH$_3$	-105	-231	-73 (13)	-80 (56)	-4	-157	-74
Methanimine	-122	-326	-95 (13)	-118 (50)	-5	-239	-87
HCN	-37	-70	-33 (13)	-20 (20)	-2	-55	-15

Cooperativity is also large when dealing with nitrogen atoms belonging to aromatic rings as in the case of imidazole and pyridine (see Figure 9.3a,b). It is worth noting that these cooperative effects are particularly strong in the pyridine complex, where the electron density at the halogen BCP increases by 0.142 a.u. and the bond shrinks by 0.501 Å (from 2.227 to 1.726 Å). Concomitantly, the beryllium bond is also reinforced significantly, its electron density increasing by 0.075 a.u. and the $Be\cdots F$ distance

shrinking 0.522 Å (from 2.000 to 1.478 Å). This indicates that the charge transfer from F towards Be is very large. The consequence is a dramatic enhancement of the electronegativity of the F atom, which recovers part of the charge transferred to BeH_2 by depopulating the F-Cl bonding region, a phenomenon known as the bond activation reinforcement (BAR) rule [341]. Consistently, the electron density at the F-Cl BCP decreases dramatically and the F-Cl bond almost cleaves. The near cleavage of the F-Cl bond favors the formation of a dihydrogen bond between one of the BeH_2 hydrogen atoms and one of the CH hydrogens of the pyridine ring. Once more, this description is in agreement with the changes observed in the atomic energy components. As illustrated in Figure 9.3b, the stabilization of the Cl atom is much larger than in the methyl amines and methanimine, and similarly larger than in imidazole. As well, the stabilization of F is much larger in pyridine than in the complexes involving other N-containing Lewis bases. It is also worth noting that the formation of the aforementioned dihydrogen bond between the BeH_2 group and the aromatic ring is reflected in a dramatic destabilization of the CH hydrogen of the ring with respect to the other ring hydrogens (+315 *vs.* +30 to +59 kJ mol^{-1}) and also by a larger destabilization of the hydrogen atom attached to Be which participates in the dihydrogen bond, with respect to the one that does not participate in this interaction (+94 *vs.* +62 kJ mol^{-1}).

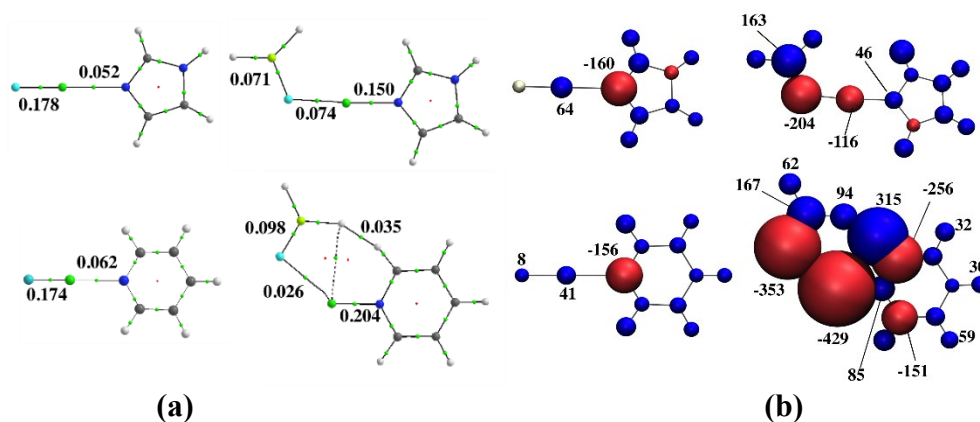(a)   (b)

Figure 9.3 Complexes involving imidazole and pyridine. **a)** Molecular graphs; **b)** Change in atomic energy upon formation of the complexes. Same conventions as in Figure 9.1.

9.4.3 Carbonyl bases

In general terms, the behavior observed for complexes involving different carbonyl Lewis bases is similar to the one described above for N-containing Lewis bases. By comparing the results for formaldehyde, acetaldehyde and acetone it is apparent that both perspectives – the molecular graphs and the atomic energy components – indicate an increase in the cooperativity between beryllium and halogen bonds with increasing number of methyl substituents (See Figure 9.4). In addition, both descriptions indicate that substitution by an amino group, going from formaldehyde to formamide also leads to an enhancement of cooperativity, whereas substitution by a hydroxyl group on going from formaldehyde to formic acid has the opposite effect: smaller changes in BCP values and reduced energy changes for Be, F and Cl. It is worth noting that, as discussed above for HCN, here again the cooperative effect is largely diminished when analyzing the atomic energy components of formic acid: The chlorine has a negligible energy change, the sum of the atomic energies of the $H_2Be\cdots FCl$ group is destabilizing ($+9$ kJ mol^{-1}), and the F-Cl bond critical point has a much smaller decrease in electron density. These results clearly ratify that cooperativity between beryllium and halogen bonds is a general phenomenon that depends on the intrinsic basicity of the Lewis base, and that in general the stronger the base the larger the cooperative effects.

It is also interesting to emphasize that some subtle effects are detected with the two approaches we are considering for our analysis. For instance, for the $H_2Be\cdots FCl\cdots$acetaldehyde complex, the topology of the electron density shows the existence of an intramolecular hydrogen bond between a hydrogen atom of the methyl group and the Cl atom, and also of a dihydrogen bond between the same methyl hydrogen and one of the hydrogen atoms in the BeH_2 group. The analysis of the changes in the atomic energy components shows that this methyl hydrogen atom in the $H_2Be\cdots FCl\cdots$acetaldehyde complex is more destabilized (63 kJ mol^{-1}) than the other two (25 kJ mol^{-1}), and that concomitantly the H atom of the BeH_2 group interacting with it is also more destabilized (24 kJ mol^{-1}) than the other one (15 kJ mol^{-1}).
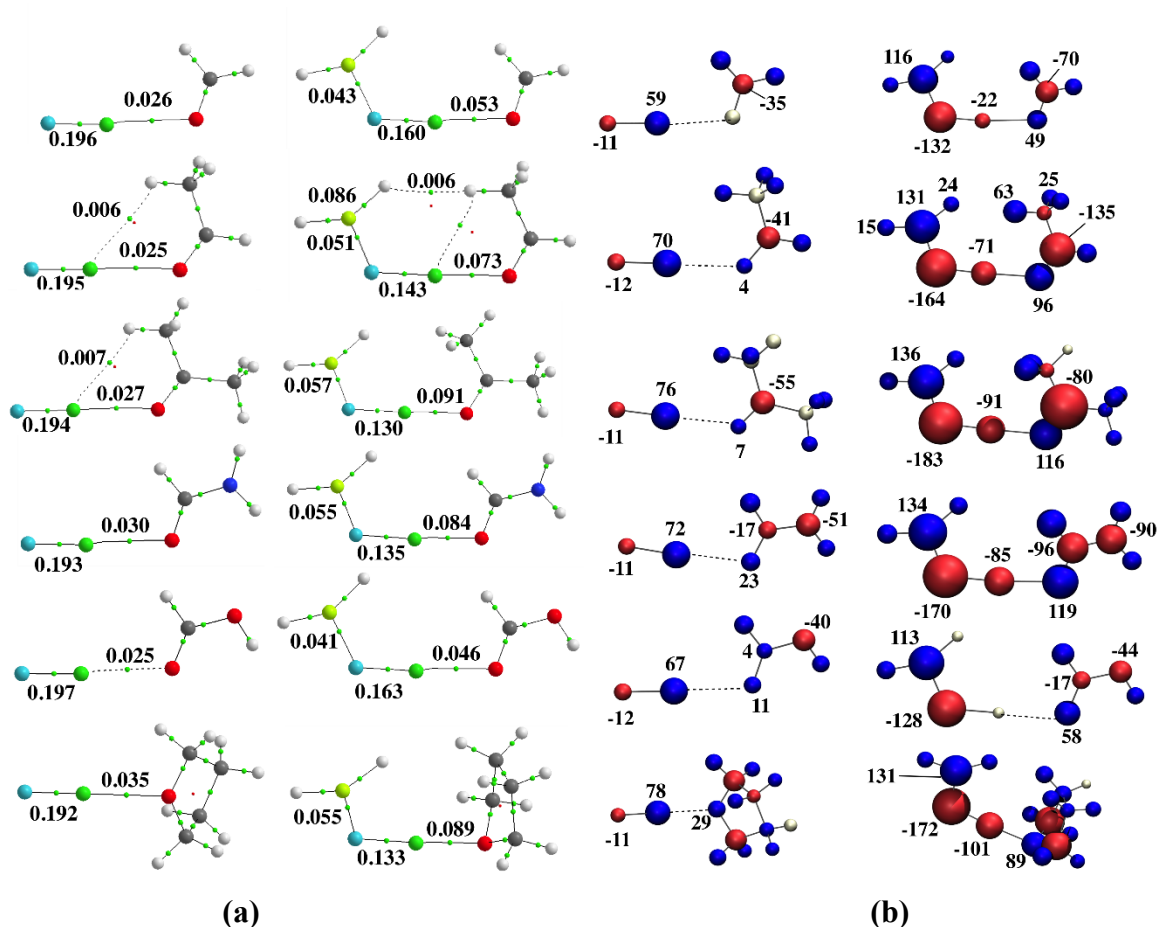
Figure 9.4 Complexes involving carbonyl bases: formaldehyde, acetaldehyde, acetone, formamide, formic acid and tetrahydrofuran. **a)** Molecular graphs; **b)** Change in atomic energy upon formation of the complexes. Same conventions as in Figure 9.1.

Finally, it is interesting to note that the complex with tetrahydrofuran becomes symmetric when it interacts with BeH_2. In the FCl··· tetrahydrofuran complex the FCl molecule practically aligns with the O atom of tetrahydrofuran, the FClO angle being 177.1º, yet the complex has no symmetry, belonging to the C_1 point group. However, in the H_2Be···FCl···tetrahydrofuran complex, not only the FClO arrangement remains practically linear (FClO angle = 176.1º), but the whole complex has C_s symmetry, because the $H_2BeFClO$ group lies in a symmetry plane which bisects the H_2C-CH_2 bond of the five-membered ring opposite to the O atom. This arrangement seems to favor a stabilizing non-bonding interaction between the negatively charged hydrogen attached to Be with the positively charged H atoms of the H_2C-CH_2 mentioned above.

154

9.5 Conclusions

In agreement with previous studies of water clusters interacting with beryllium hydride, the decomposition of the interaction energies into atomic components is found to be a very reliable tool to describe different closed-shell interactions such as halogen bonds. Both the topological analysis of the electron density and the changes in the atomic energy components of the interaction energy show the existence of strong cooperative effects between beryllium and halogen bonds. In some cases this cooperativity is so intense that halogen or beryllium bonds that were initially rather weak, for example between FCl and pyridine and between H_2Be and FCl, become both much shorter and stronger because of their mutual interaction. In general, there is some correlation between the intrinsic basicity of the Lewis base participating in the halogen bond and the cooperativity, in the sense that the stronger the base the larger the cooperative effects. This explains why cooperativity increases with methyl substitution either for N or for O containing bases, and why it increases when a methyl group is replaced by an amino group, which enhances the basicity of the system through the conjugation of the amino lone-pair with the basic site. Also interestingly, the analysis in terms of atomic energy components permits the quantification of some anti-cooperative effects, undetectable using only bond critical point electron densities.

9.6 Acknowledgments

Supporting Information

Benchmark evaluation, discussion of atomic energy scaling, relevant AIM properties and Cartesian coordinates for all structures are included in the supporting information. This material is available free of charge via the Internet at http://pubs.acs.org.

9.7 Chapter Summary and Relevance

In this chapter the decomposition of interaction energies into atomic components is found to be a useful tool to describe halogen bonds combining with beryllium bonds. There is a general correlation between the intrinsic basicity of the Lewis base participating in the halogen bond and the cooperativity, in the sense that the stronger the base the larger the cooperative effects. These cooperative effects were effectively demonstrated by visualization of the increase in the local energy changes for the interacting atoms.

Chapter 10   Future Work

Initially this thesis was meant to include a chapter on the local energy changes in water molecules as they solvate the amino acids, evaluated using Car-Parinello molecular dynamics (CPMD) and QTAIM analysis. This largely came about because of interesting discussion surrounding the important role of water in protein folding. The project was not completed, largely due to time limitations because the necessary groundwork for the QTAIM energy analysis had to be completed before a discussion of larger systems could be made with confidence. While the project did not make it past the preliminary CPMD stage, it would be wonderful in the future to use AIM to explore any correlation between the local influence of the amino acids on their solvating water's structure and the role of each amino acid's solvation in the folding of proteins.

One other project which remains to be completed is a benchmark evaluation of the atomic energies in a large series of diatomic and triatomic homo- and hetero-molecular systems. Although the local analysis of water clusters and other systems which involve hydrogen bonding has been well-explored in this thesis, it would be beneficial to explore the nature of systems containing a larger variety of atoms. Some calculations for this project have been completed, however the analysis remains to be finished.

It is my hope that the future will see further exploration of chemical phenomena using the quantum theory of atoms in molecules energy analysis.

Chapter 11   Conclusions

In this thesis, electron density topology as described in the quantum theory of atoms in molecules was used to evaluate the local energy changes in a range of systems including water clusters, water wires interacting with alkali, alkaline earth metal and halide ions, small systems demonstrating cooperative, non-cooperative and anti-cooperative hydrogen bonding interactions, and closed-shell interactions combining beryllium, hydrogen and halogen bonding. The energy changes reflect atomic stabilities and are used to create a visual representation of the local stability for systems with interactions as described above. Important conclusions from each thesis chapter are summarized below.

In Chapters 4 and 5, evaluation of water clusters $(H_2O)_{n=2-6}$ reveals that, relative to the water monomer, all oxygen atoms have a decrease in atomic energy (indicating stabilization) and hydrogen atoms increase in atomic energy (indicating destabilization), with the exception of the water dimer. Hydrogen bond cooperativity for the cyclic clusters is demonstrated at an atomic level by an increase in energy change that matches the increase in stability. Small variations in atomic energies within these clusters are correlated to water geometry and reflect variations in hydrogen bond strengths. In the water hexamers, the simple cooperativity that was observed in the cyclic systems is diminished as the linearity and symmetry of the hydrogen bond interactions are lost. The prism, cage and bag clusters demonstrate a large range of local water stabilities, due to multiple bonding partners and competing cooperative and anti-cooperative interactions.

Analysis of the interaction between BeX_2 (X = H, F) and the water dimer and trimer in Chapter 6 reveals a significant electron density redistribution within the whole system, as a result of the formation of strong beryllium bonds between water molecules and the BeX_2 derivative. There is a substantial change in the proton donor and proton acceptor capacity of the water molecules involved. Cooperative and anti-cooperative effects are again demonstrated at the atomic level through the atomic stability analysis. The changes in the atomic energy components are correlated with the changes in the strength of these interactions, providing a quantitative measure of cooperative effects directly in terms of energies.

In the study of water wires interacting with a set of alkali, alkaline earth metal and halide ions (Chapter 7), local stability within the water wire reveals that, relative to the neutral water wire, water is stabilized when interacting with F^-, H^+, Li^+, and Na^+ ions and destabilized when interacting with K^+, Ca^{2+}, Cl^-, and Br^- ions. These trends match properties of kosmotropic *vs.* chaotropic ions. Visualization of the changing atomic energies clearly represents increased local stability at the position of the proton for the protonated water wires. Systems that contain two ions separated by an n=7 water wire demonstrate that the local water stability in the presence of a counter ion is essentially the sum of the individual influences of each isolated ion.

In Chapter 8, atomic stabilities were evaluated for cooperative, anti-cooperative and non-cooperative clusters of methanol, water and formaldehyde, respectively. While the cooperatively interacting clusters show increasing stability at the atomic level as the cluster size increases, this is not observed in non-cooperative arrangements of formaldehyde. This indicates that the atomic energy analysis can correctly represent these non-covalent interactions. Furthermore, the atomic energy analysis was able to reveal local stability insight that was not available using BCP or total energy analysis alone. The changes in the atomic energy components correlate with changing types of interactions, providing a direct, quantitative evaluation of cooperative effects in terms of energies.

In the final chapter, atomic energy analysis combined with an evaluation of bond critical points shows the existence of strong cooperative effects between beryllium and halogen bonds. There is a general correlation between the intrinsic basicity of the Lewis base participating in the halogen bond and the resulting cooperativity, in the sense that the stronger the base the larger the cooperative effects. This general correlation is supported by the atomic energies representation of increasing local stabilities for the systems with stronger Lewis bases.

In conclusion, the atomic energy analysis made available through Bader's QTAIM topological evaluation of the electron density is an exceptionally useful tool for evaluating the distribution of local stability in weakly interacting systems, in particular for hydrogen bonding and closed-shell interactions. Energy changes can reflect the cooperativity in these systems and the visualization of the resulting atomic stabilities provides a unique perspective of the nature of these chemical interactions.

References

1. Bader, R. F. W. *Atoms in Molecules. A Quantum Theory;* Carendon Press: Oxford, 1990.

2. Matta, C.; Castillo, N.; Boyd, R. Atomic Contributions to Bond Dissociation Energies in Aliphatic Hydrocarbons. *J. Chem. Phys.* **2006,** *125,* 204103.

3. Taylor, A.; Taylor, J.; Watson, G. W.; Boyd, R. J. Electronic Energy Changes Associated with Guanine Quadruplex Formation: An Investigation at the Atomic Level. *J. Phys.Chem. B* **2010,** *114,* 9833-9839.

4. Albrecht, L.; Boyd, R. J. Visualizing Internal Stabilization in Weakly Bound Systems Using Atomic Energies: Hydrogen Bonding in Small Water Clusters. *J. Phys. Chem. A* **2012,** *116* (15), 3946-3951.

5. Albrecht, L.; Chowdhury, S.; Boyd, R. J. Hydrogen Bond Cooperativity in Water Hexamers: Atomic Energy Perspective of Local Stabilities. *J. Phys. Chem. A* **2013,** *117* (41), 10790-10799.

6. Albrecht, L.; Boyd, R. J.; Mó, O.; M., Y. Cooperativity Between Hydrogen Bonds and Beryllium Bonds in $(H_2O)_nBeX_2$ (n = 1–3, X = H, F) Complexes. A New Perspective. *Phys. Chem. Chem. Phys.* **2012,** *14* (42), 14540-14547.

7. Albrecht, L.; Boyd, R. J. Atomic Energy Analysis of Cooperativity, Anti-cooperativity, and Non-cooperativity in Small Clusters of Methanol, Water, and Formaldehyde. *Comp. Theo. Chem.* **2014,** *in press,* DOI: 10.1016/j.comptc.2014.08.022.

8. Albrecht, L.; Boyd, R. J.; Mó, O.; Yáñez, M. Changing Weak Halogen Bonds into Strong Ones Through Cooperativity With Beryllium Bonds. *J. Phys. Chem. A* **2014,** *118* (23), 4205–4213.

9. Gatti, C., Macchi, P., Eds. *Modern Charge-Density Analysis;* Springer: New York, 2012.

10. Ludwig, R. Water: From Clusters to the Bulk. *Angew. Chem. Int. Ed.* **2001,** *40,* 1808-1827.

11. Weinhold, F.; Klein, R. A. What is a Hydrogen Bond? Mutually Consistent Theoretical and Experimental Criteria for Characterizing H-bonding Interactions. *Mol. Phys.* **2012,** *110,* 565-579.

12. Arunan, l.; Desiraju, G. R.; Klein, R. A.; Sadle, J.; Scheiner, S.; Alkorta, I.; Clary, D. C.; Crabtree, R. H.; Dannenberg, J. J.; Hobza, P.; Kjaergaard, H. G.; Legon, A. C.; Mennucci, B.; Nesbitt, D. J. Definition of the Hydrogen Bond. *Pure Appl. Chem.* **2011,** *83* (8), 1637-1641.

13. Xantheas, S. Cooperativity and Hydrogen Bonding Network in Water Clusters. *Chem. Phys.* **2000,** *258* (2-3), 225-231.

14. Freire, E. The Thermodynamic Linkage Between Protein Structure, Stability, and Function. *Meth. Mol. Biol.* **2008,** *168,* 37-68.

15. Dannenberg, J. J. The Importance of Cooperative Interactions and a Solid-state Paradigm to Proteins: What Peptide Chemists Can Learn From Molecular Crystals. *Adv. Protein Chem.* **2006,** *72,* 227-273.

16. Becke, A. D. Fifty Years of Density-functional Theory in Chemical Physics. *J. Chem. Phys.* **2014,** *140,* 18A301(18).

17. Temelso, B.; Archer, K. A.; Shields, G. C. Benchmark Structures and Binding Energies of Small Water Clusters with Anharmonicity Corrections. *J. Phys. Chem. A* **2011,** *115,* 12034-12046.

18. Morrone, J. A.; Lin, L.; Car, R. Tunneling and Delocalization Effects in Hydrogen Bonded Systems: A Study in Position and Momentum Space. *J. Chem. Phys.* **2009,** *130,* 204511(13).

19. Brioch, J. Discovering Water: James Watt, Henry Cavendish, and the Nineteenth-Century "Water Controversy". *Vic. Stud.* **2006,** *48,* 574-576.

20. Marechal, Y. *The Hydrogen Bond and the Water Molecule: The Physics and Chemistry of Water, Aqueous and Bio Media;* Elsevier: Amsterdam, Netherlands, 2007.

21. Grzesieka, S.; Cordiera, F.; Jaravinea, V.; Barfieldb, M. Insights into Biomolecular Hydrogen Bonds from Hydrogen Bond Scalar Couplings. *Prog. Nuc. Mag. Res. Spec.* **2004,** *45,* 275-300.

22. Smith, J. D.; Cappa, C. D.; Messer, B. D.; Drisdell, W. S. Probing the Local Structure of Liquid Water by X-ray Absorption Spectroscopy. *J. Phys. Chem. B* **2006,** *110,* 20038-20045.

23. Pinga, Z. H.; Nguyenb, Q. T.; Chena, S. M.; Zhoua, J. Q.; Dinga, Y. D. States of Water in Different Hydrophilic Polymers — DSC and FTIR Studies. *Polymer* **2001,** *42,* 8461-8467.

24. Rupley, J. A.; Careri, G. Protein Hydration and Function. In *Advances in Protein Chemistry;* Anfinsen, C. B., Edsall, J. T., Richards, F. M., Eds.; Academic Press, 1991; Vol. 41. pp 31-172.

25. Bondar, A.-N.; Elstner, M.; Suhai, S.; Smith, J. C.; Fischer, S. Mechanism of Primary Proton Transfer in Bacteriorhodopsin. *Structure* **2004,** *12,* 1281-1288.

26. Tarek, M.; Tobias, D. J. The Dynamics of Protein Hydration Water: A Quantitative Comparison of Molecular Dynamics Simulations and Neutron-scattering Experiments. *Biophys. J.* **2000,** *79,* 3244-3257.

27. Persson, E.; Halle, B. Nanosecond to Microsecond Protein Dynamics Probed by Magnetic Relaxation Dispersion of Buried Water Molecules. *J. Am. Chem. Soc.* **2008,** *130,* 1774-1787.

28. Miranda, P. B.; Shen, Y. R. Liquid Interfaces: A Study by Sum-Frequency Vibrational Spectroscopy. *J. Phys. Chem. B* **1999,** *103,* 3292-3307.

29. Liu, D.; Ma, G.; Levering, L. M.; Allen, H. C. Vibrational Spectroscopy of Aqueous Sodium Halide Solutions and Air−Liquid Interfaces: Observation of Increased Interfacial Depth. *J. Phys. Chem. B* **2004,** *108,* 2252-2260.

30. Schrödinger, E. An Undulatory Theory of the Mechanics of Atoms and Molecules. *Phys. Rev. 28* **1926,** *28,* 1049-1070.

31. Born, M.; Oppenheimer, R. Zur Quantentheorie der Molekeln. *Ann. Phys. (Leipzig)* **1927,** *84* (20), 457-484.

32. Møller, C.; Plesset, M. S. Note on an Approximation Treatment for Many-electron Systems. *Phys. Rev.* **1934,** *46,* 618-622.

33. Hohenberg, P.; Kohn, W. Inhomogeneous Electron Gas. *Phys. Rev.* **1964,** *3B* (136), 864-871.

34. Kohn, W.; Sham, L. J. Self-Consistent Equations Including Exchange and Correlation Effects. *Phys. Rev.* **1965,** *140,* A1133-A1138.

35. Koch, W.; Holthausen, M. C. *A Chemist's Guide to Density Functional THeory,* 2nd ed.; Wiley-VCH, Weinham, 2001.

36. Jensen, F. *Introduction to Computational Chemistry,* 2nd ed.; Wiley: England, 2006.

37. Grimme, S. Semiempirical GGA-type Density Functional Constructed with a Long-range Dispersion Correction. *J. Comp. Chem.* **2006,** 1787-1799.

38. Wu, Q.; Yang, W. Empirical Correction to Density Functional Theory for van der Waals Interactions. *J. Chem. Phys.* **2002,** *116* (2), 515-524.

39. Becke, A. D.; Johnson, E. R. Exchange-Hole Dipole Moment and the Dispersion Interaction. *J. Chem. Phys.* **2005,** 154104.

40. Becke, A. D.; Johnson, E. R. Exchange-Hole Dipole Moment and the Dispersion Interaction Revisited. *J. Chem. Phys.* **2007,** *127,* 154180.

41. Burns, L. A.; Vázquez- Mayagoitia, Á.; Sumpter, B. G.; Sherril, C. D. Density-functional Approaches to Noncovalent Interactions: A Comparison of Dispersion Corrections (DFT-D), Exchange-Hole Dipole Moment (XDM) Theory, and Specialized Functionals. *J. Chem. Phys.* **2011,** *134,* 084107.

42. Boys, S. F.; Bernardi, F. The Calculation of Small Molecular Interactions by the Diffrences of Separate Total Energies. Some Procedures With Reduced Errors. *Mol. Phys.* **1970,** *19* (4), 553-566.

43. Hobza, P.; Havlas, Z. Counterpoise-corrected Potential Energy Surfaces of Simple H-bonded Systems. *Theo. Chem. Acc.* **1998,** *99,* 372-377.

44. Salvador, P.; Paizs, B.; Duran, M.; Suhai, S. On the Effect of the BSSE on Intermolecular Potential Energy Surfaces. Comparision of A Priori and A Posteriori BSSE Correction Schemes. *J. Comp. Chem.* **2001,** *22,* 765-786.

45. Xantheas, S.; Burnham, C. J.; Harrison, R. J. Development of Transferable Interaction Models for Water. II. Accurate Energetics of the First Few Water Clusters from First Principles. *J. Chem. Phys.* **2002,** *116* (4), 1493-1499.

46. Tomasi, J.; Mennucci, B.; Cammi, R. Quantum Mechanical Continuum Solvation Models. *Chem. Rev.* **2005,** *105,* 2999-3093.

47. Lange, A. W.; Herbert, J. M. Polarizable Continuum Reaction-field Solvation Models Affording Smooth Potential Energy Surfaces. *J. Phys. Chem. Lett.* **2010,** *1,* 556-561.

48. Roux, B.; Simonson, T. Implicit Solvent Models. *Biophys. Chem.* **1999,** *78,* 1-20.

49. Feig, M.; Brooks, C. L. Recent Advances in the Development and Application of Implicit Solvent Models in Biomolecule Simulations. *Curr. Opin. Struct. Bio.* **2004,** *14,* 217-224.

50. Baker, N. A. Improving Implicit Solvent Simulations: a Poisson-centric View. *Curr. Opin. Struct. Biol.* **2005,** *15,* 137-143.

51. Tomasi, B.; Mennucci, E.; Cances, E. The IEF Version of the PCM Solvation Method: An Overview of a New Method Addressed to Study Molecular Solutes at the QM Ab Initio Level. *J. Mol. Struct. (Theochem)* **1999,** *464,* 211-226.

52. Lewars, E. G. The Concept of the Potential Energy Surface. In *Computational Chemistry;* 2, Ed.; Springer, 2011; pp 9-43.

53. Schlegel, H. B. Exploring Potential Energy Surfaces for Chemical Reactions: An Overview of Some Practical Methods. *J. Comput. Chem.* **2003,** *24,* 1514-1527.

54. Peng, C.; Ayala, P. Y.; Schlegel, H. B.; Frisch, M. J. Using Redundant Internal Coordinates to Optimize Equilibrium Geometries and Transition States. *J. Comp. Chem.* **1996,** *17,* 49-56.

55. Fisherman, G. S. *Monte Carlo: Concepts, Algorithms, and Applications;* Springer: New York NY, 1995.

56. Bader, R. F. W. Nearsightedness as Seen by a Physicist and a Chemist. *J. Phys. Chem. A* **2008,** *112,* 13717-13728.

57. Matta, C. F., Boyd, R. J., Eds. *The Quantum Theory of Atoms in Molecules: From Solid State to DNA and Drug Design;* Wiley-VCH: Weinheim, 2007.

58. Lu, H.; Wang, Y.; Wu, Y.; Yang, P.; Li, L.; Li, S. Hydrogen-bond Network and Local Structure of Liquid Water: An Atoms-in-molecules Perspective. *J. Chem. Phys.* **2008,** *129,* 124512.

59. Bader, R. F. W. Principle of Stationary Action and the Definition of a Proper Open System. *Phys. Rev. B* **1994,** *49,* 13348-13356.

60. Bader, R. F. W. Everyman's Derivation of the Theory of Atoms in Molecules. *J. Phys. Chem. A* **2007,** *111,* 7966-7972.

61. Magnoli, D. E.; Murdoch, J. R. Obtaining Self−consistent Wave Functions Which Satisfy the Virial Theorem. *Int. J. Quantum Chem.* **1982,** *22,* 1249-1262.

62. Löwdin, P.-O. Scaling Problem, Virial Theorem, and Connected Relations in Quantum Mechanics. *J. Mol. Spectr.* **1959,** *3,* 46-66.

63. Matta, C. F. How Dependent are Molecular and Atomic Properties on the Electronic Structure Method? Comparison of Hartree–Fock, DFT, and MP2 on a Biologically Relevant set of Molecules. *J. Comput. Chem.* **2010,** *31,* 1297-1311.

64. McNaught, A. D.; Wilkinson, A. *IUPAC. Compendium of Chemical Terminology (the "Gold Book"),* 2nd ed.; Blackwell Scientific Publications: Oxford, 1997; Vol. 2.3.3.

65. University of Texas at Austin. Code: Bader Charge Analysis. http://theory.cm.utexas.edu/henkelman/code/bader/ (accessed Oct 16, 2014).

66. The ABINIT Group. abinit.org. www.abinit.org (accessed Oct 16, 2014).

67. Scientific Computing & Modelling. ADF: powerful DFT code for modeling molecules. https://www.scm.com/ADF/ (accessed Oct 16, 2014).

68. Ortiz, J.; Jané, B. C. Xaim. http://www.quimica.urv.es/XAIM/ (accessed Oct 16, 2014).

69. Keith, T. A. *AIMAll (Version 11.12.19);* TK Gristmill Software: Overland Park, KS USA, 2011.

70. Frisch, M. J.; Trucks, G. W.; Schlegel, H. B.; Scuseria, G. E.; Robb, M. A.; Cheeseman, J. R.; Scalmani, G.; Barone, V.; Mennucci, B.; Petersson, G. A.; Nakatsuji, H.; Caricato, M.; Li, X.; Hratchian, H. P.; Izmaylov, A. F.; Bloino, J., *et al. Gaussian 09, Revision D.01;* Gaussian, Inc: Wallingford CT, CT, USA, 2013.

71. Cortés-Guzmàn, F.; Bader, R. F. W. Transferability of Group Energies and Satisfaction of the Virial Theorem. *Chem. Phys. Lett.* **2003,** *379,* 183-192.

72. Nagy, Á. Regional Virial Theorem in Density-functional Theory. *Phys. Rev. A* **1992,** *46* (9), 5417-5419.

73. Rodríguez, J. I.; Ayers, P. W.; Götz, A. W.; Castillo-Alvarado, F. L. Virial Theorem in the Kohn-Sham Density-functional Theory Formalism; Accurate Calculation of the Atomic Quantum Theory of Atoms in Molecules Energies. *J. Chem. Phys.* **2009,** *131,* 021101-021104.

74. Rose, G. D.; Wolfenden, R. Hydrogen Bonding, Hydrophobicity, Packing, and Protein Folding. *Annu. Rev. Biophys. Biomol. Struct.* **1993,** *22,* 381-415.

75. Lazaridis, T.; Karplus, M. Thermodynamics of Protein Folding: a Microscopic View. *Biophys. Chem.* **2003,** *100,* 367-395.

76. Nienaber, V. L.; Richardson, P. L.; Klighofer, V.; Bouska, J. J.; Giranda, V. L.; Greer, J. Discovering Novel Ligands for Macromolecules using X-ray Crystallographic Screening. *Nature Biotech.* **2000,** *18,* 1105 - 1108.

77. Mittermaier, A.; Kay, L. E. New Tools Provide New Insights in NMR Studies of Protein Dynamics. *Science* **2006,** *312,* 224-228.

78. Edgecomb, S. P.; Murphy, K. P. Structural Energetics of Protein Folding and Binding. *Curr. Opin. Biotechnol.* **2000,** *11,* 62-66.

79. Baker, D. A Surprising Simplicity to Protein Folding. *Nature* **2000,** *405,* 39-42.

80. Harano, Y.; Roth, R.; Kinoshita, M. On the Energetics of Protein Folding in Aqueous Solution. *Chem. Phys. Lett.* **2006,** *432,* 275-280.

81. Sackett, D. L.; Sept, D. Protein-protein Interactions: Making Drug Design Second Nature. *Nat. Chem.* **2009,** *1,* 596-597.

82. Gromiha, M. M.; Selvaraj, S. Importance of Long Range Interactions in Protein Folding. *BioPhys. Chem.* **1999,** *77,* 49-68.

83. Matta, C.; Bader, R. An atoms-in-molecules Study of the Genetically-encoded Amino Acids: I. Effects of Conformation and of Tautomerization on Geometric, Atomic, and Bond Properties. *PROTEINS* **2000,** *40,* 310-329.

84. Jissy, A. K.; Ashik, U. M. P.; Datta, A. Nucleic Acid G-quartets: Insights into Diverse Patterns and Optical Properties. *J. Phys. Chem. C* **2011,** *115,* 12530-12546.

85. Stillinger, F. H. Water Revisited. *Science* **1980,** *209,* 451-457.

86. Bouteiller, Y.; Perchard, J. P. The Vibrational Spectrum of $(H_2O)_2$: Comparison Between Anharmonic Ab Initio Calculations and Neon Matrix Infrared Data Between 9000 and 90 cm−1. *Chem. Phys.* **2004,** *305,* 1-12.

87. Keutsch, F. N.; Cruzan, J. D.; Saykally, R. J. The Water Trimer. *Chem. Rev.* **2003,** *103,* 2533-2578.

88. Tremblay, B.; Madebène, B.; Alikhani, M. E.; Perchard, J. P. The Vibrational Spectrum of the Water Trimer: Comparison Between Anharmonic Ab Initio Calculations and Neon Matrix Infrared Data Between 11,000 and 90 cm^{-1}. *Chem. Phys.* **2010,** *378,* 27-36.

89. Nielsen, I. M. B.; Seidl, E. T.; Janssen, C. L. Accurate Structures and Binding Energies for Small Water Clusters: The Water Trimer. *J. Chem. Phys.* **1999,** *110,* 9435-9443.

90. Ramírez, F.; Hadad, C. Z.; Guerra, D.; David, J.; Restrepo, A. Structural Studies of the Water Pentamer. *Chem. Phys. Lett.* **2011,** *507,* 229-233.

91. Smith, J. D.; Cappa, C. D.; Wilson, K. R.; Messer, B. M.; Cohen, R. C.; Saykally, R. J. Energetics of Hydrogen Bond Network Rearrangements in Liquid Water. *Science* **2004,** *306,* 851-853.

92. Laage, D.; Hynes, J. T. A Molecular Jump Mechanism of Water Reorientation. *Science* **2006,** *311,* 832-835.

93. Wernet, P.; Nordlund, D.; Bergmann, U.; Cavalleri, M.; Odelius, M.; Ogasawara, H.; Näslund, L. Å.; Hirsch, T. K.; Ojamäe, L.; Glatzel, P.; Pettersson, L. G. M.; Nilsson, A. The Structure of the First Coordination Shell in Liquid Water. *Science* **2004,** *304,* 995-999.

94. Shields, R. M.; Temelso, B.; Archer, K. A.; Morrell, T. E.; Shields, G. C. Accurate Predictions of Water Cluster Formation, $(H_2O)_{n=2-10}$. *J. Phys. Chem.* **2010,** *114,* 11725-11737.

95. Kolb, B.; Thonhauser, T. van der Waals Density Functional Study of Energetic, Structural, and Vibrational Properties of Small Water Clusters and Ice Ih. *Phys. Rev.* **2011,** 045116(6).

96. Xantheas, S. S.; Dunning, T. H. Ab Initio Studies of Cyclic Water Clusters $(H_20)_n$, n=1-6. I. Optimal Structures and Vibrational Spectra. *J. Chem. Phys.* **1993,** 8774-8792.

97. Lyssenko, K. A.; Nelyubina, Y. V.; Kostyanovsky, R. G.; Antipin, M. Y. Water Clusters in Crystal: Beyond the "Hydrogen-Bonding Graphs". *Chem. Phys. Chem. Comm.* **2006,** 2453-2455.

98. Klein, R. A. Cooperativity in Large Water Clusters, Liquid Water, Ice and Clathrates. *NIC Series* **2006,** *32,* 65-74.

99. Bader, R. F. W. The Quantum Mechanical Basis of Conceptual Chemistry. *Monatsh. Chem.* **2005,** *136,* 819-854.

100. Bader, R. F. W.; Beddall, P. M.; Peslak Jr., J. Theoretical Development of a Virial Relationship for Spatially Defined Fragments of Molecular Systems. *J. Chem. Phys.* **1973,** *58,* 557-566.

101. Bader, R. F. W.; Larouche, A.; Gatti, C.; Carroll, M. T.; MacDougall, P. J. Properties of Atoms in Molecules: Dipole Moments and Transferability of Properties. *J. Chem. Phys.* **1987,** *87,* 1142-1152.

102. Bushmarinov, I. S.; Lyssenko, K. A.; Antipin, M. Y. Atomic Energy in the 'Atoms in Molecules' Theory and Its Use for Solving Chemical Problems. *Russ. Chem. Rev.* **2009,** *74,* 283-302.

103. Bader, R. F. W.; Carroll, M. T.; Cheeseman, J. R.; Chang, C. Properties of Atoms in Molecules: Atomic Volumes. *J. Am. Chem. Soc.* **1987,** *109,* 7968-7979.

104. Wiberg, K. B.; Bader, R. F. W.; Lau, C. D. H. A Theoretical Analysis of Hydrocarbon Properties: I. Bonds, Structures, Charge Concentrations and Charge Relaxations. *J. Am. Chem. Soc.* **1987,** *109,* 985-1001.

105. Matta, C. F.; Arabi, A. A.; Keith, T. A. Atomic Partitioning of the Dissociation Energy of the P-O(H) Bond in Hydrogen Phosphate Anion ($HPO_4{}^{2-}$): Disentangeling the effect of Mg^{2+}. *J. Phys. Chem. A* **2007**.

106. Mandado, M.; Mosquera, R. A.; Van Alsenoy, C. A Scheme Estimating the Energy of Intramolecular Hydrogen Bonds in Diols. *Tetrahedron* **2006,** *62,* 4243-4252.

107. Lorenzo, L.; Gonzalez, M.; Marıa, J.; Mandado, M.; Mosquera, R. A. Do the Neighboring Residues in a Polypeptide Affect the Electron Distribution of an Amino Acid Significantly? A Quantitative Study Using the Quantum Theory of Atoms in Molecules (QTAIM). *J. Chem. Inf. Mod.* **2006,** *46,* 2056-2065.

108. Bushmarinov, I. S.; Fedyanin, I. V.; Lyssenko, K. A.; Lapteva, V. L.; Pisarev, S. A.; Palyulin, V. A. The "Hockey Sticks" Effect Revisited: The Conformational and Electronic Properties of 3,7-Dithia-1,5-diazabicyclo[3.3.1]nonane from the QTAIM Perspective. *J. Phys. Chem. A* **2011,** *15,* 12738–12745.

109. Santra, B.; Michaelides, A.; Scheffler, M. On the Accuracy of Density-functional Theory Exchange Correlation Functionals for H bonds in Small Water Clusters: Benchmarks Approaching the Complete Basis Set Limit. *J. Chem. Phys.* **2007,** *127* (18), 184104.

110. Kendall, R. A.; Dunning, T. H. . J.; Harrison, R. J. Electron Affinities of the First-row Atoms Revisited. Systematic Basis Sets and Wave Functions. *J. Chem. Phys.* **1992,** 6796-6806.

111. Wieczorek, R.; Haskamp, L.; Dannenberg, J. J. Molecular Orbital Calculations of Water Clusters on Counterpoise-corrected Potential Energy Surfaces. *J. Phys. Chem. A* **2004,** *108,* 6713-6723.

112. Simon, S.; Duran, M.; Dannenberg, J. J. Effect of Basis Set Superposition Error on the Water Dimer Surface Calculated at Hartree–Fock, Moller-Plesset, and Density Functional Theory Levels. *J. Phys. Chem. A* **1999,** *103* (11), 1640-1643.

113. Bader, R. F. W.; Preston, H. J. T. The Kinetic Energy of Molecular Charge Distributions and Molecular Stability. *Int. J. Quantum Chem.* **1969,** *3,* 327-347.

114. Humphrey, W.; Dalke, A.; Schulten, K. VMD - Visual Molecular Dynamics. *J. Mol. Graph.* **1996,** *14,* 33-38.

115. King, B. F.; Weinhold, F. Structure and Spectroscopy of (HCN)n clusters: Cooperative and Electronic Delocalization Effects in C–HN Hydrogen Bonding. *J. Chem. Phys.* **1995,** *103,* 333-347.

116. Weinhold, F. Nature of H-bonding in Clusters, Liquids, and Enzymes: An Ab Initio, Natural Bond Orbital Perspective. *Comp. Theo. Chem.* **1997,** *398-399,* 181-197.

117. Xantheas, S. Ab Initio Studies of Cyclic Water Clusters $(H_2O)N$, N = 1–6. II. Analysis of Many–Body Interactions. *J. Chem. Phys.* **1994,** *100,* 7523-7753.

118. Wendler, K.; Thar, J.; Zahn, S.; Kirchner. Estimating the Hydrogen Bond Energy. *J. Phys. Chem. A* **2010,** *114,* 9529-9536.

119. Brown, M. G.; Keutsch, F. N.; Saykally, R. J. The Bifurcation Rrearrangement in Cyclic Water Clusters: Breaking and Making Hydrogen Bonds. *J. Chem. Phys.* **1998,** *109,* 9645-9647.

120. Lee, H. M.; Suh, S. B.; Lee, J. Y.; Tarakeshwar, P.; Kim, K. S. Structures, Energies, Vibrational Spectra, and Electronic Properties of Water Monomer to Decamer. *J. Chem. Phys.* **2000,** *112* (22), 9759-9772.

121. Paul, J.; Collier, C.; Saykally, R.; Scherer, J.; OKeefe, A. Direct Measurement of Water Cluster Concentrations by Infrared Cavity Ringdown Laser Absorption Spectroscopy. *J. Pys. Chem. A* **1997,** *101,* 5211-5214.

122. Brudermann, J.; Melzer, M.; Buc, U.; Kazimirski, J. K.; Bush, V. The Asymmetric Cage Structure of (H2O)7 From a Combined Spectroscopic and Computational Study. *J. Chem. Phys.* **1999,** *110* (22), 10649-10652.

123. Kim, J.; Majumdar, D.; Lee, H. M.; Kim, K. S. Structures and Energetics of the Water Heptamer: Comparison with the Water Hexamer and Octamer. *J. Chem. Phys.* **1999,** *110* (18), 9128-9134.

124. Cybulski, H.; Sadlej. On the Calculations of the Vibrational Raman Spectra of Small Water Clusters. *J. Chem. Phys.* **2007,** *342,* 163-172.

125. Falk, M.; Ford, T. A. Infrared Spectrum and Structure of Liquid Water. *Can. J. Chem.* **1966,** *44,* 1699-1707.

126. Hankins, D.; Moskowitz, J. W.; Stillinger, F. H. Water Molecule Interactions. *J. Chem. Phys.* **1970,** *53,* 4544–4554.

127. Mó, O.; Yáñez, M.; Elguero, J. Cooperative (Nonpairwise) Effects in Water Trimers: Nn Ab Initio Molecular Orbital Study. *J. Chem. Phys.* **1992,** *97,* 6628-6638.

128. Masella, M.; Gresh, N.; Flament, J.-P. A Theoretical Study of Nonadditive Effects in Four Water Tetramers. *J. Chem. Soc., Faraday Trans.* **1998,** 2745-2753.

129. Keutsch, F. N.; Saykally, R. J. Water clusters: Untangling the Mysteries of the Liquid, One Molecule at a Time. *Proc. Nat. Acad. Sci.* **2001,** *98* (19), 10533-10540.

130. Ohno, K.; Okimura, M.; Akai, N.; Katsumoto, Y. The Effect of Cooperative Hydrogen Bonding on the OH Stretching-Band Shift for Water Clusters Studied by Matrix-Isolation Infrared Spectroscopy and Density Functional Theory. *Phys. Chem. Chem. Phys.* **2005,** *7,* 3005-3014.

131. Hirabayashi, S.; Ito, F.; Yamada, K. Infrared Spectra of the $(H_2O)_n–SO_2$ Complexes in Argon Matrices. *J. Chem. Phys.* **2006,** *125,* 034508-0345016.

132. Cobar, E. A.; Horn, P. R.; Bergman, R. G.; Head-Gordon, M. Examination of the Hydrogen-Bonding Networks in Small Water Clusters (n = 2–5, 13, 17) Using Absolutely Localized Molecular Orbital Energy Decomposition Analysis. *Phys. Chem. Chem. Phys.* **2012,** *14,* 15328-15339.

133. Tainter, C. J.; Ni, Y.; Shi, L.; Skinner, J. L. Hydrogen Bonding and OH-stretch Spectroscopy in Water: Hexamer (Cage), Liquid Surface, Liquid, and Ice. *Phys. Chem. Lett.* **2013,** *4,* 12-17.

134. Medders, G. R.; Babin, V.; Paesani, F. A Critical Assessment of Two-body and Three-body Interactions in Water. *J. Chem. Theo. Comp* **2013,** *9,* 1103-1114.

135. Pérez, C.; Muckle, M. T.; Zaleski, D. P.; Seifert, N. A.; Temelso, B.; Shields, G. C.; Kisiel, Z.; Pate, B. H. Structures of Cage, Prism, and Book Isomers of Water Hexamer from Broadband Rotational Spectroscopy. *Science* **2012,** *336* (3083), 897-901.

136. Pérez, C.; Lobsiger, S.; Seifert, N. A.; Zaleski, D. P.; Temelso, B. Broadband Fourier Transform Rotational Spectroscopy for Structure Determination: The Water Heptamer. *Chem. Phys. Lett.* **2013,** *571,* 1-15.

137. Skinner, C. J.; Tainter, J. L. The Water Hexamer: Three-body Interactions, Structures, Energetics, and OH-stretch Spectroscopy at Finite Temperature. *J. Chem. Phys.* **2012,** *137,* 104304(6).

138. Kim, K.; Jordan, K.; Zwier, T. Low-energy Structures and Vibrational Frequencies of the Water Hexamer Comparison with Benzene-$(H_2O)_6$. *J. Am. Chem. Soc.* **1994,** *116,* 11568-11569.

139. Liu, K.; Brown, M.; Saykally, R. Terahertz Laser Vibration-rotation Tunneling Spectroscopy and Dipole Moment of a Cage Form of the Water Hexamer. *J. Phys. Chem. A* **1997,** *101,* 8995-9010.

140. Liu, K.; Brown, M.; Carter, C.; Saykally, R.; Gregory, J.; Clary, D. Characterization of a Cage Form of the Water Hexamer. *Nature* **1996,** *381,* 501-503.

141. Gregory, J.; Clary, D. Theoretical Study of the Cage Water Hexamer Structure. *J. Phys. Chem. A* **1997,** *101,* 6813-6819.

142. Pedulla, J.; Kim, K.; Jordan, K. Theoretical Study of the n-body Interaction Energies of the Ring, Cage and Prism Forms of $(H_2O)_6$. *Chem. Phys. Lett.* **1998,** *291,* 78-84.

143. Nauta, K.; Miller, R. Formation of Cyclic Water Hexamer in Liquid Helium: The Smallest Piece of Ice. *Science* **2000,** *287,* 293-295.

144. Tissandier, M. D.; Singer, S. J.; Coe, J. V. Enumeration and Evaluation of the Water Hexamer Cage Structure. *J. Phys. Chem. A* **2000,** *104,* 752-757.

145. Fajardo, M.; Tam, S. Observation of the Cyclic Water Hexamer in Solid Parahydrogen. *J. Chem. Phys.* **2001,** *115,* 6807-6811.

146. Losada, M.; Leutwyler, S. Water Hexamer Clusters: Structures, Energies, and Predicted mid IR Spectra. *J. Chem. Phys.* **2002,** *117* (5), 2003-2016.

147. Steinbach, C.; Andersson, P.; Melzer, M.; Kazimirski, J.; Buck, U.; Buch, V. Detection of the Book Isomer from the OH-stretch Spectroscopy of Size Selected Water Hexamers. *Phys. Chem. Chem. Phys.* **2004,** *6,* 3320-3324.

148. Bates, D.; Tschumper, G. CCSD(T) Complete Basis Set Limit Relative Energies for Low-Lying Water Hexamer Structures. *J. Phys. Chem. A* **2009,** *113* (15), 3555-3559.

149. Chen, Y.; Li, H. Intermolecular Interaction in Water Hexamer. *J. Phys. Chem. A* **2010,** *114,* 11719-11724.

150. Hincapié, G.; Acelas, N.; Castaño, M.; David, J.; Restrepo, A. Structural studies of the water hexamer. *J. Phys. Chem. A* **2010,** *114,* 7809-7814.

151. Wang, Y.; Babin, V.; Bowman, J. M.; Paesani, F. The Water Hexamer: Cage, Prism, or Both. Full Dimensional Quantum Simulations Say Both. *J. Am. Chem. Soc.* **2012,** *134,* 11116-11119.

152. Ludwig, R. The Importance of Tetrahedrally Coordinated Molecules for the Explanation of Liquid Water Properties. *Chem. Phys. Chem.* **2007,** *8,* 938-943.

153. Head-Gordon, T.; Johnson, M. E. Tetrahedral Structure or Chains for Liquid Water. *Proc. Nat. Acad. Sci.* **2006,** *130* (21), 7973-7977.

154. Kitaura, K.; Morokuma, K. A New Energy Decomposition Scheme for Molecular Interactions Within the Hartree–Fock Approximation. *Int. J. Quantum Chem.* **1976,** *10,* 325-340.

155. Hayes, I. C.; Stone, A. J. An Intermolecular Perturbation Theory for the Region of Moderate Overlap. *Mol. Phys.* **1984,** *53* (1), 83-105.

156. Jeziorski, B.; Moszynski, R.; Szalewicz, K. Perturbation Theory Approach to Intermolecular Potential Energy Surfaces of van der Waals Complexes. *Chem. Rev.* **1994,** *94* (7), 1887-1930.

157. Glendening, E. D. Natural Energy Decomposition Analysis: Extension to Density Functional Methods and Analysis of Cooperative Effects in Water Clusters. *J. Phys. Chem. A* **2005,** *109* (51), 11936-11940.

158. Li, H.; Gordon, M. S.; Jensen, J. H. Charge Transfer Interaction in the Effective Fragment Potential Method. *J. Chem. Phys.* **2006,** *124,* 214108(16).

159. Khaliullin, R. Z.; Cobar, E. A.; Lochan, R. C.; Bell, A. T.; Head-Gordon, M. Unravelling the Origin of Intermolecular Interactions Using Absolutely Localized Molecular Orbitals. *J. Phys. Chem. A* **2007,** *111* (36), 8753-8765.

160. Auer, B.; Pak, M.; Hammes-Schiffer, S. Nuclear-Electronic Orbital Method Within the Fragment Molecular Orbital Approach. *J. Phys. Chem. C* **2010,** *114,* 5582.

161. Góra, U.; Podeszwa, R.; Cencek, W.; Szalewicz, K. Interaction Energies of lLarge Clusters from Many-body Expansion. *J. Chem. Phys.* **2011,** *135,* 224102.

162. Gordon, M. S.; Fedorov, D. G.; Pruitt, S. R.; Slipchenko, L. V. Fragmentation Methods: A Route to Accurate Calculations on Large Systems. *Chem. Rev.* **2012,** *112* (1), 632-672.

163. Dahlke, E. E.; Olson, R. O.; Leverentz, H. R.; Truhlar, D. G. Assessment of the Accuracy of Density Functionals for Prediction of Relative Energies and Geometries of Low-Lying Isomers of Water Hexamers. *J. Phys. Chem. A* **2008,** *112,* 3976-3984.

164. Pakiari, A. H.; Eskandari, K. Closed Shell Oxygen–oxygen Bonding Interaction Based on Electron Density Analysis. *J. Mol. Struct. THEO.* **2007,** *806* (1-3), 1-7.

165. Jenkins, S.; Restrepo, A.; David, J.; Yin, D.; Kirk, S. Spanning QTAIM Topology Phase Diagrams of Water Isomers W4, W5, and W6. *Phys. Chem. Chem. Phys.* **2011,** *13,* 11644-11656.

166. Dehnicke, K.; Neumuller, B. Neues aus der Chemie des Berylliums. *Z. Anorg. Allg. Chem.* **2008,** *634,* 2703-2728.

167. Walsh, K. A., Ed. *Beryllium Chemistry and Processing;* ASM International : Materials Park, OH, 2009.

168. Puchta, R. A Brighter Beryllium. *Nat. Chem.* **2011,** *3,* 416-416.

169. Silliman, H. F. Beryllium-Copper Alloys. *Ind. Eng. Chem.* **1936,** *28,* 1424-1428.

170. Baskerville, E. E. Analysis of Beryllium-Copper Alloys. *Anal. Chem.* **1949,** *21,* 1089-1091.

171. Baboian, R.; Haynes, G. S. *J. Electrochem. Soc.* **1977,** *124,* C95-C95.

172. Gassert, R.; Chapuis, D.; Bleuler, H.; Burdet, E. Sensors for Applications in Magnetic Resonance Environments. *IEEE-ASME Trans. Mechatron.* **2008,** *13,* 335-344.

173. Figueroa, A. I.; Bartolome, J.; del Pozo, J. M. G.; Arauzo, A.; Guerrero, E.; Tellez, P.; Bartolome, F.; Garcia, L. M. Low Temperature Radio-frequency Transverse Susceptibility Measurements Using a CMOS Oscillator Circuit. *J. Magn. Magn. Mater.* **2012,** *324,* 2669-2675.

174. Powell, R. W. The Thermal and Electrical Conductivities of Beryllium. *Philosoph. Magaz.* **1953,** *44,* 645-663.

175. Darmo, J.; Schaffer, F.; Forster, A.; Kordos, P. *Beryllium doped low-temperature-grown MBE GaAs: material for photomixing in the THz frequency range;* IEEE: New York, 2000; pp 147-150.

176. Delatte, M. L. *Ultralight Weight Beryllium Mirror Development;* Spie - Int Soc Optical Engineering: Bellingham, 1993.

177. Widdowson, A.; Coad, J. P.; de Temmerman, G.; Farcage, D.; Hole, D.; Ivanova, D.; Leontyev, A.; Rubel, M.; Semerok, A.; Schmidt, A.; Thro, P. Y.; Contributors, J. E. *Removal of Beryllium-containing Films Deposited in JET from Mirror Surfaces by Laser Cleaning;* Culham Science Centr: Abingdon, UK, 2010.

178. Lightsey, P. A.; Atkinson, C.; Clampin, M.; Feinberg, L. D. James Webb Space Telescope: Large Deployable Cryogenic Telescope in Space. *Opt. Eng.* **2012,** *51,* 011003(9).

179. Marotta, E. E.; Fletcher, L. S. Thermal Contact Conductance of Refractory Ceramic Coatings. *J. Thermophys. Heat Transf.* **1996,** *10,* 10-18.

180. Parsonage, T. Beryllium Metal Matrix Composites for Aerospace and Commercial Applications. *Mater. Sci. Technol.* **2000,** *16,* 732-738.

181. Makurin, Y. N.; Kiiko, V. S.; Shein, I. R.; Maslov, V. A.; Ivanovskii, A. L. Single Crystals and Light-transmitting BeO-ceramic for Electronic Technology. *Refract. Ind. Ceram.* **2010,** *51,* 167-171.

182. de Faoite, D.; Browne, D. J.; Chang-Diaz, F. R.; Stanton, K. T. A Review of the Processing, Composition, and Temperature-dependent Mechanical and Thermal Properties of Dielectric Technical Ceramics. *J. Mater. Sci.* **2012,** *47,* 4211-4235.

183. Pascucci, L. M. Pulmonary Disease in Workers Exposed to Beryllium Compounds; Its Roentgen Characteristics. *Radiology* **1948,** *50,* 23-36.

184. Stoeckle, J. D.; Hardy, H. L.; Weber, A. L. Chronic Beryllium Disease. Long-term Follow-up of Sixty Cases and Selective Review of the Literature. *Am. J. Med.* **1969,** *46,* 545-561.

185. Virji, M. A.; Park, J. Y.; Stefaniak, A. B.; Stanton, M. L.; Day, G. A.; Kent, M. S.; Kreiss, K.; Schuler, C. R. Sensitization and Chronic Beryllium Disease at a Primary Manufacturing Facility, Part 1: Historical Exposure Reconstruction. *Scand. J. Work Environ. Health* **2012,** *38,* 247-258.

186. McCleskey, T. M.; Ehler, D. S.; Keizer, T. S.; Asthagiri, D. N.; Pratt, L. R.; Michalczyk, R.; Scott, B. L. Beryllium Displacement of H^+ from Strong Hydrogen Bonds. *Angew. Chem.-Int. Edit.* **2007,** *4,* 2669-2671.

187. Scott, B. L.; McCleskey, T. M.; Chaudhary, A.; Hong-Geller, S. E. The Bioinorganic Chemistry and Associated Immunology of Chronic Beryllium Disease. *Chem. Commun.* **2008,** *25,* 2837-2847.

188. Gnanakaran, S.; Scott, B.; McCleskey, T. M.; Garcia, A. E. Perturbation of Local Solvent Structure by a Small Dication: A Theoretical Study on Structural, Vibrational, and Reactive Properties of Beryllium Ion in Water. *J. Phys. Chem. B* **2008,** *112,* 2958-2963.

189. McCleskey, T. M.; Scott, B. L. Beryllium and Strong Hydrogen Bonds. *J. Occup. Environ. Hyg.* **2009,** *6,* 751-757.

190. Silva, S.; Ganguly, K.; Fresquez, T. M.; Gupta, G.; McCleskey, T. M.; Chaudhary, A. Beryllium Alters Lipopolysaccharide-Mediated Intracellular Phosphorylation and Cytokine Release in Human Peripheral Blood Mononuclear Cells. *J. Occup. Environ. Hyg.* **2009,** *6,* 775-782.

191. Yáñez, M.; Sanz, P.; Mó, O.; Alkorta, I.; Elguero, J. Beryllium Bonds, Do They Exist? *J. Chem Theor. Comput.* **2009,** *5,* 2763-2771.

192. Kleeberg, H.; Klein, D.; Luck, W. A. P. Quantitative Infrared Spectroscopic Investigations of Hydrogen-bond Cooperativity. *J. Phys. Chem.* **1987,** *91,* 3200-3203.

193. Hannachi, Y.; Silvi, B.; Bouteiller, Y. Ab Initio Study of the Structure, Cooperativity, and Vibrational Properties of the Water-hydrogen Fluoride Dimer (H_2O:$(HF)_2$) hydrogen-bonded complex. *J. Chem. Phys.* **1992,** *97,* 1911-1918.

194. Karpfen, A.; Yanovitskii, O. Cooperativity in Hydrogen Bonded Clusters: An Improved Ab Initio SCF Study on the Structure and Energetics of Neutral, Protonated and Deprotonated Chains and of Neutral, Cyclic Hydrogen Fluoride Oligomers. *Theochem-J. Mol. Struct.* **1994,** *120,* 211-227.

195. Suhai, S. Cooperativity and Electron Correlation Effects on Hydrogen Bonding in Infinite Systems. *Int. J. Quantum Chem.* **1994,** *52,* 395-412.

196. González, L.; Mó, O.; Yáñez, M.; Elguero, J. Cooperative Effects in Water Trimers. The Performance of Density Functional Approaches. *Theochem* **1996,** *371,* 1-10.

197. Latajka, Z.; Scheiner, S. Structure, Energetics and Vibrational Spectra of Dimers, Trimers, and Tetramers of HX (X = Cl, Br, I). *Chem. Phys.* **1997,** *216,* 37-52.

198. Li, G. S.; Ruiz-López, M. F.; Maigret, B. Ab Initio Study of 4(5)-Methylimidazole in Aqueous Solution. *J. Phys. Chem. A* **1997,** *101,* 7885-7892.

199. Lozynski, M.; RusinskaRoszak, D.; Mack, H. G. MP2 and Density Functional Studies of Hydrogen Bonding in Model Trioses -D-(+)-Glyceraldehyde and Dihydroxyacetone. *J. Phys. Chem. A* **1997,** *101,* 1542-1548.

200. Bryce, R. A.; Vincent, M. A.; Malcolm, N. O. J.; Hillier, I. H.; Burton, N. A. Cooperative Effects in the Structuring of Fluoride Water Clusters: Ab Initio Hybrid Quantum Mechanical/Molecular Mechanical Model Incorporating Polarizable Fluctuating Charge Solvent. *J. Chem. Phys.* **1998,** *109,* 3077-3085.

201. Cabaleiro-Lago, E. M.; Ríos, M. A. Ab Initio Study of Interactions in Methylamine Clusters. The Significance of Cooperative Effects. *J. Chem. Phys.* **2000,** *112,* 2155-2163.

202. Dannenberg, J. J. Cooperativity in Hydrogen Bonded Aggregates. Models for Crystals and Peptides. *J. Mol. Struct.* **2002,** *615 ,* 219-226.

203. Raveendran, P.; Wallen, S. L. Cooperative CH… O Hydrogen Bonding in CO_2-Lewis Base Complexes: Implications for Solvation in Supercritical CO_2. *J. Am. Chem. Soc.* **2002,** *124,* 12590-12599.

204. Wieczorek, R.; Dannenberg, J. J. Hydrogen-Bond Cooperativity, Vibrational Coupling, and Dependence of Helix Stability on Changes in Amino Acid Sequence in Small 3_{10}-Helical Peptides. A Density Functional Theory Study. *J. Am. Chem. Soc.* **2003,** *125,* 14065-14071.

205. Mó, O.; Yáñez, M.; Del Bene, J. E.; Alkorta, L.; Elguero, J. Cooperativity and Proton Transfer in Hydrogen-Bonded Triads. *Chem. Phys. Chem.* **2005,** *6,* 1411-1418.

206. Chen, Y. F.; Viswanathan, R.; Dannenberg, J. J. Through Hydrogen-Bond Vibrational Coupling in Hydrogen-Bonding Chains of 4-Pyridones with Implications for Peptide Amide I Absorptions: Density Functional Theory Compared with Transition Dipole Coupling. *J. Phys. Chem. B* **2007,** *111,* 8329-8334.

207. Grabowski, S. J.; Leszczynski, J. The Enhancement of X-H•••π Hydrogen Bond by Cooperativity Effects - Ab Initio and QTAIM Calculations. *Chem. Phys.* **2009,** *355,* 169-176.

208. Nagaraju, M.; Sastry, G. N. Comparative Study on Formamide-water Complex. *Int. J. Quant. Chem.* **2010,** *110,* 1994-2003.

209. Alkorta, I.; Blanco, F.; Elguero, J. A Computational Study of the Cooperativity in Clusters of Interhalogen Derivatives. *Struct. Chem.* **2009,** *20,* 63-71.

210. Mó, O.; Yáñez, M.; Alkorta, I.; Elguero, J. Modulating the Strength of Hydrogen Bonds through Beryllium Bonds. *J. Chem. Theory Comput.* **2012,** *8,* 2293-2300.

211. Dressel, M. P.; Nogai, S.; Berger, R. J. F.; Schmidbaur, H. Beryllium Dichloride Coordination by Nitrogen Donor Molecules. *Z. Naturforsch* **2002,** *58b,* 173-182.

212. Azam, S. S.; Hofer, T. S.; Bhattacharjee, A.; Lim, L. H. V.; Pribil, A. B.; Randolf, B. R.; Rode, B. M. Beryllium(II): The Strongest Structure-Forming Ion in Water? A QMCF MD Simulation Study. *J. Phys. Chem. B* **2009,** *113,* 9289-9295.

213. Rudolph, W. W.; Fischer, D.; Irmer, G.; Pye, C. C. Hydration of Beryllium(II) in Aqueous Solutions of Common Inorganic Salts. A Combined Vibrational Spectroscopic and Ab Initio Molecular Orbital Study. *Dalton Trans.* **2009,** 6513-6527.

214. Becke, A. D. Density-functional Thermochemistry. III. The Role of Exact Exchange. *J. Chem. Phys.* **1993,** *98,* 5648-5652.

215. Lee, C.; Yang, W.; Parr, R. G. Development of the Colle-Salvetti Correlation-energy Formula into a Functional of the Electron Density. *Phys. Rev. B* **1988,** *37,* 785-789.

216. González, L.; Mó, O.; Yáñez, M. High-level Ab Initio Versus DFT Calculations on $(H_2O_2)_2$ and H_2O_2-H_2O Complexes as Prototypes of Multiple Hydrogen Bond Systems. *J. Comput. Chem.* **1997,** *18,* 1124-1135.

217. González, L.; Mó, O.; Yáñez, M. High Level Ab Initio and Density Functional Theory Studies on Methanol-water Dimers and Cyclic Methanol(water)2 Trimer. *J. Chem. Phys.* **1998,** *109,* 139-150.

218. Reed, A. E.; Curtiss, L. A.; Weinhold, F. Intermolecular Interactions from a Natural Bond Orbital, Donor-acceptor Viewpoint. *Chem. Rev.* **1988,** *88,* 899-926.

219. Wiberg, K. B. Application of the Pople-Santry-Segal Complete Neglect of Differential Overlap Method to the Cyclopropyl-carbinyl and Cyclobutyl Cation and to Bicyclobutane. *Tetrahedron* **1968,** *24,* 1083-1096.

220. Schleyer, P. v. R. The Contrasting Strain Energies of Small Ring Carbon and Silicon Rings. The Relationship with Free Radical Energies. *NATO Adv. Study Inst. Ser. C* **1986,** *189,* 69-73.

221. Alcamí, M.; Mó, O.; Yáñez, M. G2 Ab Initio Calculations on Three-Membered Rings: Role of Hydrogen Atoms. *J. Comput. Chem.* **1998,** *19,* 1072-1086.

222. Wiberg, K. B.; Schleyer, P. V.; Streitwieser, A. The Role of Hydrogens in Stabilizing Organic Ions. *Can. J. Chem.* **1996,** *74,* 892-900.

223. Sánchez-Sanz, G.; Alkorta, I.; Elguero, J.; Yáñez, M.; Mó, O. Strong Interactions Between Copper Halides and Unsaturated Systems: New Metallocycles? Or the Importance of Deformation. *Phys. Chem. Chem. Phys.* **2012,** *14,* 11468–11477.

224. Saha, B. K.; Nangia, A. Helical Water Chains in Aquapores of Organic Hexahost: Remarkable Halogen-substitution Effect on the Handedness of Water Helix. *Chem. Comm.* **2005,** 3024-3026.

225. Sreenivasulu, B.; Vittal, J. J. Helix inside a Helix: Encapsulation of Hydrogen-Bonded Water Molecules in a Staircase Coordination Polymer. *Angew. Chem.* **2004,** *43,* 5769-5772.

226. Fei, Z.; Zhao, D.; Geldbach, T. J.; Scopelliti, R.; Dyson, P. J.; Antonijevic, S.; Bodenhausen, G. A Synthetic Zwitterionic Water Channel: Characterization in the Solid State by X-ray Crystallography and NMR Spectroscopy. *Angew. Chem. Int. Ed.* **2005,** *44,* 5720-5725.

227. Cox, M. J.; Timmer, R. L. A.; Bakker, H. J.; Park, S.; Agmon, N. Distance-dependent Proton Transfer Along Water Wires Connecting Acid-base Pairs. *J. Phys. Chem. A* **2009,** *113,* 6599-6606.

228. Hassanali, A.; Prakash, M. K.; Eshet, H.; Parrinello, M. On the Recombination of Hydronium and Hydroxide Ions in Water. *Proc. Nat. Am. Soc.* **2011,** *108* (51), 20410-20415.

229. Cui, Q.; Karplus, M. Is a "Proton Wire" Concerted or Stepwise? A Model Study of Proton Transfer in Carbonic Anhydrase. *J. Phys. Chem. B* **2003,** *107,* 1071-1078.

230. Cárdenas, D. J.; Cuerva, J. M.; Alías, M.; Buñuel, E.; Campaña, A. G. Water-Based Hydrogen-Atom Wires as Mediators in Long-Range Proton-Coupled Electron Transfer in Enzymes: A New Twist on Water Reactivity. *Chem. Eur. J.* **2011,** *17,* 8318-8323.

231. Hummer, G.; Rasaiah, J. C.; Noworyta, J. P. Water Conduction Through the Hydrophobic Channel of a Carbon Nanotube. *Nature* **2001,** *414,* 188-190.

232. Won, C. Y.; Aluru, N. R. Water Permeation through a Subnanometer Boron Nitride Nanotube. *J. Am. Chem. Soc.* **2007,** *129,* 2748-2749.

233. Alexiadis, A.; Kassinos, S. Molecular Simulation of Water in Carbon Nanotubes. *Chem. Rev.* **2008,** *108,* 5014-5034.

234. Cao, Z.; Peng, Y.; Yan, T.; Li, S.; Li, A.; Voth, G. A. Mechanism of Fast Proton Transport along One-Dimensional Water Chains Confined in Carbon Nanotubes. *J. Am. Chem. Soc.* **2010,** *132,* 11395-11397.

235. Köfinger, J.; Hummera, G.; Dellago, C. Single-file Water in Nanopores. *Phys. Chem. Chem. Phys.* **2011,** *13,* 15403-15417.

236. Dellago, C.; Naor, M. M.; Hummer, G. Proton Transport through Water-Filled Carbon Nanotubes. *Phys. Rev. Lett.* **2003,** *90* (10), 105902(4).

237. Natarajan, R.; Charmant, J. P. H.; Orpen, A. G.; Davis, A. P. Water Chains in Hydrophobic Crystal Channels: Nanoporous Materials as Supramolecular Analogues of Carbon Nanotubes. *Angew. Chem. Int. Ed.* **2010,** *49,* 5125-5129.

238. Asthagiri, D.; Bashford, D. Continuum and Atomistic Modeling of Ion Partitioning into a Peptide Nanotube. *Biophys. J.* **2002,** *82,* 1176-1189.

239. Raghavender, U. S.; Kantharaju; Aravinda, S.; Shamala, N.; Balaram, P. Hydrophobic Peptide Channels and Encapsulated Water Wires. *J. Am. Chem. Soc.* **2009,** *132,* 1075-1086.

240. Rahmat, F.; Thamwattana, N.; Cox, B. J. Modelling Peptide Nanotubes for Artificial Ion Channels. *Nanotech.* **2011,** *22,* 445707-445715.

241. Tajkhorshid, E.; Nollert, P.; Jensen, M.; Miercke, L. J. W.; O'Connell, J.; Stroud, R. M.; Schulten, K. Control of the Selectivity of the Aquaporin Water Channel Family by Global Orientational Tuning. *Science* **2002,** *296,* 525-530.

242. Åqvist, J.; Luzhkov, V. Ion Permeation Mechanism of the Potassium Channel. *Nature Lett.* **2000,** *404,* 881-884.

243. DeCoursey, T. E. Voltage-gated Proton Channels: Molecular Biology, Physiology, and Pathophysiology of the Hv Family. *Physiol. Rev.* **2013,** *93,* 599-652.

244. Brewer, M. L.; Schmitt, U. W.; Voth, G. A. The Formation and Dynamics of Proton Wires in Channel Environments. *Biophys. J.* **2001,** *80,* 1691-1702.

245. DeCoursey, T. E.; Hosler, J. Philosophy of Voltage-gated Proton Channels. *J. R. Soc. Interface* **2014,** *11,* 20130799.

246. Aqvist, J.; Warshel, A. Energetics of Ion Permeation Through Membrane Channels. Solvation of Na+ by Gramicidin A. *Biophys. J.* **1989,** *56,* 171-182.

247. Pomes, R.; Roux, B. Structure and Dynamics of a Proton Wire: A Theoretical Study of H+ Translocation along the Single-File Water Chain in the Gramicidin A Channel. *Biophys. J.* **1996,** *71,* 19-39.

248. Henry, R. M.; Yu, C.-H.; Rodinger, T.; Pomès, R. Functional Hydration and Conformational Gating of Proton Uptake in Cytochrome c Oxidase. *J. Mol. Biol.* **2009,** *387,* 1165-1185.

249. Wraight, C. A. Chance and Design—Proton Transfer in Water, Channels and Bioenergetic Proteins. *Biochim. Biophys. Acta* **2006,** *1757,* 886-912.

250. Bucher, D.; Kuyucak, S. Importance of Water Polarization for Ion Permeation in Narrow Pores. *Chem. Phys. Lett.* **2009,** *477,* 207-210.

251. Voth, G. A. Computer Simulation of Proton Solvation and Transport in Aqueous and Biomolecular Systems. *Acc. Chem. Res.* **2006,** *39,* 143-150.

252. Brancato, G.; Tuckerman, M. E. A Polarizable Multistate Empirical Valence Bond Model for Proton Transport in Aqueous Solution. *J. Chem. Phys.* **2005,** 224507(11).

253. Scheiner, S. Sensitivity of Noncovalent Bonds to Intermolecular Separation: Hydrogen, Halogen, Chalcogen, and Pnicogen Bonds. *Cryst Eng. Comm.* **2013,** *15,* 3119-3124.

254. Ojamie, L.; Hermansson, K. Ab Initio Study of Cooperativity in Water Chains: Binding Energies and Anharmonic Frequencies. *J. Phys. Chem.* **1994,** *98,* 4271-4282.

255. Parthasarathi, R.; Elango, M.; Subramanian, V.; Sathyamurthy, N. Structure and Stability of Water Chains (H2O)n, n = 5-20. *J. Phys. Chem.* **2009,** *113,* 3744-3749.

256. Karahka, M.; Kreuzer, H. J. Water Whiskers in High Electric Fields. *Phys. Chem. Chem. Phys.* **2011,** *13,* 11027-11033.

257. Neela, Y. I.; Mahadevi, A. S.; Sastry, G. N. Hydrogen Bonding in Water Clusters and Their Ionized Counterparts. *J. Phys. Chem. B* **2010,** *114,* 17162-17171.

258. Mahadevi, A. S.; Sastry, G. N. Modulation of Hydrogen Bonding upon Ion Binding: Insights into Cooperativity. *Int. J. Quant. Chem.* **2013,** *114,* 145-153.

259. Smith, J. D.; Saykally, R. J.; Geissler, P. L. The Effects of Dissolved Halide Anions on Hydrogen Bonding in Liquid Water. *J. Am. Chem. Soc.* **2007,** *129,* 13847-13856.

260. Schultz, J. W.; Hornig, D. F. The Effect of Dissolved Alkali Halides on the Raman Spectrum of Water. *J. Phys. Chem.* **1961,** *65,* 2131-2138.

261. Marcus, Y. Effect of Ions on the Structure of Water: Structure Making and Breaking. *Chem. Rev.* **2009,** *109,* 1346-1370.

262. Jungwirth, P.; Winter, B. Ions at Aqueous Interfaces: From Water Surface to Hydrated Proteins. *Annu. Rev. Phys. Chem.* **2008,** *59,* 343-366.

263. Relph, R. A.; Guasco, T. L.; Elliott, B. M.; Kamrath, M. Z.; McCoy, A. B.; Steele, R. P.; Schofield, D. P.; Jordan, K. D.; Viggiano, A. A.; Ferguson, E. E.; Johnson, M. A. How the Shape of an H-Bonded Network Controls Proton-Coupled Water Activation in HONO Formation. *Science* **2010,** *327,* 308-312.

264. Bankura, A.; Carnevale, V.; Klein, M. L. Hydration Structure of Salt Solutions From Ab Initio Molecular Dynamics. *J. Chem. Phys.* **2013,** *138,* 014501(10).

265. Scheu, R.; Rankin, B. M.; Chen, Y.; Jena, K. C.; Ben-Amotz, D.; Roke, S. Charge Asymmetry at Aqueous Hydrophobic Interfaces and Hydration Shells. *Angew. Chem.* **2014,** *126,* 1-5.

266. Nagle, J. F.; Morowitz, H. J. Molecular Mechanisms for Proton Transport in Membranes. *Proc. Natl. Acad. Sci. USA* **1978,** *75* (1), 298-302.

267. Cremer, D.; Kraka, E. Chemical Bonds Without Bonding Electron Density — Does the Difference Electron-Density Analysis Suffice for a Description of the Chemical Bond? *Angew. Chem. Int. Ed. Eng.* **1984,** *8,* 627-628.

268. Koch, U.; Popelier, P. L. A. Characterization of C-H-0 Hydrogen Bonds on the Basis of the Charge Density. *J. Phys. Chem.* **1995,** *99,* 9747-9754.

269. Espinosa, E.; Souhassou, M.; Lachekar, H.; Lecomte, C. Topological Analysis of the Electron Density in Hydrogen Bonds. *Acta. Cryst.* **1999,** *B55,* 563-572.

270. Espinosa, E.; Alkorta, I.; Elguero, J.; Molins, E. From Weak to Strong Interactions: A Comprehensive Analysis of the Topological and Energetic Properties of the Electron Density Distribution Involving X–H···F–Y Systems. *J. Chem. Phys.* **2002,** *117* (12), 5529-5542.

271. Boyd, R. J.; Choi, S. C. A Bond-length-bond-order Relationship for Intermolecular Interactions Based on the Topological Properties of Molecular Charge Distributions. *Chem. Phys. Lett.* **1985,** *120,* 80-85.

272. Parthasarathi, R.; Subramanian, V.; Sathyamurthy, N. Hydrogen Bonding without Borders: An Atoms-in-Molecules Perspective. *J. Chem. Phys. Lett.* **2006,** *110,* 3349-3351.

273. Scheiner, S. Proton Transfers in Hydrogen-Bonded Systems. Cationic Oligomers of Water. *J. Am. Chem. Soc.* **1981,** *103,* 315-320.

274. Laila, V. R. I.; Hummer, G. Energetics and Dynamics of Proton Transfer Reactions Along Short Water Wires. *Phys. Chem. Chem. Phys.* **2011,** *13,* 13207-13215.

275. Bader, R. F. W.; Matta, C. F. Atoms in Molecules as Non-overlapping, Bounded, Space-filling Open Quantum Systems. *Found.s Chem.* **2013,** *15* (3), 253-276.

276. Bone, R. G. A.; Bader, R. F. W. Identifying and Analyzing Intermolecular Bonding Interactions in van der Waals Molecules. *J. Phys. Chem.* **1996,** *100,* 10892-10911.

277. Graña, A. M.; Mosquera, R. A. Transferability in Aldehydes and Ketones. II. Alkyl Chains. *J. Chem. Phys.* **2000,** *113,* 1492-1500.

278. Graña, A. M.; Mosquera, R. A. The Transferability of the Carbonyl Group in Aldehydes and Ketones. *J. Chem. Phys.* **1999,** *110,* 6606-6616.

279. Kollman, P. A.; Allen, L. C. Theory of the Hydrogen-Bond. *Chem. Rev.* **1972,** *72* (3), 283-303.

280. Allen, L. C. A Simple Model of Hydrogen Bonding. *J. Am. Chem. Soc.* **1975,** *97* (24), 6921-6940.

281. Scheiner, S. *Hydrogen Bonding: A Theoretical Perspective;* Oxford University Press, 1997.

282. Mó, O.; Yáñez, M.; Elguero, J. Study of the Methanol Trimer Potential Energy Surface. *J. Chem. Phys.* **1997,** *107* (9), 3691-3601.

283. Ludwig, R.; Reis, O.; Winter, R. Quantum Cluster Equilibrium Theory of Liquids: Temperature Dependence of Hydrogen Bonding in Liquid N-methylacetamide Studied by IR Spectra. *J. Phys. Chem. B* **1998,** *102* (46), 9312-9318.

284. Parra, R. D.; Zeng, X. C. Hydrogen Bonding and Cooperative Effects in Mixed Dimers and Trimers of Methanol and Trifluoromethanol: An Ab Initio Study. *J. Chem. Phys.* **1999,** *110,* 6329-6338.

285. Masella, M.; Flament, J.-P. A Theoretical Study of Five Water/Ammonia/Formaldehyde Cyclic Trimers: Influence of Cooperative Effects. *J. Chem. Phys.* **1999,** *110* (15), 7245-7255.

286. Steiner, T. The Hydrogen Bond in the Solid State. *Angew. Chem. Int. Ed* **2002,** *41* (1), 48-76.

287. Kobko, N.; Paraskevas, L.; del Rio, E.; Dannenberg, J. J. Cooperativity in Amide Hydrogen Bonding Chains: Implications for Protein-folding Models. *J. Am. Chem. Soc.* **2001,** *123,* 4348-4349.

288. Sum, A. K.; Sandler, S. I. Ab Initio Calculations of Cooperativity Effects on Clusters of Methanol, Ethanol, 1-Propanol, and Methanethiol. *J. Phys. Chem. A* **2000,** *104,* 1121-1129.

289. Provencal, R. A.; Casaes, R. N.; Roth, K.; Paul, J. B.; Chapo, C. N.; Saykally, R. J.; Tschumper, G. S.; Schaefer, I. H. F. Hydrogen Bonding in Alcohol Clusters: A Comparative Study by Infrared Cavity Ringdown Laser Absorption Spectroscopy. *J. Phys. Chem. A.* **2000,** *104,* 1423-1429.

290. Mandado, M.; Graña, A. M.; Mosquera, R. A. On the Structures of the Methanol Trimer and their Cooperative Effects. *Chem. Phys. Lett.* **2003,** *381,* 22-29.

291. Hunter, C. A.; Ihekwaba, N.; Misuraca, M. C.; Segarra-Maseta, M. D.; Turegaa, S. M. Cooperativity in Multiply H-bonded Complexes. *Chem. Comm.* **2009,** 3964-3966.

292. Tielrooij, K. J.; Garcia-Araez, N.; Bonn, M.; Bakker, H. J. Cooperativity in Ion Hydration. *Science* **2010,** *328,* 1006-1009.

293. Deshmukh, V.; Lee, S.-L.; Chaudhari, A. Cooperativity Effects in Linear Formaldehyde Oligomers using Density Functional Theory Calculations. *J. Mol. Mod.* **2012,** *18,* 3723-3729.

294. Clark, T.; Hennemann, M.; Murray, J. S.; Politzer, P. Halogen Bonding: The Sigma-Hole. *J. Mol. Mod.* **2007,** *13,* 291-296.

295. Politzer, P.; Lane, P.; Concha, M. C.; Ma, Y.; Murray, J. S. An Overview of Halogen Bonding. *J. Mol. Mod.* **2007,** *13,* 305-311.

296. Politzer, P.; Murray, J. S. Halogen Bonding: An Interim Discussion. *Chem. Phys. Chem.* **2013,** *14* (2), 278-294.

297. Frontera, A.; Quiñonero, D.; Garau, C.; Costa, A.; Ballester, P.; Deyà, P. M. MP2 Study of Cation-(π)n-π Interactions (n = 1-4). *Phys. Chem. Lett.* **2006,** *110* (30), 9307-9309.

298. Escudero, D.; Frontera, A.; Quiñonero, D.; Deyà, P. M. Interplay Between anion-π and Hydrogen Bonding Interactions. *J. Comp. Chem.* **2009,** *30* (1), 75-82.

299. Estarellas, C.; Frontera, A.; Quiñonero, D.; Alkorta, I.; Deyà, P. M.; Elguero, J. Energetic vs. Synergetic Stability: A Theoretical Study. *J. Phys. Chem.* **2009,** *117,* 3266-3273.

300. Lankau, T. (H2O)6 on a Virtual Metal Surface: Many-Body Effects in the Bilayer Structure. *J. Phys. Chem. A* **2002,** *106,* 6154-6160.

301. Kovács, A.; Varga, Z. Halogen Acceptors in Hydrogen Bonding. *Coord. Chem. Rev.* **2006,** *250,* 710-727.

302. Grabowski, S. J. Cooperativity of Hydrogen and Halogen Bond Interactions. *Theor. Chem. Acc.* **2013,** *132,* 1347-1357.

303. Estarellas, C.; Frontera, A.; Quiñonero, D.; Deyà, P. M. Interplay Between Cation–π and Hydrogen Bonding Interactions: Are Non-Additivity Effects Additive? *Chem. Phys. Lett.* **2009,** *479,* 316-320.

304. Alkorta, I.; Blanco, F.; Deyà, P. M.; Elguero, J.; Estarellas, C.; Frontera, A.; Quiñonero, D. Cooperativity in Multiple Unusual Weak Bonds. *Theor. Chem. Acc.* **2010,** *126* (1-2), 1-14.

305. Del Bene, J. E.; Alkorta, I.; Elguero, J. Ab initio Study of Ternary Complexes X:(HCNH)(+):Z wth X, Z = NCH, CNH, FH, ClH, and FCl: Diminutive Cooperative Effects on Structures, Binding Energies, and Spin-spin Coupling Constants Across Hydrogen Bonds. *J. Phys. Chem. A* **2011,** *115,* 12677-12687.

306. Rivelino, R.; Chaudhuri, P.; Canuto, S. Quantifying Multiple-body Interaction Terms in H-bonded HCN Chains with Many-body Perturbation/Coupled-cluster Theories. *J. Chem. Phys.* **2003,** *118* (23), 10593-10601.

307. Li, F.; Wang, L.; Zhao, J.; Xie, R.-H.; Riley, K. E.; Chen, Z. What is the Best Density Functional to Describe Water Clusters: Evaluation of Widely Used Density Functionals with Various Basis Sets for (H$_2$O)n (n=1–10). *Theor. Chem. Acc.* **2011,** *13,* 341-352.

308. Roztoczyńska, A.; Kaczmarek-Kędziera, A.; Góra, R. W.; Bartkowiak, W. How Does the Boys and Bernardi Counterpoise Correction Scheme Affect the Calculated Interaction-induced Electric Properties? Model Hydrogen-bonded Systems as a Case Study. *Chem. Phys. Lett.* **2013,** *571,* 28-33.

309. Boyd, S.; Boyd, R. J. A Density Functional Study of Methanol Clusters. *J. Chem. Theory Comput.* **2007,** *3,* 54-61.

310. Palke, W. E.; Kirtman, B. The C-H Bond Energy of Formaldehyde. *Chem. Phys. Lett.* **1988,** *148* (2-3), 202-204.

311. Vila, A.; Graña, A. M.; Mosquera, R. A. Electron Density Characterisation of Intermolecular Interactions in the Formaldehyde Dimer and Trimer. *Chem. Phys.* **2002,** *281,* 11-22.

312. Kar, T.; Scheiner, S. Comparison of Cooperativity in CH-O and OH-O Hydrogen Bonds. *J. Phys. Chem.* **2004,** *108,* 9161-9168.

313. Karpfen, A. Cooperative Effects in Hydrogen Bonding, in *Advances in Chemical Physics, Vol 123;* Prigogine, I.; Stuart, A. R., Eds.; John Wiley & Sons Inc: New York, 2002; Vol. 123, pp 469-510.

314. Dolgonos, G. A. Which Isomeric Form of Formaldehyde Dimer is the Most Stable – A High-level Coupled-cluster Study. *Chem. Phys. Lett.* **2013,** *585,* 37-41.

315. Lovas, F. J.; Suenram, R. D.; Coudert, L. H.; Blake, T. A.; Grant, K. J.; Novick, S. E. The Torsional–rotational Spectrum and Structure of the Formaldehyde Dimer. *J. Chem. Phys.* **1990,** *92* (2), 891-898.

316. Hermida-Ramón, J. M.; Ríos, M. A. A New Intermolecular Polarizable Potential for a Formaldehyde Dimer. Application to Liquid Simulations. *J. Phys. Chem. A* **1998,** *102* (52), 10818-10827.

317. Ford, T. A.; Glasser, L. Ab Initio Calculations of the Structural, Energetic and Vibrational Properties of Some Hydrogen Bonded and van der Waals Dimers Part 3. The formaldehyde dimer. *J. Mol. Struct. THEOCHEM* **1997,** *398-399,* 381-394.

318. Mahadevi, S. A.; Neela, I. Y.; Sastry, G. N. Hydrogen Bonded Networks in Formamide [HCONH$_2$]n (n = 1 − 10) Clusters: A Computational Exploration of Preferred Aggregation Patterns. *J. Chem. Sci.* **2012,** *124,* 35-42.

319. Pimentel, G. C.; McClelland, A. L. *The Hydrogen Bond;* W.H. Freeman and Co. : San Francisco, 1960.

320. Weissmann, M.; Blum, L.; Cohan, N. V. On the Hydrogen Bond in an Ice-like Structure. *Chem. Phys. Lett.* **1967,** *1,* 95-98.

321. Rahman, A.; Stillinger, F. H. Molecular Dynamics Study of Liquid Water. *J. Chem. Phys.* **1971,** *55,* 3336-3359.

322. Del Bene, J. E. Theoretical Study of Open Chain Dimers and Trimers Containing CH3OH and H2O. *J. Chem. Phys.* **1971,** *55,* 4633-4637.

323. Mó, O.; Yáñez, M.; Elguero, J. Cooperative Effects in the Cyclic Trimer of Methanol. An Ab initio Molecular Orbital Study. *J. Mol. Struct. Theochem* **1994,** *314,* 73-81.

324. Masella, M.; Flament, J. P. Relation Between Cooperative Effects in Cyclic Water, Methanol/Water, and Methanol Trimers and Hydrogen Bonds in Methanol/Water, Ethanol/Water, and Dimethylether/Water Heterodimers. *J. Chem. Phys.* **1998,** *2,* 1643-1650.

325. Philp, D.; Robinson, J. M. A Computational Investigation of Cooperativity in Weakly Hydrogen-Bonded Assemblies. *J. Chem. Soc.-Perkin Trans. 2* **1998,** 1643-1650.

326. Parra, R. D.; Gong, B.; Zeng, X. C. Energetics and Cooperativity in Three-center Hydrogen Bonding interactions. II. Intramolecular Hydrogen Bonding Systems. *J. Chem. Phys.* **2001,** *115,* 6036-6041.

327. Rincón, L.; Almeida, R.; Garcia-Aldea, D.; Riega, H. D. Y. Hydrogen Bond Cooperativity and Electron Delocalization in Hydrogen Fluoride Clusters. *J. Chem. Phys.* **2001,** *114,* 5552-5561.

328. Tsuzuki, S.; Houjou, H.; Nagawa, Y.; Goto, M.; Hiratani, K. Cooperative Enhancement of Water Binding to Crownophane by Multiple Hydrogen Bonds: Analysis by High Level Ab initio Calculations. *J. Am. Chem. Soc.* **2001,** *123,* 4255-4258.

329. Kriz, J.; Dybal, J. Cooperative H-Bonds of Macromolecules. 1. Binding of Low-Molecular-Weight Ligands to Polymers. *J. Phys. Chem. B* **2005,** *109,* 13436-13444.

330. Znamenskiy, V. S.; Green, M. E. Quantum Calculations on Hydrogen Bonds in Certain Water Clusters Show Cooperative Effects. *J. Chem. Theory Comput.* **2007,** *3,* 103-114.

331. Alkorta, I.; Elguero, J.; Solimannejad, M. Dihydrogen Bond Cooperativity in (HCCBeH)(n) Clusters. *J. Chem. Phys.* **2008,** *129,* 064115.

332. Solimannejad, M.; Malekani, M.; Alkorta, I. Cooperative and Diminutive Unusual Weak Bonding In $F_3CX \cdots HMgH \cdots Y$ and $F_3CX \cdots Y \cdots HMgH$ Trimers (X = Cl, Br; Y = HCN, and HNC). *J. Phys. Chem. A* **2010,** *114,* 12106-12111.

333. Parra, R. D.; Streu, K. Hydrogen Bond Cooperativity in Polyols: A DFT and AIM Study. *Comput. Theor. Chem.* **2011,** *967,* 12-18.

334. Bakhmutov, V. I. *Dihydrogen Bond: Principles, Experiments, and Applications;* John Wiley & Sons: Hoboken, NJ, 2008; doi:10.1002/9780470226759.fmatter.

335. Metrangolo, P.; Resnati, G. Halogen Bonding: A Paradigm in Supramolecular Chemistry. *Chem.-Eur. J.* **2001,** *7,* 2511-2519.

336. Zahn, S.; Frank, R.; Hey-Hawkins, E.; Kirchner, B. Pnicogen Bonds: A New Molecular Linker? *Chem.-Eur. J.* **2011,** *17,* 6034-6038.

337. Del Bene, J. E.; Alkorta, I.; Sanchez-Sanz, G.; Elguero, J. Interplay of F-H⋯F Hydrogen Bonds and P⋯N Pnicogen Bonds. *J. Phys. Chem. A* **2012,** *116*.

338. Yáñez, M.; Mó, O.; Alkorta, I.; Elguero, J. Can Conventional Bases and Unsaturated Hydrocarbons Be Changed into Gas-Phase Superacids Stronger than Most of the Known Oxyacids? The Role of Beryllium Bonds. *Chem. Eur. J* **2013,** *35,* 11637-11643.

339. Alkorta, I.; Elguero, J.; Yáñez, M.; Mó, O. Cooperativity in Beryllium Bonds. *Phys. Chem. Chem. Phys.* **2014,** *16,* 43054312.

340. Zhao, Y.; Truhlar, D. G. The M06 Suite of Density Functionals for Main Group Thermochemistry, Thermochemical Kinetics, Noncovalent Interactions, Excited States, and Transition Elements: Two New Functionals and Systematic Testing of Four M06-Class Functionals and 12 other Function. *Theor. Chem. Acc.* **2008,** *120,* 215-241.

341. Alcamí, M.; Mó, O.; Yáñez, M. Computational Chemistry. A Useful (Some Times Mandatory) Tool in Mass Spectrometry Studies. *Mass Spectrom. Rev.* **2001,** *20,* 195-245.

342. Yu, H.; Gunsteren, W. F. v. Accounting for Polarization in Molecular Simulation. *Comp. Phys. Comm.* **2005,** *172,* 69-85.

343. Chaplin, M. Water Models. http://www.lsbu.ac.uk/water/models.html (accessed May 12, 2013).

344. Mao, Y.; Zhang, Y. Thermal Conductivity, Shear Viscosity and Specific Heat of Rigid Water Models. *Chem. Phys. Lett.* **2012,** *542,* 37-41.

345. Ren, P.; Ponder, J. W. Polarizable Atomic Multipole Water Model for Molecular Mechanics Simulation. *J. Chem. Phys. B* **2003,** *107,* 5933-5947.

346. Wang, J.; Cieplak, P.; Cai, Q.; Hsieh, M.-J.; Wang, J.; Duan, Y.; Luo, R. Development of Polarizable Models for Molecular Mechanical Calculations. 3. Polarizable Water Models Conforming to Thole Polarization Screening Schemes. *J. Phys. Chem. B* **2012,** *116,* 7999-8008.

347. Guillot, B. A Reappraisal of What We Have Learnt During Three Decades of Computer Simulations on Water. *J. Mol. Liq.* **2002,** *101,* 219-260.

348. Swanson, J. M. J.; Maupin, C. M.; Chen, H.; Petersen, M. K.; Xu, J.; Wu, Y.; Voth, G. A. Proton Solvation and Transport in Aqueous and Biomolecular Systems: Insights From Computer Simulations. *J. Phys. Chem.* **2007,** *111,* 4300-4314.

349. Bagchi, B. From Anomalies in Neat liquid to Structure, Dynamics and Function in the Biological World. *Chem. Phys. Lett.* **2012,** *529,* 1-9.

350. Müller, A. M. K. Explicit Approximate Relation Between Reduced Two- and One-particle Density Matrices. *Phys. Lett. A* **1984,** *105,* 446-452.

Appendix A   Supporting Information for Chapter 3

A.1 Modelling Water Classically

Water can be represented as a model species with several point charges or smeared charged regions centered either at nuclei or between nuclei to mimic the real electron distribution within the water molecule. Properties such as polarization can be implicitly included [342] and flexibility may be incorporated using harmonic or anharmonic bond stretching potentials, though these come with increasing computational expense. The water models most commonly applied for large-scale biochemical analysis are usually simple models such as TIP3P or SPC/E. Figure A.1 provides a comparison of the performance of some classical water models with respect to experimental values. They are classified into groups of rigid models (R), rigid and polarizable models (R,P), flexible models (F), and flexible and polarizable models (F,P). It is clear that even within model types, the performance can vary considerably.
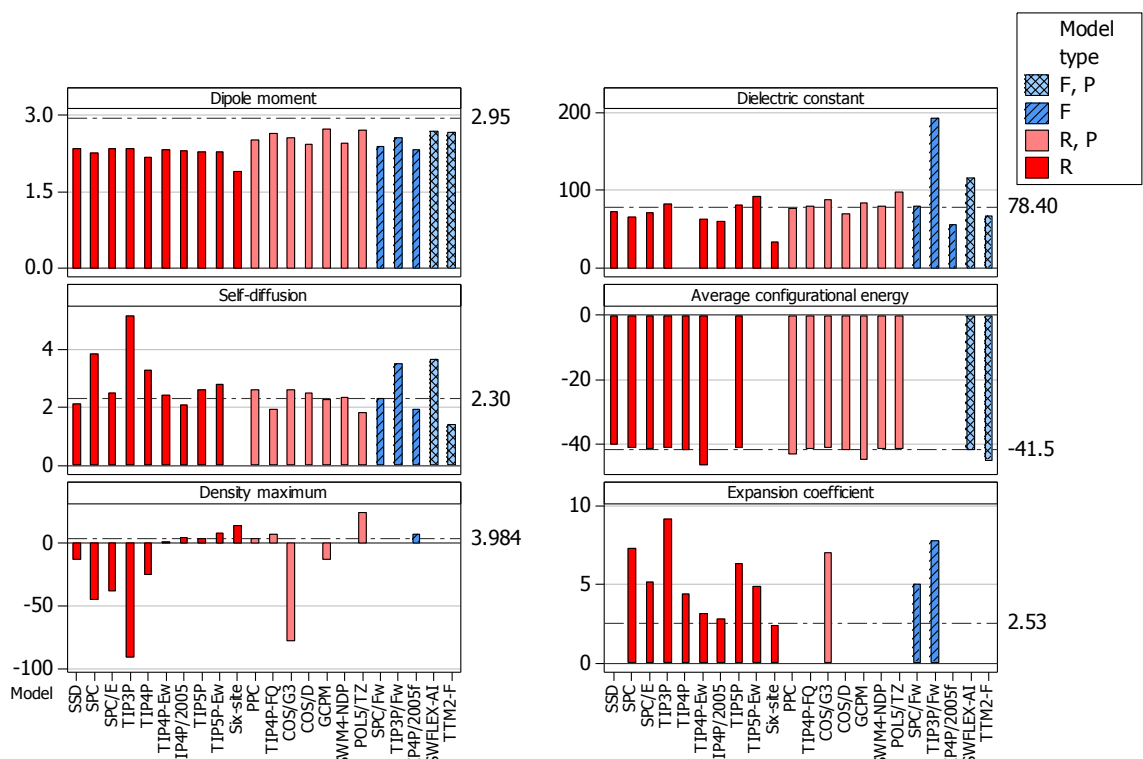
Figure A.1 Some physical properties of water models. Model type is defined as F=flexible, P=polarizable, R=rigid. Horizontal dashed lines are the experimental properties, with values included on the left. Data was obtained from reference [343]. The dipole moment is the averaged bulk value. Self-diffusion is a measure of the influence of hydrogen bonds on translational movement. The density maximum is the temperature at which the model yields the highest density for bulk water. Notice that the SPC/E model fares surprisingly well for a simple rigid model.

The large variety in performance of each model indicates that great care should be used in setting up a simulation. If the property of interest is heat transfer or dynamic ability involving water flow, a multi-site model such at TIP5P would be a good choice. For analyses requiring a dynamic response to temperature variation (for example in the heat denaturing of a protein), a simpler model such as TIP3P would be a wiser option [344]. No model has yet managed to reproduce all properties of bulk water with any great deal of accuracy. These errors in water models are derivative from the inherent differences between a classically modeled water system and "real" water molecules. Some of these characteristics, and the steps taken to account for them in the models, are listed below.

Water molecules are highly polarizable and susceptible to the surrounding environment.
Nearby ions, charges or reaction fields can affect the electron density within a real water molecule, redistributing it according to the surrounding environment. In some cases this promotes formation of elsewise unstable water structures, such as the long water chains observed in mass spectrometer experiments [256]. Although polarization is inherently an electronic property, there are several ways of including polarizability in classical water models [342]. This can include adjustment of partial atomic charges and introduction of dipoles at or near the oxygen charge center (see for example reference [345]). Many simple adjustments aim to improve correlation with bulk water behaviour. There may be consequential errors to this when describing the electrostatic interactions of water in non-bulk environments, such as near biomolecules and membrane interfaces. More complicated ways to improve polarizability are also available, involving induced-dipole models, Drude-oscillator models, and fluctuating-charge models [346].

Water molecules in bulk liquid are non-equivalent.
This is a result of polarization as well as the cooperative nature of the hydrogen bond. Each new bonding interaction from a water molecule (or a solute molecule) can either enhance or diminish the existing water hydrogen bonds, depending on the orientation of the water molecules. This is especially evident within small water clusters [5, 127]. The cooperative effect in water is an electronic effect, which is difficult to mimic using classical approaches. Polarizable models aid in providing a better description of the varying hydrogen bond strengths in water, however they do not reproduce possible changes in geometry, such as fluctuating bond lengths and angles. Flexible models allow variation in geometries, however they have been criticized because of their tendency to produce a narrowing of the HOH bond angle (to ~100° from 104°) [347]. It is worth noting that experimental and *ab initio* values for gas phase water clusters (often considered to be descriptive templates for true bulk water substructure) report that the HOH bond angle can be as narrow as 101° [135]. Considering that many rigid bulk water models fail to reproduce the proper complexity of the potential energy surface observed in bulk water, this progression in flexible models may prove useful.

183

Water is capable of proton transport

This is the driving force behind many acid-base reactions, enzyme catalysis, and energy transfer and conversion processes in biomolecules, and it is perhaps the most complicated property of water. It involves the making and breaking of both covalent and hydrogen bonds, potential quantum effects such as proton tunneling and large zero point energies, and a protonic charge that can be delocalized over multiple water molecules (rather than the classical definition of an isolated H_3O^+ species). Proton transport is all but impossible to model using classical methods. Specialized models such as the Multistate Empirical Valence Bond Method (MS-EVB) [348] are capable of modelling proton transport using MD deterministic methods. *Ab initio* molecular dynamics (AIMD) models are also available; however, they require considerable computation time and are only realistic for small systems. Interpretation of AIMD results is also dependent on an understanding of the underlying quantum theory, and care must be taken in modeling the types of electron-electron interactions as observed in hydrogen bonds.

Water is more than just "H_2O"

Finally, even if a water model could capture all of the above properties, there would still remain serious difficulties in transferring models to real situations: "pure bulk water" does not consist purely of water molecules. It is a system of molecular species including ortho and para water molecules, isotopic contributions, and hydrogen ion and hydroxide species.

Despite these shortcomings, the models developed in the past 40 years do allow us to mimic some of water's behaviour and have proven invaluable in the understanding of biomolecular systems through their dependence on water. The answers to many experimental anomalies have been clarified through application of molecular modelling [349]. A more thorough review of current models in use, as well as their performance with respect to experimental observations, is available in reference [347], and a current discussion of water models (as well as many characteristics of water) is available in reference [343].

A.2 SCVS Implementation in Gaussian 09

The SCVS method was first available commercially in the Gaussian 09 (G09) program in version B.01 and improved in version C.01. There is no keyword, but sample inputs are available in test935-test939 and test945 in the G09 test directory included with the program installation. An example input for a SCVS optimization of formamide is provided in Figure A.2.

Figure A.2 Sample input for SCVS implementation in Gaussian 09Rev.C.01 (test937.com).

```
#p opt=tight mp2(full)/6-311g** extralinks=l112 density=current
int=readb

Gaussian Test Job 937:
Formamide mp2(full)/6-311G**//mp2(full)/6-311G** SCVS

0 1
 C                -0.15457920     0.41470365     0.00000000
 O                -1.19796161    -0.26101347     0.00000000
 N                 1.08304695    -0.16570783     0.00000000
 H                -0.15135510     1.52911778     0.00000000
 H                 1.17773711    -1.15080964     0.00000000
 H                 1.90345745     0.38153249     0.00000000
```

A.3 Obtaining Accurate .wfn/.wfx Files from Gaussian

Although it is preferable to use AIMQB to transform a formatted checkpoint file into a usable .wfx or .wfn file, in some instances (such as when pseudopotentials are present) it is necessary to use Gaussian 09 to write the .wfx or .wfn file. This can be achieved using the OUTPUT=WFX or OUTPUT=WFN command in the route section. If the .wfn file for a post-Hartree Fock calculation such as MP2 is generated in Gaussian 09 using a version older than B.01 then there are some important considerations. For post-SCF correlated calculations the virial ratio will be written incorrectly to the .wfn file, reflecting the SCF energy rather than correlated values. This must be manually updated to the correct virial using the total correlated energy (*i.e.*, EUMP2) and the kinetic energy (KE). Note that this is not required for later versions of Gaussian or if AIMQB is used to write the .wfx file. The keyword DENSITY=CURRENT is required for post-SCF correlated methods, so that the natural orbitals of the correlated first order density matrix

are written to the .wfn file. In the case of a single point calculations, even if AIMQB is used to write the .wfx file it is necessary to include DENSITY=CURRENT in the Gaussian route section so that the correlated first-order density appears in the .chk file and thus .fchk file. Also for single point calculations, it is recommended that the FORCE keyword is included so that nuclear coordinate energy gradients will be written to the .fchk file. If an unrestricted post-SCF calculation is required (*i.e.* UMP2 or UCCSD(T), *etc.*), POP=NOAB must be included in the route section so that the alpha and beta natural spin orbitals of the first-order density matrix are written separately to the traditional AIM .wfn file. This is not required if the .fchk file is to be used by AIMQB to write the .wfx file. Finally, there is a small chance (in Gaussian03) that the molecular orbital coefficients will be written to the .wfn file in standard orientation but the nuclear coordinates will remain in the input orientation. This can be avoided by including the NOSYMM keyword, or by using AIMQB to write the .wfx file from the .fchk file.

Appendix B   Supporting Information for Papers

The supporting information for the majority of the chapters in this thesis is available online. In particular, information such as Cartesian coordinates for optimized structures and raw data for atomic properties can be accessed online using the doi for each paper.

B.1 Chapter 4: Visualizing Internal Stabilization in Weakly Bound Systems Using Atomic Energies: Hydrogen Bonding in Small Water Clusters

L. Albrecht, R. J. Boyd, *J. Phys. Chem. A*, (2012), 116 (15), 3946–3951. DOI: 10.1021/jp301006g.

Supporting Information Available: Geometric parameters for MP2 optimized water molecules, QTAIM atomic properties, and NPA charges. This material is available free of charge via the Internet at http://pubs.acs.org.

B.2 Chapter 5: Atomic Energy Evaluation of Eight Low-Lying Water Hexamer Structures

L. Albrecht, S. Chowdhury, R. J. Boyd, *J. Phys. Chem. A,* (2013) 117(41), 10790-9, DOI: 10.1021/jp407371c.

Supporting Information Available: Geometric parameters for SCVS-MP2 optimized water hexamers and QTAIM atomic properties including bond critical point data. This material is available free of charge via the Internet at http://pubs.acs.org.

B.3 Chapter 6: Cooperativity between hydrogen bonds and beryllium bonds in $(H_2O)nBeX_2$ (n = 1–3, X = H, F) complexes. A new perspective.

L. Albrecht, R. J. Boyd, O. Mó, M. Yáñez, *Phys. Chem. Chem. Phys.* (2012) 14, 14540-14547 (DOI: 10.1039/C2CP42534C).

Additional supporting information: B3LYP/6-31+G(d,p) optimized geometries for the water dimer and trimer, and the $(H_2O)_nBeX_2$ (n =1-3, X = H, F) complexes are available online at www.rsc.org/pccp.

Table B.1 CCSD(T)/aug-cc-pVQZ//CCSD/6-31+g(d,p) total energies (E, hartrees) and relative free energies (ΔG, kJ mol^{-1}) for WD(BeH$_2$)a and WD(BeH$_2$)b clusters.

Cluster	E	ΔG
WD(BeH$_2$)a	-168.6327986	0.0
WD(BeH$_2$)b	-168.6309422	5.6

Table B.2 B3LYP/6-31+G(d,p) optimized geometries for the water dimer and trimer, and the (H$_2$O)$_n$ BeX$_2$ (n =1-3, X = H, F) complexes. Coordinates are in Å.

(H$_2$O)$_2$				(H$_2$O)$_3$			
8	0.007035	-0.004858	-0.097332	8	-0.101541	0.040752	-0.188709
1	0.051539	-0.001213	0.871549	8	-0.104155	0.112758	2.597583
1	0.921804	0.004924	-0.391940	8	2.297625	-0.086707	1.210611
8	-0.036388	-0.000158	2.801888	1	-0.459409	0.144352	0.712880
1	-0.480854	0.761251	3.188979	1	0.855712	0.037268	2.435930
1	-0.463204	-0.772899	3.186401	1	1.678129	-0.061769	0.456557
				1	2.863824	-0.851074	1.071128
				1	-0.216065	0.760200	3.298802
				1	-0.521876	0.713425	-0.731370

H$_2$O:BeH$_2$				H$_2$O:BeF$_2$			
8	-0.005288	-0.086058	0.031365	8	0.006243	-0.109381	0.039354
1	0.090649	0.043361	0.981203	1	0.097696	0.050165	0.984616
1	0.831224	0.032487	-0.431610	1	0.828029	0.051275	-0.436231
4	-1.461878	-0.468328	-0.729727	4	-1.430742	-0.626080	-0.699025
1	-2.416897	-0.554075	0.227869	9	-2.428713	-0.762837	0.313671
1	-1.217990	-0.569053	-2.058924	9	-1.189281	-0.761918	-2.100199

WD(BeH$_2$)a				**WD(BeF$_2$)a**			
8	0.231893	-0.355351	0.065392	8	-0.010017	0.034757	-0.004271
1	0.432347	-0.257056	1.032568	1	-0.046112	0.009449	0.991300
1	0.878889	-0.869867	-0.425130	1	0.877659	-0.015587	-0.368897
8	-0.176819	0.133774	2.562190	8	-0.883847	-0.272349	2.404471
1	0.071117	0.878418	3.118954	1	-1.076897	0.353437	3.108835
1	-1.031620	0.365476	2.137819	1	-1.720902	-0.444878	1.929394
4	-1.310974	-0.039255	-0.407613	4	-1.386141	-0.441314	-0.782538
1	-1.970435	0.480978	0.690091	9	-2.428108	-0.585736	0.231617
1	-1.574879	-0.353119	-1.694842	9	-1.249944	-0.614030	-2.190441

WD(BeH$_2$)b				**WD(BeF$_2$)b**			
8	0.304537	-0.040250	-0.037072	8	0.017861	-0.006769	0.012679
1	0.170000	-0.165803	0.909899	1	0.015296	0.012662	0.978246
1	1.078731	0.522567	-0.157365	1	0.935105	0.014565	-0.288829
4	-1.126013	0.800783	-0.711415	4	-0.801538	1.459704	-0.580612
1	-2.075746	0.721716	0.298837	8	-2.163994	0.881044	-1.569202
1	-0.590441	1.849569	-1.447553	1	-2.064318	1.231212	-2.463671
8	-1.703397	-0.356897	-1.950329	1	-2.983005	1.230609	-1.195441
1	-1.704272	0.084302	-2.808197	9	0.142248	2.005527	-1.572662
1	-2.611625	-0.605349	-1.740576	9	-1.453064	2.003772	0.624599

WT(BeH$_2$)a				**WT(BeF$_2$)a**			
8	-0.827683	0.083689	0.074616	8	-0.028250	0.027247	-0.030927
8	0.287437	0.887919	2.262396	8	0.072458	0.028553	2.532292

8	2.199576	-0.877434	1.695828	8	2.699190	-0.401141	2.545822
1	-0.462637	0.444054	0.943649	1	-0.072476	0.025687	0.982083
1	1.092861	0.316417	2.258671	1	1.042671	-0.081777	2.706743
1	1.704271	-1.366450	0.996093	1	2.810317	-0.486046	1.575322
1	2.852349	-1.477902	2.065362	1	3.419055	0.150782	2.863962
1	-0.136975	0.765965	3.117031	1	-0.381606	-0.635957	3.059658
1	-1.429185	0.701403	-0.350782	1	-0.839691	0.341338	-0.439828
4	-0.289252	-1.218040	-0.739715	4	1.308890	-0.195358	-0.933229
1	0.677684	-1.897025	-0.031915	9	2.475327	-0.505945	-0.107312
1	-0.891914	-1.379670	-1.941900	9	1.085779	-0.028414	-2.335528
WT(BeH$_2$)b				**WT(BeF$_2$)b**			
8	0.283775	0.054532	0.308774	8	0.021612	0.034822	0.033028
1	0.107100	0.108950	1.272917	1	-0.058286	-0.114557	1.001832
1	1.176398	0.297623	-0.019611	1	0.894945	-0.114750	-0.395060
8	-1.167379	-0.276968	2.458295	8	-1.179101	0.041413	2.359225
1	-1.670910	0.294853	3.045302	1	-1.109237	0.471667	3.215979
1	-1.764328	-0.523872	1.723960	1	-1.837810	0.539012	1.839335
4	-0.863284	-0.429113	-0.710910	4	-1.084826	0.933459	-0.724780
1	-2.032304	-0.733909	-0.055011	8	1.835702	0.211935	-1.847792
1	-0.420297	-0.430796	-2.012225	1	1.095799	0.663529	-2.295747
8	2.062638	0.515757	-1.551315	1	2.226300	-0.392317	-2.485442
1	1.282838	0.184650	-2.040023	9	-0.680538	1.262990	-2
1	2.828460	0.052713	-1.903750	9	-2.221351	1.237377	0.129047
WT(BeH$_2$)c				**WT(BeF$_2$)c**			
8	0.159874	-0.449575	0.121021	8	-0.016461	0.013474	0.018584
1	0.076286	-0.157034	1.061387	1	-0.010186	0.044088	1.009334
1	0.692270	0.185488	-0.368030	1	0.888184	0.031171	-0.312244
8	-0.919111	0.035527	2.478394	8	-0.615930	0.581222	2.528472
1	-1.151170	0.850253	2.934092	1	-0.151209	1.036058	3.236433
1	-1.669413	-0.174614	1.867314	1	-1.158324	1.251088	2.059041
4	-1.406948	-0.675919	-0.581906	4	-0.947961	1.304548	-0.635112
1	-2.333360	-0.599734	0.489155	8	-2.268733	0.555991	-1.579772
1	-1.446556	-0.031491	-1.806540	1	-3.118613	0.844953	-1.224240
8	-1.429830	-2.421233	-1.006456	1	-2.188359	0.901825	-2.478376
1	-2.121690	-2.885423	-0.520600	9	-1.695164	1.909980	0.528584
1	-1.638583	-2.479684	-1.946537	9	-0.135357	1.960595	-1.674566
WT(BeF$_2$)d				**WT(BeF$_2$)d**			
8	0.012415	-0.122697	0.049398	8	-0.020480	0.104705	0.008291
1	-0.092572	-0.168611	1.048406	1	-0.081595	0.055967	1.026376
1	0.904144	-0.286281	-0.268392	1	0.869150	-0.008011	-0.344076
8	-0.957059	-0.332416	2.391789	8	-0.734289	-0.226274	2.401041
1	-1.072113	0.397652	3.026301	1	-0.912178	0.503055	3.027897
1	-1.785612	-0.397808	1.883284	1	-1.589775	-0.506165	2.020181
4	-1.357415	-0.334551	-0.823198	4	-1.336934	-0.549844	-0.725830
1	-2.415549	-0.320963	0.064688	8	-1.240832	1.853233	4.214542
1	-1.157889	-0.480706	-2.155757	1	-1.855019	2.572044	4.018121
8	-1.310468	1.770723	4.249033	1	-1.337395	1.655869	5.154800
1	-1.699249	2.620257	4.016735	9	-2.388749	-0.729809	0.273745
1	-1.575835	1.592357	5.157053	9	-1.200535	-0.837213	-2.121250

Table B.3 B3LYP/6-311+G(3df,2p)//B3LYP/6-31+G(d,p) total energies (hartrees).

water	-76.463373
water dimer	-152.934352
water trimer	-229.41373
BeH_2	-15.9234856
BeF_2	-214.689368
$H_2O:BeH2$	-92.4161175
$H_2O:BeF2$	-291.1860227
WD(BeH₂)a	-168.9017818
WD(BeH₂)b	-168.896473
WD(BeF₂)a	-367.674095
WD(BeF₂)b	-367.6694464
WT(BeH₂)a	-245.3850267
WT(BeH₂)b	-245.3837711
WT(BeH₂)c	-245.3815168
WT(BeH₂)d	-245.3753606
WT(BeF₂)a	-444.1586208
WT(BeF₂)b	-444.158092
WT(BeF₂)c	-444.1559868
WT(BeF₂)d	-444.1479908
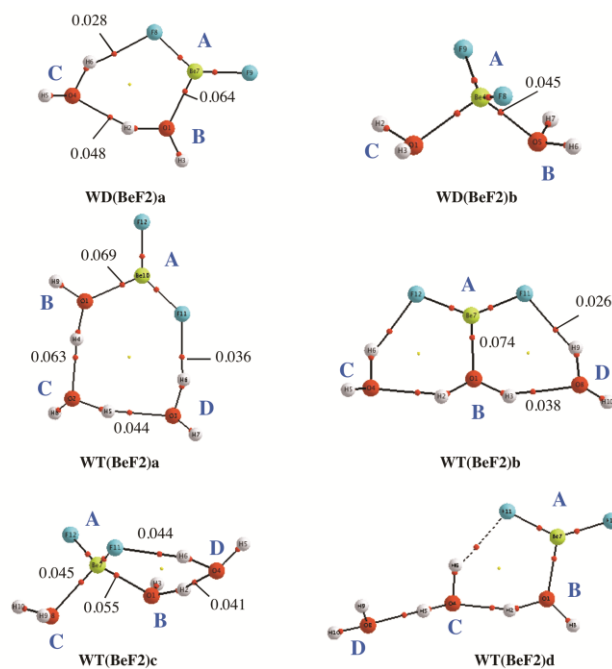
Figure B.1 Molecular graphs of the optimized clusters formed by two and three water molecules with BeF_2. Red dots denote BCPs. Electron densities are in a.u.. **A** and **B** denote respectively the BeH_2 molecule and the water molecule attached to through a beryllium bond.
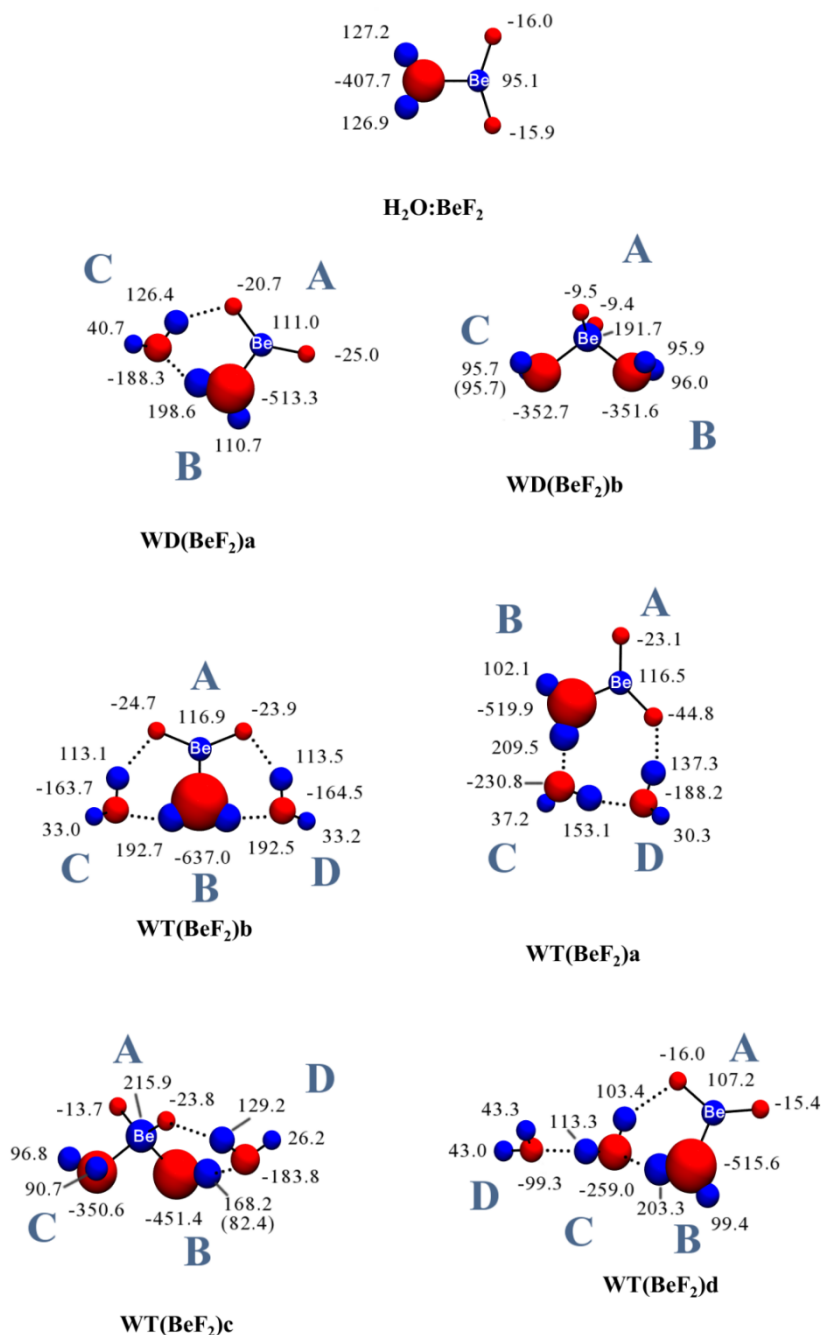
Figure B.2 Change in atomic energy for the formation of $BeF_2:(H_2O)_n$, n=1-3, systems. Values for the relative energy change of each atom are labeled (kJ mol^{-1}). Stabilized atoms are red, destabilized atoms are blue. Atom size corresponds to the magnitude of energy change. **A**, **B**, **C**, and **D** denote labels as in Figure 9.1. For hydrogens which are hidden the energy is included in parentheses. The atomic energies for the atoms in BeF_2 and H_2O monomers are: Be (-3.7x10^5), F (-2.63x10^3), and O (1.98x10^5), H (1.03x10^3), respectively, in kJ mol^{-1}.

191

B.4 Chapter 8: Atomic Energy Analysis of Cooperativity, Anti-cooperativity, and Non-cooperativity in Small Clusters of Water, Methanol, and Formaldehyde.

L. Albrecht and R. J. Boyd, *Comp. Theo. Chem.,* (2014) *In press.* DOI: 10.1016/j.comptc.2014.08.022 –

Supporting information available: Benchmark data for Dunning basis set, SCVS calculations, and CCSD(T)//MP2 *vs.* CCSD(T)//B3LYP energies are included below. Relevant AIM parameters including charges, scaled and unscaled energies, L(A) values, and BCP energy densities can be found online at http://dx.doi.org/10.1016/j.comptc.2014.08.022.

B.4.1 Benchmark Calculations

Methanol energies were optimized with B3LYP functional to compare our MP2 values with previous studies. The CCSD(T) energies are closer to the MP2 energies regardless of which method is used to optimize the geometry (Table B.4).

Table B.4 Comparison of CCSD(T) energies at B3LYP and MP2 optimized geometries for clusters of methanol, n=1-4.

Method	Monomer	Dimer	Trimer	Tetramer	Eint$_n$			E/nHB			Coop	
					n=2	n=3	n=4	n=2	n=3	n=4	n=3	n=4
MP2/6-311++G(d,p)	-115.445220	-230.901300	-346.365781	-461.835152	-6.8	-18.9	-34.1	-6.8	-6.3	-8.5	0.52	-1.7
CCSD(T)6-311++G(d,p)// MP2/6-311++G(d,p)	-115.477241	-230.965263	-346.461647	-461.962494	-6.8	-18.8	-33.6	-6.8	-6.3	-11.2	0.51	-4.4
B3LYP/6-311+G(d,p)	-115.764942	-231.539165	-347.322080	-463.108123	-5.8	-17.1	--	-5.8	-5.7	--	0.12	--
CCSD(T)6-311++G(d,p)// B3LYP//6-311+G(d,p)	-115.477186	-230.965001	-346.461358		-6.7	-18.7	--	-6.7	-6.2	--	0.44	--

Table B.5 Comparison of Pople and Dunning basis sets for selected water, methanol, and formaldehyde clusters.

		E(Hartree)			E_{int} (kcal mol^{-1})		
Water	**Monomer**	**Dimer**	**Trimer (cyclic)**	**Trimer (anticoop)**	**n=2**	**n=3 (cyc)**	**n=3 (anti)**
MP2/6-311++G(d,p)	*-76.274920*	*-152.559525*	*-228.853104*	*-228.841888*	-6.1	-17.8	-10.7
MP2/aug-cc-PVTZ	*-76.328992*	*-152.666240*	*-229.012934*	*-229.001723*	-5.2	-16.3	-9.3
Methanol	**Monomer**	**Dimer**			**n=2**		
MP2/6-311++G(d,p)	*-115.445220*	*-230.901300*			-6.8		
MP2/aug-cc-PVTZ	*-115.529008*	*-231.067846*			-6.2		
Formaldehyde	**Monomer**	**Dimer(C$_{2h}$)**	**Trimer (cyclic)**	**Trimer (stacked)**	**n=2**	**n=3 (cyc)**	**n=3 (stacked)**
MP2/6-311++G(d,p)	*-114.241772*	*-228.488602*	*-342.736017*	*-342.735147*	-3.2	-6.7	-6.2
MP2/aug-cc-PVTZ	*-114.316410*	*-228.638766*	*-342.961202*	*-342.960701*	-3.7	-7.5	-7.2

For the AIM analysis, SCVS scaling is preferable to minimize the forces on the wavefunction along with the energies during the SCF procedure. We found that the time it took for this minimization on all clusters was prohibitively long, however we have evaluated tetramer structures for each monomer set to compare the differences in scaled energies with and without SCVS scaling. Although the absolute values for the scaled atomic energies (K_scaled(Atom)) differ on average by up to 6 kcal mol^{-1} (Table B.6), the relative differences in energy for the cluster formation (ΔE(Atom)) differ by less than a kcal mol^{-1} (Table B.7).

Table B.6 Average difference in energy (AVE) and standard deviation (STDEV) comparing the influence of SCVS on scaled atomic energies (K_scaled(A)) in tetramer and monomer clusters. Energies in kcal mol^{-1}.

Atom Energy (scaled)	Water		Methanol		Formaldehyde	
	AVE	STDEV	AVE	STDEV	AVE	STDEV
K_scaled(O)	-0.265	0.018	5.181	0.235	5.713	0.095
K_scaled(C)			-5.675	0.216	-5.916	0.079
K_scaled(H)	0.153	0.036	0.152	0.036	0.165	0.018

Table B.7 Average difference in energy (AVE) and standard deviation (STDEV) comparing the influence of SCVS on atomic energy stabilities for tetramer formation. ΔE(Atom)=E(atom in monomer) – E(atom in cluster). Energies in kcal mol^{-1}.

ΔE(Atom)	Water		Methanol		Formaldehyde	
	AVE	STDEV	AVE	STDEV	AVE	STDEV
ΔE(O)	0.046	0.000	0.588	0.000	0.237	0.001
ΔE(C)			-0.539	0.002	-0.198	0.001
ΔE(H)	-0.014	0.039	-0.008	0.056	-0.017	0.019

B.4.2 Bond Critical Point Data

Table B.8 Bond critical point electron densities for water clusters.

Cluster		Density at BCP[a]		
		OH^{nHB}	OH^{HB}	$OH{\cdots}O$[b]
Monomer				
		0.364		
Dimer				
A		0.365	0.356	0.23
B		0.362		
Trimer				
Cyclic cooperative	A	0.363	0.349	0.024^{AB}
	B	0.363	0.348	0.026^{BC}
	C	0.363	0.348	0.025^{CA}
Linear anti-cooperative	A		0.358	
	B	0.362		0.021^{AB}
	C	0.362		0.012^{AC}
Tetramer				
Cyclic cooperative[c]		0.362	0.339	0.034
Cyclic anti-cooperative	A		0.360	0.019
	B		0.360	
	C	0.360		
	D	0.360		

[a] BCP densities in a.u. [b] Superscripts indicate interacting monomers. [c] In cases where only one value is given for all monomers, the BCP densities are the same.

Table B 9 Bond critical point electron densities for methanol clusters.

Cluster	Density at BCP[a]					
	CO	OH	$OH{\cdots}O$[b]	$C\text{-}H^{trans}$	$C\text{-}H^{inner}$	$C\text{-}H^{outer}$
Monomer[c]						
	0.251	0.367	--	0.283	0.278	0.278
Dimer						
A	0.256	0.357	0.028	0.281	0.277	0.277
B	0.243	0.364		0.281	0.280	0.280
Trimer						
A	0.249	0.349	0.029^{AC}	0.282	0.279	0.279
B	0.250	0.348	0.030^{BA}	0.282	0.278	0.279
C	0.250	0.349	0.028^{CB}	0.282	0.278	0.279
Tetramer[c]	0.249	0.337	0.041	0.281	0.278	0.279

[a] BCP densities in a.u. [b] Superscripts indicate interacting monomers. [c] In cases where only one value is given for all monomers, the BCP densities are the same due to symmetry.

Table B.10 Bond critical point electron densities for formaldehyde clusters.

Cluster		Density at BCP[a]				
		C=O	CH^{HB}	CH^{nHB}	CH···O[b]	C···O[b]
Monomer						
		0.398	--	0.277	--	--
Dimer						
C_s^c		0.394	0.281	0.277	0.008	
C_{2h}	A	0.394	0.280	0.278	0.009	0.013
	B	0.395		0.279		
Trimer						
Cyclic^c		0.392	0.282	0.277	0.010	--
Stacked	A	0.394	0.281	0.277	.0.008	--
	B	0.390	0.281	--	0.008	--
	C	0.394	0.281	0.277	0.008	--
Bucket	A	0.392	0.282	0.278	0.006^{AB} 0.009^{AC}	0.013^{AB}
	B	0.393	--	0.280	0.006^{BA}	0.013^{AB} 0.008^{BC}
	C	0.395	--	0.280 0.278	--	0.008^{BC}
Tetramer						
Cyclic^c		0.392	0.283	0.277	0.010	--
Stacked	A	0.394	0.281	0.277	0.008	--
	B	0.391	0.281	--	0.008	--
	C	0.391	0.281	--	0.008	--
	D	0.394	0.281	0.277	0.008	--
Bucket	A	0.393	0.281	0.278	0.006^{AD} 0.009^{AC} 0.008^{AB}	0.013^{AB}
	B	0.392	0.280	0.280	0.008^{AB}	0.012^{BC} 0.013^{AB}
	C	0.391	0.282	0.279	0.009^{AC} 0.007^{CD}	0.012^{BC} 0.012^{CD}
	D	0.0394	0.280	0.278	0.007^{CD}	0.012^{CD}

[a] BCP densities in a.u. [b] Superscripts indicate interacting monomers. [c] In cases where only one value is given for all monomers, the BCP densities are the same.

B.5 Chapter 9: Changing Weak Halogen Bonds into Strong Ones through Cooperativity with Beryllium Bonds

Supporting information available: Benchmark evaluation and a discussion of atomic energy scaling is included below. Relevant AIM properties and Cartesian coordinates for all structures are included in the supporting information online at http://pubs.acs.org.

B.5.1 Benchmark Data
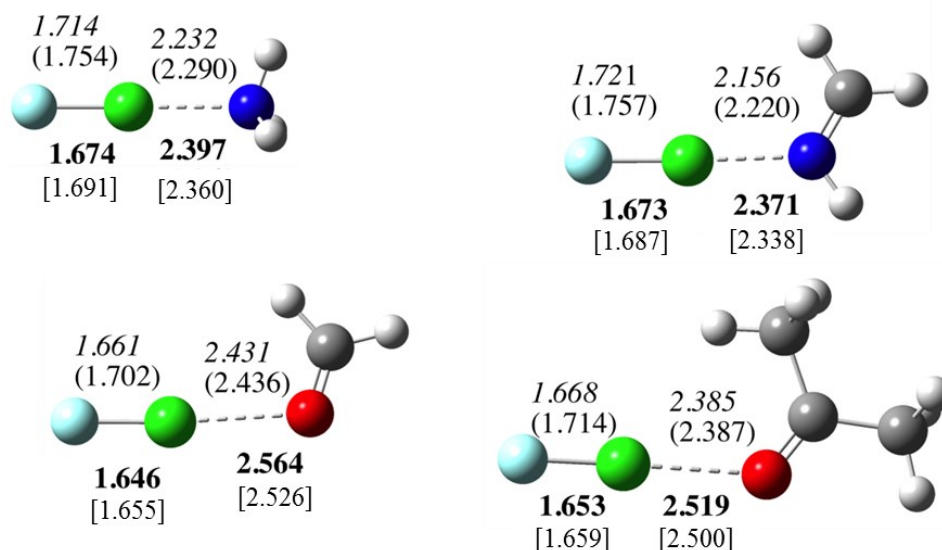
Figure B.3 Optimized bond distances (in Å) for complexes between FCl and different Lewis bases. Values in bold and italic were obtained at the CCSD/aug-cc-pVTZ and MP2/aug-cc-pVTZ levels of theory, respectively. The values within parentheses and brackets were obtained using the B3LYP and the M06-2X functionals, respectively. In both cases the 6-31+G(d,p) basis set was used.

Table B.11 Interaction energies, E_{int} and the two- and three-body interaction energy components (Δ^2E and Δ^3E) for ABC (A = BeH$_2$, B = FCl, C = Lewis Base) complexes calculated at the M062X/6-31+G(d,p) level. The values within brackets correspond to CCSD(T)/aug-cc-pVTZ calculations carried out on the M062X/6-31+G(d,p) optimized geometries . All values are in kJ mol^{-1}.

Lewis Base	E_{int}	$\Delta^2E(AB)$	$\Delta^2E(BC)$	$\Delta^2E(AC)$	$\Sigma\Delta^2E$	Δ^3E
NH$_3$	-231	-73	-80	-4	-157	-74
	[-209]	[-55]	[-64]	[-9]	[-123]	[-86]
Methaneimine	-326	-95	-118	-5	-239	-87
	[-292]	[-114]	[-84]	[-7]	[-205]	[-87]
HCN	-70	-33	-20	-2	-55	-15
	[-67]	[-28]	[-21]	[-2]	[-52]	[-16]

Table B 12 Bond lengths (Å) for FCl, H$_2$Be-FCl, FCl-Base and H$_2$Be-FCl-Base complexes evaluated at M06-2X/6-31+G(d,p).

Base	FCl-Base Complex		H$_2$Be-FCl-Base Complex		
	r(F-Cl)	r(Cl-Base)	r(Be-F)	r(F-Cl)	r(Cl-Base)
Ammonia	1.691	2.360	1.602	1.888	1.974
Methylamine	1.715	2.234	1.572	1.969	1.894
Dimethylamine	1.731	2.177	1.557	2.026	1.858
Trimethylamine	1.739	2.155	1.548	2.067	1.846
Methanimine	1.687	2.338	1.559	2.019	1.796
HCN	1.650	2.662	1.768	1.699	2.462
Imidazol	1.697	2.289	1.570	2.053	1.845
Pyridine	1.708	2.227	1.478	2.541	1.726
Formaldehyde	1.655	2.526	1.709	1.734	2.230
Acetaldehyde	1.656	2.526	1.660	1.781	2.092
Acetone	1.659	2.500	1.631	1.821	2.007
Formamide	1.661	2.463	1.640	1.803	2.041
Formic Acid	1.653	2.544	1.723	1.724	2.276
Tetrahydrofuran	1.663	2.410	1.639	1.812	2.029
FCl	1.639				
BeFCl			2.000	1.659	
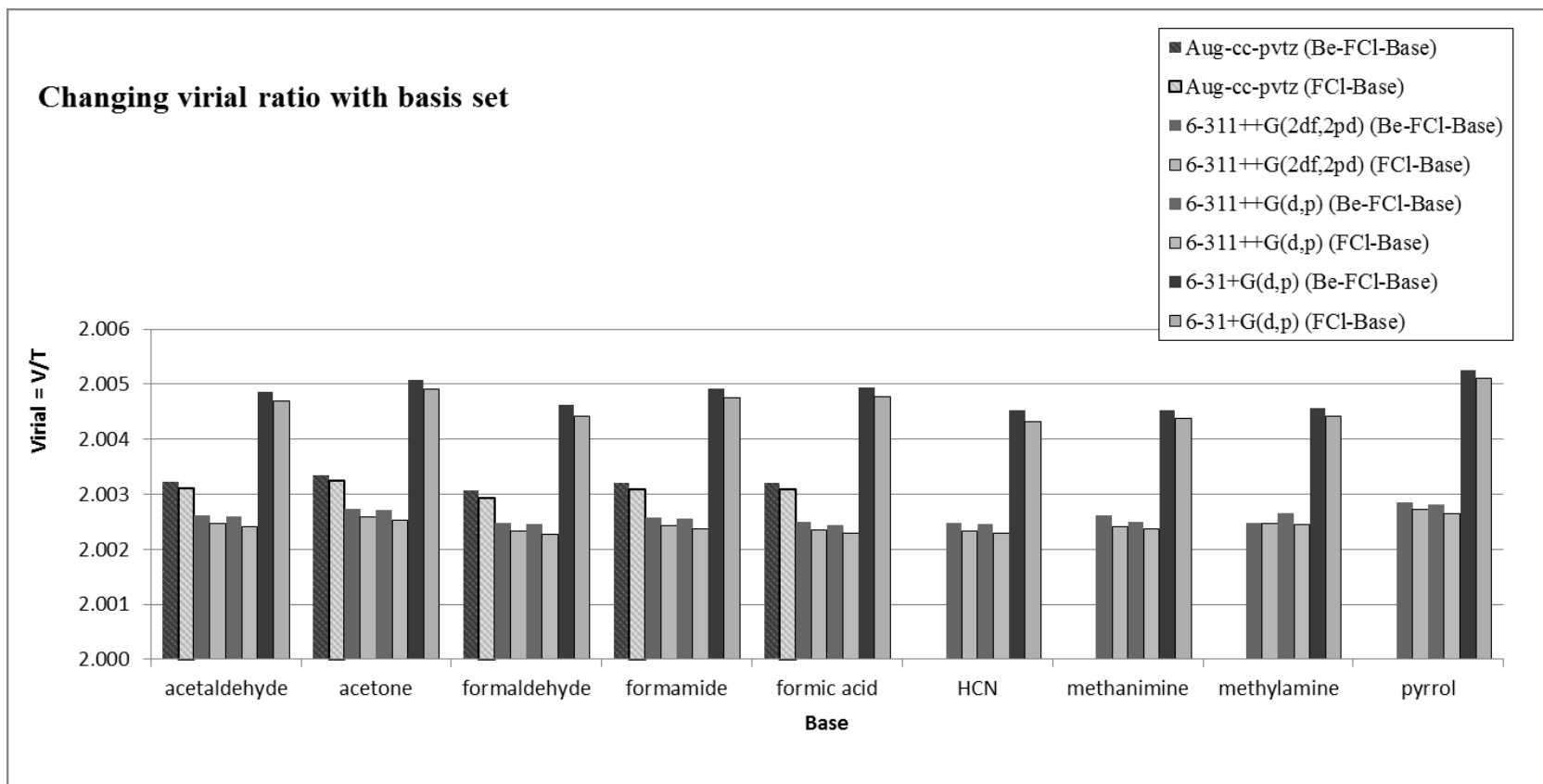
Figure B.4 Virial ratio for set of complexes at four basis sets: 6-31+G(d,p), 6-311++G(d,p), 6-311++G(2df,2pd), aug-cc-pVTZ for representative systems.
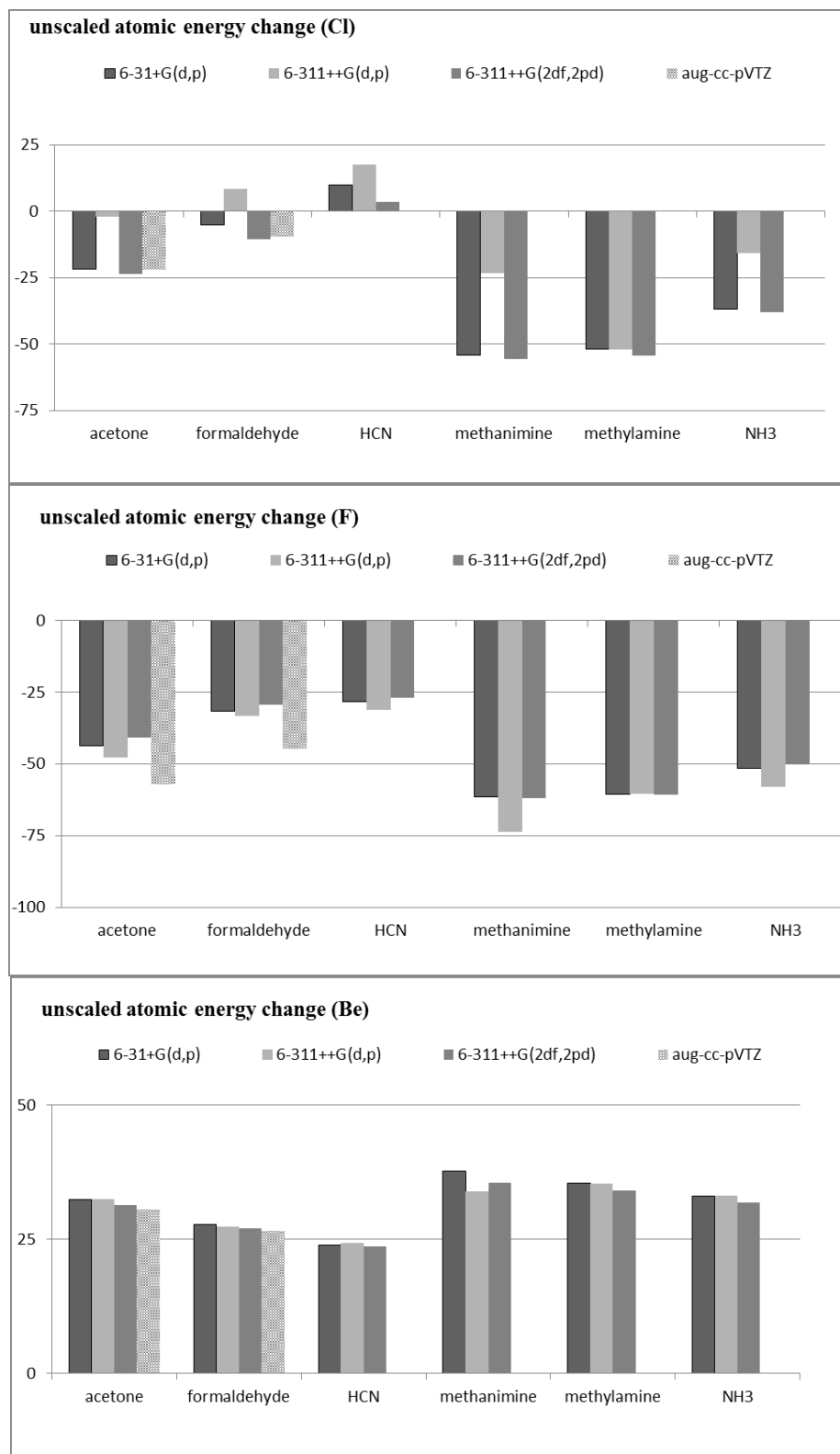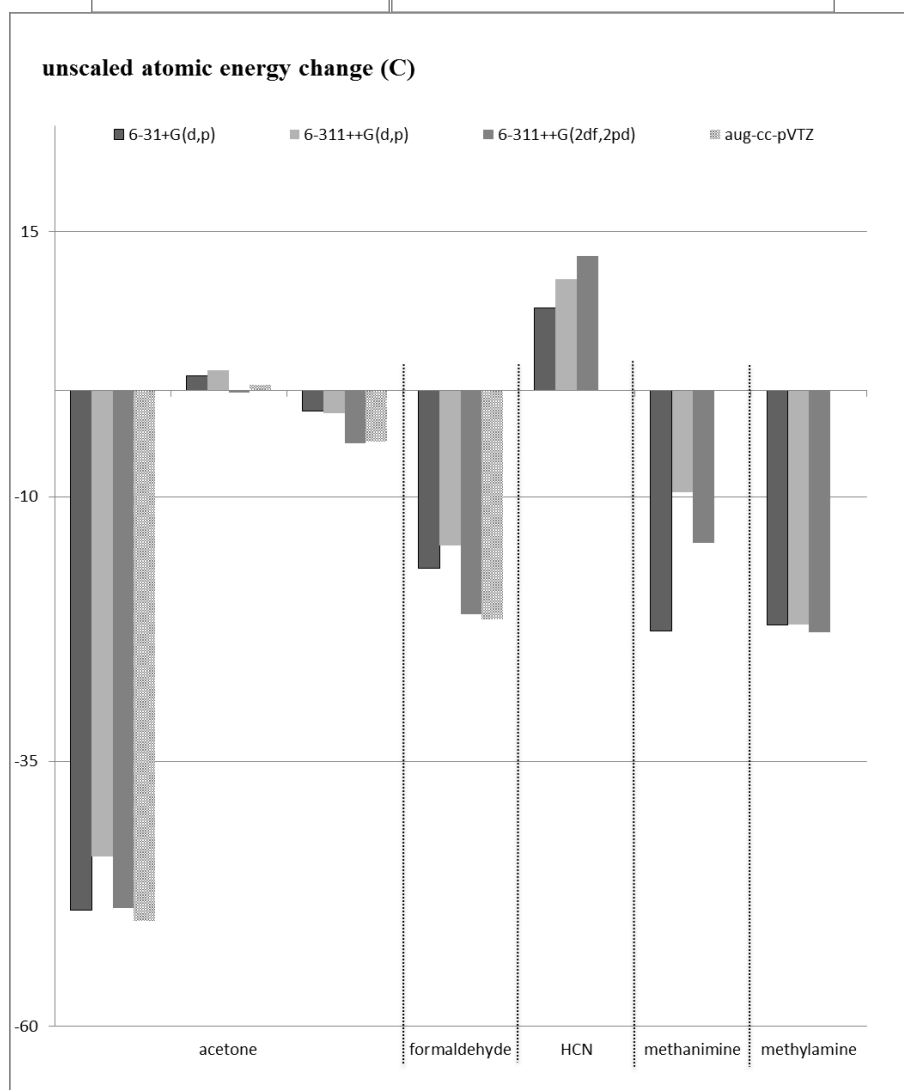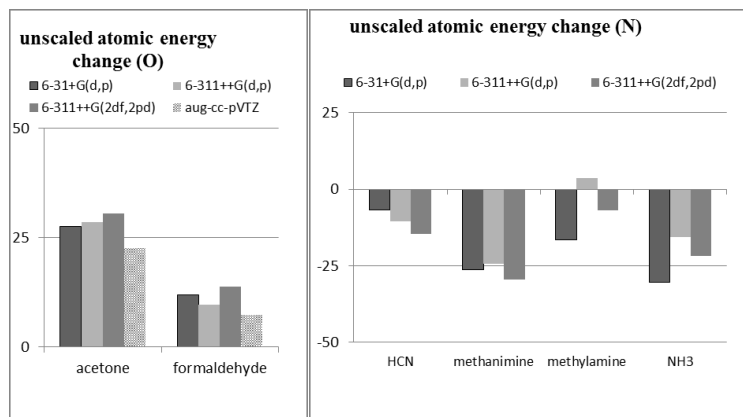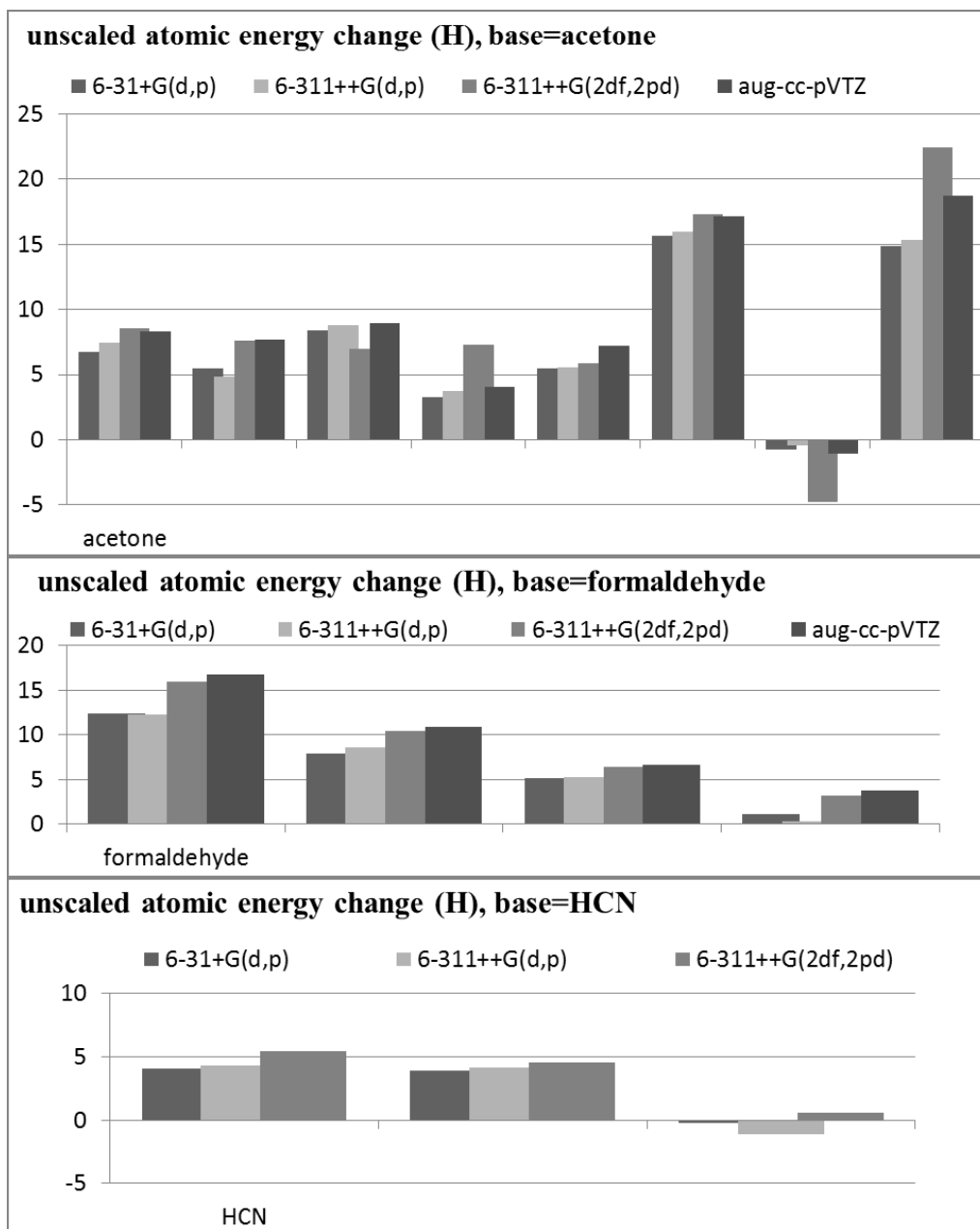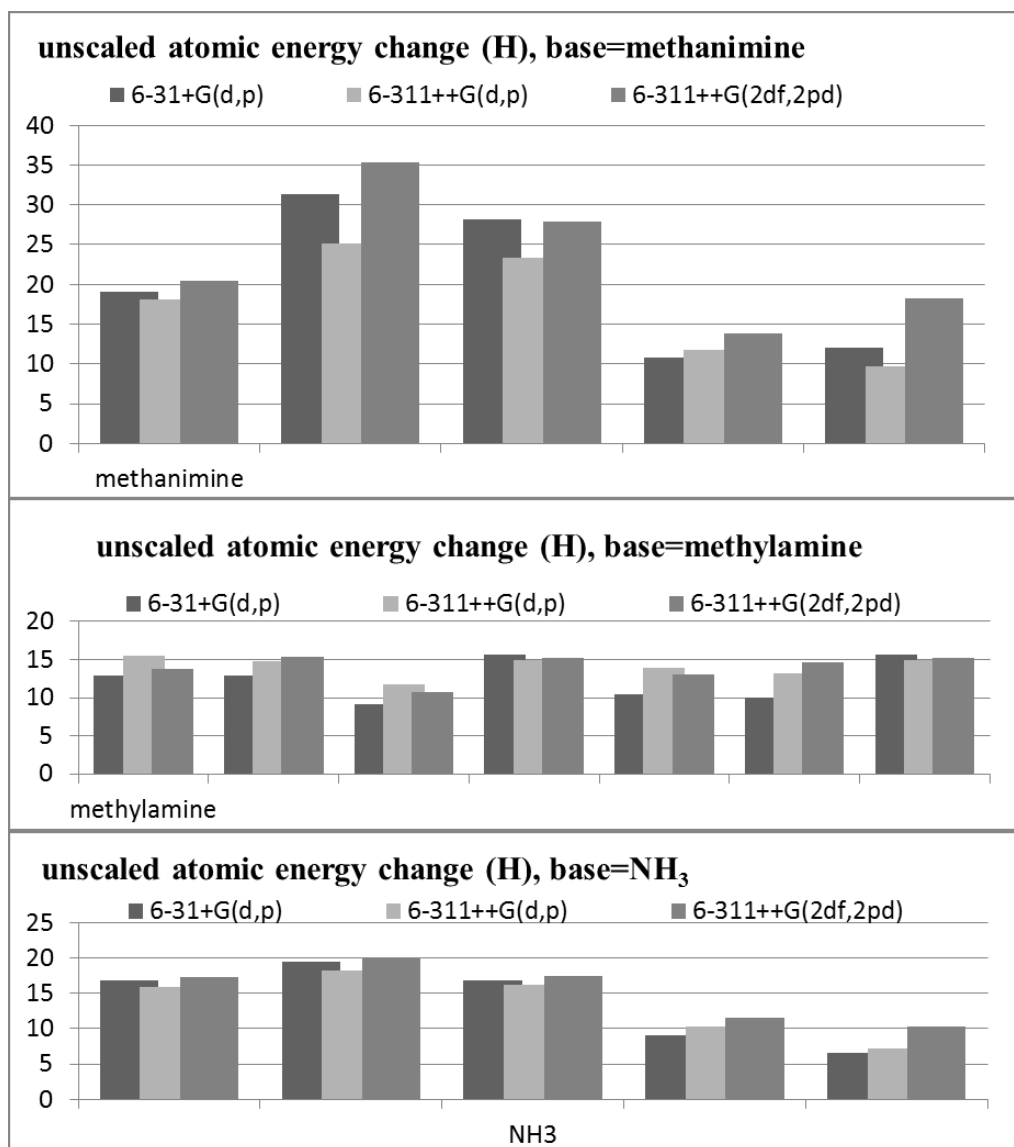
Figure B.5 Unscaled atomic energy changes for the interaction BeH_2 + FCl-Base $\rightarrow$ H_2Be-FCl-Base for representative systems (Dunning basis set only for acetone and formaldehyde. Energy scale in kcal mol^{-1}).

X-axis = unscaled atomic energies, Y-axis = scaled atomic energies (energy in kcal mol^{-1})
sm = 6-31+G(d,p); bb = 6-311++G(d,p); bg = 6-311++G(2df,2pd).
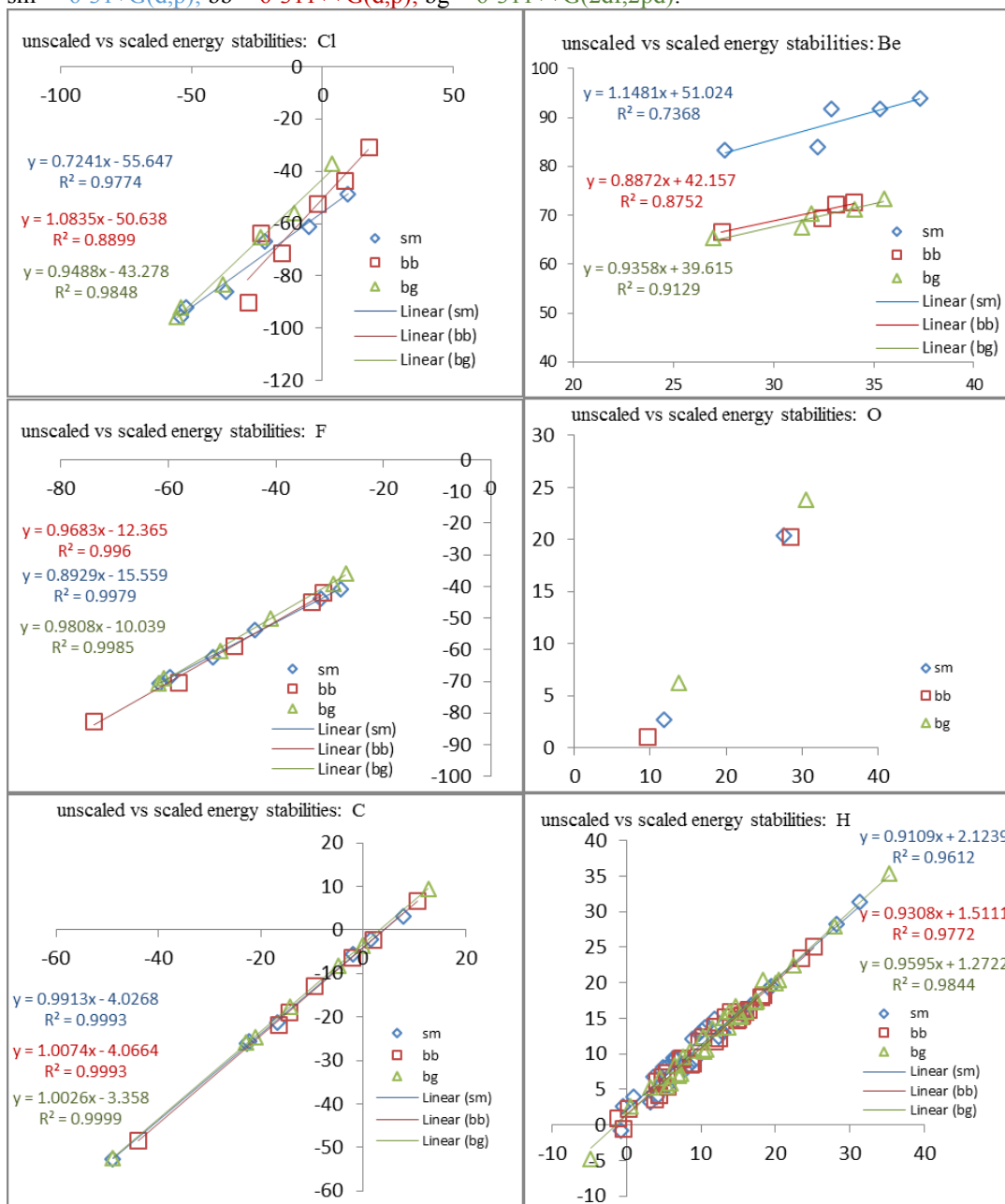
Figure B.6 Unscaled *vs.* scaled energies for representative systems at three basis sets, sm: 6-31+G(d,p), bb: 6-311++G(d,p), bg: 6-311++G(2df,2pd).

B.5.2 Scaled Atomic Energies and the AIM Method

The virial theorem for a molecule at a stationary state on the potential energy surface reduces to $-V/T = 2$, where V and T are the potential and kinetic energies, respectively. In AIM theory this can be extended to atoms, Ω, that are defined by zero-flux surfaces, giving atomic energy

$$E(\Omega) = -T(\Omega) = -\frac{1}{2}V(\Omega)$$

The sum of E(Ω) for all atoms in a molecule returns the molecular energy, E. Because the wavefunctions used in practice are approximate, there will be some deviation from this virial relationship and summation of E(Ω) does not exactly yield E. Ideally, one would remove or at least minimize this deviation by simultaneously minimizing the energy with respect to a scaling factor for all coordinates, molecular orbital coefficients, and the molecular geometry [63]. This procedure (self-consistent virial scaling, SCVS [71]) can be very computationally costly, and is not currently available for DFT methods such as M06-2X in the Gaussian 09 software. An alternative and much cheaper approach is to simply scale the final atomic energy components by the amount of deviation from the virial relationship,

$$E_{scaled}(\Omega) = T(\Omega)(1 + \gamma)$$

where $\gamma = -V/T$. This provides satisfactory results for comparison of energies in different systems because $(1 + \gamma)$ is usually small and γ generally scales linearly with $T(\Omega)$. In the case of Kohn-Sham (KS) DFT, however, the kinetic energy is obtained from KS molecular orbitals (KS-MOs) where $T(\Omega)$ is now $T_0(\Omega)$, the non-interacting kinetic energy. This deviates from the total kinetic energy by

$$T(\Omega) = T_0(\Omega) + \Delta T_C(\Omega)$$

Here $\Delta T_C(\Omega)$ is the correlation kinetic energy contained in the exchange-correlation functional [72-73].

The implication for AIM analysis is that the relationship used to define the scaling factor is no longer $V/T = \gamma$, but is actually $V/T_0 = \gamma$ and is thus missing $\Delta T_C(\Omega)$, which can vary in size depending on the atom and may be positive or negative. The use of $(1 + \gamma)$ to scale the energies now becomes a first approximation to the correct energy and will either over- or underestimate the actual value [73]. In this report we choose to use

unscaled energy values to minimize any exaggeration of atomic energy *change* resulting from comparing an overestimated value in one complex with an underestimated value in another. We further minimize possible error by using a pruned ultrafine integration grid (99,590) and very tight convergence criteria (RMS force $< 10^{-6}$ and RMS displacement $< 4\times10^{-5}$). As an explorative tool for investigating changing local stabilities within molecules, the use of atomic energies remains highly useful and provides a great deal of insight that would be otherwise unattainable. We hope that in the future it will be possible to attain DFT-based energies that incorporate in some way the missing $T_C(\Omega)$. Both the scaled and unscaled atomic energy values have been included in this supporting information document, as well as other relevant data from the AIM analysis.

Appendix C   Copyright Permissions

C.1 American Chemical Society

C.2 Royal Society of Chemistry

Acknowledgements to be used by RSC authors

Authors of RSC books and journal articles can reproduce material (for example a figure) from the RSC publication in a non-RSC publication, including theses, without formally requesting permission providing that the correct acknowledgement is given to the RSC publication. This permission extends to reproduction of large portions of text or the whole article or book chapter when being reproduced in a thesis.

The acknowledgement to be used depends on the RSC publication in which the material was published and the form of the acknowledgements is as follows:

- For material being reproduced from an article in *New Journal of Chemistry* the acknowledgement should be in the form:

  - [Original citation] - Reproduced by permission of The Royal Society of Chemistry (RSC) on behalf of the Centre National de la Recherche Scientifique (CNRS) and the RSC

- For material being reproduced from an article *Photochemical & Photobiological Sciences* the acknowledgement should be in the form:

  - [Original citation] - Reproduced by permission of The Royal Society of Chemistry (RSC) on behalf of the European Society for Photobiology, the European Photochemistry Association, and RSC

- For material being reproduced from an article in *Physical Chemistry Chemical Physics* the acknowledgement should be in the form:

  - [Original citation] - Reproduced by permission of the PCCP Owner Societies

- For material reproduced from books and any other journal the acknowledgement should be in the form:

  - [Original citation] - Reproduced by permission of The Royal Society of Chemistry

The acknowledgement should also include a hyperlink to the article on the RSC website.

The form of the acknowledgement is also specified in the RSC agreement/licence signed by the corresponding author.

Except in cases of republication in a thesis, this express permission does not cover the reproduction of large portions of text from the RSC publication or reproduction of the whole article or book chapter.

A publisher of a non-RSC publication can use this document as proof that permission is granted to use the material in the non-RSC publication.

C.3 Elsevier